UNIVERSITAT DE BARCELONA

Design and synthesis of sphingosine-1-phosphate lyase inhibitors and fluorogenic probes for the development of HTS assays

Pol Sanllehí Figuerola

UNIVERSITAT DE BARCELONA

FACULTAT DE FARMÀCIA I CIÈNCIES DE L'ALIMENTACIÓ

DEPARTAMENT DE FARMACOLOGIA, TOXICOLOGIA I QUÍMICA TERAPÈUTICA

CONSELL SUPERIOR D'INVESTIGACIONS CIENTÍFIQUES

INSTITUT DE QUÍMICA AVANÇADA DE CATALUNYA

DESIGN AND SYNTHESIS OF SPHINGOSINE-1-PHOSPHATE LYASE INHIBITORS AND FLUOROGENIC PROBES FOR THE DEVELOPMENT OF HTS ASSAYS

POL SANLLEHÍ FIGUEROLA

2016

UNIVERSITAT DE BARCELONA

FACULTAT DE FARMÀCIA I CIÈNCIES DE L'ALIMENTACIÓ

PROGRAMA DE DOCTORAT DE QUÍMICA ORGÀNICA EXPERIMENTAL I INDUSTRIAL

DESIGN AND SYNTHESIS OF SPHINGOSINE-1-PHOSPHATE LYASE INHIBITORS AND FLUOROGENIC PROBES FOR THE DEVELOPMENT OF HTS ASSAYS

Memòria presentada per Pol Sanllehí Figuerola per optar al títol de doctor per la Universitat de Barcelona

Directors:

Dr. Antonio Delgado Cirilo
Dr. Jordi Bujons Vilas

Tutor:

Dr. Antonio Delgado Cirilo

Doctorand:

Pol Sanllehí Figuerola

POL SANLLEHÍ FIGUEROLA
2016

The present doctoral thesis has been carried out at the Institute of Advanced Chemistry of Catalonia (IQAC), which belongs to the Spanish National Research Council (CSIC).

This work was supported by grants from the Spanish Ministry of Economy and Competitiveness (Project CTQ2014-54743-R) and 'Fundació la Marató de TV3' (20112130 and 20112132).

The work reported in this Doctoral Thesis has given rise to the following publications:

1) Sanllehí, P.; Casasampere, M.; López, O.; Abad, J. L.; Fabriàs, G.; Bujons, J.; Casas, J.; Delgado, A. Improved Fluorogenic Probes for the *in vivo* Monitoring of Sphingosine-1-Phosphate Lyase Activity (manuscript in preparation).

2) Sanllehí, P.; Abad, J. L.; Bujons, J.; Casas, J.; Delgado, A. Studies on the Inhibition of Sphingosine-1-Phosphate Lyase by Stabilized Reaction Intermediates and Stereodefined Azido Phosphates. *Eur*. *J*. *Med*. *Chem*. **2016**, *123*, 905–915.

3) Sanllehí, P.; Abad, J. L.; Casas, J.; Bujons, J.; Delgado, A. Bacterial versus Human Sphingosine-1-Phosphate Lyase (S1PL) in the Design of Potential S1PL Inhibitors. *Bioorg*. *Med*. *Chem*. **2016**, *24* (18), 4381–4389.

4) Sanllehí, P.; Abad, J. L.; Casas, J.; Delgado, A. Inhibitors of Sphingosine-1-Phosphate Metabolism (sphingosine Kinases and Sphingosine-1-Phosphate Lyase). *Chem*. *Phys*. *Lipids* **2016**, *197*, 69–81.

5) Nieves, Í.; Sanllehí, P.; Abad, J. L.; Fabriàs, G.; Casas, J.; Delgado, A. Chemical Probes of Sphingolipid Metabolizing Enzymes. In *Bioactive Sphingolipids in Cancer Biology and Therapy*; Hannun, Y. A., Luberto, C., Mao, C., Obeid, L. M., Eds.; Springer International Publishing: Switzerland, **2015**; pp 437–469.

A les meves àvies

Agraïments

En primer lloc vull agrair a totes les persones que m'han ajudat durant la realització d'aquest treball.

Als Drs. José Luís Abad, Gemma Fabriàs i Josefina Casas, i en especial al Dr. Antonio Delgado, per haver-me donat l'oportunitat de realitzar aquesta tesi doctoral al RUBAM. Per la vostra proximitat i confiança, per la vostra gran disponibilitat i per la llibertat transmesa en tot moment. També vull donar les gràcies al Dr. Jordi Bujons per haver estat el codirector d'aquest treball. Pels teus valuosos consells i pel criteri transmès com a investigador. Moltes gràcies per la immensa quantitat de coses apreses durant aquest temps.

A tots els companys del laboratori amb els que he anat coincidint, per la quantitat d'experiències viscudes i per tot allò que m'heu anat ensenyant. Gràcies per les extenses discussions químiques i per les rialles compartides.

Als meus amics, per el vostre recolzament i atenció encara que la majoria no hi entengueu de reaccions o de molècules. Gràcies per la vostra confiança, per escoltar-me i aconsellar-me quan més ho he necessitat i per ser com sou.

Finalment m'agradaria donar especialment les gràcies a la meva família.

Als meus pares, pels valors transmesos, per el recolzament i consells rebuts a l'hora de prendre decisions i per l'estimació i afecte mostrats. Gràcies per ajudar-me en les diferents etapes de la vida que he anat iniciant. Una abraçada ben forta.

A la meva germana Maria, per saber que puc comptar sempre amb tu tot i no veure'ns tan com abans. Per la teva simpatia i tendresa, et desitjo el millor.

A les meves dues àvies, per la força i la perseverança mostrades en els moments més difícils. Sou un exemple per a mi, us estimo.

I a tu, Íngrid, per tots els moments que hem viscut junts, pel teu recolzament incondicional i per saber com fer-me feliç.

A tots vosaltres, moltes gràcies.

Abbreviations

3–kdhSo	3–Ketodihydrosphingosine
AcCl	Acetyl chloride
aCDase	Acid ceramidase
AFU	Arbitray fluorescence units
aq.	Aqueous
aSMase	Acid sphingomyelinase
ATP	Adenosine triphosphate
Boc	*tert*–Butoxycarbonyl
cat.	Catalytic
C1P	Ceramide–1–phosphate
CBz	Carboxybenzyl
Cer	Ceramide
CerK	Ceramide kinase
CerS	Ceramide synthase
CNS	Central nervous system
CuAAC	Copper(I)–catalyzed alkyne-azide cycloaddition
DAG	Diacylglycerol
DAIH	2–Diphenylacetyl–1,3–indandione–1–hydrazone
DCM	Dichloromethane
Des1	Dihydroceramide desaturase
dhCer	Dihydroceramide
dhS1P	Dihydrosphingosine–1–phosphate
dhSo	Dihydrosphingosine; sphinganine
DIPEA	*N*,*N*–Diisopropylethylamine
DMAP	4–(Dimethylamino)pyridine
DMF	*N*,*N*–Dimethylformamide
DMP	Dess–Martin periodinane
DMSO	Dimethyl sulfoxide
DOP	4–Deoxypyridoxine
DOP−P	4–Deoxypyridoxine 5'−phosphate
DTT	DL–Dithiothreitol
EAE	Experimental autoimmune encephalomyelitis

EAP	Ethanolamine phosphate
EDC	*N*–(3–Dimethylaminopropyl)–*N′*–ethylcarbodiimide hydrochloride
EDTA	Ethylenediaminetetraacetic acid
ee	Enantiomeric excess
ELS	Evaporative light scattering
equiv.	Equivalent(s)
ER	Endoplasmic reticulum
Et_2O	Diethyl ether
EtOAc	Ethyl acetate
EtOH	Ethanol
FD	Fluorescence detector
Fmoc	9–Fluorenylmethoxycarbonyl
GC/MS	Gas chromatography/mass spectrometry
GCase	Acid–β–glucosidase; Glucocerebrosidase
GC	Glucosyl ceramide
GCS	Glucosyl ceramide synthase
GSL	Glycosphingolipids
h	Hour(s)
HATU	1–[Bis(dimethylamino)methylene]–1*H*–1,2,3–triazolo[4,5–b] pyridinium 3–oxide hexafluorophosphate
HEPES	4–(2–Hydroxyethyl)piperazine–1–ethanesulfonic acid
HOBt	1–Hydroxybenzotriazole
HPLC	High–performance liquid chromatography
HRMS	High–resolution mass spectrometry
HTS	High–throughput screening
IC_{50}	Half maximal inhibitory concentration
IMAC	Immobilized–metal affinity chromatography
IPTG	Isopropyl–β–D–thiogalactoside
ISA·HCl	1*H*–imidazole–1–sulfonylazide hydrochloride
K_I	Enzyme inhibitor (inhibition) constant
LB	Luria–Bertani broth
LC/MS	Liquid chromatography/mass spectrometry
LPA	Lysophosphatidic acid

LPP	Lipid phosphate phosphatases
MEF	Mouse embryonic fibroblast
MeOH	Methanol
min	Minute(s)
MPA	α–Methoxy–α–phenylacetic acid
nCDase	Neutral ceramidase
NMR	Nuclear magnetic resonance
nSMase	Neutral sphingomyelinase
Nu	Nucleophile
OCM	Olefin cross–metathesis
PA	Phosphatidic acid
PDA	Photodiode array
PDXK	Pyridoxal kinase
PFBHA	*O*–(2,3,4,5,6–pentafluorobenzyl)hydroxylamine
PG	Protecting group
PhytoSo	Phytosphingosine
PLP	Pyridoxal 5'–phosphate
p-TsCl	*p*–Toluenesulfonyl chloride
p-TsOH	*p*–Toluenesulfonic acid
quant.	Quantitative
RP	Reversed–phase
rt	Room temperature
R_T	Retention time
S1P	Sphingosine–1–phosphate
S1PL	Sphingosine–1–phosphate lyase
S1PPase	Sphingosine–1–phosphate phosphatase
sat.	Saturated
LSC	Liquid scintillation counting
SDS–PAGE	Sodium dodecyl sulfate polyacrylamide gel electrophoresis
SK	Sphingosine kinase
SLs	Sphingolipids
SM	Sphingomyelin
So	Sphingosine

SPT	Serine palmitoyltransferase
TBAF	Tetrabutylammonium fluoride
TBDPS	*tert*–Butyldiphenylsilyl ether
TBDPSCl	*tert*–Butyl(chloro)diphenylsilane
TBS	*tert*–Butyldimethylsilyl ether
TEA	Triethylamine
TEAA	Triethylammonium acetate
THF	Tetrahydrofuran
THI	2–Acetyl–4–tetrahydroxybutylimidazole
TLC	Thin layer chromatography
TMSBr	Bromotrimethylsilane
TOF	Time of flight
UPLC	Ultra–performance liquid chromatography
UV	Ultraviolet
WT	Wild type

Table of contents

1. Introduction

1.1 Sphingolipids

Sphingolipids (SLs) are ubiquitous structural components of eukaryotic cell membranes. Since their discovery in 1884 by J. L. W. Thudichum and until very recently, SLs have been considered inert components of membranes with merely structural roles. However, several studies conducted over the past decades revealed that some SLs, including ceramide (Cer), sphingosine (So), and their phosphorylated forms, ceramide–1–phosphate (C1P) and sphingosine–1–phosphate (S1P), are bioactive molecules that can control vital biological functions, ranging from regulation of signal transduction pathways to the mediation of cell–to–cell interactions and recognition.[1]

SLs, in association with other lipids and cholesterol, are also involved in the formation of specific membrane domains, called rafts, which are important in determining the biophysical properties of membranes. These lipid microdomains, together with membrane proteins, are able to form fluctuating nanoscale assemblies, which also play important roles in membrane signaling and trafficking.[2,3]

Dysregulation of sphingolipid metabolism leads to the establishment and progression of diseases. Sphingolipidoses are the most characteristic disorders linked to alterations in sphingolipid metabolism. These metabolically inherited diseases are rare syndromes caused by mutations in the sphingolipid metabolizing enzyme genes that result in defective enzyme activities and accumulation of lipids inside the cell organelles. Altered sphingolipid metabolism also occurs in higher economic impact diseases, such as neurodegenerative and cardiovascular diseases, chronic inflammation, or cancer.[4] In this context, several sphingolipid metabolizing enzymes have become important therapeutic targets.[5]

1.1.1 Structure

From a chemical point of view, SLs are a class of naturally occurring lipids containing a C18 carbon backbone with a 2–amino–1,3–diol motif, known as sphingoid base (Figure 1.1) In mammals, most SLs derive from So, which has a (2*S*,3*R*)–*erythro* configuration, although a minor portion arise from its saturated analogue dihydrosphingosine (dhSo) or its 4–hydroxy derivative phytosphingosine (PhytoSo), being the latter the central scaffold for the synthesis of most fungal and plant SLs.[6]

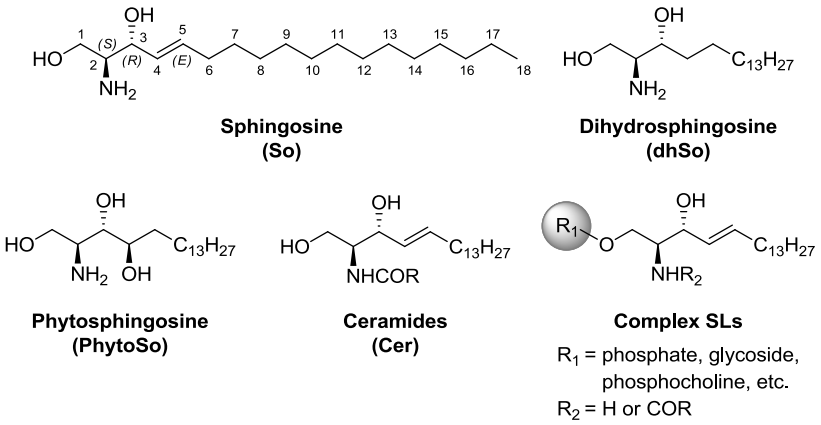

Figure 1.1. General structure of SLs.

Sphingoid bases can be *N*–acylated with a variety of fatty acids giving ceramides (Cer). Despite the generic term "ceramide" comprises a family of several molecular species differing in the unsaturation of the sphingoid base as well as in the nature of the *N*–acyl chain,[7] in this section we will refer to Cer to indicate the C18 monounsaturated species shown in Figure 1.1, unless otherwise stated.

Functionalization at the C1–OH with different polar groups gives rise to complex SLs. Depending on the nature of the *O*–linked moiety, this large family of metabolites may range from simple phosphate or phosphocholine derivatives to complex glycoconjugated ceramide species (see below).

1.1.2 Metabolism and compartmentalization

The biosynthesis of SLs comprises a highly organized system that takes place in different intracellular compartments (Figure 1.2). Thus, the so–called *de novo* biosynthesis takes place in the endoplasmic reticulum (ER) and starts with the condensation of L–serine with palmitoyl–CoA to give 3–ketodihydrosphingosine (3–kdhSo) (Figure 1.3) in a reaction catalyzed by serine palmitoyltransferase (SPT). By the action of a reductase, the ketone group of 3–kdhSo is stereospecifically reduced to a hydroxyl group to afford dihydrosphingosine (dhSo), which is *N*–acylated to dihydroceramides (dhCer) by specific ceramide synthases (CerS) of different chain length specificities.[8] The oxidation of dhCer to ceramide (Cer) by dhCer desaturase (Des1) constitutes the last step of the biosynthetic pathway.[9]

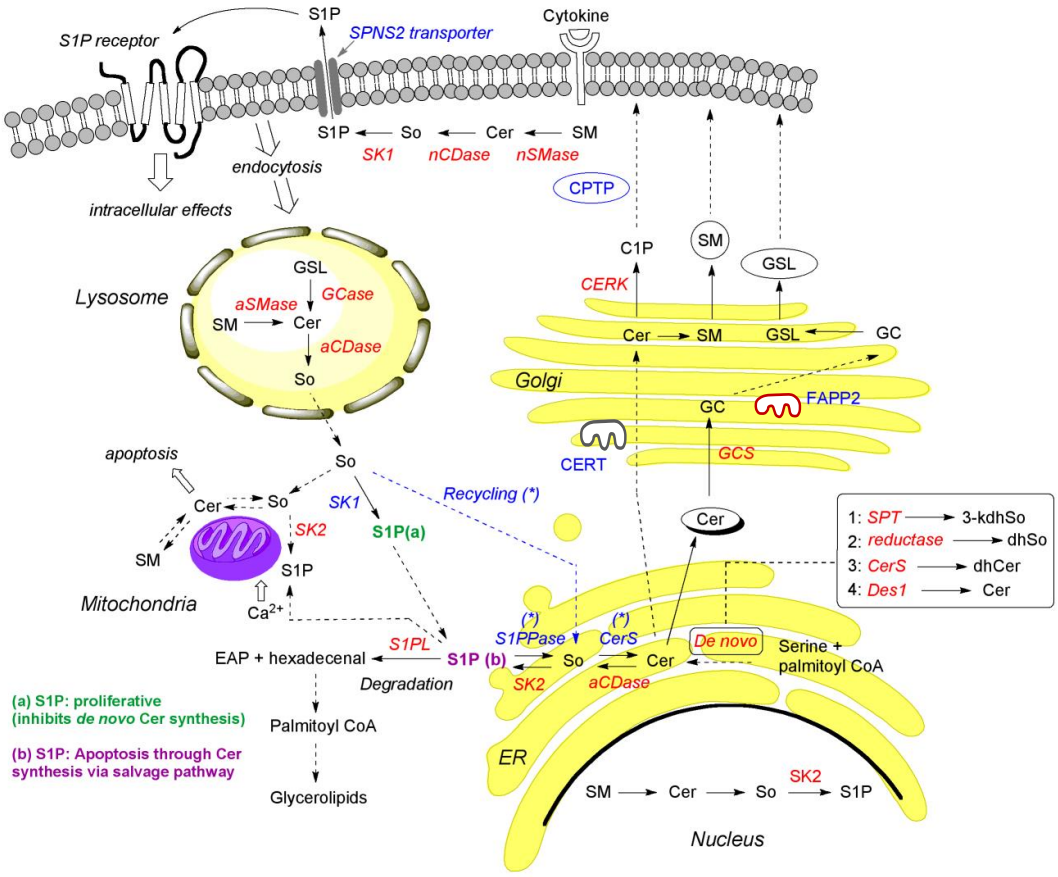

Figure 1.2. Compartmentalization of SLs biosynthesis. For the structures, see Figure. 1.3. Adapted from ref. 10; (*): salvage pathway.

Due to the metabolic inter–relations between Cer and other SL metabolites, Cer has been considered as the metabolic hub of SLs biosynthesis.[1] Part of the Cer generated in the ER is transported to the *trans*–Golgi apparatus by means of the specific transporter protein CerT[11] for its further transformation into sphingomyelin (SM), the major SL constituent of the cell membranes. Alternatively, after vesicular transport of Cer to the *cis*–Golgi, biosynthesis of glucosyl ceramide (GC) by means of glucosyl ceramide synthase (GCS) takes place, prior to its subsequent transport to *trans*–Golgi by FAPP2 to give complex glycosphingolipids (GSL). As with SM, GSL are transported by vesicular pathways to the cell membrane where they exert several and capital functions concerning cell–cell communications and responses to external stimuli.[12]

By the action of specific cytokines or by other external stimuli, activation of neutral forms of sphingomyelinase (nSMase) and ceramidase (nCDase) can give rise to a buildup of So at the membrane level. Phosphorylation of So by the action of the specific

sphingosine kinase–1 (SK1) leads to sphingosine–1–phosphate (S1P), which is secreted to elicit a plentiful of extracellular actions by interaction with specific receptors (see below). In addition to the biosynthesis *de novo*, which provides a flux of SLs from the ER to the cell membrane, these membrane SLs can also be internalized by endocytosic pathways and degraded in the lysosome by acidic forms of acid sphingomyelinase (aSMase), glycosidases (GCase) and acid ceramidase (aCDase). The So thus generated can be recycled back to Cer (by the action of CerS) in what is known as the salvage pathway (Figure 1.2). In an alternative degradation process, S1P can be generated at the ER to be further transformed by sphingosine–1–phosphate lyase (S1PL) into 2–hexadecenal and ethanolamine phosphate (EAP).

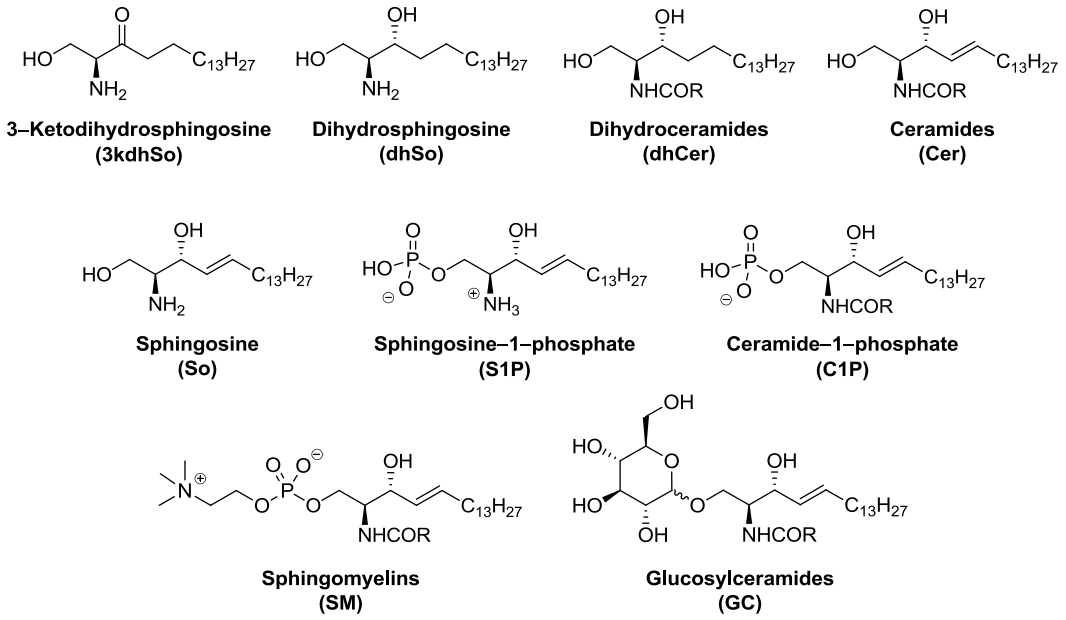

Figure 1.3. Chemical structures of the most relevant SLs.

1.2 Phosphorylated sphingolipids

An important group of SLs metabolites are those showing a phosphate group at the terminal hydroxyl group. In this context, ceramide–1–phosphate (C1P) and sphingosine–1–phosphate (S1P) are nowadays recognized as signaling molecules that regulate cell differentiation, survival, inflammation, angiogenesis, calcium homeostasis and immunity, among other functions.[13] In general, the roles of phosphorylated SLs are opposed to those of ceramides, which are potent inducers of cell cycle arrest and

apoptosis.[14] Since phosphorylation and dephosphorylation are closely interconnected metabolic pathways in the cell, the balance between these two types of metabolites is crucial for cell fate and homeostasis.

1.2.1 Ceramide–1–phosphate (C1P)

Ceramide kinase (CerK)[15,16] catalyzes the biosynthesis of C1P in the *trans*–Golgi, despite other localizations for this kinase have been shown.[17,18] Further transport by the specific transporter CPTP[19] is involved in the transfer of C1P to the plasma membrane, where it is probably rapidly degraded to Cer by specific phosphatases. Nevertheless, C1P, together with S1P, have been implicated in the regulation of inflammatory responses[20] and, particularly, C1P has been shown to directly activate cytosolic phospholipase A2 (cPLA2a), thus stimulating arachidonic acid release and the subsequent synthesis of prostaglandins.[21] In addition, the CerK/C1P pathway is required for PLA2 activation in response to cytokines.[22] The finding that bone marrow-derived macrophages from CerK deficient mice still have significant levels of C1P, suggests that other metabolic pathways may be implicated in the formation of C1P.[23] The ability of C1P to induce macrophage migration when administered exogenously, has led to hypothesize on the existence of a specific extracellular, low affinity G_i–coupled C1P receptor, which has emerged as a potential drug target for the treatment of disorders associated to macrophage migration as the main cause of the pathology, such as chronic inflammation or metastasis of malignant tumors.[24]

1.2.2 Sphingosine–1–phosphate (S1P)

S1P is a key signaling lipid that is present in all mammalian cells. It is released into the extracellular milieu by a variety of cell types, making it one of the most abundant biologically active lysophospholipids in circulation, with concentrations in plasma ranging from 100 to 400 nM, depending on the population, and reaching up to 1 μM depending on the method used to isolate plasma.[25,26]

S1P is generated in the plasma membrane from the pools of SM and the successive action of nSMase, nCDase and SK1 (Figure 1.2). The S1P thus generated is transported, via the Spinster homologue 2 (SPNS2) transporter, across the membrane to exert its extracellular roles associated to the binding to specific lipid G–protein coupled $S1P_{1–5}$

receptors in an autocrine (also known as "inside–out" signaling) or paracrine manner, to give rise to a series of downstream signaling pathways that play essential roles in vascular development and endothelial integrity, control of cardiac rhythm, and immunity responses including lymphocyte trafficking and differentiation, cell growth, cell survival, and cytokine and chemokine production, among others[10,27–31] (Table 1.1).

In mammals, $S1P_{1–3}$ receptors are expressed ubiquitously, whereas $S1P_4$ and $S1P_5$ are restricted to certain tissues. $S1P_1$, in particular, is highly expressed in mature T cells and is the most important S1P receptor in the immune system, since it regulates numerous aspects of immune function including lymphocyte trafficking between the blood and lymphoid tissues.[32,33] Interestingly, the family of GPCRs $S1P_{1–5}$ receptors share around 40 % sequence identity.[30] In addition, the crystal structure of the $S1P_1$ receptor in complex with a selective antagonist sphingolipid mimic has been reported.[34]

Most of the research aimed at the pharmacological intervention of the S1P signaling pathway has focused on synthetic agonists of S1P receptors. This has boosted the development of specific S1P receptor modulators, some of which have gained relevance in clinical practice, as, for example, FTY720 (Fingolimod, Gilenya®) (Figure 1.7). Detailed pharmacological studies carried out on this compound showed that it is a pro–drug that requires an (*S*)–enantioselective phosphorylation by SK2 for activation as S1P receptor agonist.[35] Fingolimod was the first orally active drug approved for the treatment of relapsing–remitting multiple sclerosis for its ability to act as a $S1P_{1,3–5}$ agonist at nM concentrations.[36,37] The design of FTY720 analogs with improved receptor selectivity has been an active field of research. In this context, several selective agonists and antagonists on the different S1P receptors have been reported.[38,39]

S1P play pivotal roles in the egress of activated lymphocytes from secondary lymphoid organs, a process that is dependent on the expression of $S1P_1$ on the cell surface. Downregulation of this receptor by FTY720 leads to retention of the lymphocytes, which thus cannot reach sites of inflammation, an effect that is desired in the treatment of autoimmune diseases.[5] S1P acts as a potent chemoattractant for $S1P_1$–dominant cells, so lymphocytes migrate in response to a S1P gradient between tissues (low S1P concentrations) and circulation (high S1P concentrations). This S1P gradient mediates lymphocyte egress from lymphoid organs to lymph and further to blood.[40]

Table 1.1. Distribution and functions of sphingosine-1-phosphate receptors; modified from ref. 32.

Receptor	Tissue expression	Functional expression
$S1P_1$	Endothelial cells Smooth muscle cells Cardiomyocytes Immune cells (dendritic cells, macrophages, eosinophils, mastocytes, lymphocytes T and B, NK, NKT) Neuronal cells	Angiogenesis Endothelial integrity Cardiomyocytes survival in ischemia/reperfusion Vascular tone regulation (relaxation) Lymphocyte circulation Migration Neurogenesis
$S1P_2$	Smooth muscle cells Cardiomyocytes Immune cells (dendritic cells, macrophages, eosinophils, mastocytes, NKT)	Cardiomyocytes survival in ischemia/reperfusion Vascular system and audition Vascular tone regulation (contraction) Neuronal excitability Inhibition of migration Mastocytes degranulation
$S1P_3$	Endothelial cells Smooth muscle cells Cardiomyocytes Immune cells (dendritic cells, eosinophils, lymphocytes T) Neuronal cells	Cardiomyocytes survival in ischemia/reperfusion Vascular tone regulation (relaxation) Heart rate regulation
$S1P_4$	Immune cells (dendritic cells, lymphocytes T, NKT)	Maintenance of dendritic cells functions Inhibition of T cell proliferation
$S1P_5$	Immune cells (dendritic cells, NK) Neuronal cells (oligodendrocytes)	NK circulation Oligodendrocytes survival

NK = natural killer; NKT = natural killer T.

A functional consequence of (*S*)–FTY720P, the phosphorylated (*S*)–active form of FTY720, binding to $S1P_1$ is receptor internalization and intracellular degradation which eventually leads to its down–regulation in the cell surface.[41] Thus, lymphocytes lose their response to the S1P gradient thereby preventing their release from secondary lymphoid tissues and resulting in peripheral lymphopenia.[13] Although (*S*)–FTY720P acts initially as an agonist at S1P receptors, it could be considered as 'functional antagonist', since its effects are inhibitory in the longer term on S1P receptor function.

Erythrocytes and platelets constitute a buffer system for S1P in blood. They efficiently incorporate and store S1P, and protect it from cellular degradation. Despite they are not able to biosynthesize S1P, they can phosphorylate So as an additional pathway to account for the high levels of intracellular S1P.[25] Another reason for the high levels of S1P found in these types of cells has been attributed to their lack of both SPL and the specific S1P transporter SPNS2.[42,43] Nevertheless, the S1P produced in erythrocytes can also be exported to the extracellular space by the ATP-binding cassette ABCC1[44] to reach S1P receptors after binding to albumin and high–density lipoprotein (HDL).[31]

On the other hand, recent findings have revealed that S1P modulates many noxious processes that follow CNS injury (apoptotic cell death, lipid hydrolysis, oxidative stress and tissue damage), while supporting growth and trophic factor activities, angiogenesis and neurogenesis.[45,46] Thus, pharmacological agents that either promote or mimic S1P activities may be therapeutic in the context of acute CNS injury and perhaps neurodegenerative diseases. Due to its crucial role on cell fate (see below), the control of the S1P/Cer balance might be exploited for the discovery of potential neuroprotective and/or neuro–restorative therapies with applications in traumatic brain injury, spinal cord injury, and stroke.

In contrast to the well characterized receptor–mediated effects of S1P, much less is known about its intracellular actions. Recent studies evidenced that S1P can also act inside the cell as a secondary messenger during inflammation.[31] In this regard, S1P is unique in that it can be biosynthesized in the nucleus of endothelial cells and T cells by the action of SK2, where it exerts important immune functions as a result of the activation of gene transcription by inhibition of histone deacetylases 1 and 2 (HDAC 1 and 2).[31,47]

1.3 Modulation of S1P metabolism

The levels of S1P depend on the balance of three different processes: (a) phosphorylation of So at the 1–position by specific kinases, which use ATP as phosphate source and present different cellular localizations, (b) dephosphorylation of S1P by ubiquitous general lipid phosphatases or by specific S1P phosphatases located at the ER, and (c) degradation of S1P by the action of the specific lyase S1PL, also located at the ER. Together with C1P, the dynamic balance between phosphorylated and non–phosphorylated SL, as well as their subcellular localization, turns out to be crucial for cell fate. Thus, phosphorylated SLs exert mitogenic effects while Cer and other sphingoid bases are considered pro–apoptotic. Based on these premises, the notion that the ratio S1P/Cer can act as a "sphingolipid rheostat"[48,49] emerged as an important concept to understand cellular homeostasis. This concept can be better understood by also considering CerK for its ability to regulate the intracellular levels of C1P, another important phosphorylated SL.

1.3.1 Sphingosine kinases

Sphingosine kinases (SK) catalyze the transfer of phosphate from ATP to So to generate S1P. Two SK isoforms (SK1 and SK2) have been identified.[50] Concerning substrate specificity, both enzymes can also phosphorylate dhSo. However, SK2 is less restrictive and can accept a wider variety of lipid structures as, for example, PhytoSo, L–*threo*–dhSo,[50] and also FTY720, which is converted into the active (*S*)–phosphorylated form.[51]

SK1 isoform is mostly localized in the cytosol, in close proximity to the plasma membrane. It participates in the biosynthesis of S1P, which is subsequently transported to the extracellular space for autocrine or paracrine signaling to give rise, *inter alia*, to cell proliferation and inhibition of *de novo* Cer synthesis. Another location of SK1 is near the lysosomes, where it converts So to zwitterionic S1P for its subsequent degradation by SPL or its recycling, as part of the salvage pathway.[1] On the other hand, although the isoform SK2 is mostly nuclear, it can also be found in mitochondria, where S1P plays an important role in the cytochrome c–oxidase assembling required for mitochondrial respiration,[52] and in the ER, where So is phosphorylated to give S1P, which promotes Cer synthesis through the salvage pathway and induces apoptosis. (see Figure 1.2).[53]

From a functional standpoint, both SK are quite similar and partly redundant, since the absence of any of the isoforms does not give rise to severely altered phenotypes. However, the simultaneous lack of both SK1 and SK2 in a double knockout mouse is lethal due to an incomplete maturation of the vascular system and brain.[54]

The importance of SK as potential targets for drug discovery is linked to the above indicated role of phosphorylated SL, in particular S1P, in cell proliferation and its implication in several diseases as, for example, sickle cell disease, cancer, and fibrosis.[5,43]

1.3.2 Sphingosine–1–phosphate phosphatases (S1PPase)

The phosphatase super–family comprises a heterogeneous group of enzymes characterized by the presence of conserved residues essential for their catalytic activity. The mammalian lipid phosphate phosphatases (LPP) and the S1PPase are members of this superfamily. LPPs are integral membrane proteins that dephosphorylate a variety of phosphorylated lipid substrates. Three mammalian LPP isoforms have been identified, termed LPP1, LPP2 and LPP3, together with another member named PRG–1 (plasticity–related gene–1). They differ in tissue distribution but, overall, they are widely expressed. All three LPPs are capable of dephosphorylating lysophosphatidic acid (LPA), S1P, phosphatidic acid (PA) and C1P *in vitro*, thereby producing monoacylglycerol, So, diacylglycerol (DAG) and Cer, respectively. Concerning S1PPase, there are two ER–localized isoforms (named SPP1 and SPP2) that catalyze the dephosphorylation of S1P. They differ from LPP in the substrate specificity, which is limited to S1P, dhS1P, and phytosphingosine–1–phosphate, whereas LPA and PA are not substrates. Concerning tissue distribution, S1PPase1 is mainly expressed in kidney and placenta whereas S1PPase2 is predominant in the heart and kidney.[20,55,56]

1.3.3 Sphingosine–1–phosphate lyase (S1PL)

Sphingosine–1–phosphate lyase (S1PL) is a key enzyme of SLs metabolism that catalyzes the retroaldol cleavage of S1P into ethanolamine phosphate (EAP) and 2–hexadecenal (see Figure 1.4).[57] The S1PL reaction is considered the “exit gate” of the SLs metabolism since it is the only irreversible reaction in the sphingolipid pathway. In addition, it connects SLs to other metabolic routes, as both reaction products are

ultimately incorporated into the biosynthesis of phospholipids.[58] Sphinganine–1–phosphate (dhS1P), the saturated analogue of S1P (Figure 1.4), can be also catabolized by S1PL yielding EAP and the saturated fatty aldehyde hexadecanal as the degradation products. Remarkably, the enzyme exhibits specificity to only the naturally occurring D–*erythro* isomers.[59]

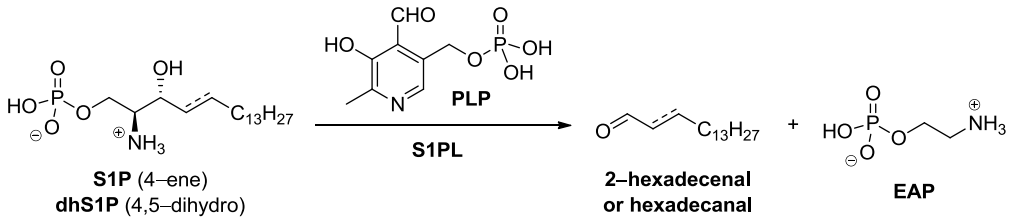

Figure 1.4. S1PL–catalyzed retroaldol cleavage of S1P.

From a mechanistic standpoint, S1PL belongs to the superfamily of pyridoxal 5'–phosphate (PLP)–dependent enzymes (see Figure 1.4). S1PL is located in the ER and possesses an *N*–terminal lumenal domain, a transmembrane segment and a soluble PLP–binding domain, responsible for its catalytic activity (Figure 1.5).[59] In 2010, Bourquin *et al*. reported the crystal structures of yeast S1PL from *Saccharomyces cerevisiae* (Dpl1p)[60] and that of a putative prokaryotic homolog from *Symbiobacterium thermophilum* (StS1PL),[61] which were expressed in *E*. *coli* (Figure 1.5).

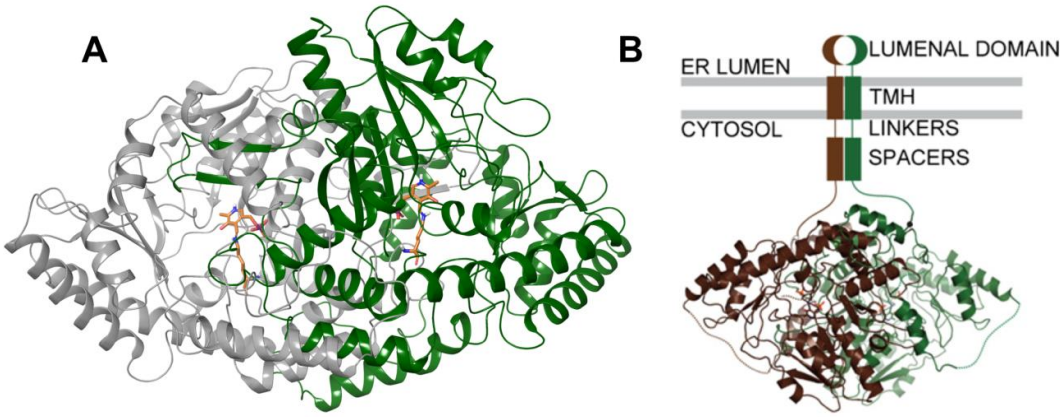

Figure 1.5. (A) Crystal structure of StS1PL (PDB 3MAD). The PLP cofactor bound to K311 is highlighted in orange. (B) Crystal structure of the PLP–binding domain of yeast S1PL (Dpl1p) and proposed arrangement on the ER membrane. TMH, transmembrane helix. Image taken from ref. 61

These structures were used as a basis for a very reliable model of the human enzyme.[61] In a more recent work published in 2014, Weiler *et al*, reported the efficient expression of hS1PL in Sf9 insect cells together with the first crystal structure of hS1PL in complex with the selective inhibitor **3b** (see Figures 1.6 and 1.9).[62] Very recently, the crystal structure of another prokaryotic S1PL from *Legionella pneumophila* (LpS1PL) has also been solved.[63]

S1PL is active as a dimer, with two catalytic cavities to which each protomer contributes residues simultaneously (Figure 1.6). hS1PL and Dpl1p are ER–resident, integral membrane proteins with a single trans–membrane domain. In contrast, bacterial StS1PL is a globular protein lacking this trans–membrane domain, which has been shown to be dispensable for enzyme activity in the human and yeast homologues.[60,64] Therefore, in order to easily obtain soluble and active forms of hS1PL and Dpl1p, they have been expressed and purified as *N*–terminally shortened variants.[61,62]

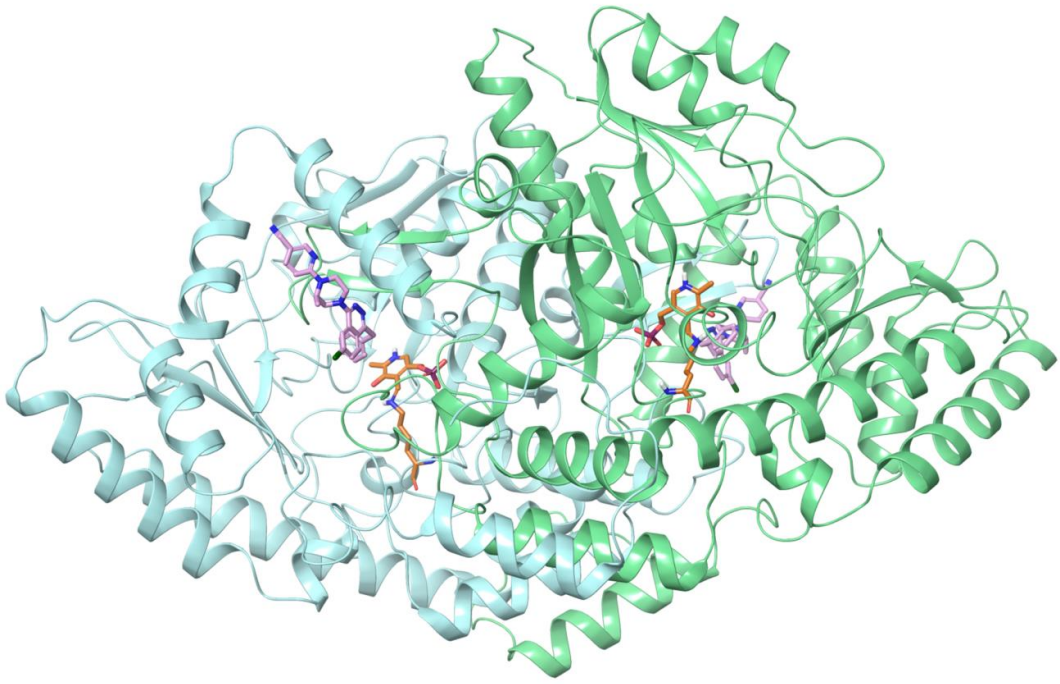

Figure 1.6. Cartoon representation of the hS1PL dimer (PDB 4Q6R). Both subunits are highlighted in light blue (chain A) and green (chain B). The PLP cofactor bound to K353 (orange) and a bound inhibitor (**3b**, light purple, structure on Figure 1.9) are also shown.

In combination with sphingosine kinases and S1PPase, S1PL is in critical position to tightly regulate intracellular levels of S1P. Notably, S1PL knockout mice featuring partial reduction of S1PL activity exhibited a significant decrease in circulating lymphocytes and presented high levels of S1P in lymphoid organs.[65] Moreover, downregulation of S1PL activity also conferred protective effects to rodents in experimental autoimmune encephalomyelitis (EAE), a model of multiple sclerosis.[62] As introduced above in Section 1.2.2, lymphocyte egress from secondary lymphoid organs is mediated by a S1P gradient between tissues and blood. Inhibition of S1PL causes a steep increase of S1P concentrations in lymphoid tissues, thereby disrupting the S1P gradient.[40] This triggers downregulation of S1P receptors on the cell membrane of lymphocytes which thus do not migrate out to circulation. Since S1PL plays pivotal roles in mediating the S1P gradient, modulation of S1PL activity has emerged as an alternative pharmacological approach in the treatment of autoimmune diseases such as multiple sclerosis or rheumatoid arthritis, among others.[5,66] S1PL expression and activity have been also involved in development[67–69] and chemotaxis.[70] Moreover, the enzyme prevents defects in reproductive structures and function,[71] acts as a tumor suppressor[57,72,73] and has an important role in chemoresistance.[74–77]

1.3.3.1 Sphingolipid analogs as SPL inhibitors

The development of selective SPL inhibitors has attracted the scientific community as an indirect way to increase the levels of S1P and because of the opportunities that S1P modulation offers for the treatment of some immunity–related disorders.[40,78] Attempts to design selective SPL inhibitors have been accomplished with varied results. The first inhibitor reported in the literature was 1–deoxysphinganine–1–phosphonate (Figure 1.7).[79] Initially described as a competitive inhibitor with a K_I = 5 μM, the compound behaves also as a substrate, but it is cleaved at reduced rate in comparison with S1P. Due to its hemolytic properties, this phosphonate was proved to be highly toxic when administered intravenously. The S1P analog 2–vinylsphinganine–1–phosphate (2–vinyl–dhS1P) (described as a mixture of stereoisomers) (Figure 1.7) has also been reported as a potent S1PL inhibitor with an IC_{50} value of 2.4 μM. Given the reactivity of the vinyl group at C2, it is presumed that this compound could interact in a covalent manner with the enzyme and, therefore, act as an irreversible inhibitor.[80]

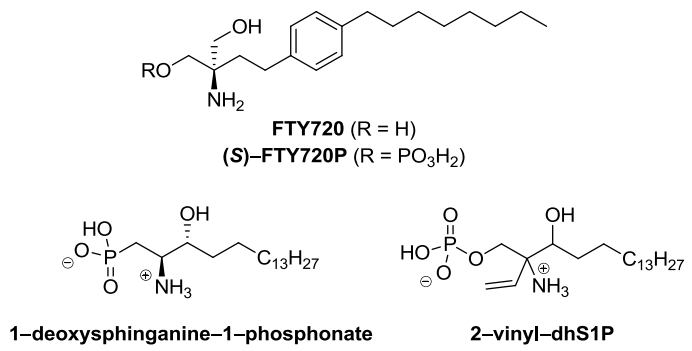

Figure 1.7. Sphingolipid analogs reported as S1PL inhibitors.

Compound FTY720, initially reported as an immunomodulatory agent due to its direct activity towards S1P receptors 1,3,4 and 5 after phosphorylation by SK2 (see Section 1.2.2), was also reported as S1PL inhibitor *in vitro*,[81] with IC_{50} values ranging from 17[62] to 52[82] μM, depending on the source of enzyme activity. However, this effect is only observed at concentrations around 100–fold higher than those required for *in vivo* activity as S1P receptors agonist.[36] In contrast, (*S*)–FTY720P, the active form of fingolimod on S1P receptors, was determined to be inactive against S1PL.[81,82]

1.3.3.2 Functional SPL inhibitors

Some compounds have been reported as functional SPL inhibitors because of their ability to reproduce a phenotypic S1PL inhibition *in vivo*, despite their lack of activity on the isolated enzyme. In this context, the vitamin B_6 antagonist 4–deoxypyridoxine (DOP) (Figure 1.8) has been reported as a S1PL inhibitor and also as a non–selective inhibitor of PLP–dependent enzymes.[40,83] Although DOP does not inhibit S1PL in either cell–free of cell–based assays,[65,84,85] it induces increased S1P concentrations in different tissues and causes reduction of circulating lymphocyte when administered *in vivo*,[40,65] suggesting that DOP can act as an indirect S1PL inhibitor. In this context, Ohtoyo *et al*. recently reported that DOP, upon phosphorylation by pyridoxal kinase (PDXK), is converted *in vitro* to 4–deoxypyridoxine 5'–phosphate (DOP–P) (Figure 1.8), which competes with PLP for the active site of apo–S1PL, resulting in the inhibition of the enzymatic activity.[86]

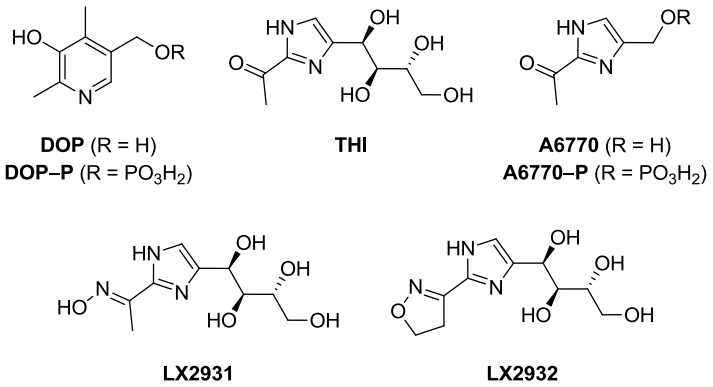

Figure 1.8. Functional S1PL inhibitors.

A similar scenario is observed for THI and structurally related analogs (Figure 1.8). Oral administration of 2–acetyl–4–tetrahydroxybutylimidazole (THI), originally identified as a minor constituent of caramel color III, caused lymphopenia in rodents,[87] leading to a phenotype similar to that observed in mice expressing reduced levels of S1PL.[65] As for DOP, these compounds only inhibit S1PL *in vivo* and its effect is reverted by excess dietary vitamin B_6.[40] However, very recently, it has been demonstrated that THI is metabolized to the smaller derivative A6770, a key metabolic intermediate that can be also phosphorylated to yield the active compound A6770–P, which inhibits S1PL in the same way as DOP–P (see above).[88] In addition, derivatives of THI, such as LX2931 and LX2932, have also been described.[41,65] LX2931, developed for the treatment of rheumatoid arthritis, was the first clinically studied inhibitor of S1PL. After evaluation in phase I clinical trial in healthy human subjects it failed at phase II, apparently due to sub–therapeutic dosing.[66]

1.3.3.3 Non lipidic S1PL inhibitors

A series of inhibitors structurally unrelated to S1P have been reported on the last years as a result of extensive HTS programs. This is the case of the oxopyridylpyrimidine **1** (Figure 1.9), which was identified as S1PL hit (IC_{50} = 2.1 μM) after a HTS performed by Lexicon. **1** increased S1P levels 275 % over controls in HepG2 cells, despite it failed to elicit an *in vivo* lymphopenic effect, probably because of tight protein binding.[65] References in the literature mentioning this compound are very scarce. Gatfield *et al*. used **1** alongside the Des1 inhibitor GT11 and the functional $S1P_1$ receptor agonist

Ponesimod[89] in order to study the role of S1PL in the physiological $S1P_1$ receptor recycling process.[90]

Kashem and coworkers from Boehringer Ingelheim, reported the development of a scintillation proximity assay compatible with HTS (See section 1.4.1) which allowed for a massive screening of an in–house library of approximately 10^6 compounds that led to the identification of structurally diverse S1PL inhibitors. Among them, compound **2** (Figure 1.9), with an IC_{50} value of 1.6 μM, was selected as an attractive starting point for the development of a new class of immunosuppressive drugs, since it induced dose–dependent lymphopenia in mice, with reduction levels similar than those described for the reference compound FTY720.[91]

On the other hand, as a result of a massive screening campaign carried out by Novartis using a corporate chemical library of around 250,000 compounds, the piperazinophthalazine derivative **3a** (Figure 1.9) was identified as an interesting S1PL inhibitor in the low micromolar range (IC_{50} = 2.4 μM).[84,85] Interestingly, the (*S*)–configured enantiomer of **3a** was significantly less potent (IC_{50} > 30 μM). As a result of a lead optimization process, compounds **3b**[85] and **3c**[62] (Figure 1.9) were later reported as improved inhibitors acting in the submicromolar and nanomolar range (IC_{50} values of 0.21 μM and 0.024 μM for **3b** and **3c**, respectively). The reported crystal structure of human S1PL in complex with **3b** demonstrated that the inhibitor is hosted in the substrate binding site, specifically at the branching point of a Y–shaped channel that links the buried active site to the exterior.[62,92] Remarkably, compound **3b** is able to induce lymphopenia and confers protection in animal models of multiple sclerosis.[62]

Very recently, an HTS program conducted by AbbVie has led to the discovery of isoxazolecarboxamide **4a** (Figure 1.9) which behaved as low micromolar S1PL inhibitor (*in vitro* IC_{50} = 1 μM, cell IC_{50} = 1.8 μM). Regarding the stereoselectivity of S1PL towards **4a**, the *S*–enantiomer (IC_{50} = 485 nM) was 2–fold more potent than the racemate, while the *R*–enantiomer was inactive. After a hit–to–lead process around **4a**, compounds **4b** and **4c** were reported as S1PL inhibitors with desirable potencies (For **4b**: *in vitro* IC_{50} = 120 nM, cell IC_{50} = 230 nM; for **4c**: *in vitro* IC_{50} = 590 nM, cell IC_{50} = 240 nM), but moderate metabolic stability.[93,94] Likewise, several S1PL potential inhibitors based on a virtual screening approach, have been suggested.[95]

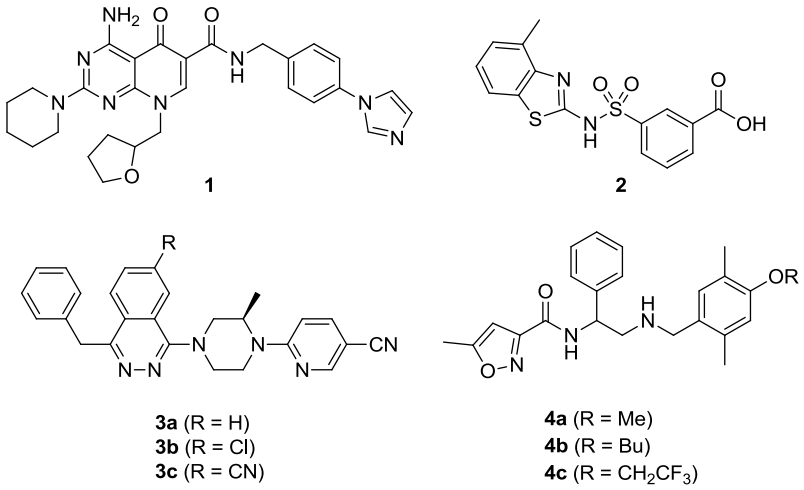

Figure 1.9. Non lipidic S1PL inhibitors.

Recently, Schümann *et al*. reported that both genetically and pharmacologically inhibition of S1PL in rodents resulted in kidney toxicity, skin irritation and platelet activation, among other effects. These results may limit the treatment of autoimmune diseases with S1PL inhibitors, if similar effects are observed in humans.[96]

1.4 Chemical probes to monitor S1PL activity

Sphingolipids regulate signal transduction pathways involved in several biological processes. Dysregulation of sphingolipid metabolism leads to the outburst and progression of diseases, from rare syndromes to disorders of high socio–economic impact. Therefore, as discussed in the preceding sections, several sphingolipid metabolism enzymes have been validated as therapeutics targets, including ceramide synthases (CerS), dihydroceramide desaturase (Des1), ceramidases (CDases) and sphingosine−1−phosphate lyase (S1PL).

In this context, the use of specific probes to monitor the enzymatic activity of specific SLs metabolizing enzymes, as well as their intracellular localization and trafficking is gaining importance in contemporary chemical biology and drug design approaches. The biological relevance and the growing amount of interest around some SLs metabolizing enzymes as a drug target highlights the need for potent and selective inhibitors that efficiently modulates their activities.

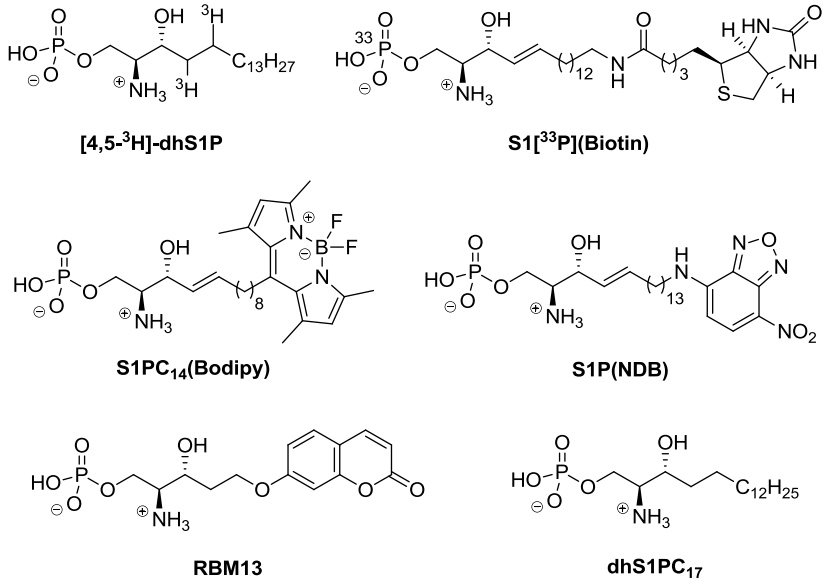

Figure 1.10. Most representative chemical probes to monitor S1PL activity.

In this regard, the rapid and efficient identification of sphingolipid metabolism enzyme inhibitors may be achieved by massive screening of chemical libraries. However, this requires the availability of high throughput screening (HTS) methods, which are currently very scarce.

S1PL is a promising target for the treatment of inflammatory, autoimmune and neurodegenerative diseases (see Section 1.3.3). Extensive research around this key enzyme has boosted the development of molecular and chemical tools to study its functions. As a result, several non–natural S1P derivatives have been reported over the past decades as chemical probes to determine S1PL activity (see Figure 1.10). Some of them have been used to develop HTS–amenable assays for library screening, which have led to the identification of novel S1PL inhibitors (see Section 1.3.3).

1.4.1 Radiolabeled probes

Until assays based on the use of fluorescent or fluorogenic substrates were implemented, most enzyme determinations were performed with radioactive substrates. The tritiated derivative [4,5–^{3}H] dhS1P (Figure 1.10) was one of the first chemical probes reported for S1PL activity measurements. In this case, upon incubation of the substrate with S1PL, followed by an extraction of the lipids into an organic phase under acidic conditions, the reaction products are separated by thin–layer chromatography.

Finally, the resulting radioactive aldehyde (and its metabolic derivatives [2,3–^{3}H]–palmitic acid and [2,3–^{3}H]–palmitol) are quantified by liquid–scintillation counting, autoradiography or phosphorimaging.[97,98]

In a more sophisticated approach, an HTS–compatible scintillation proximity assay (SPA) for S1PL has been reported (Figure 1.11). The assay requires the use of S1[^{33}P](Biotin) (Figure 1.10) as substrate and employs recombinant human full–length SPL in insect cell membrane preparations as the enzymatic source. When S1PL is absent or inhibited, binding of the substrate to streptavidin–coated SPA beads brings the β–particles emitted by ^{33}P in close proximity to the scintillating SPA beads, resulting in photon generation (high signal). Upon metabolization, however, the signal decreases, as fewer ^{33}P atoms are bound to the SPA beads.[91]

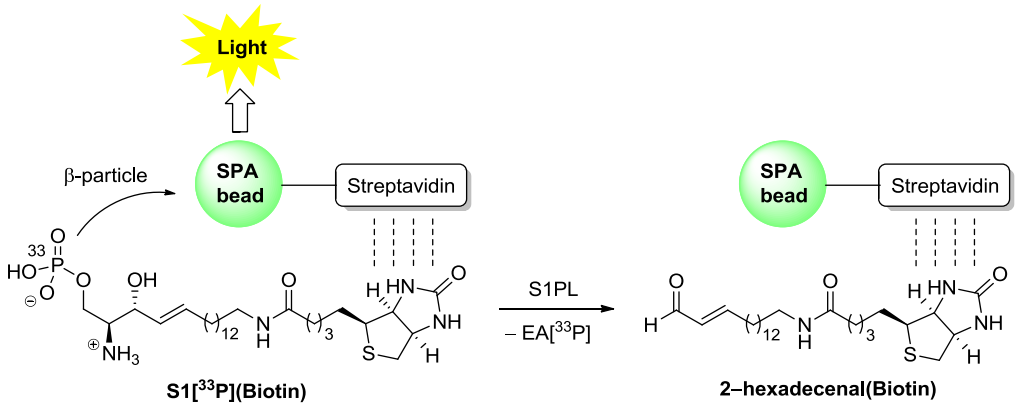

Figure 1.11. Mechanism of the scintillation proximity assay (SPA) for S1PL.

1.4.2 Fluorescent and fluorogenic probes

The disadvantages of working with radioactive materials have prompted the development of other non–natural substrates to monitor S1PL activity. This is the case of fluorescent substrates S1P(NBD)[99] and S1PC$_{14}$(Bodipy),[100] which incorporate a fluorescent reporter as part of the sphingoid base chain (Figure 1.10). In both cases, the resulting aldehyde is extracted from the incubation mixture and quantified after separation by HPLC coupled to a fluorescence detector. However, the Bodipy derivative is more extensively used due to its improved photochemical properties.[100] As mentioned before for [4,5–^{3}H] dhS1P, other fluorophore–containing metabolites such as the carboxylic acid or the corresponding alcohol are also formed *in vitro*. Therefore, the

amount of product determined for S1PL activity measurements should be expressed as a sum different products.

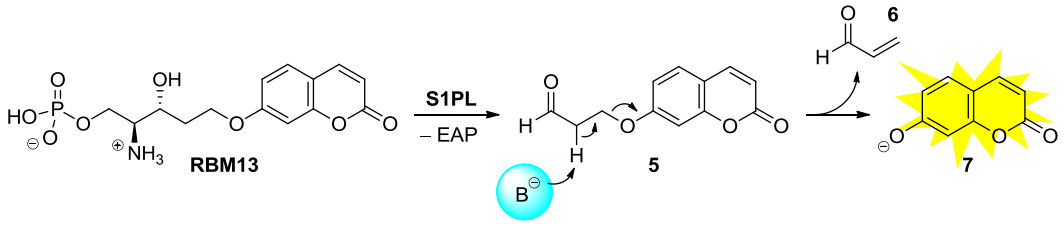

Figure 1.12. S1PL–catalyzed fluorescence release from **RBM13**.

The fluorogenic coumarin–containing substrate **RBM13** has also been reported (Figure 1.10).[101] In this case, the released aldehyde **5** undergoes a β–elimination reaction under basic conditions to give acrolein (**6**) and the fluorescent umbelliferone (**7**) (Figure 1.12). According to the reported protocol, no separation of the reaction products is necessary and the assay can be performed in multiwell plates, which is an important improvement in high throughput screening (HTS) assays of putative inhibitors.

An inherent limitation of the above fluorescent or fluorogenic substrates relies on the use of a non–natural S1PL substrate and, hence, the presence of a bulky reporter as part of the sphingoid chain. This fact can explain the lower affinity of some of these substrates towards the target enzyme, as evidenced from their higher K_M values in comparison to that of the natural substrate (see Table 1.2).

1.4.3 Natural S1P as probe

Another problem found with the use of fluorescent enzyme assays based on the use of non–natural substrates is that they may not reflect physiological conditions in cells, since they are linked to non–naturally occurring fluorophores. The specificity of fluorogenic substrates could also be a problem in assays using cell or tissue preparations, as they may be cleaved by enzymes present in the assay media. In addition, the binding affinity of the artificial substrate towards the enzyme's active site may not be the same than that of the natural one, which could ultimately lead to significant differences on the activities of potential inhibitors, depending on the substrate used.[102]

Consequently, due to their physiological relevancy, several enzymatic assays based on the use of the natural substrate itself, or a minimally modified analogue thereof, have been reported over the last years. In general, this strategy requires the use of derivatization reactions, prior to instrumental analysis or enzyme reactions specially designed to quantify the particular reaction products. In the case of S1PL, several enzymatic assays have been developed using S1P as substrate. In all cases, the generated 2–hexadecenal (2EC16–AL) is quantified upon transformation to a more stable derivative. In this context, methods involving the derivatization of 2–hexadecenal with semicarbazide and analysis of the resulting semicarbazone **8a** by LC–MS/MS,[82] 2–diphenylacetyl–1,3–indandione–1–hydrazone (DAIH) for fluorescence HPLC or LC–MS/MS analyses of **8b**[103] and isonicotinylhydrazide for LC–MS/MS quantification of the resulting isonicotinylhydrazone **8c**[62] (Figure 1.13), have been reported.

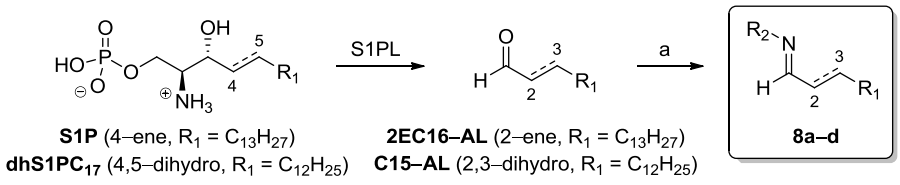

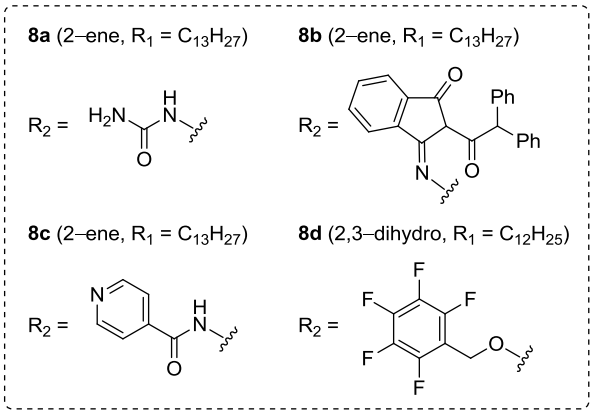

Figure 1.13. Use of the natural substrate or a minimally modified probe to monitor S1PL activity. (a) semicarbazide for **8a**, DAIH for **8b**, isonicotinylhydrazide for **8c** and PFBHA for **8d**; 2EC16–AL: (*E*)–2–hexadecenal, C15–AL: pentadecanal.

Table 1.2. Characteristic features of reported assays to determine S1PL activity.

Substrate	Analytical technique	K_M (μM)	V_{max} (pmol/min/μg)	Protein (μg)	Reaction time (min)	Ref.
[4,5-^{3}H]-dhS1P	TLC and LSC	9	0.07	variable[a]	60	97,98
S1[^{33}P](Biotin)	On–plate LSC	1.4	n.s.	0.12–0.24[b]	60	91
S1P(NBD)	HPLC/FD	14.6	~6.7[c]	15–25[d]	15	99
$S1PC_{14}$(Bodipy)	HPLC/FD	35	~1.8[e]	25[d]	30	100
RBM13	On–plate fluorescence	152	4.8 x 10^{-3}	500[f]	360	101
S1P	LC/MS/MS	5.7	0.17	5[g]	20	82
	LC/FD or LC/MS/MS	n.s.	n.s.	n.s.[h]	60	103
	LC/MS/MS	5.2	n.s.	n.s.[i]	60	62
$dhS1PC_{17}$	GC/MS	6	0.37	20[f]	60	104

(a) rat liver homogenate (b) full–length hS1PL in membrane preparations from insect cells (c) Deduced from Figure 3C of Ref. 99 (d) lysates of S1PL–overexpressing cells (e) Deduced from Figure 3B of Ref. 100; (f) lysates of WT MEF cells (g) mouse liver microsomal protein. (h) HT–29 cells (i) recombinant human S1PL (Δ1–61); FD = fluorescence detection, LSC = liquid scintillation counting, n.s. = not specified.

In an alternative approach, a minimally modified C_{17}–dihydrosphingosine–1–phosphate substrate ($dhS1PC_{17}$, Figure 1.10) was tested as S1PL activity probe.[104] In this case, determination of S1PL activity is carried out by derivatization of the released pentadecanal (C15–AL) with pentafluorobenzyl hydroxylamine (PFBHA) and quantification of the resulting oxime **8d** by GC/MS (Figure 1.13). As expected, the affinity of this minimally modified substrate rises to levels comparable to those of the natural substrate (see Table 1.2)

However, due to the more tedious and time–consuming analytical protocols, these substrates are less amenable for HTS analysis than the previously reported method based on the fluorogenic coumarin–containing substrate **RBM13**.

1.5 References

(1) Hannun, Y. A.; Obeid, L. M. Principles of Bioactive Lipid Signalling: Lessons from Sphingolipids. *Nat Rev Mol Cell Biol* **2008**, *9* (2), 139–150.

(2) Lingwood, D.; Simons, K. Lipid Rafts As a Membrane-Organizing Principle. *Science (80-.).* **2009**, *327* (5961), 46–50.

(3) Simons, K.; Toomre, D. Lipid Rafts and Signal Transduction. *Nat Rev Mol Cell Biol* **2000**, *1* (1), 31–39.

(4) Gangoiti, P.; Camacho, L.; Arana, L.; Ouro, A.; Granado, M. H.; Brizuela, L.; Casas, J.; Fabriás, G.; Abad, J. L.; Delgado, A.; et al. Control of Metabolism and Signaling of Simple Bioactive Sphingolipids: Implications in Disease. *Prog. Lipid Res.* **2010**, *49* (4), 316–334.

(5) Billich, A.; Baumruker, T. Sphingolipid Metabolizing Enzymes as Novel Therapeutic Targets. In *Lipids in Health and Disease*; Quinn, P. J., Wang, X., Eds.; Springer, 2008; pp 487–522.

(6) Warnecke, D.; Heinz, E. Recently Discovered Functions of Glucosylceramides in Plants and Fungi. *Cell. Mol. Life Sci. C.* **2003**, *60* (5), 919–941.

(7) Hannun, Y. A.; Obeid, L. M. Many Ceramides. *J. Biol. Chem.* **2011**, *286* (32), 27855–27862.

(8) Mullen, T. D.; Hannun, Y. A.; Obeid, L. M. Ceramide Synthases at the Centre of Sphingolipid Metabolism and Biology. *Biochem. J.* **2012**, *441* (3), 789–802.

(9) Fabrias, G.; Muñoz-Olaya, J.; Cingolani, F.; Signorelli, P.; Casas, J.; Gagliostro, V.; Ghidoni, R. Dihydroceramide Desaturase and Dihydrosphingolipids: Debutant Players in the Sphingolipid Arena. *Prog. Lipid Res.* **2012**, *51* (2), 82–94.

(10) Maceyka, M.; Spiegel, S. Sphingolipid Metabolites in Inflammatory Disease. *Nature* **2014**, *510* (7503), 58–67.

(11) Kumagai, K.; Yasuda, S.; Okemoto, K.; Nishijima, M.; Kobayashi, S.; Hanada, K. CERT Mediates Intermembrane Transfer of Various Molecular Species of Ceramides. *J. Biol. Chem.* **2005**, *280* (8), 6488–6495.

(12) Wennekes, T.; van den Berg, R. J. B. H. N.; Boot, R. G.; van der Marel, G. A.; Overkleeft, H. S.; Aerts, J. M. F. G. Glycosphingolipids—Nature, Function, and Pharmacological Modulation. *Angew. Chemie Int. Ed.* **2009**, *48* (47), 8848–8869.

(13) Kihara, A.; Mitsutake, S.; Mizutani, Y.; Igarashi, Y. Metabolism and Biological Functions of Two Phosphorylated Sphingolipids, Sphingosine 1-Phosphate and Ceramide 1-Phosphate. *Prog. Lipid Res.* **2007**, *46* (2), 126–144.

(14) Arana, L.; Gangoiti, P.; Ouro, A.; Trueba, M.; Gómez-Muñoz, A. Ceramide and Ceramide 1-Phosphate in Health and Disease. *Lipids Health Dis.* **2010**, *9* (1), 1–12.

(15) Bajjalieh, S.; Batchelor, R. [24] Ceramide Kinase. In *Sphingolipid Metabolism and Cell Signaling Part A*; Enzymology, B. T.-M. in, Ed.; Academic Press, 2000; Vol. Volume 311, pp 207–215.

(16) Bornancin, F. Ceramide Kinase: The First Decade. *Cell. Signal.* **2011**, *23* (6), 999–1008.

(17) Carré, A.; Graf, C.; Stora, S.; Mechtcheriakova, D.; Csonga, R.; Urtz, N.; Billich, A.;

Baumruker, T.; Bornancin, F. Ceramide Kinase Targeting and Activity Determined by Its N-Terminal Pleckstrin Homology Domain. *Biochem. Biophys. Res. Commun.* **2004**, *324* (4), 1215–1219.

(18) Van Overloop, H.; Gijsbers Sofie; Van Veldhoven, P. P. Further Characterization of Mammalian Ceramide Kinase: Substrate Delivery and (stereo)specificity, Tissue Distribution, and Subcellular Localization Studies. *J. Lipid Res.* **2006**, *47* (2), 268–283.

(19) Yamaji, T.; Hanada, K. Sphingolipid Metabolism and Interorganellar Transport: Localization of Sphingolipid Enzymes and Lipid Transfer Proteins. *Traffic* **2015**, *16* (2), 101–122.

(20) Gomez-Muñoz, A.; Gangoiti, P.; Arana, L.; Ouro, A.; Rivera, I.-G.; Ordoñez, M.; Trueba, M. New Insights on the Role of Ceramide 1-Phosphate in Inflammation. *Biochim. Biophys. Acta - Mol. Cell Biol. Lipids* **2013**, *1831* (6), 1060–1066.

(21) Pettus, B. J.; Bielawska, A.; Subramanian, P.; Wijesinghe, D. S.; Maceyka, M.; Leslie, C. C.; Evans, J. H.; Freiberg, J.; Roddy, P.; Hannun, Y. A.; et al. Ceramide 1-Phosphate Is a Direct Activator of Cytosolic Phospholipase A2. *J. Biol. Chem.* **2004**, *279* (12), 11320–11326.

(22) Pettus, B. J.; Bielawska, A.; Spiegel, S.; Roddy, P.; Hannun, Y. A.; Chalfant, C. E. Ceramide Kinase Mediates Cytokine- and Calcium Ionophore-Induced Arachidonic Acid Release. *J. Biol. Chem.* **2003**, *278* (40), 38206–38213.

(23) Boath, A.; Graf, C.; Lidome, E.; Ullrich, T.; Nussbaumer, P.; Bornancin, F. Regulation and Traffic of Ceramide 1-Phosphate Produced by Ceramide Kinase: COMPARATIVE ANALYSIS TO GLUCOSYLCERAMIDE AND SPHINGOMYELIN . *J. Biol. Chem.* **2008**, *283* (13), 8517–8526.

(24) Granado, M. H.; Gangoiti, P.; Ouro, A.; Arana, L.; González, M.; Trueba, M.; Gómez-Muñoz, A. Ceramide 1-Phosphate (C1P) Promotes Cell Migration: Involvement of a Specific C1P Receptor. *Cell. Signal.* **2009**, *21* (3), 405–412.

(25) Hänel, P.; Andréani, P.; Gräler, M. H. Erythrocytes Store and Release Sphingosine 1-Phosphate in Blood. *FASEB J.* **2007**, *21* (4), 1202–1209.

(26) Książek, M.; Chacińska, M.; Chabowski, A.; Baranowski, M. Sources, Metabolism, and Regulation of Circulating Sphingosine-1-Phosphate. *J. Lipid Res.* **2015**, *56* (7), 1271–1281.

(27) Adada, M.; Canals, D.; Hannun, Y. A.; Obeid, L. M. Sphingosine-1-Phosphate Receptor 2. *FEBS J.* **2013**, *280* (24), 6354–6366.

(28) Pulkoski-Gross, M. J.; Donaldson, J. C.; Obeid, L. M. Sphingosine-1-Phosphate Metabolism: A Structural Perspective. *Crit. Rev. Biochem. Mol. Biol.* **2015**, *50* (4), 298–313.

(29) Rosen, H.; Stevens, R. C.; Hanson, M.; Roberts, E.; Oldstone, M. B. A. Sphingosine-1-Phosphate and Its Receptors: Structure, Signaling, and Influence. *Annu. Rev. Biochem.* **2013**, *82* (1), 637–662.

(30) Sanchez, T.; Hla, T. Structural and Functional Characteristics of S1P Receptors. *J. Cell. Biochem.* **2004**, *92* (5), 913–922.

(31) Spiegel, S.; Milstien, S. The Outs and the Ins of Sphingosine-1-Phosphate in Immunity. *Nat Rev Immunol* **2011**, *11* (6), 403–415.

(32) Cuvillier, O. Les Récepteurs de La Sphingosine 1-Phosphate. *Med Sci* **2012**, *28* (11), 951–957.

(33) Delgado, A.; Martínez-Cartro, M. Therapeutic Potential of the Modulation of Sphingosine-1-Phosphate Receptors. *Current Medicinal Chemistry*, 2016, *23*, 242–264.

(34) Hanson, M. A.; Roth, C. B.; Jo, E.; Griffith, M. T.; Scott, F. L.; Reinhart, G.; Desale, H.; Clemons, B.; Cahalan, S. M.; Schuerer, S. C.; et al. Crystal Structure of a Lipid G Protein–Coupled Receptor. *Science (80-.)*. **2012**, *335* (6070), 851–855.

(35) Albert, R.; Hinterding, K.; Brinkmann, V.; Guerini, D.; Müller-Hartwieg, C.; Knecht, H.; Simeon, C.; Streiff, M.; Wagner, T.; Welzenbach, K.; et al. Novel Immunomodulator FTY720 Is Phosphorylated in Rats and Humans To Form a Single Stereoisomer. Identification, Chemical Proof, and Biological Characterization of the Biologically Active Species and Its Enantiomer. *J*. *Med*. *Chem*. **2005**, *48* (16), 5373–5377.

(36) Brinkmann, V.; Billich, A.; Baumruker, T.; Heining, P.; Schmouder, R.; Francis, G.; Aradhye, S.; Burtin, P. Fingolimod (FTY720): Discovery and Development of an Oral Drug to Treat Multiple Sclerosis. *Nat*. *Rev*. *Drug Discov*. **2010**, *9* (11), 883–897.

(37) Strader, C. R.; Pearce, C. J.; Oberlies, N. H. Fingolimod (FTY720): A Recently Approved Multiple Sclerosis Drug Based on a Fungal Secondary Metabolite. *J*. *Nat*. *Prod*. **2011**, *74* (4), 900–907.

(38) Cahalan, S. M. Chemical and Genetic Tools to Explore S1P Biology. In *Sphingosine-1-Phosphate Signaling in Immunology and Infectious Diseases*; Oldstone, M. B. A., Rosen, H., Eds.; Springer, 2014; pp 55–83.

(39) Roberts, E.; Guerrero, M.; Urbano, M.; Rosen, H. Sphingosine 1-Phosphate Receptor Agonists: A Patent Review (2010 – 2012). *Expert Opin*. *Ther*. *Pat*. **2013**, *23* (7), 817–841.

(40) Schwab, S. R.; Pereira, J. P.; Matloubian, M.; Xu, Y.; Huang, Y.; Cyster, J. G. Lymphocyte Sequestration Through S1P Lyase Inhibition and Disruption of S1P Gradients. *Science (80-.)*. **2005**, *309* (5741), 1735–1739.

(41) Bagdanoff, J. T.; Donoviel, M. S.; Nouraldeen, A.; Carlsen, M.; Jessop, T. C.; Tarver, J.; Aleem, S.; Dong, L.; Zhang, H.; Boteju, L.; et al. Inhibition of Sphingosine 1-Phosphate Lyase for the Treatment of Rheumatoid Arthritis: Discovery of (E)-1-(4-((1 R,2 S,3 R)-1,2,3,4-Tetrahydroxybutyl)-1 H -Imidazol-2-Yl)ethanone Oxime (LX2931) and (1 R,2 S,3 R)-1-(2-(Isoxazol-3-Yl)-1 H -Imidazol-4-Yl)but. *J*. *Med*. *Chem*. **2010**, *53*, 8650–8662.

(42) Ito, K.; Anada, Y.; Tani, M.; Ikeda, M.; Sano, T.; Kihara, A.; Igarashi, Y. Lack of Sphingosine 1-Phosphate-Degrading Enzymes in Erythrocytes. *Biochem*. *Biophys*. *Res*. *Commun*. **2007**, *357* (1), 212–217.

(43) Santos, W. L.; Lynch, K. R. Drugging Sphingosine Kinases. *ACS Chem*. *Biol*. **2015**, *10* (1), 225–233.

(44) Mitra, P.; Oskeritzian, C. A.; Payne, S. G.; Beaven, M. A.; Milstien, S.; Spiegel, S. Role of ABCC1 in Export of Sphingosine-1-Phosphate from Mast Cells. *Proc*. *Natl*. *Acad*. *Sci*. **2006**, *103* (44), 16394–16399.

(45) Lu, L.; Barfejani, A. H.; Qin, T.; Dong, Q.; Ayata, C.; Waeber, C. Fingolimod Exerts Neuroprotective Effects in a Mouse Model of Intracerebral Hemorrhage. *Brain Res*. **2014**, *1555*, 89–96.

(46) Singh, I. N.; Hall, E. D. Multifaceted Roles of Sphingosine-1-Phosphate: How Does This Bioactive Sphingolipid Fit with Acute Neurological Injury? *J. Neurosci. Res.* **2008**, *86* (7), 1419–1433.

(47) Hait, N. C.; Allegood, J.; Maceyka, M.; Strub, G. M.; Harikumar, K. B.; Singh, S. K.; Luo, C.; Marmorstein, R.; Kordula, T.; Milstien, S.; et al. Regulation of Histone Acetylation in the Nucleus by Sphingosine-1-Phosphate. *Science (80-.).* **2009**, *325* (5945), 1254–1257.

(48) Newton, J.; Lima, S.; Maceyka, M.; Spiegel, S. Revisiting the Sphingolipid Rheostat: Evolving Concepts in Cancer Therapy. *Exp. Cell Res.* **2015**, *333* (2), 195–200.

(49) Spiegel, S.; Milstien, S. Sphingosine-1-Phosphate: An Enigmatic Signalling Lipid. *Nat Rev Mol Cell Biol* **2003**, *4* (5), 397–407.

(50) Liu, H.; Sugiura, M.; Nava, V. E.; Edsall, L. C.; Kono, K.; Poulton, S.; Milstien, S.; Kohama, T.; Spiegel, S. Molecular Cloning and Functional Characterization of a Novel Mammalian Sphingosine Kinase Type 2 Isoform. *J. Biol. Chem.* **2000**, *275* (26), 19513–19520.

(51) Paugh, S. W.; Payne, S. G.; Barbour, S. E.; Milstien, S.; Spiegel, S. The Immunosuppressant FTY720 Is Phosphorylated by Sphingosine Kinase Type 2. *FEBS Lett.* **2003**, *554* (1-2), 189–193.

(52) Strub, G. M.; Paillard, M.; Liang, J.; Gomez, L.; Allegood, J. C.; Hait, N. C.; Maceyka, M.; Price, M. M.; Chen, Q.; Simpson, D. C.; et al. Sphingosine-1-Phosphate Produced by Sphingosine Kinase 2 in Mitochondria Interacts with Prohibitin 2 to Regulate Complex IV Assembly and Respiration. *FASEB J.* **2011**, *25* (2), 600–612.

(53) Maceyka, M.; Sankala, H.; Hait, N. C.; Le Stunff, H.; Liu, H.; Toman, R.; Collier, C.; Zhang, M.; Satin, L. S.; Merrill, A. H.; et al. SphK1 and SphK2, Sphingosine Kinase Isoenzymes with Opposing Functions in Sphingolipid Metabolism. *J. Biol. Chem.* **2005**, *280* (44), 37118–37129.

(54) Mizugishi, K.; Yamashita, T.; Olivera, A.; Miller, G. F.; Spiegel, S.; Proia, R. L. Essential Role for Sphingosine Kinases in Neural and Vascular Development. *Mol. Cell. Biol.* **2005**, *25* (24), 11113–11121.

(55) Brindley, D. N. Lipid Phosphate Phosphatases and Related Proteins: Signaling Functions in Development, Cell Division, and Cancer. *J. Cell. Biochem.* **2004**, *92* (5), 900–912.

(56) Pyne, S.; Kong, K.-C.; Darroch, P. I. Lysophosphatidic Acid and Sphingosine 1-Phosphate Biology: The Role of Lipid Phosphate Phosphatases. *Semin. Cell Dev. Biol.* **2004**, *15* (5), 491–501.

(57) Bandhuvula, P.; Saba, J. D. Sphingosine-1-Phosphate Lyase in Immunity and Cancer: Silencing the Siren. *Trends Mol. Med.* **2007**, *13* (5), 210–217.

(58) Bourquin, F.; Capitani, G.; Grütter, M. G. PLP-Dependent Enzymes as Entry and Exit Gates of Sphingolipid Metabolism. *Protein Sci.* **2011**, *20* (9), 1492–1508.

(59) Ikeda, M.; Kihara, A.; Igarashi, Y. Sphingosine-1-Phosphate Lyase SPL Is an Endoplasmic Reticulum-Resident, Integral Membrane Protein with the Pyridoxal 5′-Phosphate Binding Domain Exposed to the Cytosol. *Biochem. Biophys. Res. Commun.* **2004**, *325* (1), 338–343.

(60) Mukhopadhyay, D.; Howell, K. S.; Riezman, H.; Capitani, G. Identifying Key Residues of Sphinganine-1-Phosphate Lyase for Function in Vivo and in Vitro. *J. Biol. Chem.*

2008, *283* (29), 20159–20169.

(61) Bourquin, F.; Riezman, H.; Capitani, G.; Grütter, M. G. Structure and Function of Sphingosine-1-Phosphate Lyase, a Key Enzyme of Sphingolipid Metabolism. *Structure* **2010**, *18*, 1054–1065.

(62) Weiler, S.; Braendlin, N.; Beerli, C.; Bergsdorf, C.; Schubart, A.; Srinivas, H.; Oberhauser, B.; Billich, A. Orally Active 7-Substituted (4-Benzylphthalazin-1-Yl)-2-Methylpiperazin-1-Yl]nicotinonitriles as Active-Site Inhibitors of Sphingosine 1-Phosphate Lyase for the Treatment of Multiple Sclerosis. *J*. *Med*. *Chem*. **2014**, *57*, 5074–5084.

(63) Rolando, M.; Escoll, P.; Nora, T.; Botti, J.; Boitez, V.; Bedia, C.; Daniels, C.; Abraham, G.; Stogios, P. J.; Skarina, T.; et al. Legionella Pneumophila S1P-Lyase Targets Host Sphingolipid Metabolism and Restrains Autophagy. *Proc*. *Natl*. *Acad*. *Sci*. **2016**, *113* (7), 1901–1906.

(64) Van Veldhoven, P. P.; Gijsbers, S.; Mannaerts, G. P.; Vermeesch, J. R.; Brys, V. Human Sphingosine-1-Phosphate Lyase: cDNA Cloning, Functional Expression Studies and Mapping to Chromosome 10q221. *Biochim*. *Biophys*. *Acta - Mol*. *Cell Biol*. *Lipids* **2000**, *1487* (2–3), 128–134.

(65) Bagdanoff, J. T.; Donoviel, M. S.; Nouraldeen, A.; Tarver, J.; Fu, Q.; Carlsen, M.; Jessop, T. C.; Zhang, H.; Hazelwood, J.; Nguyen, H.; et al. Inhibition of Sphingosine-1-Phosphate Lyase for the Treatment of Autoimmune Disorders. *J*. *Med*. *Chem*. **2009**, *52*, 3941–3953.

(66) Bigaud, M.; Guerini, D.; Billich, A.; Bassilana, F.; Brinkmann, V. Second Generation S1P Pathway Modulators: Research Strategies and Clinical Developments. *Biochim*. *Biophys*. *Acta - Mol*. *Cell Biol*. *Lipids* **2014**, *1841* (5), 745–758.

(67) Herr, D. R.; Fyrst, H.; Phan, V.; Heinecke, K.; Georges, R.; Harris, G. L.; Saba, J. D. Sply Regulation of Sphingolipid Signaling Molecules Is Essential for Drosophila Development. *Development* **2003**, *130* (11), 2443–2453.

(68) Kihara, A.; Ikeda, M.; Kariya, Y.; Lee, E.-Y.; Lee, Y.-M.; Igarashi, Y. Sphingosine-1-Phosphate Lyase Is Involved in the Differentiation of F9 Embryonal Carcinoma Cells to Primitive Endoderm. *J*. *Biol*. *Chem*. **2003**, *278* (16), 14578–14585.

(69) Li, G.; Foote, C.; Alexander, S.; Alexander, H. Sphingosine-1-Phosphate Lyase Has a Central Role in the Development of Dictyostelium Discoideum. *Development* **2001**, *128* (18), 3473–3483.

(70) Kumar, A.; Wessels, D.; Daniels, K. J.; Alexander, H.; Alexander, S.; Soll, D. R. Sphingosine-1-Phosphate Plays a Role in the Suppression of Lateral Pseudopod Formation during Dictyostelium Discoideum Cell Migration and Chemotaxis. *Cell Motil*. *Cytoskeleton* **2004**, *59* (4), 227–241.

(71) Phan, V. H.; Herr, D. R.; Panton, D.; Fyrst, H.; Saba, J. D.; Harris, G. L. Disruption of Sphingolipid Metabolism Elicits Apoptosis-Associated Reproductive Defects in Drosophila. *Dev*. *Biol*. **2007**, *309* (2), 329–341.

(72) Oskouian, B.; Sooriyakumaran, P.; Borowsky, A. D.; Crans, A.; Dillard-Telm, L.; Tam, Y. Y.; Bandhuvula, P.; Saba, J. D. Sphingosine-1-Phosphate Lyase Potentiates Apoptosis via p53- and p38-Dependent Pathways and Is down-Regulated in Colon Cancer. *Proc*. *Natl*. *Acad*. *Sci*. **2006**, *103* (46), 17384–17389.

(73) Reiss, U.; Oskouian, B.; Zhou, J.; Gupta, V.; Sooriyakumaran, P.; Kelly, S.; Wang, E.;

Merrill, A. H.; Saba, J. D. Sphingosine-Phosphate Lyase Enhances Stress-Induced Ceramide Generation and Apoptosis. *J. Biol. Chem.* **2004**, *279* (2), 1281–1290.

(74) Alexander, S.; Min, J.; Alexander, H. Dictyostelium Discoideum to Human Cells: Pharmacogenetic Studies Demonstrate a Role for Sphingolipids in Chemoresistance. *Biochim. Biophys. Acta - Gen. Subj.* **2006**, *1760* (3), 301–309.

(75) Li, G.; Alexander, H.; Schneider, N.; Alexander, S. Molecular Basis for Resistance to the Anticancer Drug Cisplatin in Dictyostelium. *Microbiology* **2000**, *146* (9), 2219–2227.

(76) Min, J.; Stegner, A. L.; Alexander, H.; Alexander, S. Overexpression of Sphingosine-1-Phosphate Lyase or Inhibition of Sphingosine Kinase in Dictyostelium Discoideum Results in a Selective Increase in Sensitivity to Platinum-Based Chemotherapy Drugs. *Eukaryot. Cell* **2004**, *3* (3), 795–805.

(77) Min, J.; Van Veldhoven, P. P.; Zhang, L.; Hanigan, M. H.; Alexander, H.; Alexander, S. Sphingosine-1-Phosphate Lyase Regulates Sensitivity of Human Cells to Select Chemotherapy Drugs in a p38-Dependent Manner. *Am. Assoc. Cancer Res.* **2005**, *3* (5), 287–296.

(78) Matloubian, M.; Lo, C. G.; Cinamon, G.; Lesneski, M. J.; Xu, Y.; Brinkmann, V.; Allende, M. L.; Proia, R. L.; Cyster, J. G. Lymphocyte Egress from Thymus and Peripheral Lymphoid Organs Is Dependent on S1P Receptor 1. *Nature* **2004**, *427* (6972), 355–360.

(79) Stoffel, W.; Grol, M. Chemistry and Biochemistry of 1-Desoxysphinganine-1-Phosphonate (dihydrosphingosine-1-Phosphonate). *Chem. Phys. Lipids* **1974**, *13*, 372–388.

(80) Boumendjel, A.; Miller, S. P. F. Synthesis of an Inhibitor of Sphingosine- 1-Phosphate Lyase. *Tetrahedron Lett.* **1994**, *35* (6), 819–822.

(81) Bandhuvula, P.; Tam, Y. Y.; Oskouian, B.; Saba, J. D. The Immune Modulator FTY720 Inhibits Sphingosine-1-Phosphate Lyase Activity. *J. Biol. Chem.* **2005**, *280*, 33697–33700.

(82) Berdyshev, E. V.; Goya, J.; Gorshkova, I.; Prestwich, G. D.; Byun, H. S.; Bittman, R.; Natarajan, V. Characterization of Sphingosine-1-Phosphate Lyase Activity by Electrospray Ionization-Liquid Chromatography/tandem Mass Spectrometry Quantitation of (2E)-Hexadecenal. *Anal. Biochem.* **2011**, *408* (1), 12–18.

(83) Bassi, R.; Anelli, V.; Giussani, P.; Tettamanti, G.; Viani, P.; Riboni, L. Sphingosine-1-Phosphate Is Released by Cerebellar Astrocytes in Response to bFGF and Induces Astrocyte Proliferation through Gi-Protein-Coupled Receptors. *Glia* **2006**, *53* (6), 621–630.

(84) Billich, A.; Beerli, C.; Bergmann, R.; Bruns, C.; Loetscher, E. Cellular Assay for the Characterization of Sphingosine-1-Phosphate Lyase Inhibitors. *Anal. Biochem.* **2013**, *434* (2), 247–253.

(85) Loetscher, E.; Schneider, K.; Beerli, C.; Billich, A. Assay to Measure the Secretion of Sphingosine-1-Phosphate from Cells Induced by S1P Lyase Inhibitors. *Biochem. Biophys. Res. Commun.* **2013**, *433* (3), 345–348.

(86) Ohtoyo, M.; Tamura, M.; Machinaga, N.; Muro, F.; Hashimoto, R. Sphingosine 1-Phosphate Lyase Inhibition by 2-Acetyl-4-(tetrahydroxybutyl)imidazole (THI) under Conditions of Vitamin B6 Deficiency. *Mol. Cell. Biochem.* **2015**, *400* (1), 125–133.

(87) Gugasyan, R.; Coward, A.; O'Connor, L.; Shortman, K.; Scollay, R. Emigration of Mature T Cells from the Thymus Is Inhibited by the Imidazole-Based Compound 2-Acetyl-4-Tetrahydroxybutylimidazole. *Immunology* **1998**, *93* (3), 398–404.

(88) Ohtoyo, M.; Machinaga, N.; Inoue, R.; Hagihara, K.; Yuita, H.; Tamura, M.; Hashimoto, R.; Chiba, J.; Muro, F.; Watanabe, J.; et al. Component of Caramel Food Coloring, THI, Causes Lymphopenia Indirectly via a Key Metabolic Intermediate. *Cell Chem. Biol.* **2016**, *23* (5), 555–560.

(89) D'Ambrosio, D.; Freedman, M. S.; Prinz, J. Ponesimod, a Selective S1P1 Receptor Modulator: A Potential Treatment for Multiple Sclerosis and Other Immune-Mediated Diseases. *Ther. Adv. Chronic Dis.* **2016**, *7* (1), 18–33.

(90) Gatfield, J.; Monnier, L.; Studer, R.; Bolli, M. H.; Steiner, B.; Nayler, O. Sphingosine-1-Phosphate (S1P) Displays Sustained S1P1 Receptor Agonism and Signaling through S1P Lyase-Dependent Receptor Recycling. *Cell. Signal.* **2014**, *26*, 1576–1588.

(91) Kashem, M. A.; Wa, C.; Wolak, J. P.; Grafos, N. S.; Ryan, K. R.; Sanville-Ross, M. L.; Fogarty, K. E.; Rybina, I. V; Shoultz, A.; Molinaro, T.; et al. A High-Throughput Scintillation Proximity Assay for Sphingosine-1-Phosphate Lyase. *Assay Drug Dev. Technol.* **2014**, *12* (5), 293–302.

(92) Cosconati, S.; Novellino, E. The First Sphingosine 1-Phosphate Lyase Inhibitors against Multiple Sclerosis: A Successful Drug Discovery Tale. *J. Med. Chem.* **2014**, *57*, 5072–5073.

(93) Dinges, J.; Harris, C. M.; Wallace, G. A.; Argiriadi, M. A.; Queeney, K. L.; Perron, D. C.; Dominguez, E.; Kebede, T.; Desino, K. E.; Patel, H.; et al. Hit-to-Lead Evaluation of a Novel Class of Sphingosine 1-Phosphate Lyase Inhibitors. *Bioorg. Med. Chem. Lett.* **2016**, *26* (9), 2297–2302.

(94) Argiriadi, M. A.; Banach, D.; Radziejewska, E.; Marchie, S.; DiMauro, J.; Dinges, J.; Dominguez, E.; Hutchins, C.; Judge, R. A.; Queeney, K.; et al. Creation of a S1P Lyase Bacterial Surrogate for Structure-Based Drug Design. *Bioorg. Med. Chem. Lett.* **2016**, *26* (9), 2293–2296.

(95) Deniz, U.; Ozkirimli, E.; Ulgen, K. O. A Systematic Methodology for Large Scale Compound Screening: A Case Study on the Discovery of Novel S1PL Inhibitors. *J. Mol. Graph. Model.* **2016**, *63*, 110–124.

(96) Schümann, J.; Grevot, A.; Ledieu, D.; Wolf, A.; Schubart, A.; Piaia, A.; Sutter, E.; Côté, S.; Beerli, C.; Pognan, F.; et al. Reduced Activity of Sphingosine-1-Phosphate Lyase Induces Podocyte-Related Glomerular Proteinuria, Skin Irritation, and Platelet Activation. *Toxicol. Pathol.* **2015**.

(97) Van Veldhoven, P. P.; Mannaerts, G. P. Subcellular Localization and Membrane Topology of Sphingosine-1-Phosphate Lyase in Rat Liver. *J. Biol. Chem.* **1991**, *266* (19), 12502–12507.

(98) Van Veldhoven, P. P. [28] Sphingosine-1-Phosphate Lyase. In *Sphingolipid Metabolism and Cell Signaling Part A*; Enzymology, B. T.-M. in, Ed.; Academic Press, 2000; Vol. Volume 311, pp 244–254.

(99) Bandhuvula, P.; Fyrst, H.; Saba, J. D. A Rapid Fluorescence Assay for Sphingosine-1-Phosphate Lyase Enzyme Activity. *J. Lipid Res.* **2007**, *48* (12), 2769–2778.

(100) Bandhuvula, P.; Li, Z.; Bittman, R.; Saba, J. D. Sphingosine 1-Phosphate Lyase Enzyme Assay Using a BODIPY-Labeled Substrate. *Biochem. Biophys. Res. Commun.* **2009**, *380*

(2), 366–370.

(101) Bedia, C.; Camacho, L.; Casas, J.; Abad, J. L.; Antonio, D.; Van Veldhoven, P. P.; Fabriàs, G. Synthesis of a Fluorogenic Analogue of Sphingosine-1-Phosphate and Its Use to Determine Sphingosine-1-Phosphate Lyase Activity. *ChemBioChem* **2009**, *10* (5), 820–822.

(102) Motabar, O.; Goldin, E.; Leister, W.; Liu, K.; Southall, N.; Huang, W.; Marugan, J. J.; Sidransky, E.; Zheng, W. A High Throughput Glucocerebrosidase Assay Using the Natural Substrate Glucosylceramide. *Anal*. *Bioanal*. *Chem*. **2012**, *402* (2), 731–739.

(103) Lüth, A.; Neuber, C.; Kleuser, B. Novel Methods for the Quantification of (2E)-Hexadecenal by Liquid Chromatography with Detection by Either ESI QTOF Tandem Mass Spectrometry or Fluorescence Measurement. *Anal*. *Chim*. *Acta* **2012**, *722*, 70–79.

(104) Reina, E.; Camacho, L.; Casas, J.; Van Veldhoven, P. P.; Fabrias, G. Determination of Sphingosine-1-Phosphate Lyase Activity by Gas Chromatography Coupled to Electron Impact Mass Spectrometry. *Chem*. *Phys*. *Lipids* **2012**, *165* (2), 225–231.

2. Objectives

Taking into account the considerations introduced in the preceding section, the following objectives were considered in the present doctoral thesis:

1. The design and synthesis of new S1PL inhibitors. This objective involves:

    1.1. The structure–based design of potential S1PL inhibitors using both human and bacterial S1PL crystal structures. Based on this design, a library o potential S1PL inhibitors will be designed and synthesized.

    1.2. The design of S1PL inhibitors based on S1PL mechanistic considerations: According to the proposed mechanism for the S1PL catalyzed reaction (see Section 3.2.1), a small family of chemically modified analogs of some of the key reaction intermediates involved in the S1PL catalytic cycle, as well as a series of substrate analogs, will be designed and synthesized.

2. The development of HTS enzymatic assays for library screening of putative S1PL inhibitors. This goal includes:

    2.1. The development of an on–plate S1PL activity assay based on the previously reported fluorogenic substrate **RBM13**, in which recombinant bacterial or human S1PL will be used as enzyme sources.

    2.2. The validation of StS1PL as a reliable model of the human enzyme in the identification of potential hS1PL inhibitors.

    2.3. The design and synthesis of new fluorogenic substrates in order to expand the chemical toolbox for monitoring S1PL activity. In this regard, different coumarin–containing probes with potential applicability in HTS assays will be rationally designed and synthesized as analogs of the parent compound **RBM13**.

3. The determination of *in vitro* activity of the synthesized compounds resulting from objective 1. To this end, the different families of compounds will be tested as S1PL inhibitors using the previously developed enzymatic assays (see objective 2).

3. Results and discussion

3.1 Design of S1PL inhibitors based on docking approaches from bacterial and human enzyme structures

3.1.1 Introduction

Sphingosine–1–phosphate lyase (S1PL) is a key enzyme of sphingolipid catabolism. Together with SK and S1PPase (see section 1.3), S1PL tightly regulates the levels of S1P and contributes to the so–called 'sphingolipid rheostat', a system that controls cell fate based on the ratio of intracellular proliferative S1P and the apoptogenic So and Cer. Notably, S1PL was found to play an important role in regulating the immune system, since its inhibition disrupts the S1P gradient that promotes T cell egress from lymphoid tissues. In this context, S1PL has been validated as therapeutic target for the treatment of autoimmune diseases, such as multiple sclerosis[1] or rheumatoid arthritis.[2] Likewise, recent evidence indicates that S1PL may serve as target for modulation of immune responses in transplantation settings.[3]

Due to the therapeutic potential associated to the modulation of S1PL activity, a structure–based design of S1PL active site–directed inhibitors was envisaged in our group before the beginning of the present doctoral thesis. Firstly, a massive virtual screening study was required in order to identify structural features to build a common pharmacophore that guided the design of new potential S1PL binders. For that purpose, since at that time no structural data was available for the human enzyme, homology models of hS1PL were built using the published yeast and bacterial S1PL crystal structures as templates (PDB 3MC6 and 3MAD, respectively).[4]

A virtual library of about 650.000 compounds[5] was next screened *in silico* against the 3MAD–based hS1PL homology model. As a result, a subset of 28 compounds (coded as **VS01–VS28**) was chosen based on scoring, molecular diversity, price and commercial availability criteria. (see Figures 3.1.2 and 3.1.3 for the structures). These compounds were then purchased from commercial sources and tested at 250 μM in our previously reported assay using **RBM13** as substrate and cell lysates as hS1PL source.[6] The results are presented in Figure 3.1.1. Although several compounds exerted significant inhibition, it was worthy of mention the noticeable activity of compounds **VS11**, **VS19**, **VS20** and **VS21**, which showed inhibitory activities of 64, 62, 51 and 58 %, respectively. Notably, the activities exerted by the above compounds were comparable to that of the reference compound FTY720, which behaved as a modest S1PL inhibitor under our assay conditions (around 40 % inhibition at 125 μM, results not shown). All the hits of this virtual screening process shared some common structural features,

namely a carboxylate group bound to one or more aromatic rings through a short linker. Despite no potent hS1PL inhibitors were identified at this stage, the promising activities showed by some of the compounds encouraged us to continue with the design of a series of potential high affinity S1PL inhibitors.

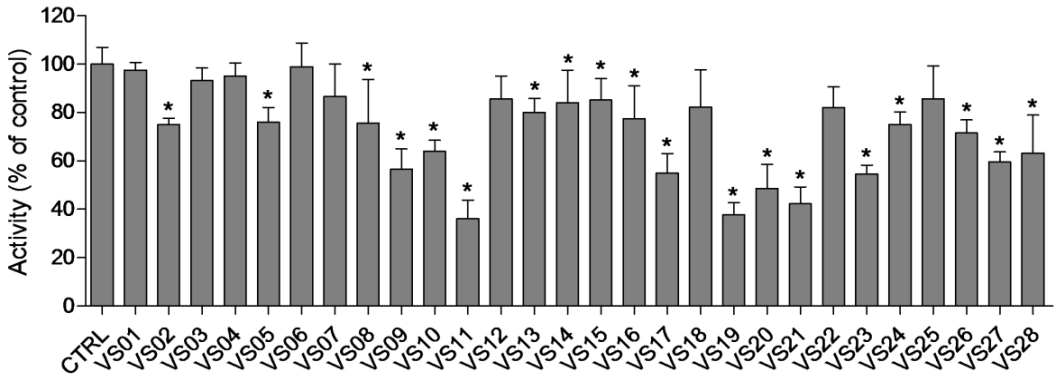

Figure 3.1.1. S1PL activity in the absence (CTRL, control) or in the presence of compounds **VS01–VS28** at a final concentration of 250 μM. HeLa cell lysates were used as enzyme source (final concentration: 0.2 mg prot./well). Compound **RBM13** was used as substrate at a final concentration of 125 μM. Data are the mean ± SD of three independent experiments with triplicates. Data were analyzed by one–way ANOVA followed by Dunnet's multiple comparison post–test if ANOVA $P < 0.05$. (*, $P < 0.05$ from control).

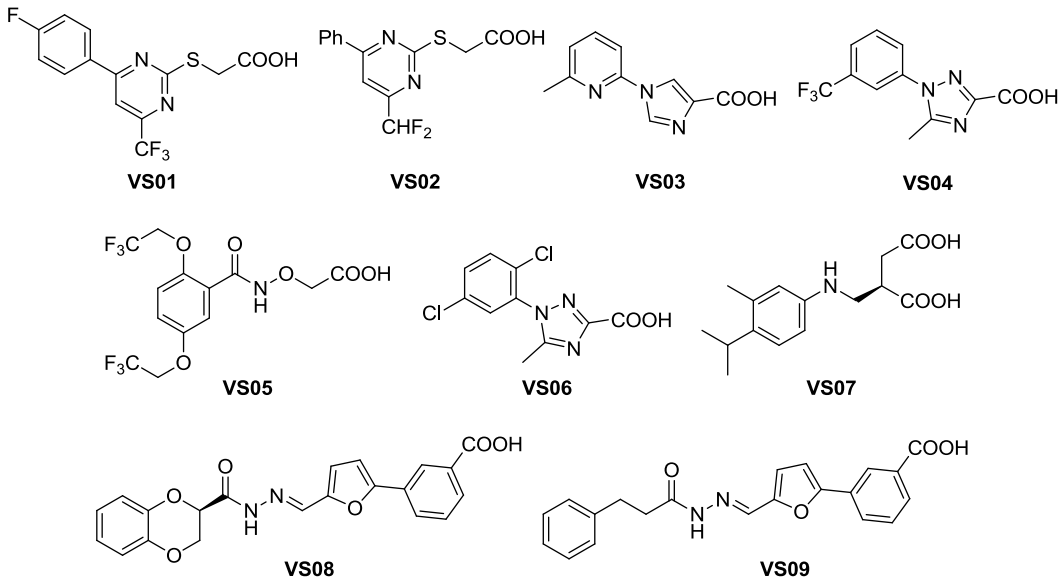

Figure 3.1.2. Selected hits resulting from virtual screening against the 3MAD–based hS1PL homology model.

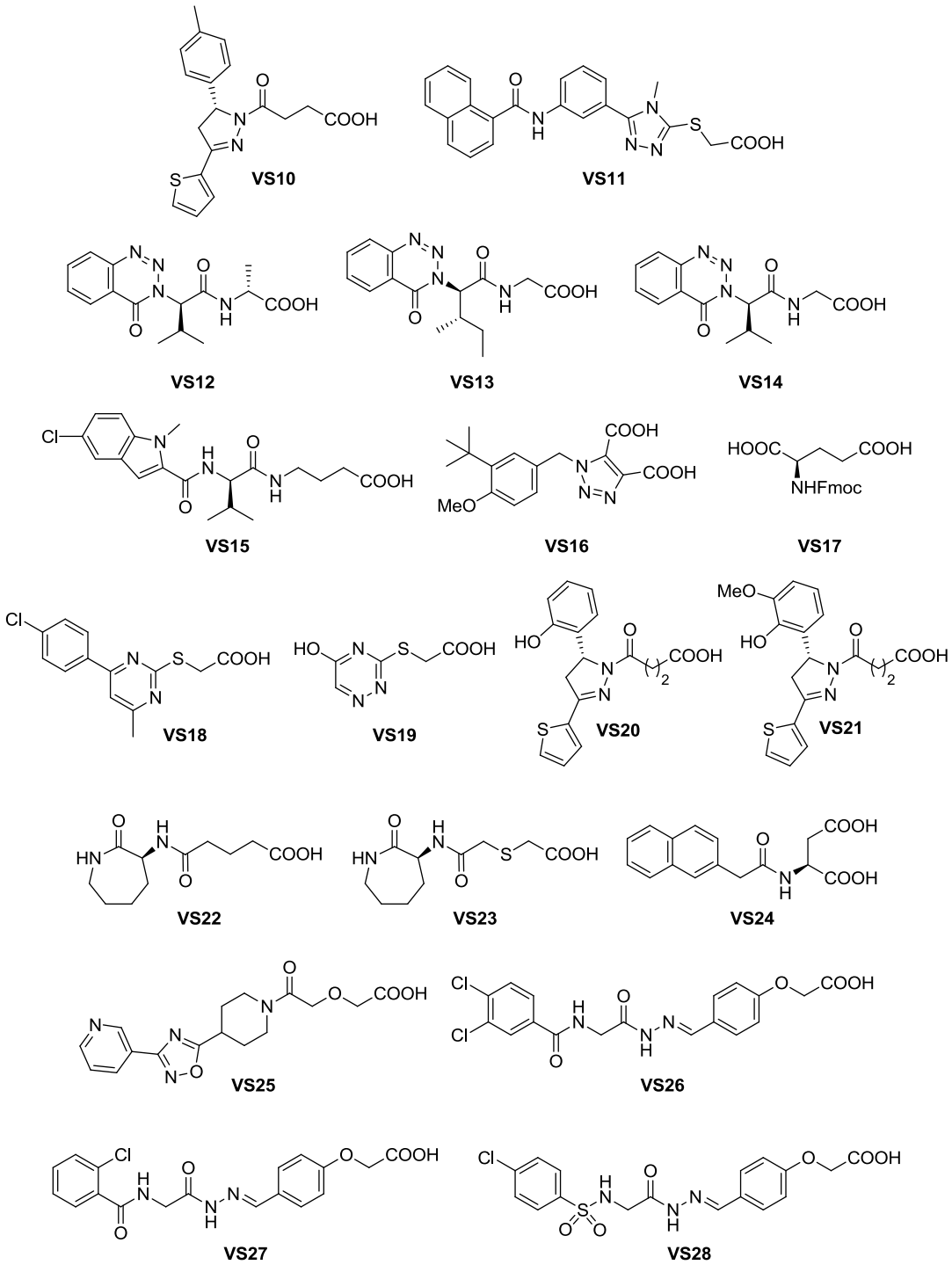

Figure 3.1.3. Selected hits resulting from virtual screening against the 3MAD–based hS1PL homology model.

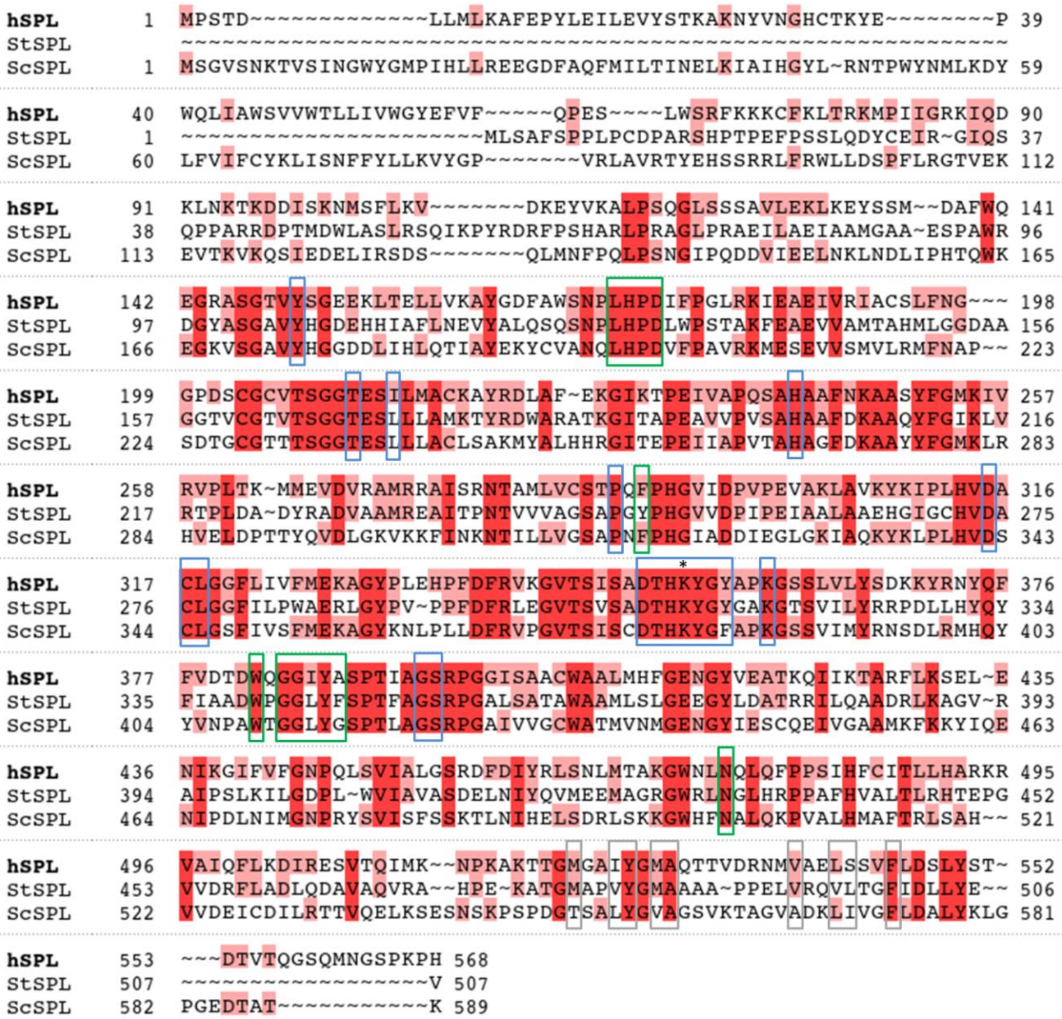

Figure 3.1.4. Alignment of human (hS1PL), *Symbiobacterium thermophilum* (StS1PL) and *Saccharomyces cerevisiae* (ScS1PL) SPL sequences according to Bourquin *et al*.[4] Residues which are identical in the three sequences are marked in red while those that are identical only in two of them are marked in pink (StS1PL vs hS1PL: 36 % identity, 51 % similarity; ScS1PL vs hS1PL: 34 % identity, 53 % similarity). Residues that constitute the active site cavity, the access channel and the outer vestibule are marked with blue, green and gray boxes, respectively. The essential Lys residue that binds to the PLP cofactor is highlighted with an asterisk on top.

Compounds **VS01–VS28** were tested using **RBM13** as S1PL substrate, since enzyme activity assays can be performed in multiwell plates that allow the simultaneous screening of a large number of compounds. However, the use of cell lysates as enzyme source presented some problems. First, it made the assay less amenable to HTS protocols, since a tedious and time consuming cell culture step is required. In addition, due to the low S1PL expression level in the cell line used, the enzymatic activity was

usually low and large amounts of cells were needed in order to properly measure the S1PL activity with the appropriate signal–to–noise ratio. All of these resulted on experiments with variable reproducibility, which pointed towards the necessity of finding an alternative source of S1PL activity. Consequently, the use of easily accessible, reliable and purified S1PL preparations was considered a crucial requirement for progress of this project.

With these antecedents, based on the high sequence homology with the human enzyme (see Figure 3.1.4) and since the DNA clone required for its overexpression in *E. coli* cultures was available in our group (a generous gift from Dr. Florence Bourquin), we envisaged the use of purified StS1PL as enzyme source.

3.1.2 Library design

As stated in the preceding section, no structural data of hS1PL had been reported at the beginning of the present doctoral thesis. Therefore, due to the high degree of homology with the human enzyme, we envisaged the use of purified StS1PL as enzyme source. Thus, we started the expression and purification process of the bacterial enzyme (see below) in order to have a suitable S1PL source to develop an activity assay using **RBM13** as substrate. However, in the course of the project, the crystal structure of human S1PL, as well as the first family of site–directed S1PL inhibitors (**3a–c**) were reported by Weiler *et. al.*[1] Consequently, with both S1PL crystal structures in hand, we decided to perform a new virtual screening against the human and bacterial proteins in order to compare the results with those previously obtained using the 3MAD–based hS1PL homology model. In light of the activities showed by compounds **VS01–VS28**, together with the results from the additional virtual screening studies, we tried to identify the common structural features required to build a general pharmacophore for the design of new S1PL inhibitors.

Comparison of the active site structures from StS1PL (PDB 3MAD)[4] and hS1PL (PDB 4Q6R)[1] revealed a high level of sequence and structural similarity (Figures 3.1.4 and 3.1.5). Thus, from 30 residues that conform their active site cavity and access channel, 26 are identical and 3 are conserved in both proteins, and the RMSD among the C_{α}–atoms of these residues is only 0.71 Å. This suggested that StS1PL could be a good active site protein model for the discovery of hS1PL inhibitors.

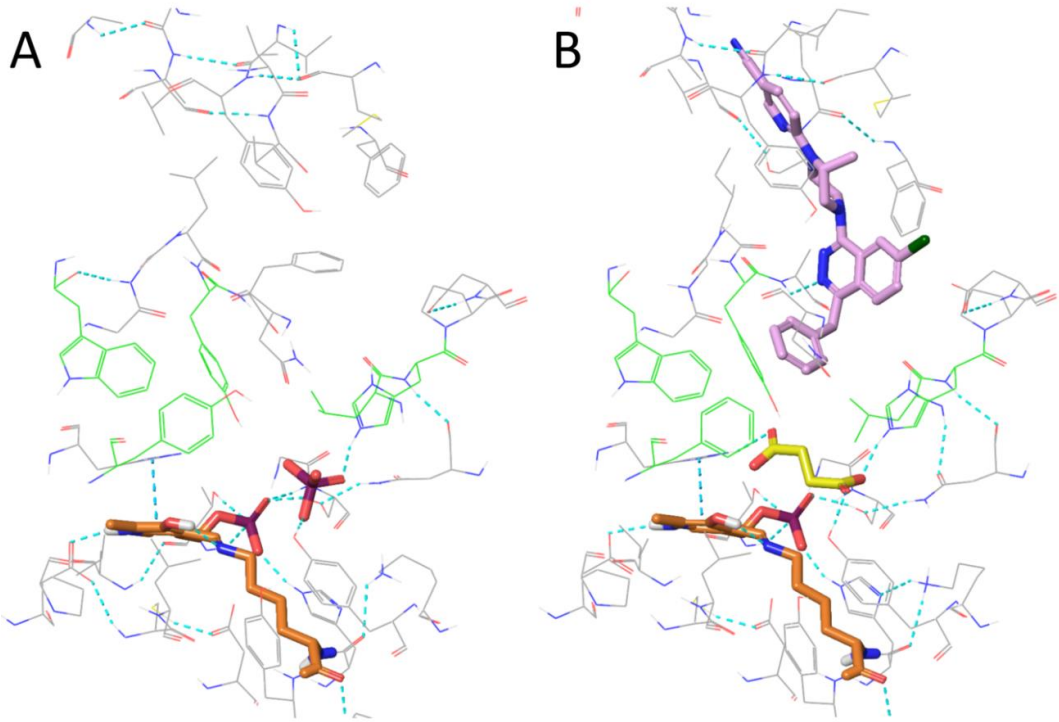

Figure 3.1.5. Crystal structure of the active site, access channel and vestibule residues of (A) StS1PL (PDB 3MAD)[4] and (B) hS1PL (PDB 4Q6R).[1] The PLP cofactor bound to the essential lysine (orange), a phosphate (A, red) and a succinate (B, yellow) anions, as well as a bound inhibitor (B, light purple) are highlighted with thick bonds. A hydrophobic patch of residues located just above the PLP cofactor is highlighted in green.

The same database of about 650,000 lead–like commercial chemical structures[5] that was used in our preliminary docking studies, was virtually screened against StS1PL and hS1PL to find potential active site binders. For that purpose, a virtual screening workflow[7] that uses the docking software Glide[8–11] to perform the flexible docking of the compounds at different levels of accuracy was employed in order to successively filter the compounds according to their predicted binding potency. Thus, initially all the compounds in the database were docked at the HTVS (high-throughput virtual screening) level, then the best 10 % was subjected to a second round of docking at the SP (standard precision) level, and finally the best 10 % was submitted to a third round of docking at the XP (extra precision) level, from which the best 10 % hits were reported.

Since during the S1PL catalytic cycle, the 3–hydroxypyridine moiety of PLP and the imino group between the essential lysine and the cofactor can go through different

ionization states,[4] two possible situations were considered to carry out the virtual screening, namely: either with the 3–hydroxypyridine and the imino groups in their neutral state, or in their ionized state (*i.e.* "phenolate–like" for the 3–hydroxypyridine moiety and the iminium forms). Among the final hits from the screening against both protein targets in the two ionization states considered, compounds that bound to the anion binding site (see below) and that exhibited scores better than –9 kcal/mol were considered as positive hits. Since Glide scores intend to correlate with binding free energies ($\Delta G_{binding}$) of ligands, it was expected that this threshold would ensure submicromolar binding.

The results of virtual screening showed that ionized carboxylic acids that bind at, or close to, an anion binding site near to the PLP cofactor (Figure 3.1.6) (see also Section 3.1.6, Figure 3.1.16 and Charts 3.1.1–3.1.4) were among the best scored hits for both targets. This site is formed by residues Y105, H129 and K317 of StS1PL, which correspond to Y150, H174 and K359 in hS1PL, and it has been postulated as the binding site for the phosphate group of the natural substrate S1P.[4] This was not surprising, since carboxylate is a well–known phosphate surrogate.[12] In addition to the carboxylate group, many of these compounds also showed, as a common feature, the presence of a variable moiety that links the carboxylate group to an aromatic ring, which, in turn, is decorated with one or more variable substituents (Figure 3.1.6) (see also Section 3.1.6, Figure 3.1.16 and Charts 3.1.1–3.1.4). The linker moiety was of variable nature, mostly formed by a short linear chain (*e.g.* $–CH_2O–$), although longer chains with different functionalities (*e.g.* amide groups) were also found.

This suggested that the binding site for the aromatic group of the hits is not in a well delimited region, but rather in a relatively large hydrophobic patch formed by residues L128, H129, Y249, W340 and Y345 of StS1PL, which correspond to L173, H174, F290, W382 and Y387 of hS1PL, respectively. Finally, the variable region decorating the aromatic ring included, in most cases, one or more additional aromatic rings, which occupied the same protein region as the known S1PL inhibitor **3b**[1] (see Figure 3.1.5B and Figure 1.9).

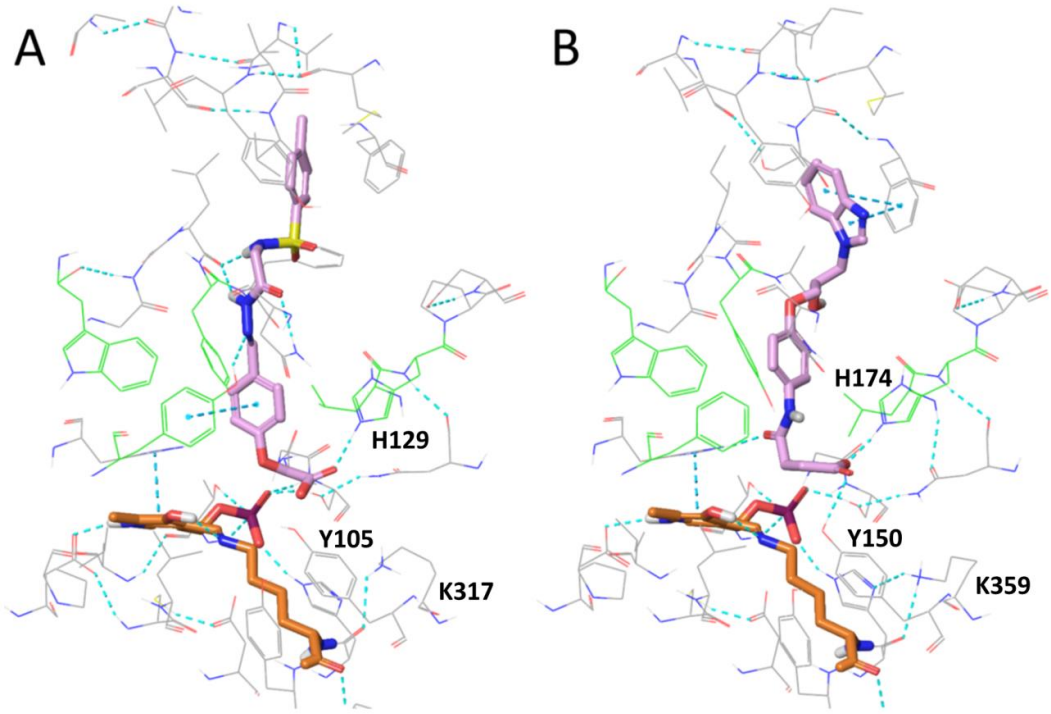

Figure 3.1.6. (A) Best docked pose for compound Sigma–Aldrich (SALOR) R125830 (see Chart 3.1.1) bound to StS1PL. (B) Best docked pose for compound Chembridge 7978434 (see Chart 3.1.2) bound to hS1PL. The 3–hydroxypyridine group from the PLP cofactor and the imino group between the essential Lys residue and PLP were both considered in their neutral state. Protein residues conforming the postulated anion binding site are labelled. The PLP cofactor bound to the essential lysine (thick, orange), the residues that constitute the hydrophobic patch (green) and the ligands (thick, light purple) are highlighted.

As shown in Charts 3.1.1–3.1.4, the hits showed similarities in their structures and in their docking scores. Therefore, it was concluded that the ionization state of the 3–hydroxypyridine–imine pair did not have much effect on the binding of these types of compounds. In addition, the results of this virtual screening were in agreement with those obtained using the hS1PL homology model, since similar structures arose from all docking studies, regardless of the target protein used.

Taking into account the above features and according to the structures of the hits identified in our preliminary screening to detect S1PL inhibitors among commercial compounds (see Section 3.1.1), we proposed **9** as a suitable scaffold to develop a small library of potential S1PL binders (see Figure 3.1.7).

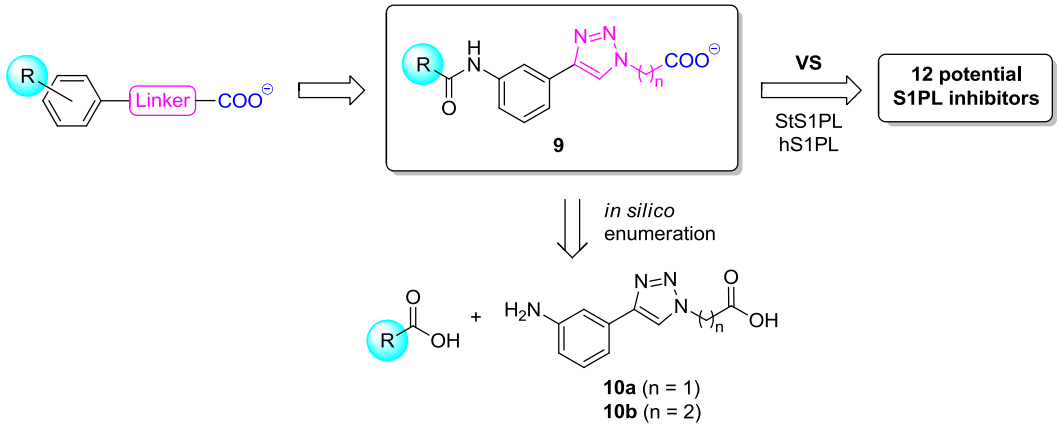

Figure 3.1.7. General structure of the putative S1PL ligands and derived scaffold structure **9**, as detected by virtual screening, and constituted by a carboxylate group, a linker and a substituted aromatic ring.

In this structure, the triazole central core was chosen as part of the linker for its synthetic availability, since it can be easily assembled using standard click chemistry protocols based on alkyne–azide cycloadditions. Furthermore, by binding to the phenyl ring, it would provide an extended aromatic region able to establish strong interactions with the aromatic residues present in the above mentioned receptor hydrophobic patch. On the other hand, an amide group bound to the phenyl ring would allow the exploration of a diversity of R–substituents, coming from suitable carboxylic acid precursors, which would interact with the more external part of the channel that leads to the active site cavity of S1PL.

Therefore, a virtual library of compounds with the general structure **9** was enumerated. For that purpose, a diverse collection of commercial carboxylic acids (R–COOH) was extracted from the clean lead–like subset from the ZINC database.[13,14] Compounds were selected according to different criteria: molecular weight < 500 g/mol, a single carboxylic group present or no undesirable chemical functions present. Additional compounds available in house were also considered resulting in a collection of 6048 carboxylic acids. These were combined *in silico* with scaffolds **10a** and **10b** (setting n = 1 or 2) using the CombiGlide[15] application of the Schrodinger Suite to enumerate a virtual library of 12096 compounds.

This library was docked against StS1PL and hS1PL using Glide,[10] but this time performing only the SP and XP docking steps and considering only the neutral state for the phenol–imine pair of the lysine–bound PLP complex, to yield 120 hits for each protein target. The hits from both proteins were then submitted to an Induced Fit Docking Protocol[16–18] of the Schrödinger Suite, which takes in consideration the flexibility of the protein residues within a given distance (5 Å) from the bound ligands, in order to refine the geometries and scores of the docked poses.

Based on their scores, the diversity of their structures and other practical criteria, like synthetic suitability or commercial availability, 12 virtual hits were selected for synthesis (Table 3.1.1) (see Section 3.1.6, Charts 3.1.5 and 3.1.6 for docking scores). These virtual hits showed similar binding modes (see Figures 3.1.17–3.1.22 from Section 3.1.6), with their carboxylate groups located at the anion binding site and the central triazole and phenyl rings interacting with the residues of the hydrophobic patch of each protein, in many cases through π–stacking interactions.

3.1.3 Synthesis of *N*–acylanilino carboxylates

The general synthetic approach to the series of *N*–acylanilino carboxylates is summarized in Scheme 3.1.1. Initially, the commercially available bromoesters **11a** and **11b** were converted to azides **RBM7–019** and **RBM7–020** by nucleophilic displacement of the bromine atom using NaN_3.[19,20] Cu–catalyzed cycloaddition[21,22] between 3–ethynylaniline and the obtained azidoesters gave scaffolds **RBM7–021** and **RBM7–022** in almost quantitative yields. Subsequent *N*–acylation with the selected carboxylic acids (see table 3.1.1), using HATU as coupling agent,[23] afforded the corresponding amides in variable yields.

Initial attempts at the synthesis of compounds **RBM7–037** and **RBM7–040** under the above conditions were unsuccessful, since the required products were obtained in very low yields (< 15 %). In this case, we hypothesized that the use of carboxylic acids containing one or more hydroxyl group may favor the formation of the corresponding *O*–acylated byproducts in the presence of a base (DIPEA), thus leading to the observed low yields. However, when the acylation reaction was performed in the absence of a base and using EDC/HOBt as coupling agents, the desired amides **RBM7–037** and **RBM7–040** were satisfactorily obtained in 83 and 87 % yield, respectively (See Section 5.1.3.2). Final alkaline hydrolysis of the intermediate methyl esters afforded the required *N*–acylanilino carboxylic acids also in variable yields (See Scheme 3.1.1 and Table 3.1.1).

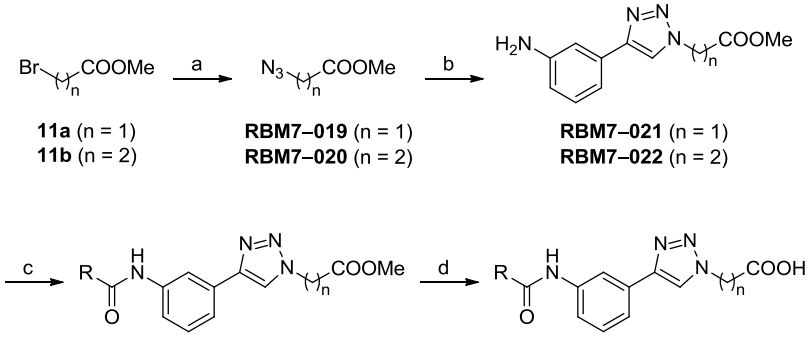

Scheme 3.1.1. Synthesis of *N*–acylanilino carboxylates. For names and structures, see Table 3.1.1. Reagents and conditions: (a) for **RBM7–019**: **11a**, NaN_3, DMSO, rt, 92 %; for **RBM7–020**: **11b**, NaN_3, H_2O/DMF (1:1), 55 ºC, 89 %; (b) 3–ethynylaniline, $CuSO_4 \cdot 5H_2O$, sodium ascorbate, H_2O/THF (1:1), rt, quant. yield for **RBM7–021** and 97 % for **RBM7–022**; (c) selected carboxylic acid and HATU, DIPEA, DMF, 40 ºC or EDC, HOBt, DMF, rt, 54–92 % (See Section 5.1.3.2); (d) LiOH, THF/H_2O (3:1), 0 ºC, 39–93 %.

Table 3.1.1. Compounds synthesized in this section.

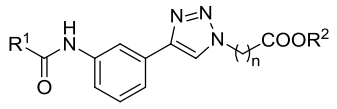

Entry	R^1	n	R^2	Compound	Yield[a]
1	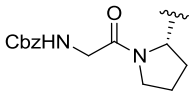	2	Me	**RBM7–028**	
2			H	**RBM7–030**	48
3		1	Me	**RBM7–027**	
4			H	**RBM7–031**	41
5	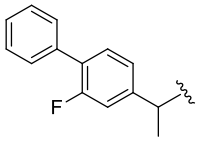	1	Me	**RBM7–034**	
6			H	**RBM7–042**	43
7	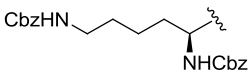	1	Me	**RBM7–035**	
8			H	**RBM7–043**	52
9	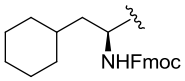	1	Me	**RBM7–033**	
10			H	**RBM7–044**	23
11	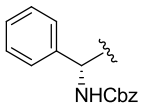	2	Me	**RBM7–038**	
12			H	**RBM7–045**	54
13	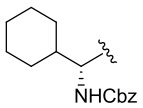	2	Me	**RBM7–039**	
14			H	**RBM7–046**	22
15	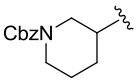	1	Me	**RBM7–041**	
16			H	**RBM7–047**	35
17	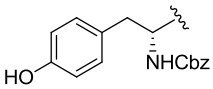	2	Me	**RBM7–040**	
18			H	**RBM7–048**	29
19	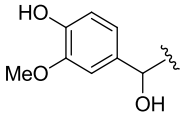	2	Me	**RBM7–037**	
20			H	**RBM7–049**	65
21	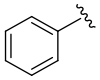	2	Me	**RBM7–065**	
22			H	**RBM7–066**	51
23	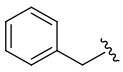	2	Me	**RBM7–054**	
24			H	**RBM7–067**	50

[a]Overall yield (from starting bromoesters, see Scheme 3.1.1 and Section 5.1.3.2)

3.1.4 Inhibition studies on StS1PL and hS1PL

3.1.4.1 Optimization of the inhibition assay using **RBM13** as substrate

Among the several assays reported for the determination of S1PL activity (see Section 1.4), those amenable to 'on–plate' analysis are particularly interesting for their application to HTS protocols. As introduced above (section 1.4.2), some time ago we developed the fluorogenic probe **RBM13**,[6] a S1PL substrate that affords the fluorescent reporter umbelliferone (**7**), after base–promoted decomposition of the intermediate aldehyde product **5** (See Figure 1.12).

So far, the only kinetic constants for **RBM13** had been determined in cell lysates of murine embryonic fibroblasts.[6] In the present thesis, however, these parameters have also been determined in purified StS1PL and hS1PL, which required a thorough protocol optimization. In this case, StS1PL was expressed and purified following an adapted version of a reported protocol (see Section 5.2.2).[4] Briefly, plasmid pQE70-StSPL, which was kindly provided by Dr. Florence Bourquin,[4] was expressed in *E. Coli* M–15 strain. This recombinant plasmid, consisting of the WT StS1PL gene subcloned in a pQE70 expression vector, encodes for the *Symbiobacterium thermophilum* full–length S1PL with six His residues added to the C–terminus (Figure 3.1.8). Although the IPTG–induced overexpression of StS1PL was evidenced by SDS–PAGE, most of the protein was expressed as inclusion bodies (See Figure 3.1.9). Nevertheless, thermal treatment of the soluble fraction to denature undesired proteins followed by IMAC purification, allowed the isolation of a highly enriched StS1PL solution, which was considered suitable for further enzymatic assays. Purity and identity of purified StS1PL was confirmed by SDS–PAGE and LC/MS analysis (See Figures 3.1.9, 3.1.10 and Section 5.2.3). In both cases, results were in full agreement with those reported by Bourquin and coworkers.[4]

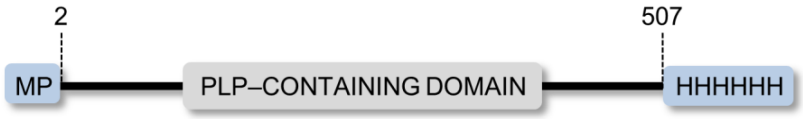

Figure 3.1.8. Encoded recombinant StS1PL from plasmid pQE70-StSPL.[4] Non–native residues are highlighted in blue. Residue numbering refers to the StS1PL WT sequence (See Figure 3.1.4). The predicted molecular mass of recombinant StS1PL is 55565 Da.

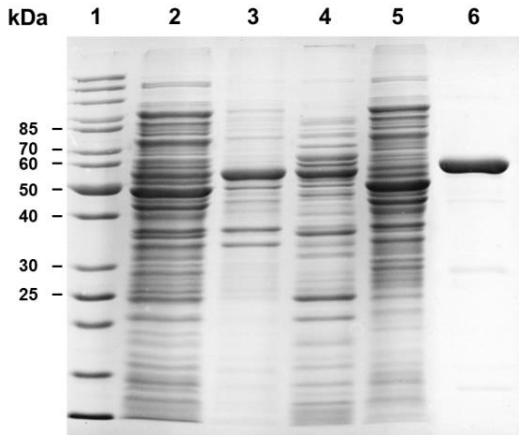

Figure 3.1.9. Coomassie Blue–stained SDS–PAGE of purified StS1PL. The gel was loaded with samples of StS1PL from supernatant of lysis (lane 2), pellet after lysis and centrifugation (lane 3), supernatant after thermal denaturation (lane 4), pellet after thermal denaturation (lane 5) and purified StS1PL after affinity chromatography (IMAC) and dialysis (lane 6). Lane 1 corresponds to the protein molecular weight marker (PageRuler^{TM} Unstained Protein Ladder 26614, Thermo Scientific). The predicted molecular mass of StSPL is 55 kDa.

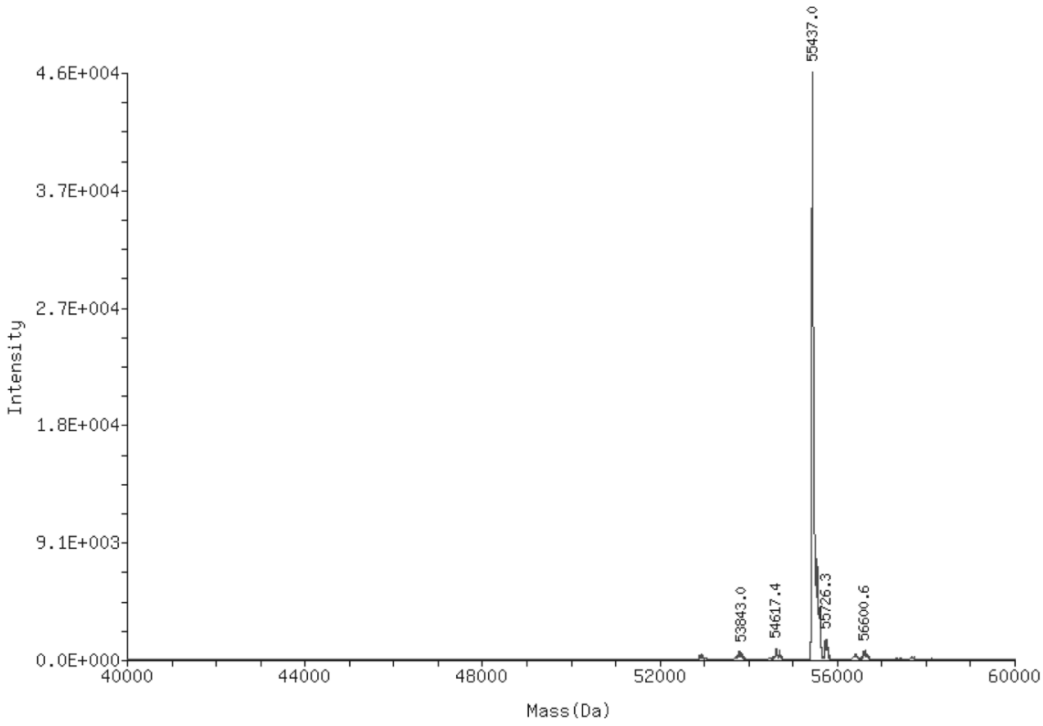

Figure 3.1.10. StS1PL mass spectrometry analysis. Calculated for pQE70–StSPL (without Met1): 55434 Da,[4] measured: 55437 Da (lit.[4] 55436 Da). Measured mass corresponds to apo–St1SPL.

On the other hand, hS1PL, as well as inhibitor **3c**, were kindly provided by Dr. Andreas Billich from Novartis Institutes for BioMedical Research (Basel, Switzerland). In this case, the recombinant human protein corresponds to a His–tagged *N*–terminally shortened variant (Δ1–61) of the WT enzyme, which had been expressed in insect cells and purified to homogeneity.[1]

Initially, **RBM13** was tested as StS1PL substrate at 62 μM, in agreement with the original protocol reported by Bourquin *et al*.[4] Incubation of **RBM13** with different amounts of StS1PL showed linearity in product formation up to 50 μg/mL of StS1PL (Figure 3.1.11A). The optimal enzyme concentration was fixed at 25 μg/mL, in which 12 % of the substrate was metabolized, with a 12–fold increase of the fluorescence signal with respect to the blank. Product formation was also time–dependent, since the amount of umbelliferone increased linearly up to 90 min (Figure 3.1.11B). From these results, an incubation time of 60 min was considered suitable for further assays. Kinetic parameters for **RBM13** against StS1PL were thus determined (Figure 3.1.11C) as K_M = 1522 ± 73 μM and V_{max} = 46 ± 2 pmol·min^{-1}·μg^{-1} (V_{max}/K_M = 0.03 ± 0.002).

Concerning hS1PL, the ability of **RBM13** as substrate was also evidenced, as shown in Figure 3.1.11D. At 3 μg/mL of hS1PL (corresponding to a 2 % substrate conversion) a 4–fold increase in the fluorescence signal was observed with respect to a blank experiment without enzyme. Under these conditions, product formation increased linearly up to 2 h of incubation time (Figure 3.1.11E). Hence, an incubation time of 60 min was considered as suitable. The reaction rate was dependent on the substrate concentration (Figure 3.1.11F), with K_M = 1994 ± 121 μM and V_{max} = 107 ± 11 pmol·min^{-1}·μg^{-1} (V_{max}/K_M = 0.05 ± 0.006). Since the determined kinetic parameters were in the same order of magnitude for both bacterial and human enzymes, a similar behavior of **RBM13** towards both enzyme sources can be inferred.

3.1.4.2 Activity of *N*–acylanilino carboxylates as StS1PL and hS1PL inhibitors

Using **RBM13** as fluorogenic substrate, the synthesized *N*–acylanilino carboxylates (Table 3.1.1) were evaluated as S1PL inhibitors at 250 μM in both enzyme sources. The recently reported potent and selective hS1PL inhibitor **3c**[1] (See Figure 1.9), was also included in this study as positive control of inhibition. The results are collected in Figure 3.1.12. The tested compounds showed activities ranging from low to moderate

against both enzyme sources. In the case of hS1PL, only carboxylates **RBM7–042**, **RBM7–043**, **RBM7–044**, **RBM7–045** and **RBM7–048** exerted significant inhibition. Compound **RBM7–043** was the most active compound of this series with a 33 % inhibition.

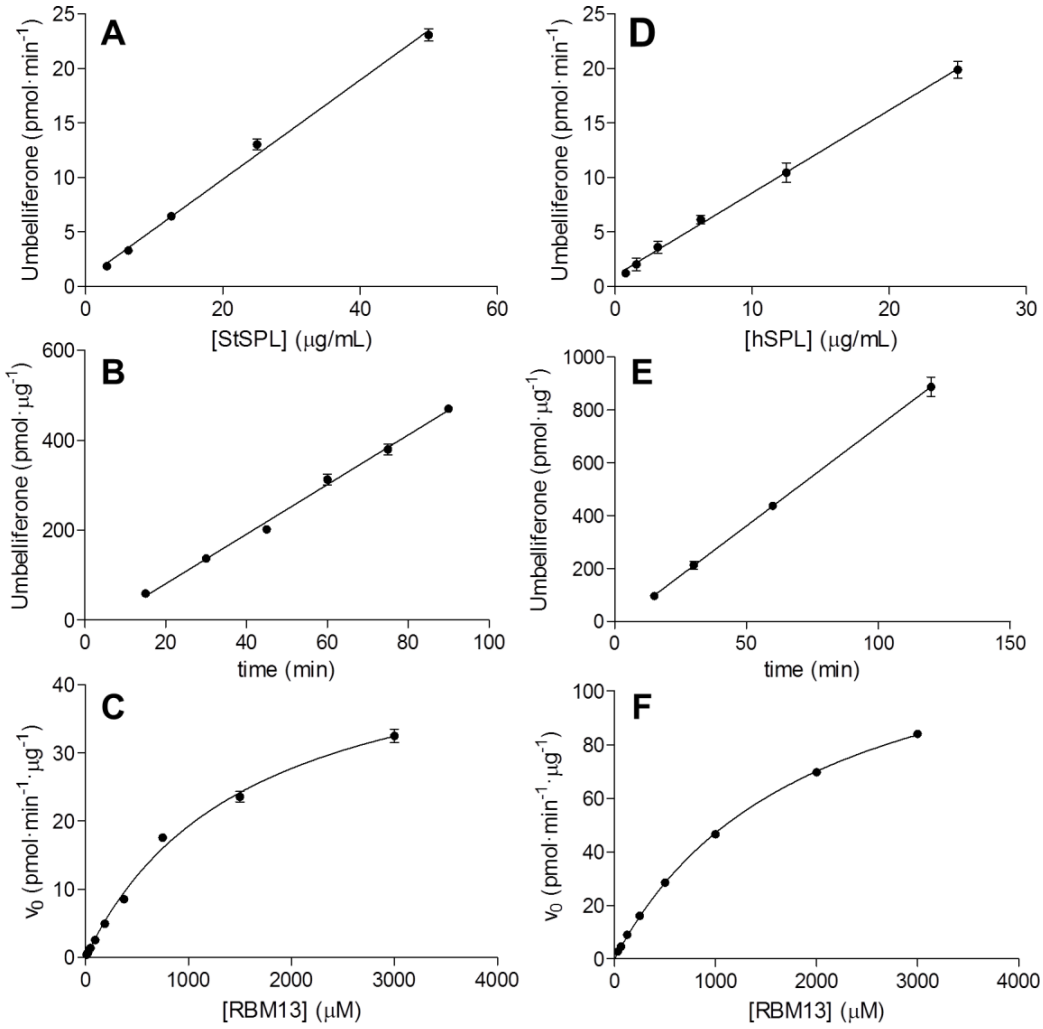

Figure 3.1.11. Enzyme concentration (A, D) and time–dependence (B, E) of the S1PL reaction using **RBM13** as substrate against StS1PL (A, B) and hS1PL (D, E). Substrate concentration was 62 µM (A, B) and 125 µM (D,E). In A and D, incubation time was 60 min. Enzyme concentration was 25 µg/mL (B) and 3 µg/mL (E). Substrate concentration dependence of the StS1PL reaction (C) and the hS1PL reaction (F) using **RBM13** as substrate at graded concentrations. In both cases, the substrate was incubated for 60 min with 25 µg/mL (C) or 3 µg/mL (F) of StS1PL and hS1PL, respectively. Data correspond to one representative experiment performed twice (with triplicates).

In contrast, compounds **RBM7–031**, **RBM7–044**, **RBM7–047**, **RBM7–048**, and **RBM7–049** showed significant inhibition on StS1PL, being carboxylate **RBM7–048** the most active compound of this series (31 % of inhibition).

Comparison of activities for the series of *N*–acylanilino carboxylates showed small differences on their behavior against each enzyme source. Only **RBM7–043** showed a significant selectivity towards hS1PL ($P < 0.001$; unpaired two–tailed t–test; $n = 6$). Conversely, **RBM7–048**, the most active compound against StS1PL, showed little selectivity. As expected, compound **3c** behaved as a potent hS1PL inhibitor in our fluorogenic assay, with a residual enzyme activity of around 2 % at 10 μM (Figure 3.1.12) and $IC_{50} = 93.5 \pm 6.0$ nM (Figure 3.1.13B), consistent with the reported value.[1] However, compound **3c** turned out to be significantly less active against StS1PL ($P < 0.001$; unpaired two–tailed t–test; $n = 6$), even at an equimolar concentration with the substrate (125 μM). Under these conditions, only a moderate decrease on the StS1PL activity (around 34 %) was observed (Figure 3.1.12).

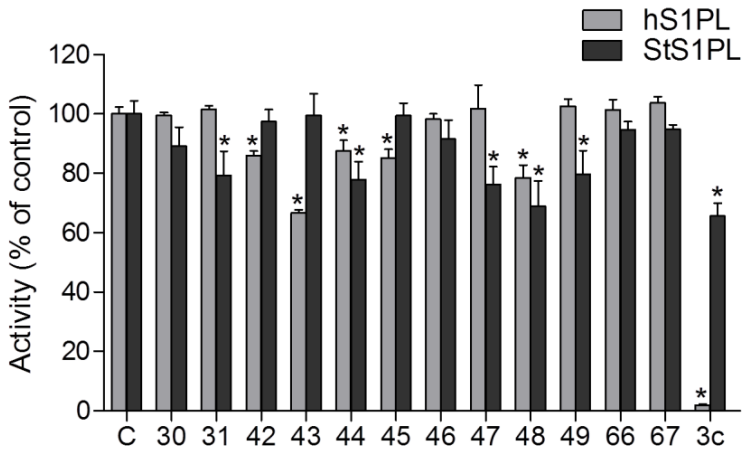

Figure 3.1.12. Activity (% of control) of hS1PL (3 μg/mL) and StS1PL (25 μg/mL) in the absence (C, control) or in the presence of compounds **RBM7** (indicated with the last two digits, for the sake of clarity) and compound **3c** (taken as positive control of inhibition). Compounds were tested at 250 μM, except for compound **3c**, which was tested at 10 μM (for hS1PL) and 125 μM (for StS1PL). In both cases, compound **RBM13** was used as substrate at a final concentration of 125 μM. Data are the mean ± SD of two independent experiments with triplicates. Data were analyzed by one–way ANOVA followed by Dunnet's multiple comparison post–test if ANOVA $P < 0.05$. (*, $P < 0.001$ from control).

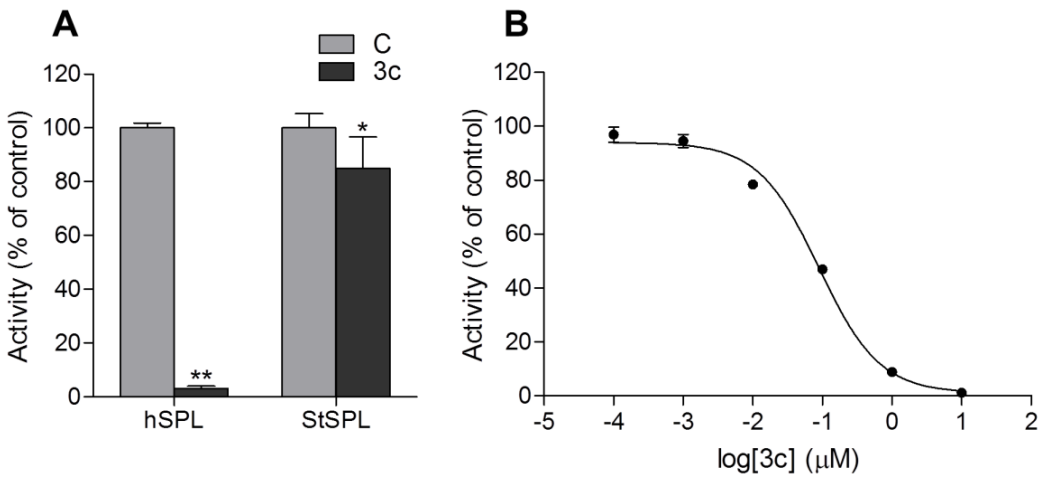

Figure 3.1.13. (A) Activity (%) of hS1PL and StS1PL (both at 0.8 μg/mL) in the absence (C, control) or presence of **3c** (50 μM). In both cases, S1P was used as substrate of the enzymatic reaction at a final concentration of 10 μM. Data correspond to the mean ± SD of four independent experiments with duplicates. Asterisks indicate statistical significance (unpaired two–tail t–test; *, $P < 0.01$; **, $P < 0.001$ from controls). (B) Activity (% of control) of hS1PL (final concentration: 3 μg/mL) at graded concentrations of **3c** using **RBM13** as substrate (final concentration: 125 μM). Data correspond to one representative experiment out of three performed (with triplicates).

This lower activity showed by compound **3c** against StS1PL was unexpected. Nonetheless, this result was confirmed using a slightly modified version of a reported LC/MS method to measure enzyme activity with natural S1P as substrate[1] (See Section 1.4.3 and Section 5.2.4.4 for experimental details). Briefly, S1PL activity in the presence of the inhibitor (50 μM) was determined using natural S1P (10 μM) as substrate and trapping the enzyme reaction product (*trans*–2–hexacedenal) as the isonicotinylhydrazone **8c** (see Figure 1.13), prior to LC/MS quantification. Under these conditions, compound **3c** also behaved as a potent hS1PL inhibitor (97 % inhibition), while it only exerted a moderate 15 % inhibition on StS1PL, consistent with the results obtained in our fluorogenic assay (See Figure 3.1.13A).

The different activity of inhibitor **3c** against hS1PL and StS1PL can be explained on the basis of the structural differences between both proteins at the access channel and vestibule to the active site cavity. Superimposition of the surface of hS1PL on the structure of StS1PL shows a protrusion from the surface of several side chain residues of the bacterial protein, in particular those of L344, F346 and L497 (Figure 3.1.14), in

agreement with a very recent report.[24] This could preclude the binding of inhibitors **3b** or **3c** at that site, as we have experimentally observed for **3c**. These structural differences between StS1PL and hS1PL should be taken into account if the more easily available StS1PL is taken as a model for the design of potential inhibitors targeting the S1PL access channel.[24,25]

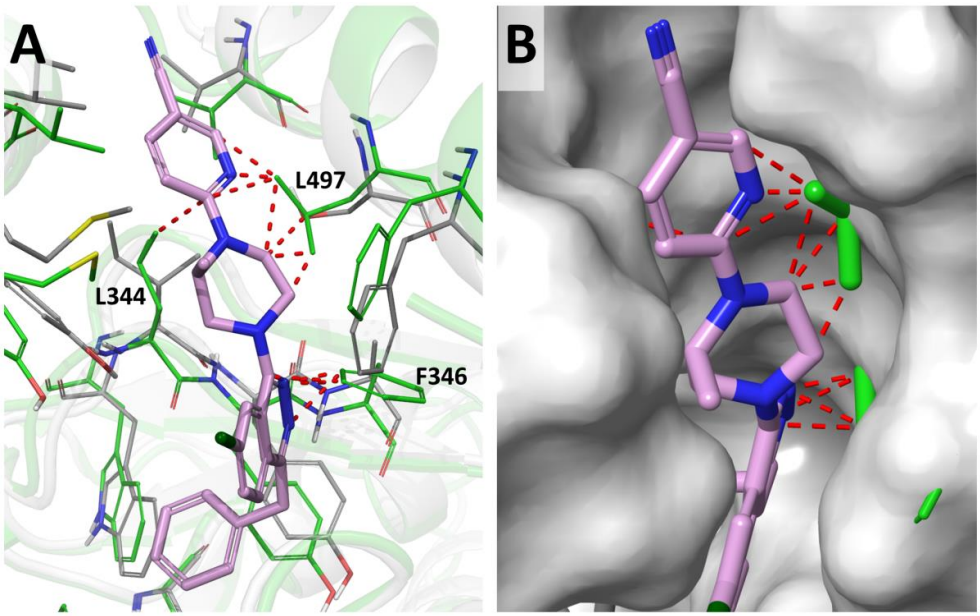

Figure 3.1.14. (A) Crystal structure of hS1PL (PDB 4Q6R, grey)[1] with the bound inhibitor **3b** (light purple) and superposed structure of StS1PL (PDB 3MAD, green).[4] StS1PL residues L344, F346 and L497 (corresponding to I386, A388 and S542 of hS1PL) are labeled. (B) A close up view of the hS1PL surface (grey) at the inhibitor binding site and StS1PL residues (green) protruding from the surface. Red dashed lines indicate bad clashes between the StS1PL residues and a hypothetically bound inhibitor **3b**.

Given the low activities found for the above carboxylates, we decided to re–evaluate compounds **VS01–VS28** as StS1PL and hS1PL inhibitors, in order to check the activities showed by these compounds in a preliminary test using cell lysates as hS1PL source (see Figure 3.1.1). In this case, compounds **VS01–VS28** were tested against our two purified S1PL enzyme sources, using **RBM13** as substrate. Results are collected in Figure 3.1.15. Shockingly, all compounds exerted low to moderate activities. Compound **VS19** was the most active compound against both enzymes (40 % StSPL inhibition and 18 % hS1PL inhibition). The remaining compounds were practically devoid of activity, especially as hS1PL inhibitors.

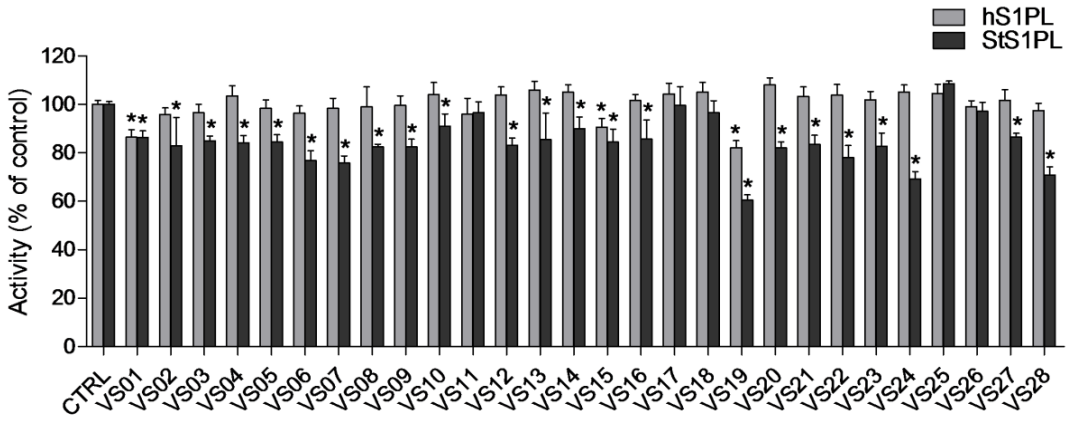

Figure 3.1.15. Activity (% of control) of hS1PL (3 μg/mL) and StS1PL (25 μg/mL) in the absence (CTRL, control) or in the presence of compounds **VS01-28** at a final concentration of 250 μM. In both cases, compound **RBM13** was used as substrate at a final concentration of 125 μM. Data are the mean ± SD of two independent experiments with triplicates. Data were analyzed by one way ANOVA followed by Dunnet's multiple comparison post–test if ANOVA $P < 0.05$. (*, $P < 0.05$ from control).

The obtained results clearly suggested that the S1PL activity assays performed with cell lysates led to the identification of false positives hits, since practically all the assayed compounds were inactive under the developed assay using purified enzymes. At this point, trying to find an explanation for this apparent discrepancy was not considered. However, one can speculate that cell lysates, in addition to S1PL, contain other factors that could facilitate the entrance of the assayed compounds into the active site cavity, to exert their inhibitory activity.

Concerning the modest activity of the above *N*–acylanilino carboxylates (Figure 3.1.12), a number of causes might explain the discrepancy with our expectations, based on the computational docking results. One concern is the ionization state of the carboxylate group present in our compounds and that of the ionizable protein residues at the anion binding site. Despite the fact that our virtual screening study considered two possibilities for the protonation state of the 3–hydroxypyridine and the imine moieties on the K359–PLP complex (in hS1PL) or K311–PLP complex (in StS1PL), the results obtained in both cases were similar (Charts 3.1.1–3.1.4, Figures 3.1.6 and 3.1.16). On the other hand, there are two additional residues at the anion binding site of both proteins that might be ionized, *i.e*. H129 and K317 of StS1PL or H174 and K359 of hS1PL. Our assumption was that these residues were in their ionic form, allowing the

establishment of strong electrostatic and hydrogen bond interactions with the ligands. This assumption is probably right when the anion is a phosphate group (either from the buffer or that present in the natural substrate S1P), and it seemed also reasonable for a carboxylate group, since there is in fact one molecule of succinic acid bound at the same site in the crystal structure of hS1PL (PDB 4Q6R, see Figure 3.1.5).[1]

However, the fact that the series of carboxylates could be less acidic than expected in the protein environment should not be disregarded, thus precluding the interaction with the protein in their anionic form. Similarly, it is conceivable that the histidine residue at the anion binding site could be in its neutral state if there is not a strongly anionic bound ligand. This could have led to an overestimation of the potency of the polar interactions between the ligands and the proteins. Moreover, scoring functions in docking software are usually too crude to rank ligands according to their binding potency[26] and results arising only from docking estimates should be taken with caution.[27] In addition, the possibility that the inhibitors do not reach the enzyme active site should not be overlooked. In any case, a strong structural similarity between hS1PL and its bacterial surrogate at the active site can be inferred from structural data and also by the similar biochemical parameters found for our fluorogenic substrate **RBM13** (see above). This justifies the use of the more easily available bacterial source when planning the design of active–site directed inhibitors, as we have observed in a series of substrate analogs (See Section 3.2) However, more caution should be taken for inhibitors targeting the active site access channel, for which alternative chimeric constructs from bacterial origin represent interesting alternatives.[24]

3.1.5 References

(1) Weiler, S.; Braendlin, N.; Beerli, C.; Bergsdorf, C.; Schubart, A.; Srinivas, H.; Oberhauser, B.; Billich, A. Orally Active 7-Substituted (4-Benzylphthalazin-1-Yl)-2-Methylpiperazin-1-Yl]nicotinonitriles as Active-Site Inhibitors of Sphingosine 1-Phosphate Lyase for the Treatment of Multiple Sclerosis. *J. Med. Chem.* **2014**, *57*, 5074–5084.

(2) Bagdanoff, J. T.; Donoviel, M. S.; Nouraldeen, A.; Carlsen, M.; Jessop, T. C.; Tarver, J.; Aleem, S.; Dong, L.; Zhang, H.; Boteju, L.; et al. Inhibition of Sphingosine 1-Phosphate Lyase for the Treatment of Rheumatoid Arthritis: Discovery of (E)-1-(4-((1 R,2 S,3 R)-1,2,3,4-Tetrahydroxybutyl)-1 H -Imidazol-2-Yl)ethanone Oxime (LX2931) and (1 R,2 S,3 R)-1-(2-(Isoxazol-3-Yl)-1 H -Imidazol-4-Yl)but. *J. Med. Chem.* **2010**, *53*, 8650–8662.

(3) Billich, A.; Baumruker, T. Sphingolipid Metabolizing Enzymes as Novel Therapeutic Targets. In *Lipids in Health and Disease*; Quinn, P. J., Wang, X., Eds.; Springer, 2008; pp 487–522.

(4) Bourquin, F.; Riezman, H.; Capitani, G.; Grütter, M. G. Structure and Function of Sphingosine-1-Phosphate Lyase, a Key Enzyme of Sphingolipid Metabolism. *Structure* **2010**, *18*, 1054–1065.

(5) MOE Leadlike Database, v. 2011.10, Chemical Comuting Group Inc.: Montreal, QC, Canada, 2011.

(6) Bedia, C.; Camacho, L.; Casas, J.; Abad, J. L.; Antonio, D.; Van Veldhoven, P. P.; Fabriàs, G. Synthesis of a Fluorogenic Analogue of Sphingosine-1-Phosphate and Its Use to Determine Sphingosine-1-Phosphate Lyase Activity. *ChemBioChem* **2009**, *10* (5), 820–822.

(7) Schrödinger Virtual Screening Workflow 2015-2, Schrödinger, LLC: New York, NY, 2015.

(8) Schrödinger Glide, Version 6.7, Schrödinger, LLC: New York, NY, 2015.

(9) Halgren, T. A.; Murphy, R. B.; Friesner, R. A.; Beard, H. S.; Frye, L. L.; Pollard, W. T.; Banks, J. L. Glide: A New Approach for Rapid, Accurate Docking and Scoring. 2. Enrichment Factors in Database Screening. *J Med Chem* **2004**, *47* (7), 1750–1759.

(10) Friesner, R. A.; Murphy, R. B.; Repasky, M. P.; Frye, L. L.; Greenwood, J. R.; Halgren, T. A.; Sanschagrin, P. C.; Mainz, D. T. Extra Precision Glide: Docking and Scoring Incorporating a Model of Hydrophobic Enclosure for Protein-Ligand Complexes. *J Med Chem* **2006**, *49* (21), 6177–6196.

(11) Friesner, R. A.; Banks, J. L.; Murphy, R. B.; Halgren, T. A.; Klicic, J. J.; Mainz, D. T.; Repasky, M. P.; Knoll, E. H.; Shelley, M.; Perry, J. K.; et al. Glide: A New Approach for Rapid, Accurate Docking and Scoring. 1. Method and Assessment of Docking Accuracy. *J Med Chem* **2004**, *47* (7), 1739–1749.

(12) Elliott, T. S.; Slowey, A.; Ye, Y.; Conway, S. J. The Use of Phosphate Bioisosteres in Medicinal Chemistry and Chemical Biology. *Med. Chem. Commun.* **2012**, *3* (7), 735–751.

(13) Irwin, J. J.; Shoichet, B. K. ZINC--a Free Database of Commercially Available Compounds for Virtual Screening. *J. Chem. Inf. Model.* **2005**, *45* (1), 177–182.

(14) Irwin, J. J.; Sterling, T.; Mysinger, M. M.; Bolstad, E. S.; Coleman, R. G. ZINC: A Free Tool to Discover Chemistry for Biology. *J*. *Chem*. *Inf*. *Model*. **2012**, *52* (7), 1757–1768.

(15) Schrödinger CombiGlide, Version 3.7, Schrödinger, LLC: New York, NY, 2015.

(16) Schrödinger Induced Fit Docking Protocol 2015-2, Scrödinger, LCC: New York, NY, 2015.

(17) Sherman, W.; Beard, H. S.; Farid, R. Use of an Induced Fit Receptor Structure in Virtual Screening. *Chem*. *Biol*. *Drug Des*. **2006**, *67* (1), 83–84.

(18) Sherman, W.; Day, T.; Jacobson, M. P.; Friesner, R. A.; Farid, R. Novel Procedure for Modeling Ligand/Receptor Induced Fit Effects. *J*. *Med*. *Chem*. **2006**, *49* (2), 534–553.

(19) Burlison, J. A.; Blagg, B. S. J. Synthesis and Evaluation of Coumermycin A1 Analogues That Inhibit the Hsp90 Protein Folding Machinery. *Org*. *Lett*. **2006**, *8* (21), 4855–4858.

(20) Duval, S.; Kindermann, M. Azido Alkanoic Acids and Derivatives Thereof in Feed for Reducing Methane Formation Emanating from the Digestive Activities of Ruminants. WO 2011/045418 A1, 2011.

(21) Díaz, L.; Bujons, J.; Casas, J.; Llebaria, A.; Delgado, A. Click Chemistry Approach to New N-Substituted Aminocyclitols as Potential Pharmacological Chaperones for Gaucher Disease. *J*. *Med*. *Chem*. **2010**, *53* (14), 5248–5255.

(22) Díaz, L.; Casas, J.; Bujons, J.; Llebaria, A.; Delgado, A. New Glucocerebrosidase Inhibitors by Exploration of Chemical Diversity of N-Substituted Aminocyclitols Using Click Chemistry and in Situ Screening. *J*. *Med*. *Chem*. **2011**, *54* (7), 2069–2079.

(23) Pittolo, S.; Gómez-Santacana, X.; Eckelt, K.; Rovira, X.; Dalton, J.; Goudet, C.; Pin, J.-P.; Llobet, A.; Giraldo, J.; Llebaria, A.; et al. An Allosteric Modulator to Control Endogenous G Protein-Coupled Receptors with Light. *Nat Chem Biol* **2014**, *10* (10), 813–815.

(24) Argiriadi, M. A.; Banach, D.; Radziejewska, E.; Marchie, S.; DiMauro, J.; Dinges, J.; Dominguez, E.; Hutchins, C.; Judge, R. A.; Queeney, K.; et al. Creation of a S1P Lyase Bacterial Surrogate for Structure-Based Drug Design. *Bioorg*. *Med*. *Chem*. *Lett*. **2016**, *26* (9), 2293–2296.

(25) Dinges, J.; Harris, C. M.; Wallace, G. A.; Argiriadi, M. A.; Queeney, K. L.; Perron, D. C.; Dominguez, E.; Kebede, T.; Desino, K. E.; Patel, H.; et al. Hit-to-Lead Evaluation of a Novel Class of Sphingosine 1-Phosphate Lyase Inhibitors. *Bioorg*. *Med*. *Chem*. *Lett*. **2016**, *26* (9), 2297–2302.

(26) Nervall, M.; Hanspers, P.; Carlsson, J.; Boukharta, L.; Åqvist, J. Predicting Binding Modes from Free Energy Calculations. *J*. *Med*. *Chem*. **2008**, *51* (9), 2657–2667.

(27) Deniz, U.; Ozkirimli, E.; Ulgen, K. O. A Systematic Methodology for Large Scale Compound Screening: A Case Study on the Discovery of Novel S1PL Inhibitors. *J*. *Mol*. *Graph*. *Model*. **2016**, *63*, 110–124.

3.1.6 Annex

Chart 3.1.1. Hits from virtual screening targeting the anion binding site of 3MAD. The 3–hydroxypyridine group from the PLP cofactor and the imino group between the essential Lys311 residue and PLP were both considered in their neutral state. Names of compounds and their Glide XP scores are shown.

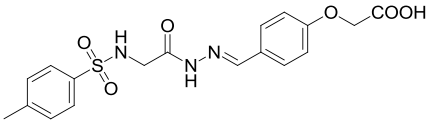

Sigma–Aldrich (SALOR) R125830
Docking score: –10.475

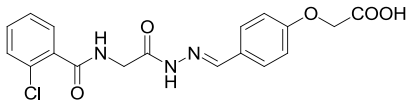

Sigma–Aldrich (SALOR) R123544
Docking score: –10.45

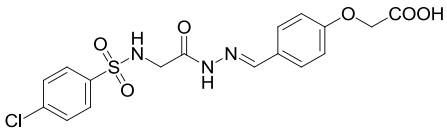

Sigma–Aldrich (SALOR) R123889
Docking score: –10.157

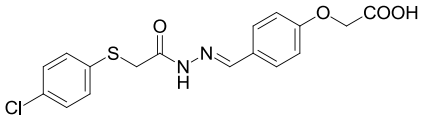

TimTec ST019382
Docking score: –10.142

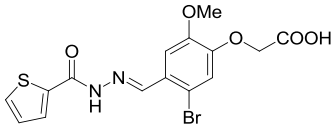

Chemstar CHS 1581259
Docking score: –10.111

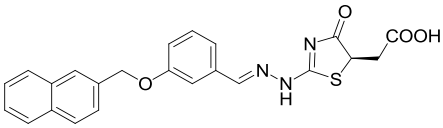

Chembridge 6641005
Docking score: –10.063

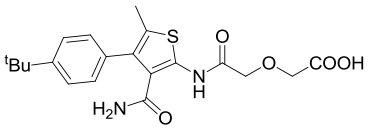

Chem T&I IVK/0000160
Docking score: –9.941

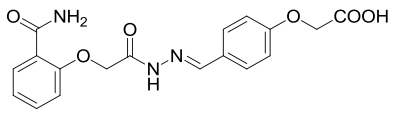

Akos OWH–AU33–M447
Docking score: –9.866

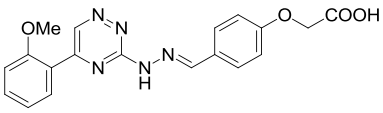

Chemdiv 4896–4529
Docking score: –9.82

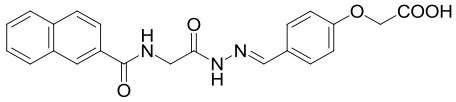

Sigma–Aldrich (SALOR) R121541
Docking score: –9.713

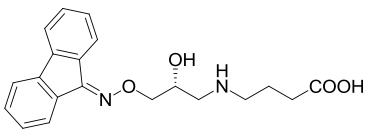

Princeton Biomolecular OSSK–474336
Docking score: –9.657

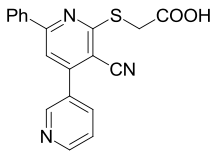

Labotest LT00234781
Docking score: –9.655

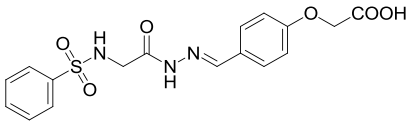

A–Synthese–Biotech EX–03254
Docking score: –9.572

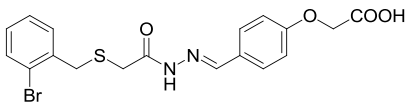

Chembridge 5627425
Docking score: –9.491

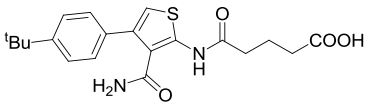

Chem T&I NSB–0096867
Docking score: –9.491

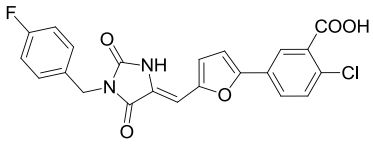

Chembridge 7124611
Docking score: –9.488

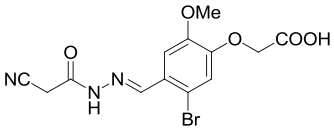

Chemstar CHS 1580328
Docking score: –9.41

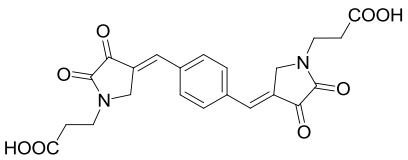

BiotechCA 376
Docking score: –9.373

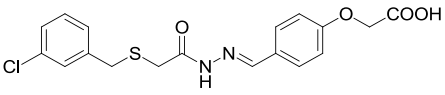

Chembridge 5627698
Docking score: –9.361

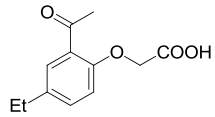

Otava 7020020679
Docking score: –9.342

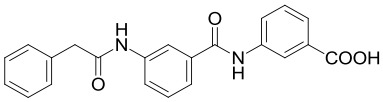

Chemdiv 2746–0238
Docking score: –9.273

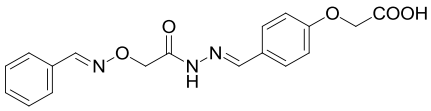

Labotest LT00245797
Docking score: –9.269

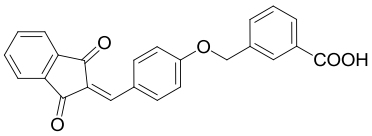

Chembridge 6222465
Docking score: –9.188

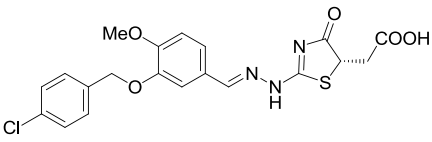

Chemdiv 4405–0798
Docking score: –9.182

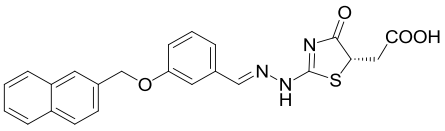

Chembridge 6663800
Docking score: –9.164

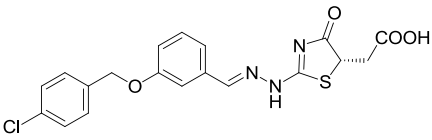

Chembridge 6664643
Docking score: –9.116

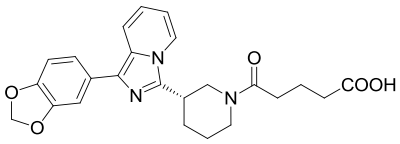

Biofocus 144–5942–1003–6684
Docking score: –9.114

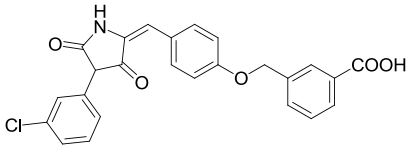

Chembridge 7377768
Docking score: –9.102

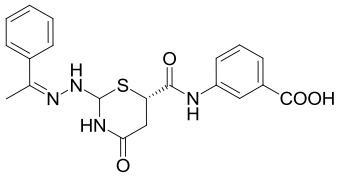

Asinex BAS 02248792
Docking score: –9.1

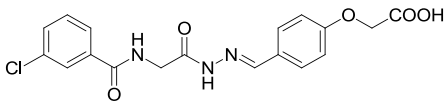

Sigma–Aldrich (SALOR) R125067
Docking score: –9.098

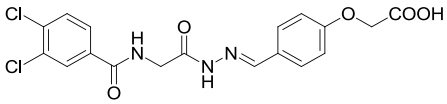

Sigma–Aldrich (SALOR) L302635
Docking score: –9.092

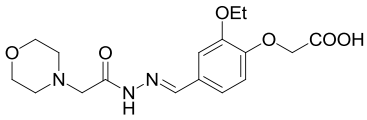

Specs AN-988/40680096
Docking score: –9.089

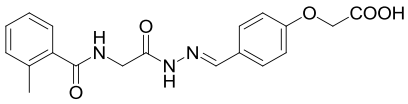

Sigma–Aldrich (SALOR) L381225
Docking score: –9.084

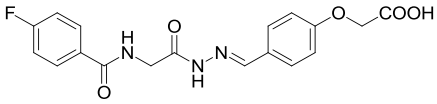

Sigma–Aldrich (SALOR) L302503
Docking score: –9.066

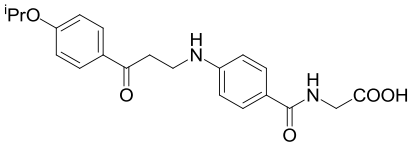

Princeton Biomolecular OSSK–484339
Docking score: –9.062

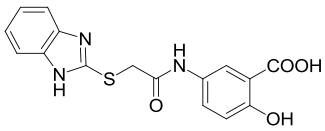

Nanosyn NS66152
Docking score: –9.049

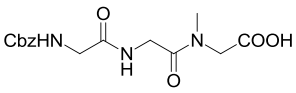

BiotechCA 8498
Docking score: –9.039

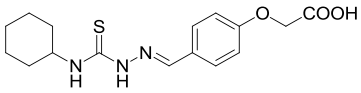

Sigma–Aldrich (SALOR) R126012
Docking score: –8.996

Chart 3.1.2. Hits from virtual screening targeting the anion binding site of 4Q6R. The 3–hydroxypyridine group from the PLP cofactor and the imino group between the essential Lys353 residue and PLP were both considered in their neutral state. Names of compounds and their Glide XP scores are shown.

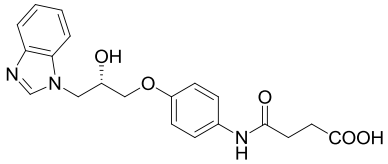

Chembridge 7978434
Docking score: –10.541

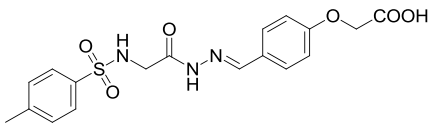

Sigma–Aldrich (SALOR) R125830
Docking score: –10.506

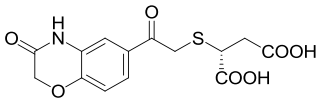

Enamine T0510–2655
Docking score: –10.214

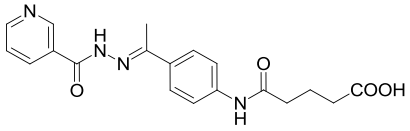

Chem T&I NSB–0095229
Docking score: –10.214

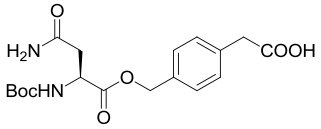

Maybridge JFD 01556
Docking score: –10.178

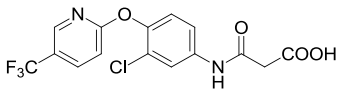

Bionet 1K–004
Docking score: –10.147

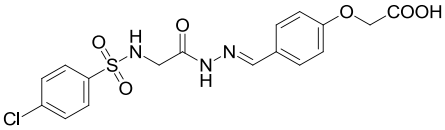

Sigma–Aldrich (SALOR) R123889
Docking score: –10.117

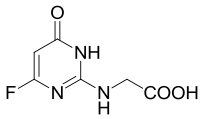

Chemdiv 1545–0020
Docking score: –10.104

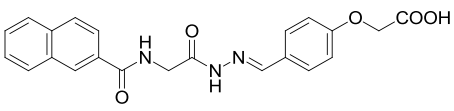

Sigma–Aldrich (SALOR) R121541
Docking score: –10.098

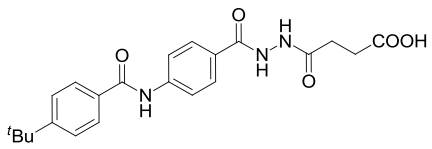

Chem T&I ARAK0131790
Docking score: –9.936

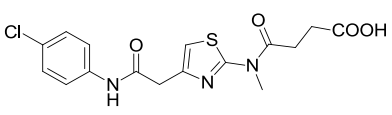

Asinex ASN 04371853
Docking score: –9.723

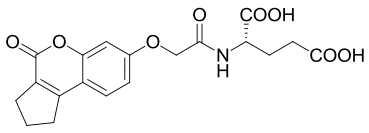

Princeton Biomolecular OSSK–456460
Docking score: –9.684

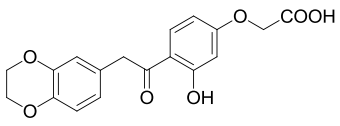

Nanosyn NS59314
Docking score: –9.551

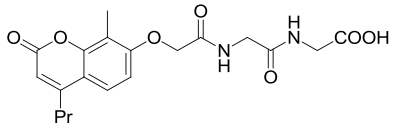

Princeton Biomolecular OSSK–295468
Docking score: –9.547

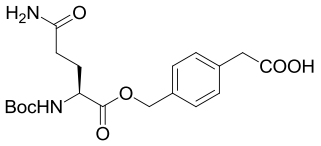

Maybridge JFD 01584
Docking score: –9.353

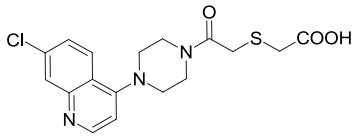

Maybridge HTS 01446
Docking score: –9.237

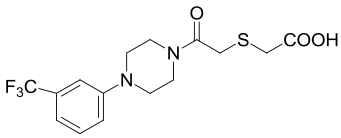

Chem T&I UZI/4036992
Docking score: –9.196

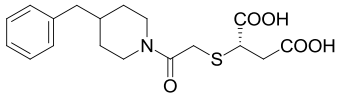

Enamine T0511–6556
Docking score: –9.174

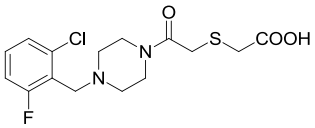

Maybridge HTS 01677
Docking score: –9.134

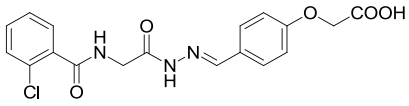

Sigma–Aldrich (SALOR) R123544
Docking score: –9.126

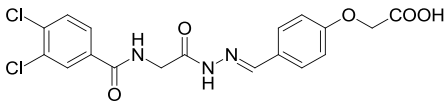

Sigma–Aldrich (SALOR) L302635
Docking score: –9.042

Chart 3.1.3. Hits from virtual screening targeting the anion binding site of 3MAD. The 3–hydroxypyridine group from the PLP cofactor and the imino group between the essential Lys311 residue and PLP were both considered in their ionized state. Names of compounds and their Glide XP scores are shown.

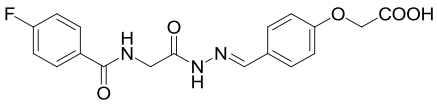

Sigma–Aldrich (SALOR) L302503
Docking score: –11.045

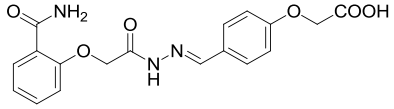

Akos OWH–AU33–M447
Docking score: –10.407

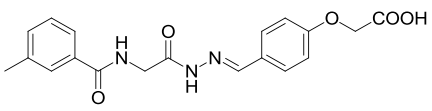

Sigma–Aldrich (SALOR) R125091
Docking score: –10.243

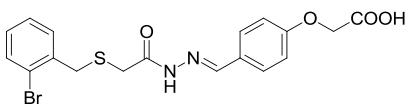

Chembridge 5627425
Docking score: –9.999

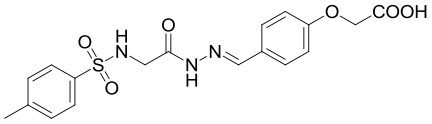

Sigma–Aldrich (SALOR) R125830
Docking score: –9.912

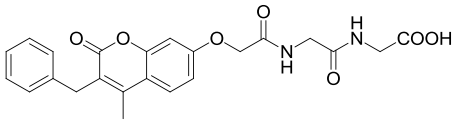

Princeton Biomolecular OSSK–295501
Docking score: –9.747

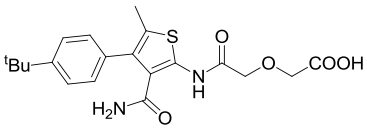

Chem T&I IVK/0000160
Docking score: –9.732

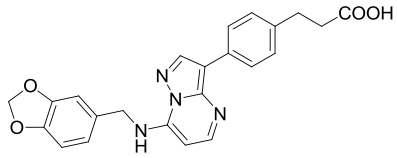

Biofocus 179–0236–0082
Docking score: –9.678

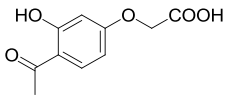

Labotest LT00239332
Docking score: –9.659

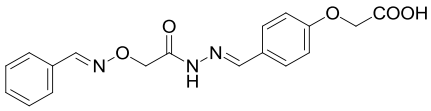

Labotest LT00245797
Docking score: –9.542

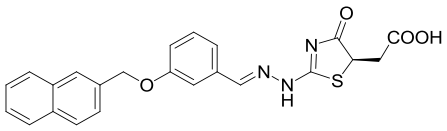

Chembridge 6641005
Docking score: –9.495

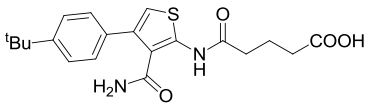

Chem T&I NSB–0096867
Docking score: –9.483

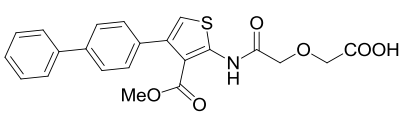

Chem T&I UZI/4040800
Docking score: –9.319

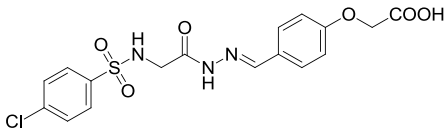

Sigma–Aldrich (SALOR) R123889
Docking score: –9.307

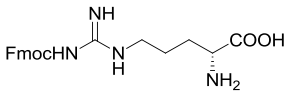

Labotest LT00441068
Docking score: –9.255

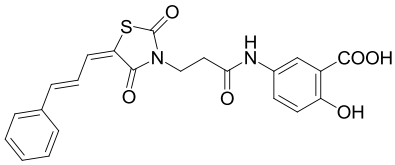

InterBioScreen STOCK5S–92848
Docking score: –9.244

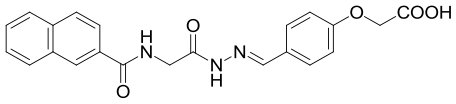

Sigma–Aldrich (SALOR) R121541
Docking score: –9.174

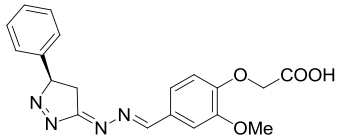

Chemdiv 6231–0020
Docking score: –9.116

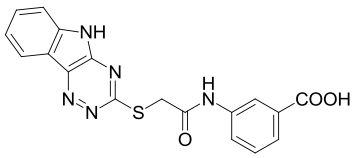

Asinex ASN 02992426
Docking score: –9.062

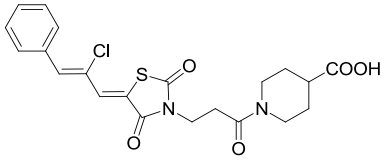

InterBioScreen STOCK5S–85371
Docking score: –8.96

Chart 3.1.4. Hits from virtual screening targeting the anion binding site of 4Q6R. The 3–hydroxypyridine group from the PLP cofactor and the imino group between the essential Lys353 residue and PLP were both considered in their ionized state. Names of compounds and their Glide XP scores are shown.

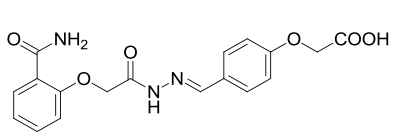

Akos OWH–AU33–M447
Docking score: –10.725

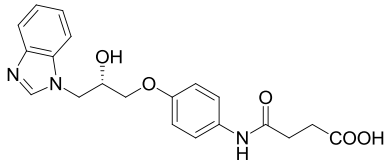

Chembridge 7978434
Docking score: –10.684

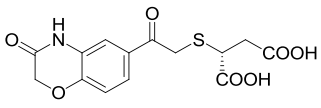

Enamine T0510–2655
Docking score: –10.45

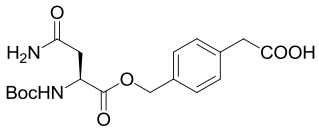

Maybridge JFD 01556
Docking score: –10.078

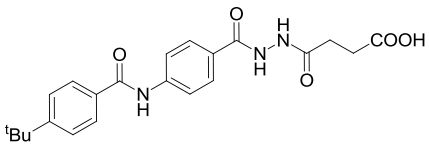

Chem T&I ARAK0131790
Docking score: –9.947

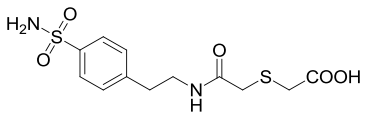

Chem T&I UZI/4036741
Docking score: –9.732

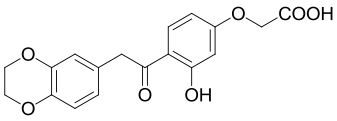

Nanosyn NS59314
Docking score: –9.539

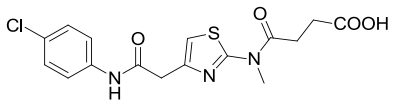

Asinex ASN 04371853
Docking score: –9.451

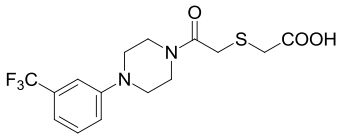

Chem T&I UZI/4036992
Docking score: –9.438

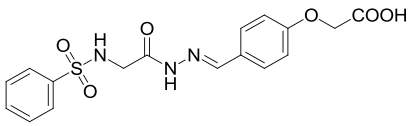

A–Synthese–Biotech EX–03254
Docking score: –9.364

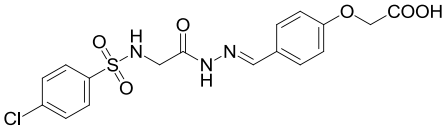

Sigma–Aldrich (SALOR) R123889
Docking score: –9.34

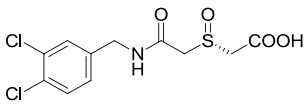

Bionet 5H–335S
Docking score: –9.267

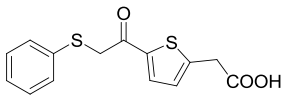

Maybridge KM 05951
Docking score: –9.151

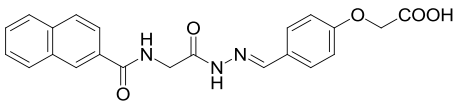

Sigma–Aldrich (SALOR) R121541
Docking score: –9.089

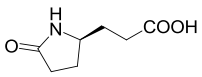

Princeton Biomolecular OSSK–427740
Docking score: –9.084

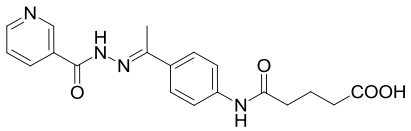

Chem T&I NSB–0095229
Docking score: –9.079

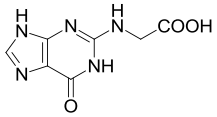

Pharmeks PHAR072306
Docking score: –9.055

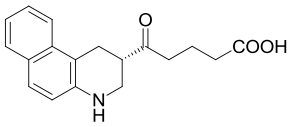

Chemical Block A3915/0166560
Docking score: –9.05

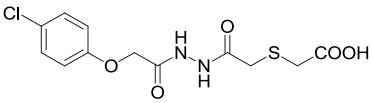

Enamine T0509–0851
Docking score: –9.044

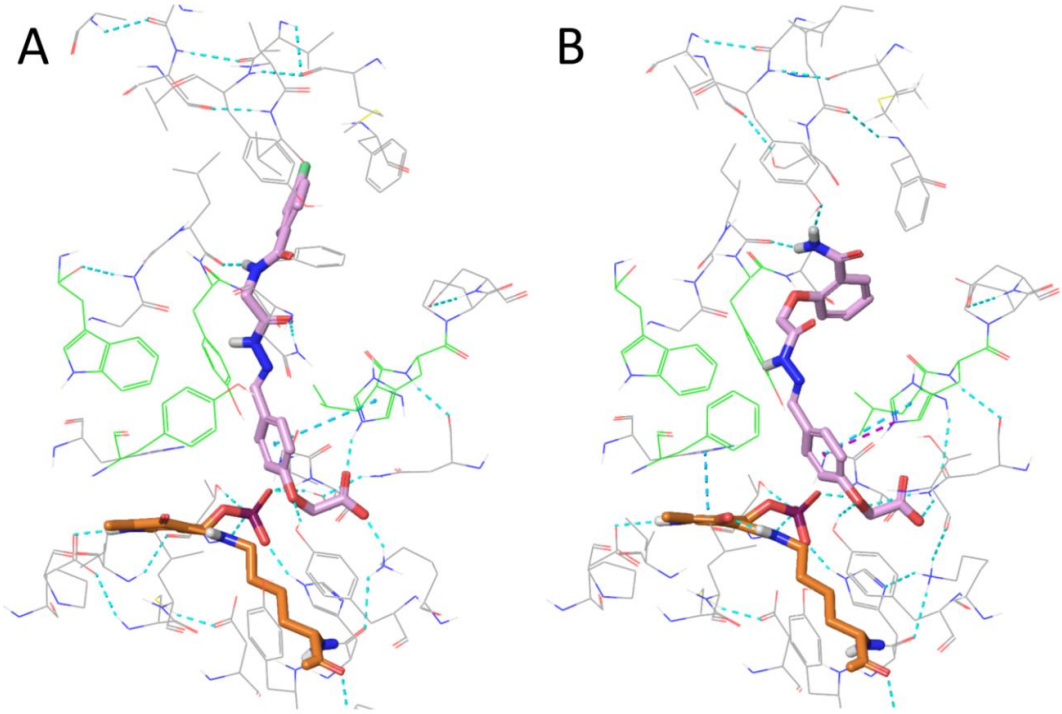

Figure 3.1.16. (A) Best docked pose for compound Sigma–Aldrich (SALOR) L302503 (see Chart 3.1.3) bound to StS1PL. (B) Best docked pose for compound Akos OWH–AU33–M447 (see Chart 3.1.4) bound to hS1PL. The 3–hydroxypyridine group from the PLP cofactor and the imino group between the essential Lys residue and PLP were both considered in their ionized state. The PLP cofactor bound to the essential lysine (thick, orange), the residues that constitute the hydrophobic patch (green) and the ligands (thick, light purple) are highlighted.

Chart 3.1.5. Hits from virtual screening/induced fit docking targeting the anion binding site of 3MAD. The 3–hydroxypyridine group from the PLP cofactor and the imino group between the essential Lys311 residue and PLP were both considered in their neutral state. Names of compounds, and their Glide XP and IFD scores are shown.

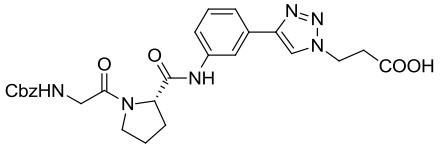

RBM7–030
Docking score: –17.506
IFDscore: –1918.783

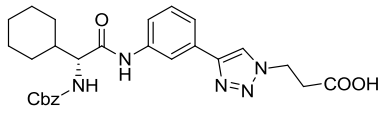

RBM7–046
Docking score: –16.242
IFDscore: –1916.286

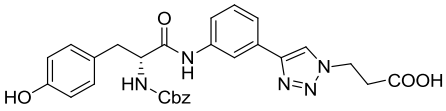

RBM7–048
Docking score: –15.893
IFDscore: –1915.981

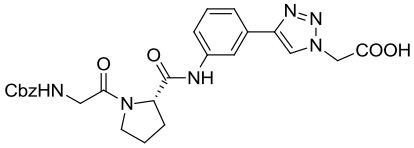

RBM7–031
Docking score: –15.694
IFDscore: –1914.717

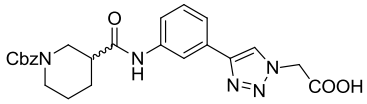

RBM7–047
Docking score: –15.511
IFDscore: –1912.283

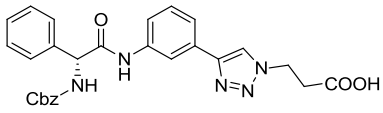

RBM7–045
Docking score: –15.408
IFDscore: –1913.314

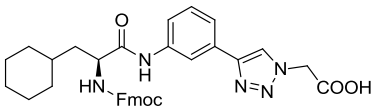

RBM7–044
Docking score: –15.355
IFDscore: –1913.598

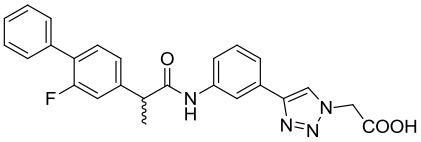

RBM7–042
Docking score: –14.152
IFDscore: –1909.293

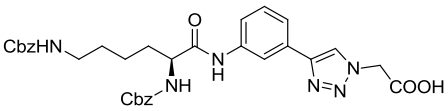

RBM7–043
Docking score: –14.019
IFDscore: –1916.836

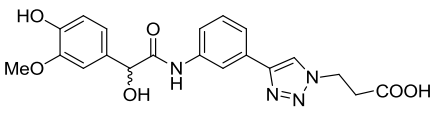

RBM7–049
Docking score: –13.629
IFDscore: –1910.676

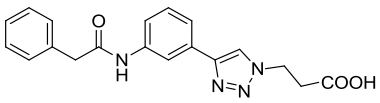

RBM7–067
Docking score: –13.589
IFDscore: –1908.111

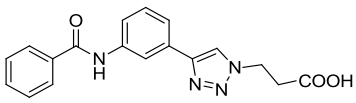

RBM7–066
Docking score: –13.554
IFDscore: –1908.181

Chart 3.1.6. Hits from virtual screening/induced fit docking targeting the anion binding site of 4Q6R. The 3–hydroxypyridine group from the PLP cofactor and the imino group between the essential Lys353 residue and PLP were both considered in their neutral state. Names of compounds and their Glide XP and IFD scores are shown.

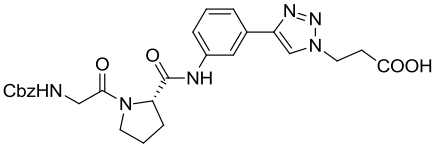

RBM7–030
Docking score: –16.421
IFDscore: –1929.944

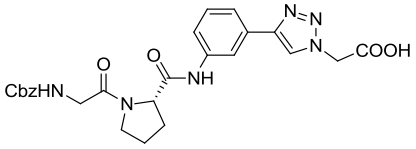

RBM7–031
Docking score: –14.758
IFDscore: –1921.526

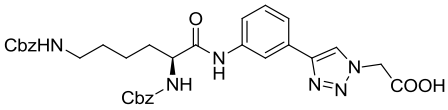

RBM7–043
Docking score: –14.033
IFDscore: –1929.027

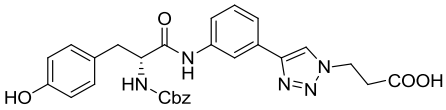

RBM7–048
Docking score: –13.706
IFDscore: –1920.181

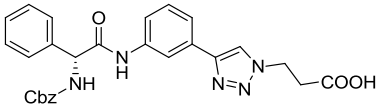

RBM7–045
Docking score: –13.553
IFDscore: –1918.46

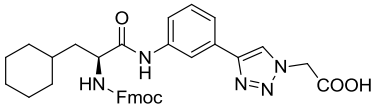

RBM7–044
Docking score: –13.149
IFDscore: –1917.512

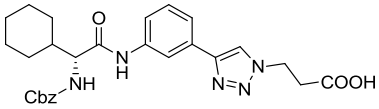

RBM7–046
Docking score: –13.03
IFDscore: –1918.507

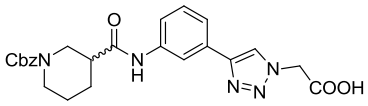

RBM7–047
Docking score: –12.759
IFDscore: –1914.839

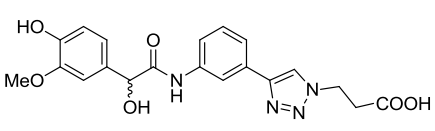

RBM7–049
Docking score: –12.61
IFDscore: –1914.152

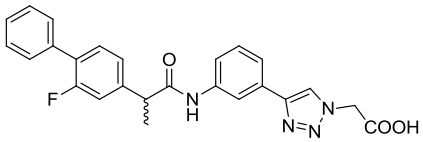

RBM7–042
Docking score: –12.364
IFDscore: –1912.363

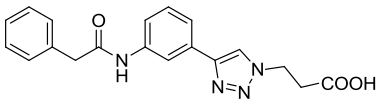

RBM7–067
Docking score: –10.581
IFDscore: –1912.063

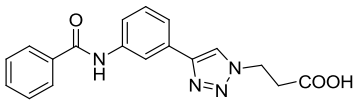

RBM7–066
Docking score: –10.545
IFDscore: –1910.988

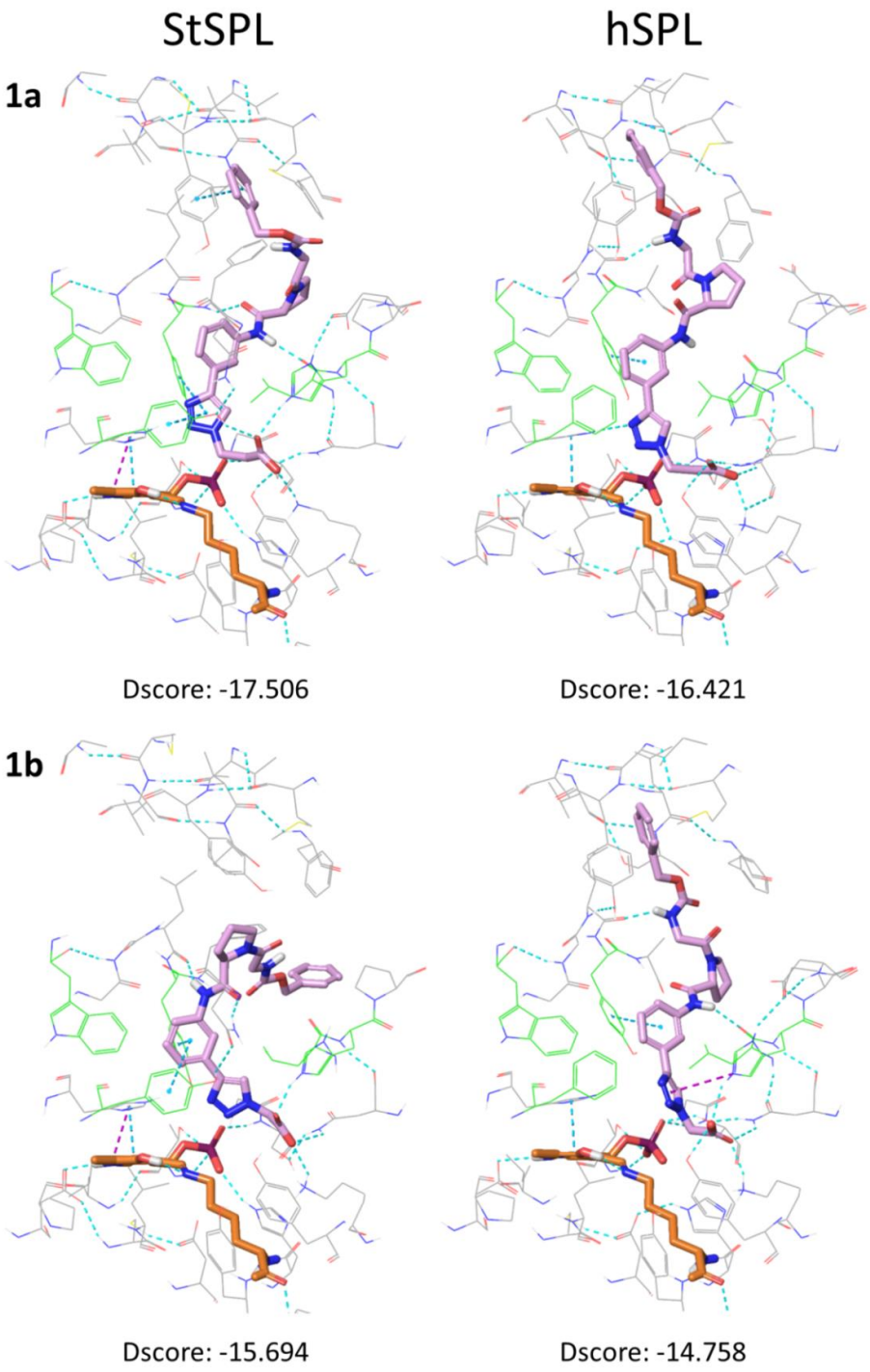

Figure 3.1.17. Docked poses for hits **1a** (**RBM7–030**) and **1b** (**RBM7–031**) bound to StS1PL and hS1PL.

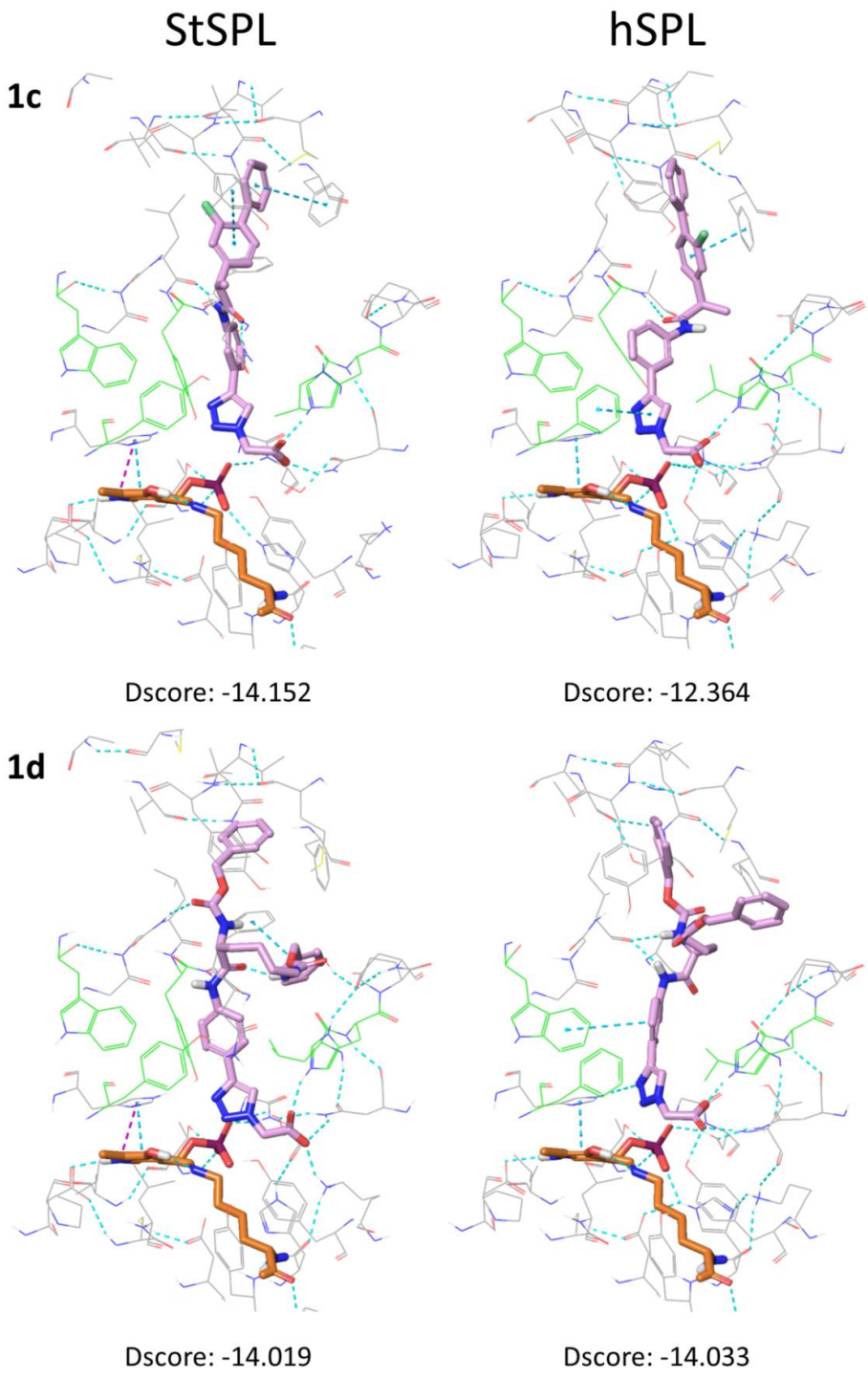

Figure 3.1.18. Docked poses for hits **1c** (**RBM7–042**) and **1d** (**RBM7–043**) bound to StS1PL and hS1PL.

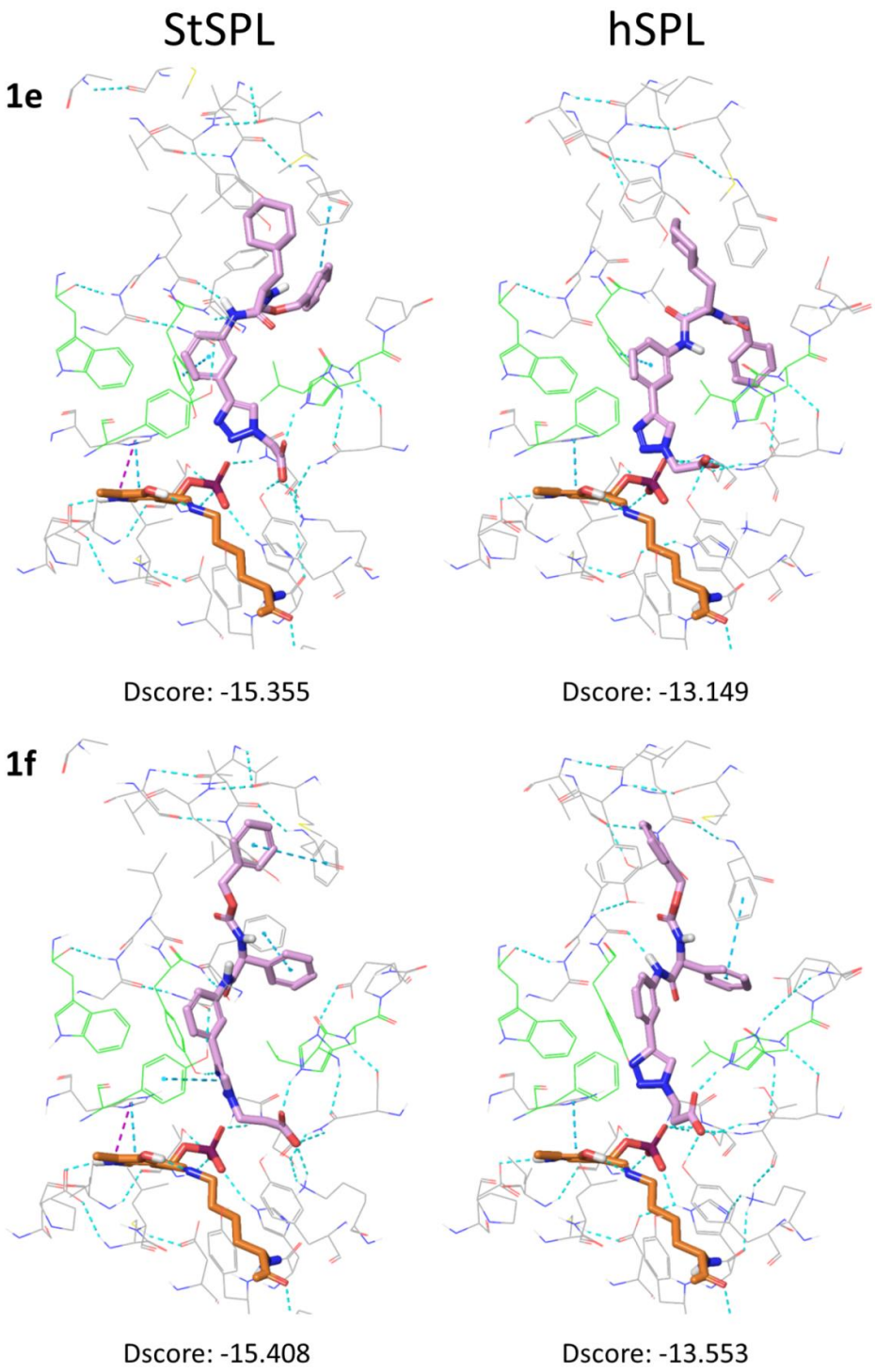

Figure 3.1.19. Docked poses for hits **1e** (**RBM7–044**) and **1f** (**RBM7–045**) bound to StS1PL and hS1PL.

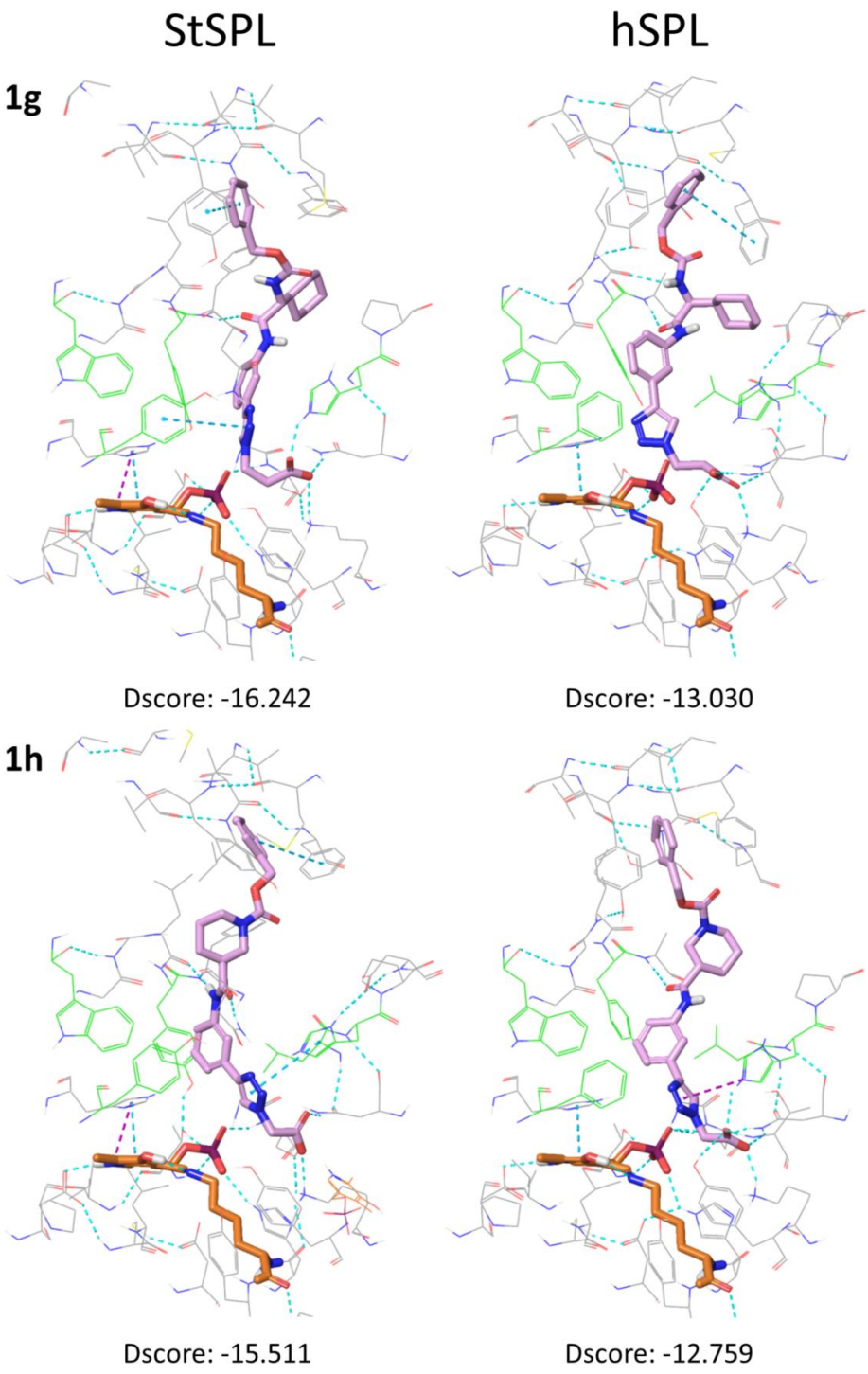

Figure 3.1.20. Docked poses for hits **1g** (**RBM7–046**) and **1h** (**RBM7–047**) bound to StS1PL and hS1PL.

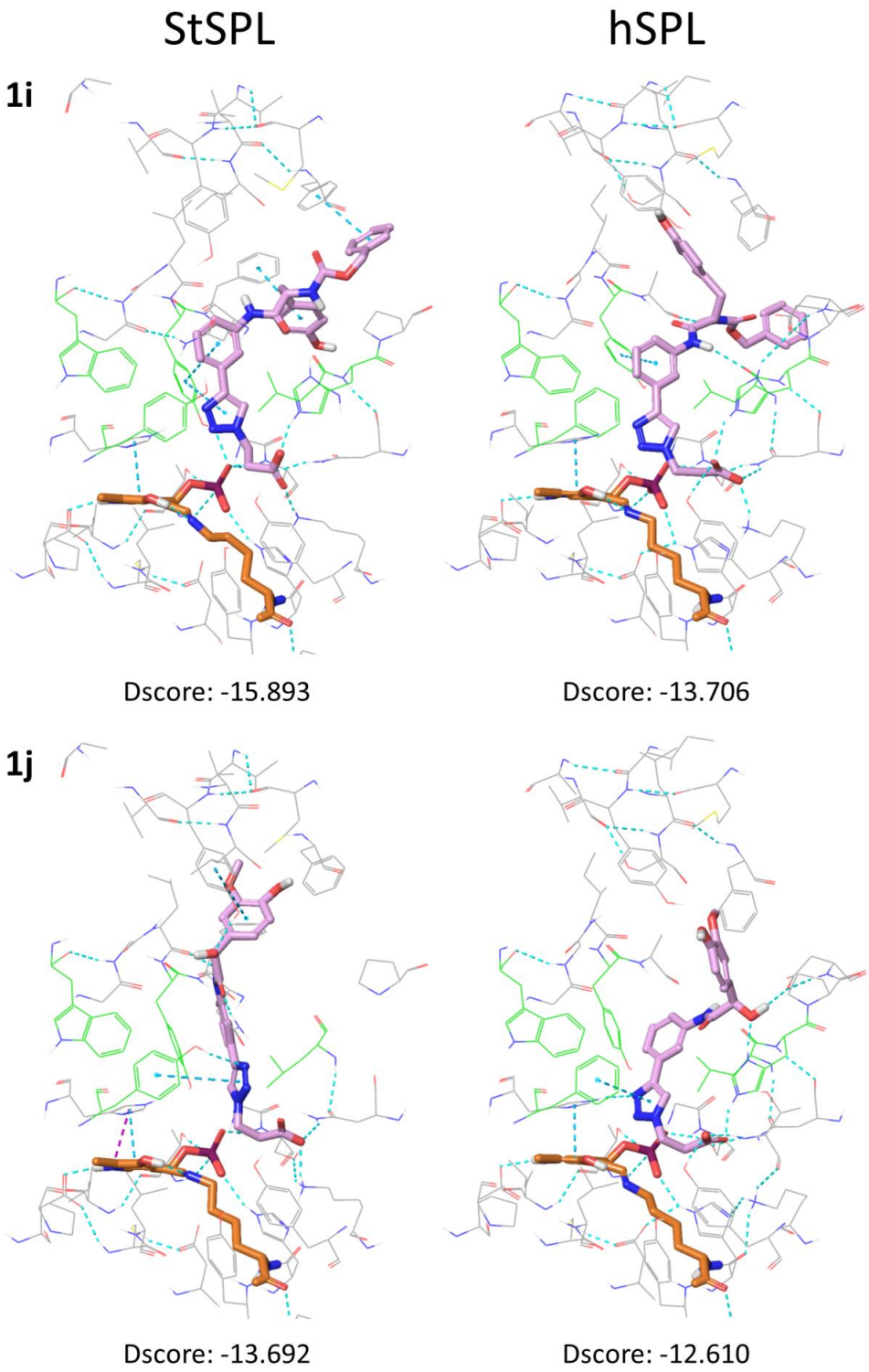

Figure 3.1.21. Docked poses for hits **1i** (**RBM7–048**)and **1j** (**RBM7–049**) bound to StS1PL and hS1PL.

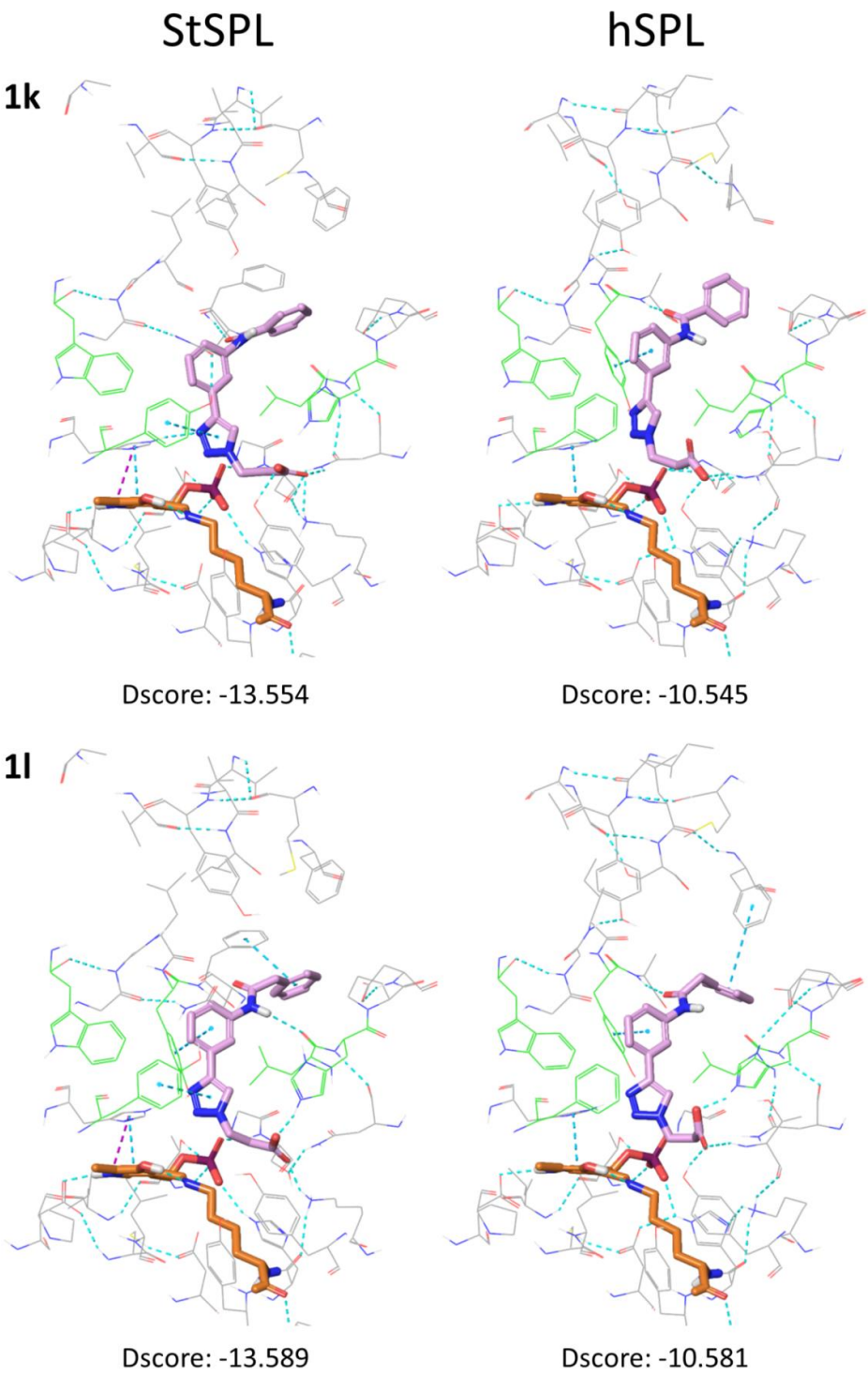

Figure 3.1.22. Docked poses for hits **1k** (**RBM7–066**) and **1l** (**RBM7–067**) bound to StS1PL and hS1PL.

3.2 New S1PL inhibitors from non–reactive enzyme reaction intermediates and substrate analogs

3.2.1 Introduction

Based on structural, biochemical and mutagenesis studies performed with bacterial and yeast S1PL, Bourquin *et al.*[1] postulated a plausible mechanism for the S1PL reaction, which is shown in Figure 3.2.1. Initially, the incoming S1P replaces the catalytic Lys in the internal aldimine **12** to form the external aldimine **13** (step 1). Proton abstraction at the C3–OH initiates the retro–aldol cleavage (step 2), which results in the release of the corresponding fatty aldehyde. Unfortunately, the identity of the basic residue involved in the deprotonation step (depicted as "B:" in Figure 3.2.1) is still unknown and its elucidation will require further structural and biochemical studies. Subsequent reprotonation of the transient quinonoid intermediate **14** leads to the external aldimine **15** (step 3). According to the authors, either the catalytic StS1PL K311 or the nearby Y105 (K353 and Y150, respectively, for hS1PL), may act as proton donors in this step. Finally, after hydrolysis of **15**, EAP is released and the internal aldimine **12** is formed again for a second enzyme turnover (step 4).

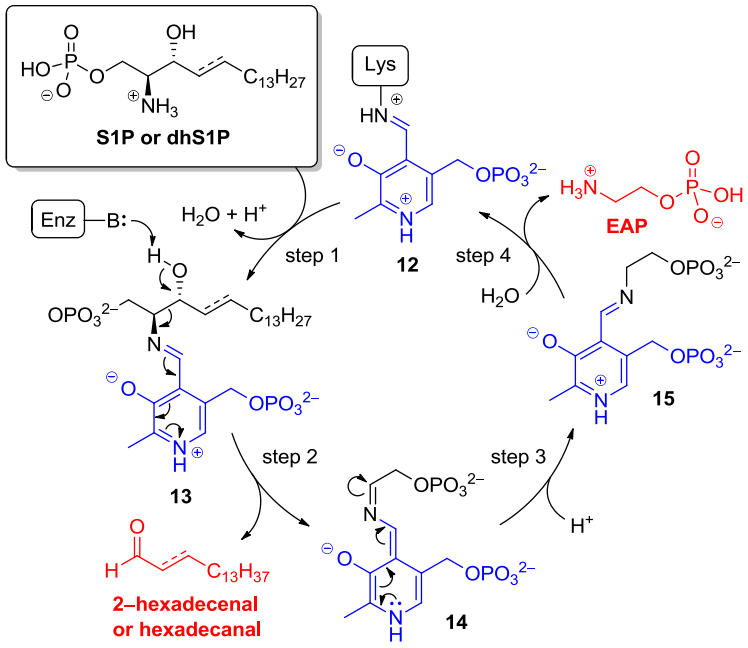

Figure 3.2.1. Catalytic cycle of sphingosine–1–phosphate lyase (S1PL). 1) S1P or dhS1P replaces Lys from **12** to form the external aldimine **13**; 2) Retro–aldol cleavage with generation of 2–hexadecenal or hexadecanal and the quinonoid intermediate **14**; 3) Formation of the aldimine system **15** by protonation of **14**; 4) Hydrolysis of **15** with release of EAP and final restoration of **12**.

An identical mechanism is accepted for the alternative S1PL substrate 4,5–dihydro–S1P (dhS1P), giving rise to EAP and hexadecanal as reaction products.

As introduced previously in Section 1.3.3.1, the repertoire of available S1PL inhibitors structurally related to the enzyme substrate is scarce. In this context, 1–deoxysphinganine–1–phosphonate and 2–vinyl–dhS1P are the only ones reported in the literature. The structurally related FTY720, a well–known S1P receptor agonist after its enantioselective phosphorylation to the (*S*)–isomer, has also been reported as a modest S1PL inhibitor *in vitro*. On the other hand, 4–deoxypyridoxine (DOP) has been described as a functional S1PL inhibitor *in vivo*, as well as THI and related analogs, whose mechanism of action have been controversial (see Section 1.3.3.2).

3.2.2 Design of new mechanism-based S1PL inhibitors

As a result of our interest in the development of sphingolipid modulators by targeting S1P metabolism,[2] we undertook the design of new S1PL inhibitors based on S1PL mechanistic considerations. Thus, compound **RBM7–001** (Figure 3.2.2) was designed as a non–hydrolyzable analog of the putative intermediate **15** (Figure 3.2.1), since the labile imine group is replaced by a hydrolytically stable secondary amine group. In contrast, compounds **RBM7–012** and **RBM7–032** (Figure 3.2.2) were designed as non–reactive analogs of the intermediate aldimine **13** (Figure 3.2.1). In this case, we envisaged that the absence of an imine group would preclude the retro–aldol cleavage, since the pyridinium ring of the PLP moiety is not conjugated with the nitrogen atom of S1P. Interestingly, dephosphorylated **RBM7–032** (compound **16**, Figure 3.2.2) had been reported in the literature as a potential S1PL inhibitor.[3] Compound **16** was expected to undergo SK1 or SK2 directed phosphorylation *in vivo* in order to generate the potentially active **RBM7–032**. However, its lack of activity in cellular and *in vivo* assays was attributed to an inadequate phosphorylation. As PLP analogs, compounds **RBM7–001**, **RBM7–012**, and **RBM7–032** were expected to displace the cofactor in the enzyme active site.

In a second approach, a series of configurationally defined azido analogs of both enzyme substrates (S1P and dhS1P) were designed as non–reactive, potential S1PL competitive inhibitors (compounds **RBM7–089**, **RBM7–098**, **RBM7–103**, and **RBM7–114**, Figure 3.2.2). Since the C2 amino group is replaced by an azido group,

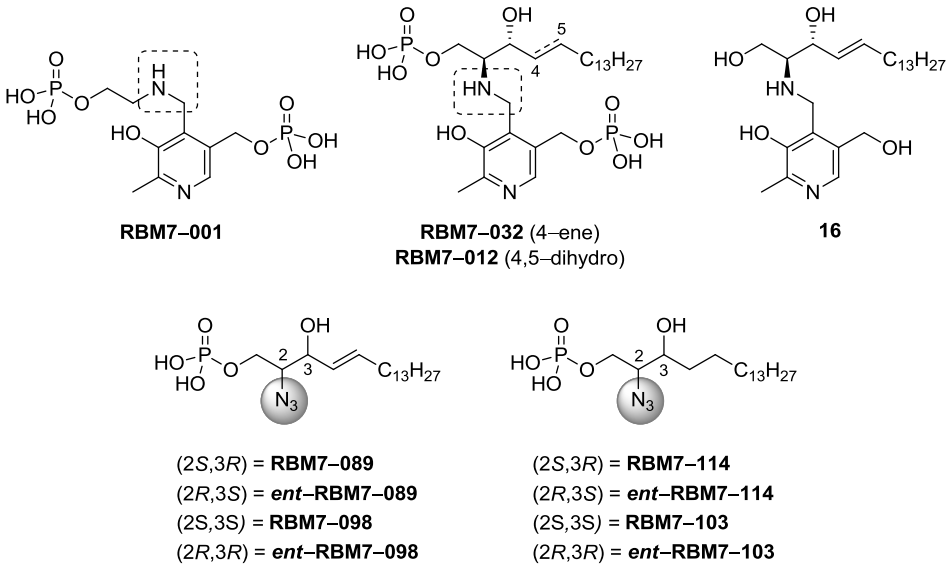

Figure 3.2.2. Non–reactive S1PL reaction intermediates and substrates.

formation of the external aldimine **13** is expected to be precluded at the enzyme active site. Apart from the inherent lack of reactivity towards imine formation and its remarkable stability *in cellulo*,[4] the azido group has also been used as a "pseudohalide" in drug design.[5] In terms of approximate size, polarity and electronic character, the azido group has been proposed to resemble a bromo substituent. As a consequence, the replacement of the amino group present in S1P with an azido group is expected to cause a significant effect in the electronic properties and on the interactions with the enzyme active site without disturbing the overall shape of the molecule. Moreover, to gain insight into the enzyme stereoselectivity towards this type of analogs, all the configurations around the C2 and C3 carbon atoms have been considered (*i.e.* compounds ***ent*–RBM7–089**, ***ent*–RBM7–098**, ***ent*–RBM7–103** and ***ent*–RBM7–114**).

3.2.3 Synthesis of PLP–derivatives RBM7–001, RBM7–012 and RBM7–032

Compounds **RBM7–001**, **RBM7–012** and **RBM7–032** were obtained as outlined in Scheme 3.2.1 by reductive amination of PLP with either *O*–phosphorylethanolamine, dhS1P or S1P, respectively (for the synthesis of S1P and dhS1P see Section 3.2.3.1). Following an adaptation of reported protocols,[6,7] the dipotassium salts of PLP and the corresponding amines were initially generated *in situ* using KO^{t}Bu, in order to ensure their total solubility. After the consumption of the starting amine was evidenced by ^{1}H NMR, reduction of the corresponding imines with $NaBH_4$ afforded the desired

diphosphates in acceptable overall yields, together with pyridoxine 5'–phosphate (compound **RBM7–002**, Scheme 3.2.1), which was also included in our S1PL inhibition assays due to its high structural similarity with PLP and DOP. On the other hand, crude diphosphates **RBM7–012** and **RBM7–032** presented a very low solubility in different organic solvents and in aqueous mixtures. Nevertheless, preparation of the corresponding triethylammonium salts afforded highly water–soluble species, which could be properly characterized in terms of chemical identity and biological activity (see Section 5.1.4.1 for experimental details).

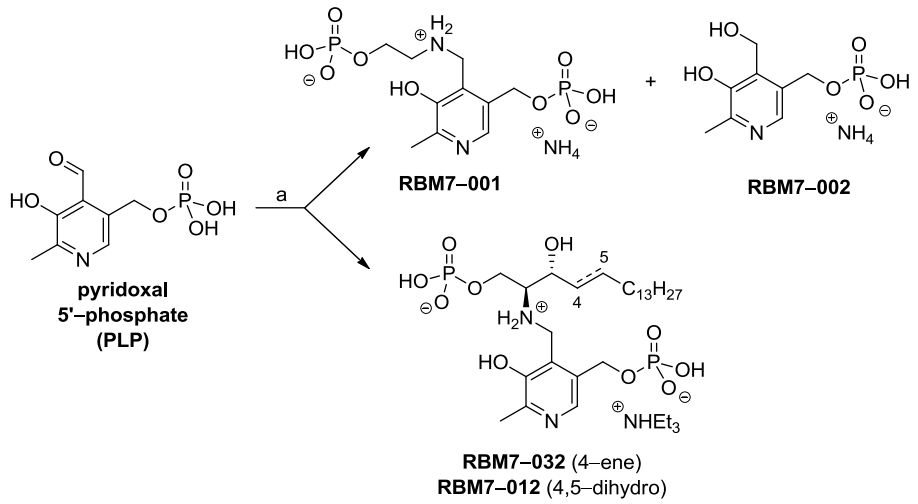

Scheme 3.2.1. Synthesis of PLP–derivatives. Reagents and conditions: (a) (i) selected amine (*O*-Phosphorylethanolamine for **RBM7–001**, S1P for **RBM7–032** and dhS1P for **RBM7–012**), KO^{t}Bu, MeOH, reflux (ii) $NaBH_4$, MeOH, 0 ºC to rt, 79 % for **RBM7–001**, 74 % for **RBM7–032**, 71 % for **RBM7–012**.

3.2.3.1 Synthesis of S1P and dhS1P

Zwitterionic aminophosphates S1P and dhS1P were prepared from their corresponding *N*–Boc protected aminodiols **RBM7–025** and **RBM7–009**, as shown in Scheme 3.2.2. Firstly, compounds **RBM7–025** and **RBM7–009**, whose synthesis will be detailed in Section 3.2.5, were site–selectively phosphorylated at the primary hydroxyl using dimethyl chlorophosphate[8] to give phosphate triesters **RBM7–026** and **RBM7–010** in good yields. In both cases, small amounts of other phosphorylated byproducts were detected by ^{31}P NMR of the crude reaction mixtures. In comparison with **RBM7–009**, phosphorylation of diol **RBM7–025** occurred with lower site–selectivity, probably as a

result of the higher nucleophilicity of the C3 allylic alcohol of **RBM7–025** in comparison with that of the saturated secondary alcohol of **RBM7–009** (see Figure 3.2.3). However, pure dimethyl phosphates were successfully obtained after careful purification of the crude reaction mixtures by flash chromatography (for the ^{31}P NMR spectra of purified compounds, see Section 7).

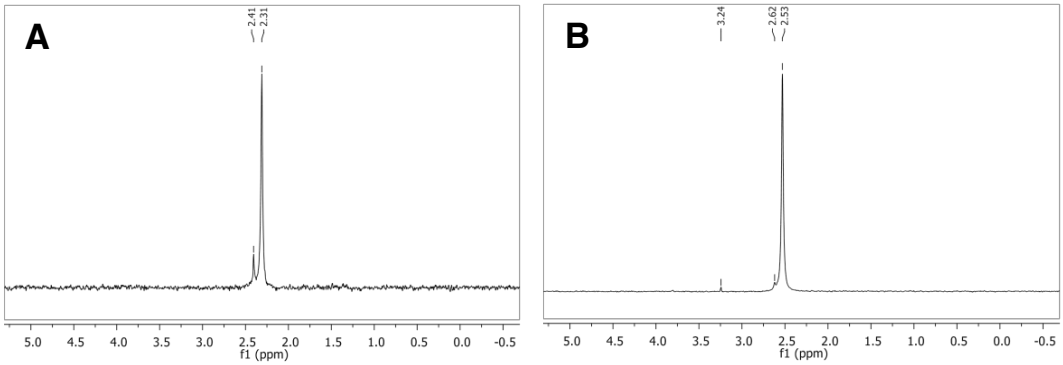

Figure 3.2.3. ^{31}P NMR spectra of crude reaction mixtures of compounds **RBM7–026** (A) and **RBM7–010** (B).

Successive TMSBr–mediated deprotection of the phosphate ester and the C2–amino groups[8] in **RBM7–026** and **RBM7–010**, gave the target aminophosphates S1P and dhS1P, respectively. Due to their high polarity and extremely low solubility, initial attempts at the purification of the crude products by flash chromatography proved fruitless. Nevertheless, recristallyzation of the crude material from THF/H_2O (2:1, v/v)[9] followed by a washing process of the resulting precipitate[10,11] gave pure S1P and dhS1P in moderate to good yields. The lower yield obtained for S1P was due to a lower recovery during the recrystallization step, since S1P presented a slightly higher solubility than its saturated analog dhS1P.

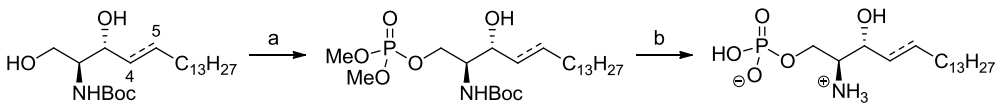

RBM7–025 (4–ene) **RBM7–009** (4,5–dihydro) | **RBM7–026** (4–ene) **RBM7–010** (4,5–dihydro) | **S1P** (4–ene) **dhS1P** (4,5–dihydro)

Scheme 3.2.2. Synthesis of S1P and dhS1P. Reagents and conditions: (a) Dimethyl chlorophosphate, *N*–methylimidazole, CH_2Cl_2, 0 ºC to rt, 76 % for **RBM7–026**, 75 % for **RBM7–010**; (b) (i) Me_3SiBr, MeCN, 0 ºC to rt (ii) MeOH/H_2O (95:5), rt, 54 % for S1P, 79 % for dhS1P.

3.2.4 Synthetic approach to the series of stereodefined azidophosphates

Our retrosynthetic analysis towards the stereomeric series of azidophosphates is depicted in Scheme 3.2.3. As described above for the synthesis of S1P and dhS1P (see section 3.2.3.1), a site–selective phosphorylation of the corresponding azidodiol derivatives was envisaged as a suitable way to access the desired compounds. The introduction of the azido group at C2 would be accomplished by diazotransfer reaction from the corresponding stereodefined amine hydrochlorides. Finally, a diastereocontrolled addition of a suitable 1–alkenyl organometallic derivative to L– or D–Garner's aldehyde would allow the construction of the differently configured sphingoid bases.

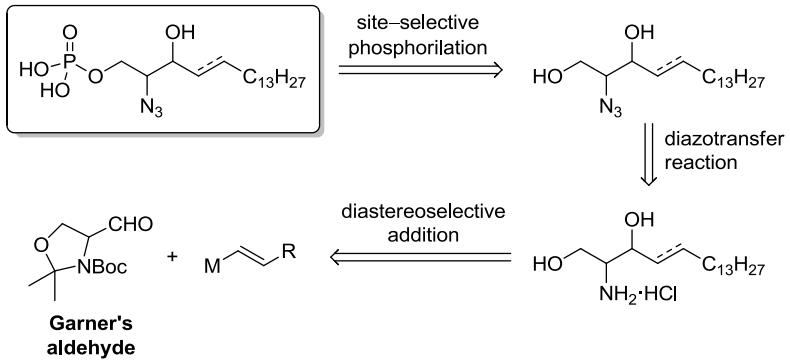

Scheme 3.2.3. Synthetic approach to the series of stereodefined azidophosphates.

3.2.5 Synthesis of sphingosines RBM7–062, RBM7–086, RBM7–095, RBM7–100 and their enantiomers

The synthesis of the desired stereodefined sphingosines started with a nucleophilic addition to L– and D– Garner's aldehydes, which were obtained over 4 steps from the corresponding enantiopure serines, according to a reported methodology.[12] Thus, the synthesis of the *anti*– adducts of the 2*S* series started with the diasteroselective addition of vinylmagneisum bromide to the L–Garner's aldehyde in THF at –78 ºC,[13,14] which gave the allylic alcohol **RBM7–023** in moderate yield (64 %) and good diastereoselectivity (dr = 86:14) (Scheme 3.2.4). In this case, both diastereomers were easily separated at this stage by flash chromatography.

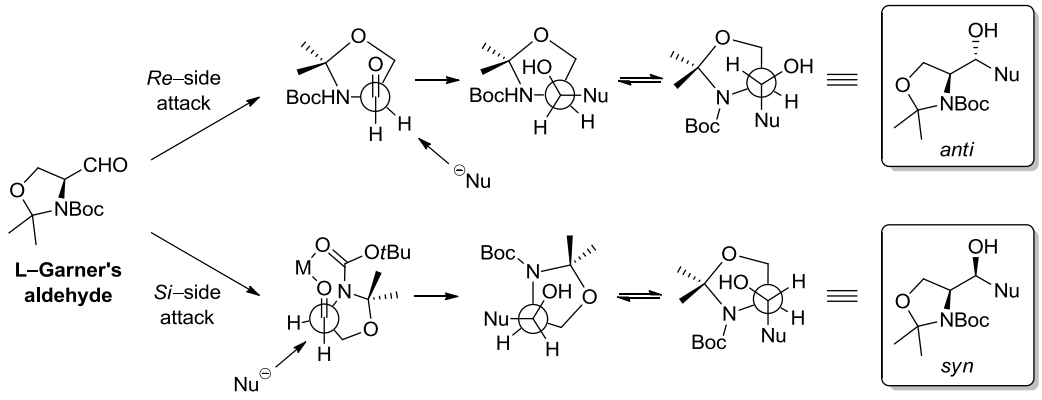

Figure 3.2.4. Stereochemical outcome of the nucleophilic addition reaction to Garner's aldehyde. Adapted from ref. 15.

The remarkable *anti*–selectivity can be rationalized with the Felkin–Anh non–chelation transition state model (see Figure 3.2.4), in which the attack of the nucleophile occurs from the sterically less hindered side (*Re*–side attack).[15] Subsequent olefin cross metathesis reaction between **RBM7–023** and 1–pentadecene[13,16] furnished alkene **RBM7–024** as an inseparable 94:6 *E*/*Z* mixture of diastereomers. Despite minor amounts of the *Z*–isomer were also detected in subsequent steps, pure *E*–isomers could be obtained by careful purification of the synthetic intermediates.

On the other hand, addition of 1–pentadecenylethylzinc to L–Garner's aldehyde in CH_2Cl_2 at –40 ºC,[17] efficiently afforded the *syn*–configured allylic alcohol **RBM7–093** in good yield (75 %) and high diastereoselectivity (dr = 93:7, only *E*). In this case, the nucleophilic organozinc derivative was generated *in situ* by a stereo– and regiospecific hydrozirconation of 1–pentadecyne using the Schwartz's reagent, followed by transmetalation of the resulting alkenylzirconocene with Et_2Zn. The major formation of the *syn* adduct can be explained by the Cram's chelation control model (see Figure 3.2.4). In this case, the chelating metal coordinates both the aldehyde and the carbamate carbonyl groups, thus forcing the nucleophile to attack from the *Si*–side with high stereocontrol.[15] Alternative mechanisms involving a coordinate delivery of the nucleophile have also been reported.[18]

Deprotection of the *N*,*O*–isopropylidene moiety of **RBM7–024** and **RBM7–093** under acidic conditions[19] yielded *anti*– and *syn*–configured *N*–Boc aminodiols **RBM7–025** and **RBM7–094** in excellent yields. In this case, both key sphingoid intermediates

proved to be spectroscopically and configurationally in agreement with reported literature data.[17,20] Further catalytic hydrogenation on Rh/Al_2O_3[21] furnished diols **RBM7–009** and **RBM7–099**, thus giving access to the 4,5–dihydro series. Finally, the acid–mediated deprotection of the Boc group of the above *N*–protected aminodiols,[4] afforded the target 2*S* sphingosines and 4,5–dihydrosphingosines, which were obtained as their corresponding amine hydrochlorides. As expected, application of the same reaction sequence from D–Garner's aldehyde led to the corresponding 2*R* enantiomeric series, namely compounds ***ent*–RBM7–086**, ***ent*–RBM7–062**, ***ent*–RBM7–095** and ***ent*–RBM7–100**.

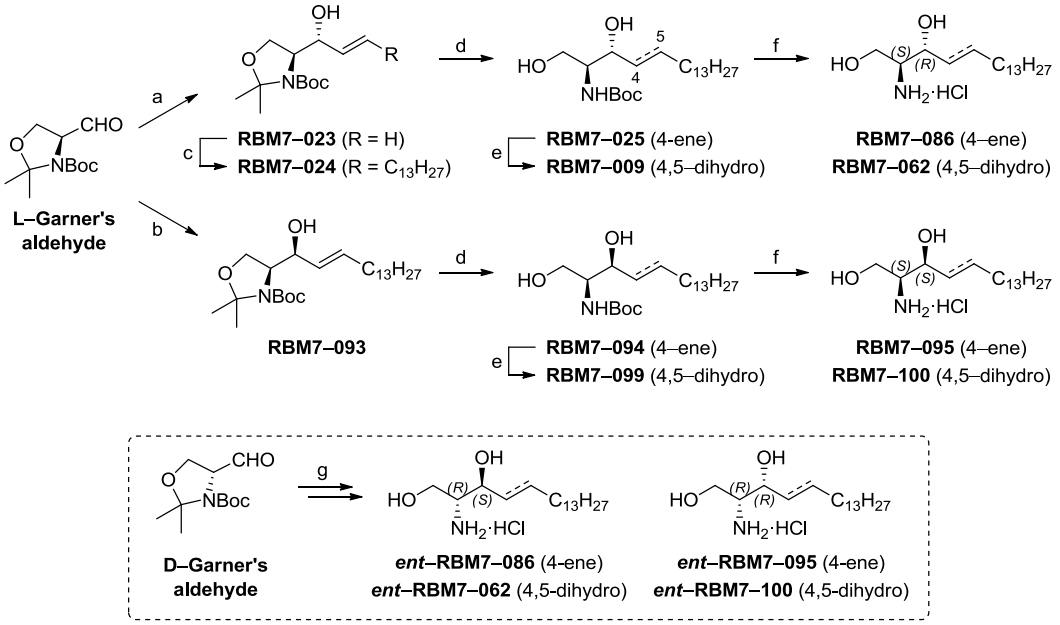

Scheme 3.2.4. Synthesis of sphingosines **RBM7–086**, **RBM7–062**, **RBM7–095**, **RBM7–100** and their enantiomers. Reagents and conditions: (a) vinylmagnesium bromide, THF, –78 ºC, 64 %, dr = 86:14; (b) (i) 1–pentadecyne, $Cp_2Zr(H)Cl$, CH_2Cl_2, 0 ºC (ii) Et_2Zn, CH_2Cl_2, –40 ºC to rt, 75 %, dr = 93:7, only *E*; (c) 1–pentadecene, Grubbs catalyst 2nd gen., CH_2Cl_2, reflux, 78 %, *E*/*Z* = 94:6; (d) *p*–TsOH, MeOH, rt, 94 % for **RBM7–025**, 92 % for **RBM7–094**; (e) H_2, 5 wt. % Rh on Al_2O_3, MeOH, rt, 97 % for **RBM7–009**, 91 % for **RBM7–099**; (f) AcCl, MeOH, 0 ºC to rt, 84 %–quant. yield; (g) same sequence as from L–Garner's aldehyde.

3.2.6 Synthesis of the stereodefined azido–S1P and dhS1P analogs

The differently configured sphingosines and 4,5–dihydrosphingosines were submitted to diazotransfer reaction with 1*H*–imidazole–1–sulfonylazide hydrochloride (ISA·HCl),[22]

a process that courses with retention of configuration at the azide carbon (Scheme 3.2.5).[23,24] Gratifyingly, the resulting azides were in agreement with the expected configuration, as evidenced by comparison of their optical rotations with those reported in the literature for azido diols **RBM7–087**,[25] **RBM7–096**,[26] and **RBM7–112**.[27] In addition, enantiomeric purity of the above azidodiols, together with that of the unreported compound **RBM7–101** was confirmed by chiral HPLC analysis, with *ee* higher than 95 % in all cases (see Section 5.1.4.2 and Figures S6–S13 from Section 7). Finally, the site–selective phosphorylation of the above azido diols gave the corresponding dimethyl phosphates derivatives in moderate to good yields. As stated above for the synthesis of **RBM7–010** and **RBM7–026**, phosphorlylation reactions with dimethyl chlorophosphate afforded little amounts of other unidentified phosphorous–containing byproducts. However, pure dimethyl phosphates were obtained after careful chromatographic purification of the corresponding crude reaction mixtures (See section 5.1.4.2). Finally, TMSBr–mediated methyl ester removal[28] afforded the required azidophosphates in 15–25 % overall yields from the starting Garner's aldehydes. Crude products were purified by RP chromatography (see section 5.1.4.2), yielding pure azidophosphates as their corresponding free acids.

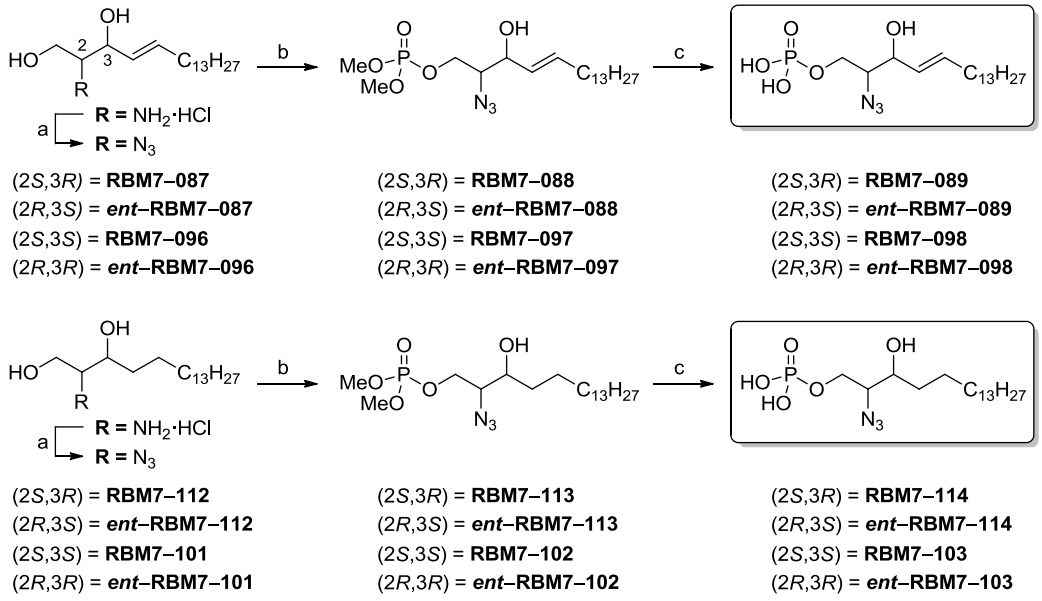

Scheme 3.2.5. Synthesis of the stereodefined azido–S1P and dhS1P analogs. Reagents and conditions: (a) 1*H*–imidazole–1–sulfonylazide hydrochloride, $CuSO_4 \cdot 5H_2O$, K_2CO_3, MeOH, rt, 80–91 %; (b) Dimethyl chlorophosphate, *N*–methylimidazole, CH_2Cl_2, 0 ºC to rt, 64–85 %; (c) (i) Me_3SiBr, MeCN, 0 ºC to rt (ii) MeOH/H_2O (95:5), rt, 56–71 %.

3.2.7 S1PL inhibition

The above compounds were tested against recombinant human (hS1PL)[29] and bacterial (StS1PL)[1] enzyme sources, using our previously developed fluorogenic substrate **RBM13**. Inhibition assays were performed under the optimized experimental conditions showed in Section 3.1.4.1. The results are collected in Table 3.2.1. Compound **RBM7–001**, designed as a mimic of the S1PL reaction intermediate **15** (see Figure 3.2.1) behaved as a weak inhibitor (around 20 % inhibition at 250 μM) in both hS1PL and StS1PL, while pyridoxine 5'–phosphate (**RBM7–002**) was practically devoid of activity. The presence of the sphingoid moiety in **RBM7–012** and **RBM7–032** led to more potent inhibitors, with IC_{50} values in the range of 50–80 μM for both enzymes (Table 3.2.1, entries 3 and 4; Figure S1 from Section 7).

Table 3.2.1. Inhibitory activity of the synthesized compounds.

			IC_{50} (μM)		**K_I (μM)[c]**
Entry	**Compound**	**Configuration**	**StS1PL**	**hS1PL**	**hS1PL**
1	**RBM7–001**	–	ni	ni[a]	nd[b]
2	**RBM7–002**	–	ni	ni	nd
3	**RBM7–012**	–	47.0	81.1	nd
4	**RBM7–032**	–	53.4	89.0	nd
5	**RBM7–089**	(2*S*,3*R*,4*E*)	12.9	10.1	9.1
6	***ent*–RBM7–089**	(2*R*,3*S*,4*E*)	13.8	5.2	5.6
7	**RBM7–098**	(2*S*,3*S*,4*E*)	16.0	28.8	20.4
8	***ent*–RBM7–098**	(2*R*,3*R*,4*E*)	11.7	22.9	17.5
9	**RBM7–114**	(2*S*,3*R*)	25.0	25.7	19.0
10	***ent*–RBM7–114**	(2*R*,3*S*)	25.7	10.8	6.3
11	**RBM7–103**	(2*S*,3*S*)	27.2	21.8	16.4
12	***ent*–RBM7–103**	(2*R*,3*R*)	24.3	28.3	36.7

[a]ni = No significant inhibition at 250 μM. [b]nd = Not determined. [c]Inhibition was competitive in all cases (see Figures S4 and S5 from Section 7).

Despite the comparable IC_{50} values for **RBM7–012** and **RBM7–032** on each of the enzyme sources, a slight selectivity towards the bacterial enzyme was observed. Furthermore, the presence of a double bond at the C4–C5 position of the sphingoid backbone seemed not crucial for S1PL inhibition. A putative unspecific inhibition due to the triethylammonium counterion present in **RBM7–012** and **RBM7–032** was disregarded since incubation of both enzymes at different concentrations of triethylamine hydrochloride (500–0.5 μM range) did not affect the enzymatic activity (results not shown). The modest results obtained with enzyme intermediate mimics **RBM7–001**, **RBM7–012** and **RBM7–032**, initially designed to occupy the enzyme PLP binding site, could be explained by their inability to displace the cofactor from its Schiff base with the postulated Lys residue at the active site (Figure 3.2.1). In addition, the bulkiness of **RBM7–012** and **RBM7–032** may prevent their access through the narrow channel linking the active site with the cytosol, as observed in the X–ray structures reported for S1PL.[1,29]

Unlike the above compounds, all the azidophosphate analogs synthesized in this work behaved as low μM inhibitors on the two S1PL tested (Table 3.2.1, entries 5–12). However, despite the subtle activity differences observed, some trends are worthy of mention. As StS1PL inhibitors, unsaturated derivatives **RBM7–089**, ***ent*–RBM7–089**, **RBM7–098** and ***ent*–RBM7–098** showed IC_{50} values in the range of 10–16 μM (Table 3.2.1, entries 5–8 and Figure S2 from Section 7), around 2–fold more active than their saturated analogs **RBM7–114**, ***ent*–RBM7–114**, **RBM7–103** and ***ent*–RBM7–103**, for which an IC_{50} value around 25 μM was determined in all cases (Table 3.2.1, entries 9–12 and Figure S2 from Section 7).

On the other hand, as hS1PL inhibitors, the *anti*–configured compounds **RBM7–089**, ***ent*–RBM7–089** and ***ent*–RBM7–114** were the most active compounds of this series, with IC_{50} values of 10.1, 5.2 and 10.8 μM, respectively (Table 3.2.1, entries 5, 6 and 10 and Figure S3 from Section 7). Interestingly, the naturally configured (2*S*,3*R*)–azidophosphate **RBM7–114** (IC_{50} = 25.7 μM) was not as active as the above derivatives. In contrast, the *syn*–configured compounds **RBM7–098**, ***ent*–RBM7–098**, **RBM7–103** and ***ent*–RBM7–103**, with IC_{50} values in the 20–30 μM range, were the less active stereoisomers of the series of azidophosphates (Table 3.2.1, entries 7, 8, 11 and 12 and Figure S3 from Section 7).

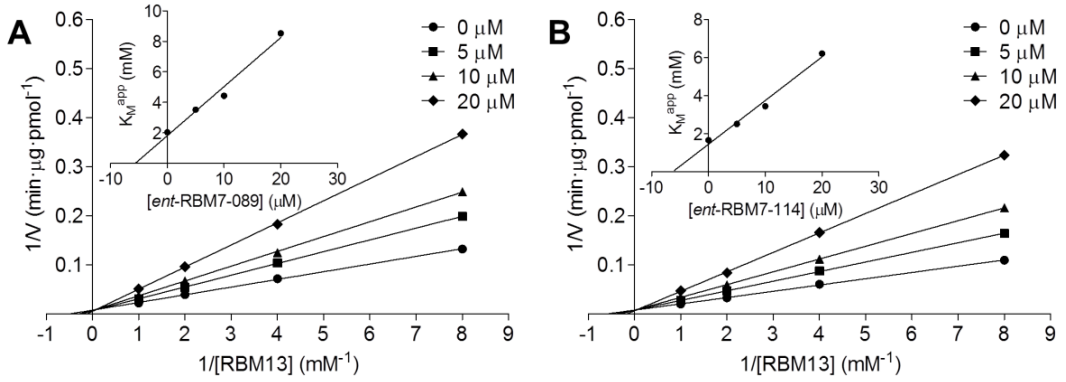

Figure 3.2.5. Lineweaver–Burk plots for inhibition of hS1PL by ***ent*–RBM7–089** (A) and ***ent*–RBM7–114** (B) at different concentrations of substrate (**RBM13**) and inhibitor. Regression lines arise from data obtained in two different experiments performed in triplicate.

The inhibition constants (K_I) against hS1PL showed a competitive inhibition pattern in all cases, with K_I values in the 5–40 μM range (see Figures S4 and S5 from Section 7) and a good correlation with the corresponding IC_{50} values. However, despite the similar inhibitory trends, compounds ***ent*–RBM7–089** and ***ent*–RBM7–114**, both with the non–natural 2*R*,3*S* configuration at the sphingoid backbone, were the most active stereoisomers of the series, with K_I values of 5.6 and 6.3 μM, respectively (Table 3.2.1, entries 6 and 10 and Figure 3.2.5). For the naturally configured series, **RBM7–089** (K_I = 9.1 μM) was found to be about two–fold more potent than its saturated analog **RBM7–114** (K_I = 19.0 μM).

Finally, in order to study the contribution of the phosphate group on S1PL activity, the corresponding azidodiols (compounds **RBM7–087**, ***ent*–RBM7–087**, **RBM7–096**, ***ent*–RBM7–096, RBM7–112**, ***ent*–RBM7–112**, **RBM7–101** and ***ent*–RBM7–101**, see Scheme 3.2.5) were also evaluated as hS1PL inhibitors. Interestingly, all compounds were inactive at 250 μM, thus suggesting that the presence of the phosphate group at C1 is critical to ensure a strong enzyme binding.

3.2.8 Computational studies

Computer docking simulations allowed proposing similar binding modes for the active azido phosphates in the active center of StS1PL and hS1PL. As indicated in Section 3.1.2, ligands were docked into the active site of both S1PL structures using the Induced Fit Docking Protocol of the Schrodinger Suite, in order to asses a possible configurational change of the protein in the presence of the ligand. In this case, The 3–hydroxypyridine and imino groups of the Lys–bound PLP prosthetic group were considered in their neutral state. Figure 3.2.6 shows the bound poses of compounds **RBM7–089** and ***ent*–RBM7–089** in the active center of both enzymes (PDB codes 3MAD and 4Q6R).[1,29] In agreement with the above suggestion, these poses show that the phosphate group can establish multiple interactions with residues of a previously identified anion binding site,[1] (See also Section 3.1.2) *i.e*. residues Y105, N126, H129 and K317 of StS1PL, and residues Y150, N171, H174 and K359 of hS1PL, thus confirming that the presence of a phosphate moiety is essential for binding.

The long aliphatic chain is always placed along the narrow hydrophobic access channel that communicates the active site of the proteins with the surface, while the azido and hydroxyl groups of both compounds are placed close to two aromatic residues (H201/Y249 in StS1PL and H242/F290 in hS1PL), which are at short distance of the PLP prosthetic group. The high similarity between the spatial arrangement of both compounds in the active sites of both proteins and the interactions that they stablish correlates well with their observed S1PL inhibitory activities. Furthermore, this docking analysis revealed that the presence or absence of the C4–double bond does not have a significant influence in the binding mode of the inhibitors, as illustrated by comparing the docked poses of azidophosphates **RBM7–089** and ***ent*–RBM7–089** (Figure 3.2.6) with those of the corresponding saturated analogs **RBM7–114** and ***ent*–RBM7–114** (Figure 3.2.7).

The similar behavior of the above azidophosphates as StS1PL and hS1PL inhibitors is also indicative of the similarities of both enzymes at their active site level. Hence, the more easily available StS1PL can be used as a reliable model of the human enzyme for putative inhibitors targeting the active site. This is not the case for inhibitors targeting the enzyme access channel, where the structural differences between both enzymes at that level may account for the lack of activity on StS1PL observed for the potent hS1PL

inhibitor **3c** (see Section 3.1.4.2). These observations justify the development of an engineered StS1PL as a model for the discovery of S1PL inhibitors.[30]

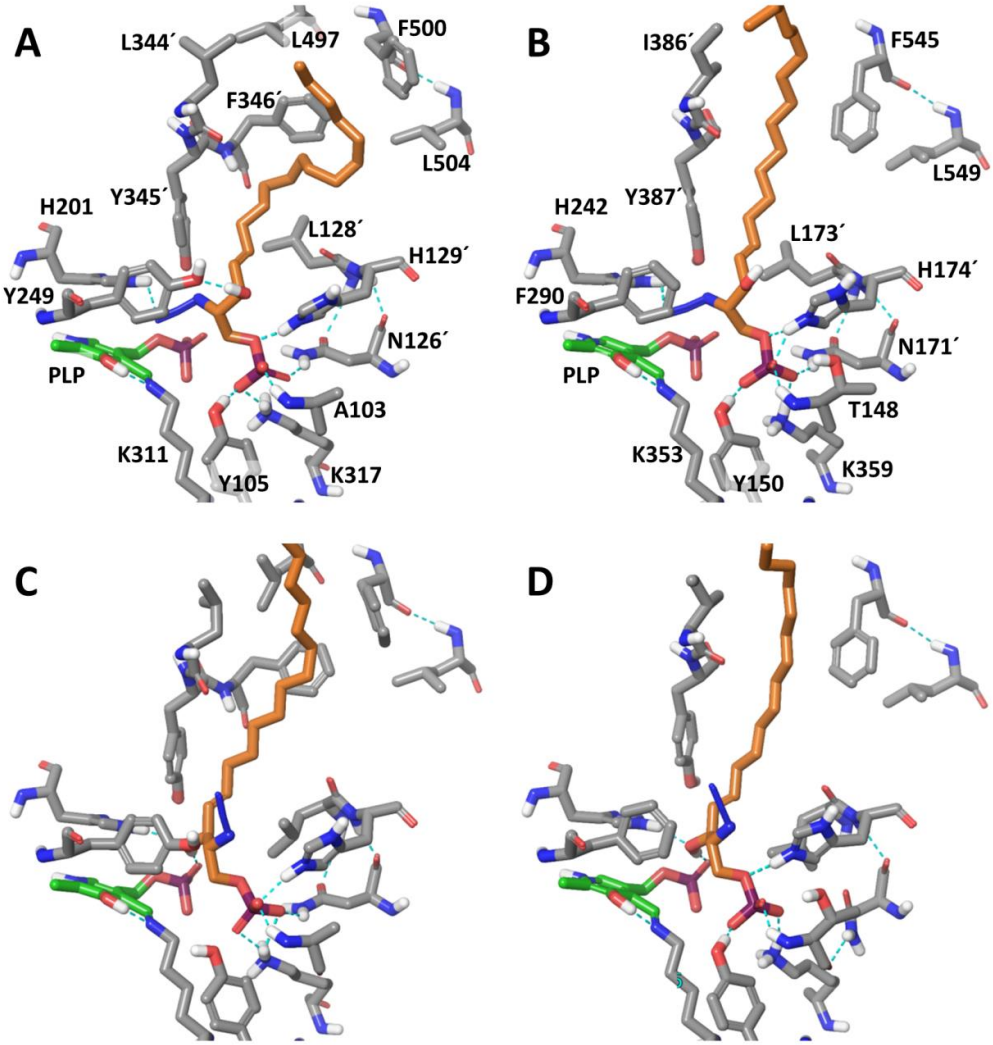

Figure 3.2.6. Best docked poses of azido phosphates **RBM7–089** (A, B) and ***ent*–RBM7–089** (C, D) bound into the active site of StS1PL (A, C) and hS1PL (B, D), as determined by an Induced Fit Docking protocol. Azido phosphates and the PLP prosthetic group are highlighted in orange and green, respectively. Protein residues interacting with the inhibitors are shown and labelled. Prime numbering indicates that residues belong to different subunits of the dimeric S1PL proteins.

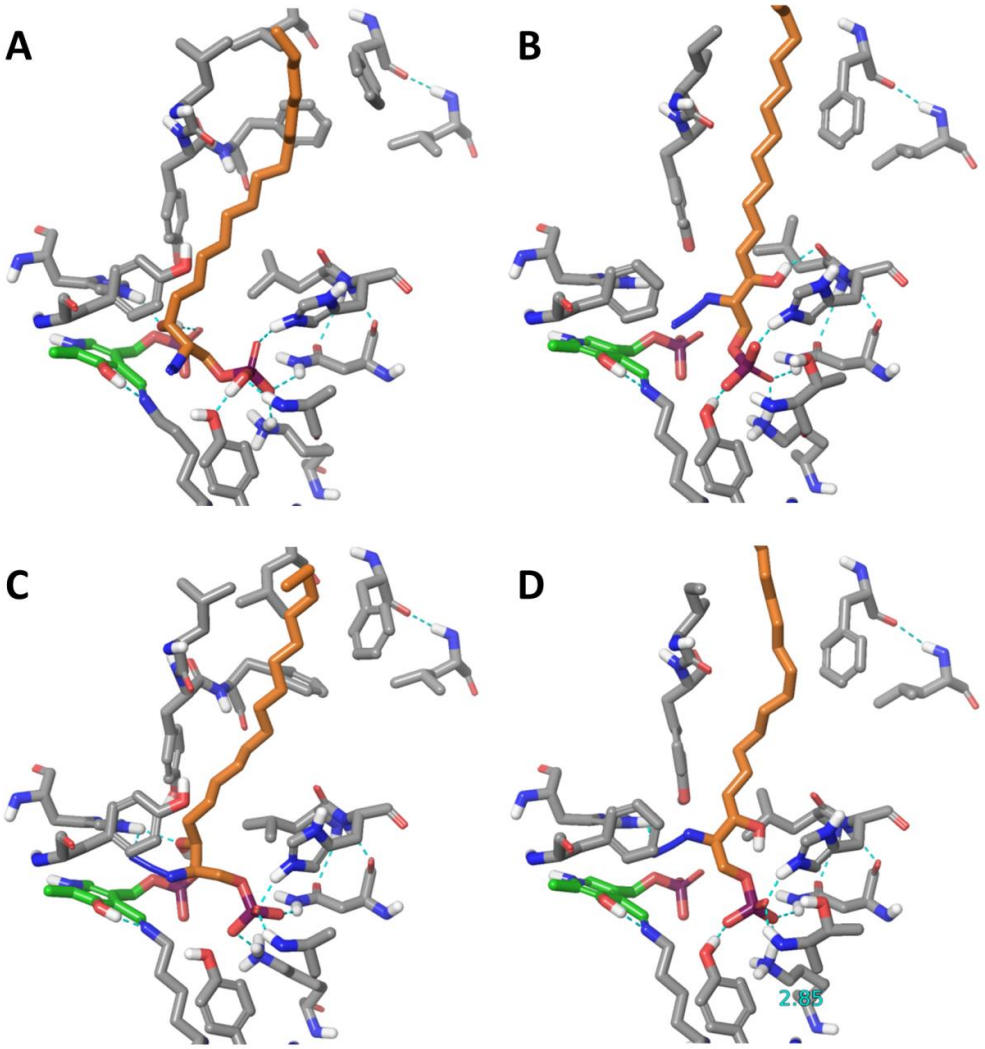

Figure 3.2.7. Best docked poses of azido phosphates **RBM7–114** (A, B) and ***ent*–RBM7–114** (C, D) bound into the active site of StS1PL (A, C) and hS1PL (B, D), as determined by an Induced Fit Docking protocol. Azido phosphates and the PLP prosthetic group are highlighted in orange and green, respectively. Protein residues interacting with the inhibitors are shown. See Figure 3.2.6 for residue numbering.

In light of the obtained results, we consider that the chemical and biological optimization of the above azidophosphates would be an interesting subject for further studies. We expect that a second generation of putative S1PL inhibitors with improved properties in terms of drug likeness may arise after the appropriate chemical modification of some key functional groups. Therefore, since the presence of a phosphate group at C1 was determined to be crucial for stablishing strong interactions with the anion binding site of S1PL, we hypothesize that its replacement by an acidic

surrogate such as a carboxylic acid, a phosphonic acid, a sulfonic acid or a tetrazole ring,[31] can lead to new families of active S1PL inhibitors. On the other hand, the replacement of the azido group with other substituents capable of stablishing additional interactions with the nearby residues of the active site would also be beneficial in terms of potency. Finally, in order to evaluate the effect of the lipophilicity on the activity of the above compounds, the synthesis and evaluation of new derivatives with truncated hydrocarbon tails could also be explored in further studies.

3.2.9 References

(1) Bourquin, F.; Riezman, H.; Capitani, G.; Grütter, M. G. Structure and Function of Sphingosine-1-Phosphate Lyase, a Key Enzyme of Sphingolipid Metabolism. *Structure* **2010**, *18*, 1054–1065.

(2) Delgado, A.; Martínez-Cartro, M. Therapeutic Potential of the Modulation of Sphingosine-1-Phosphate Receptors. *Current Medicinal Chemistry*, 2016, *23*, 242–264.

(3) Bagdanoff, J. T.; Donoviel, M. S.; Nouraldeen, A.; Tarver, J.; Fu, Q.; Carlsen, M.; Jessop, T. C.; Zhang, H.; Hazelwood, J.; Nguyen, H.; et al. Inhibition of Sphingosine-1-Phosphate Lyase for the Treatment of Autoimmune Disorders. *J. Med. Chem.* **2009**, *52*, 3941–3953.

(4) Garrido, M.; Abad, J. L.; Fabriàs, G.; Casas, J.; Delgado, A. Azide-Tagged Sphingolipids: New Tools for Metabolic Flux Analysis. *ChemBioChem* **2015**, *16* (4), 641–650.

(5) Griffin, R. J. The Medicinal Chemistry of the Azido Group. In *Progress in Medicinal Chemistry*; Ellis, G. P., Luscombe, D. K., Eds.; Elsevier, 1994; Vol. 31, pp 121–232.

(6) Tilley, K.; Akhtar, M.; Gani, D. The Stereochemical Course of Decarboxylation, Transamination and Elimination Reactions Catalysed by Escherichia Coli Glutamic Acid Decarboxylase. *J. Chem. Soc. Perkin Trans. 1* **1994**, No. 21, 3079–3087.

(7) Choi, S. Y.; Churchich, J. E. Glutamate Decarboxylase Side Reactions Catalyzed by the Enzyme. *Eur. J. Biochem.* **1986**, *160* (3), 515–520.

(8) Bedia, C.; Camacho, L.; Casas, J.; Abad, J. L.; Antonio, D.; Van Veldhoven, P. P.; Fabriàs, G. Synthesis of a Fluorogenic Analogue of Sphingosine-1-Phosphate and Its Use to Determine Sphingosine-1-Phosphate Lyase Activity. *ChemBioChem* **2009**, *10* (5), 820–822.

(9) Szulc, Z. M.; Hannun, Y. A.; Bielawska, A. A Facile Regioselective Synthesis of Sphingosine 1-Phosphate and Ceramide 1-Phosphate. *Tetrahedron Lett.* **2000**, *41* (41), 7821–7824.

(10) Boumendjel, A.; Miller, S. P. Synthesis of Sphingosine-1-Phosphate and Dihydrosphingosine-1-Phosphate. *J. Lipid Res.* **1994**, *35* (12), 2305–2311.

(11) Yang, H.; Liebeskind, L. S. A Concise and Scalable Synthesis of High Enantiopurity (−)-D-Erythro-Sphingosine Using Peptidyl Thiol Ester−Boronic Acid Cross-Coupling. *Org. Lett.* **2007**, *9* (16), 2993–2995.

(12) Campbell, A. D.; Raynham, T. M.; Taylor, R. J. K. A Simplified Route to the (R)-Garner Aldehyde and (S)-Vinyl Glycinol. *Synthesis (Stuttg).* **1998**, *1998* (12), 1707–1709.

(13) Bhabak, K. P.; Proksch, D.; Redmer, S.; Arenz, C. Novel Fluorescent Ceramide Derivatives for Probing Ceramidase Substrate Specificity. *Bioorg. Med. Chem.* **2012**, *20* (20), 6154–6161.

(14) Ojima, I.; Vidal, E. S. Rhodium-Catalyzed Cyclohydrocarbonylation: Application to the Synthesis of (+)-Prosopinine and (−)-Deoxoprosophylline. *J. Org. Chem.* **1998**, *63* (22), 7999–8003.

(15) Passiniemi, M.; Koskinen, A. M. P. Garner's Aldehyde as a Versatile Intermediate in the Synthesis of Enantiopure Natural Products. *Beilstein J. Org. Chem.* **2013**, *9*, 2641–2659.

(16) Wisse, P.; Gold, H.; Mirzaian, M.; Ferraz, M. J.; Lutteke, G.; van den Berg, R. J. B. H. N.; van den Elst, H.; Lugtenburg, J.; van der Marel, G. A.; Aerts, J. M. F. G.; et al. Synthesis of a Panel of Carbon-13-Labelled (Glyco)Sphingolipids. *Eur. J. Org. Chem.* **2015**, *2015* (12), 2661–2677.

(17) Murakami, T.; Furusawa, K. Efficient Stereodivergent Synthesis of Erythro- and Threo-Sphingosines: Unprecedented Reversal of the Stereochemistry in the Addition. *Tetrahedron* **2002**, *58* (45), 9257–9263.

(18) Coleman, R. S.; Carpenter, A. J. Diastereoselective Addition of Vinyl Organometallic Reagents to L-Serinal. *Tetrahedron Lett.* **1992**, *33* (13), 1697–1700.

(19) Triola, G.; Fabriàs, G.; Casas, J.; Llebaria, A. Synthesis of Cyclopropene Analogues of Ceramide and Their Effect on Dihydroceramide Desaturase. *J. Org. Chem.* **2003**, *68* (26), 9924–9932.

(20) Herold, P. Synthesis of D-Erythro- and D-Threo-Sphingosine Derivatives From L-Serine. *Helv. Chim. Acta* **1988**, *71* (2), 354–362.

(21) Alcaide, A.; Llebaria, A. Aziridine Ring Opening for the Synthesis of Sphingolipid Analogues: Inhibitors of Sphingolipid-Metabolizing Enzymes. *J. Org. Chem.* **2014**, *79* (7), 2993–3029.

(22) Goddard-Borger, E. D.; Stick, R. V. An Efficient, Inexpensive, and Shelf-Stable Diazotransfer Reagent: Imidazole-1-Sulfonyl Azide Hydrochloride. *Org. Lett.* **2007**, *9* (19), 3797–3800.

(23) Nyffeler, P. T.; Liang, C.-H.; Koeller, K. M.; Wong, C.-H. The Chemistry of Amine−Azide Interconversion: Catalytic Diazotransfer and Regioselective Azide Reduction. *J. Am. Chem. Soc.* **2002**, *124* (36), 10773–10778.

(24) Pandiakumar, A. K.; Sarma, S. P.; Samuelson, A. G. Mechanistic Studies on the Diazo Transfer Reaction. *Tetrahedron Lett.* **2014**, *55* (18), 2917–2920.

(25) Sandbhor, M. S.; Key, J. A.; Strelkov, I. S.; Cairo, C. W. A Modular Synthesis of Alkynyl-Phosphocholine Headgroups for Labeling Sphingomyelin and Phosphatidylcholine. *J. Org. Chem.* **2009**, *74* (22), 8669–8674.

(26) Enders, D.; Whitehouse, D. L.; Runsink, J. Diastereo- and Enantioselective Synthesis of L-Threo- and D-Erythro-Sphingosine. *Chem. – A Eur. J.* **1995**, *1* (6), 382–388.

(27) Fernandes, R. A.; Kumar, P. A Stereoselective Synthesis of Dihydrosphingosine. *Eur. J. Org. Chem.* **2000**, *2000* (20), 3447–3449.

(28) Grijalvo, S.; Llebaria, A.; Delgado, A. Straightforward Access to Simplified Sphingosine-1-Phosphate Analogues. *Synth. Commun.* **2007**, *37* (16), 2737–2751.

(29) Weiler, S.; Braendlin, N.; Beerli, C.; Bergsdorf, C.; Schubart, A.; Srinivas, H.; Oberhauser, B.; Billich, A. Orally Active 7-Substituted (4-Benzylphthalazin-1-Yl)-2-Methylpiperazin-1-Yl]nicotinonitriles as Active-Site Inhibitors of Sphingosine 1-Phosphate Lyase for the Treatment of Multiple Sclerosis. *J. Med. Chem.* **2014**, *57*, 5074–5084.

(30) Argiriadi, M. A.; Banach, D.; Radziejewska, E.; Marchie, S.; DiMauro, J.; Dinges, J.; Dominguez, E.; Hutchins, C.; Judge, R. A.; Queeney, K.; et al. Creation of a S1P Lyase Bacterial Surrogate for Structure-Based Drug Design. *Bioorg. Med. Chem. Lett.* **2016**, *26* (9), 2293–2296.

(31) Högenauer, K.; Hinterding, K.; Nussbaumer, P. S1P Receptor Mediated Activity of FTY720 Phosphate Mimics. *Bioorg*. *Med*. *Chem*. *Lett*. **2010**, *20* (5), 1485–1487.

3.3 Coumarin–derived fluorogenic probes for S1PL activity determination

3.3.1 Introduction

As discussed in section 1.4, different radiolabeled,[1–3] fluorescent[4,5] and fluorogenic[6] substrates have been described to determine S1PL activity. In this regard, we have reported an easy procedure to measure S1PL activity using the fluorogenic substrate **RBM13**, which evolves to give umbelliferone (see Figure 1.12). More recently, **RBM13** has also been validated as substrate of bacterial and human S1PL, allowing the development of an HTS–amenable assay using purified enzymes (see Section 3.1.4.1).

According to its relatively high K_M and low V_{max} values against different enzyme sources (see Table 1.2), **RBM13** should be considered as a poor S1PL substrate. Using cell lysates of mouse embryonic fibroblasts, a K_M of 152 μM was initially determined,[6] which was 25–fold higher compared to that reported for the natural S1P using mouse liver microsomes as S1PL source (K_M = 5.7 μM).[7] In comparison with other non–natural S1PL substrates bearing a bulky fluorophore on its structure such as S1P(NBD) (K_M = 14.6 μM)[4] and $S1PC_{14}$(BODIPY) (K_M = 35 μM),[5] an increase of the K_M value for **RBM13** was also significant. In addition, as shown in section 3.1.4.1, even higher K_M values were determined for **RBM13** using purified enzymes (K_M = 1522 ± 73 μM for StS1PL and K_M = 1994 ± 121 μM for hS1PL).

We speculated that the moderate affinity of **RBM13** towards S1PL is likely due to the lack of the C13 hydrocarbon tail present in S1P, which is replaced with and ether–linked umbelliferone group. Since the bulky coumarin unit is close to the reactive moiety (C2–C3 bond), we hypothesized that it could hinder the enzyme–substrate interaction, thus leading to the moderate kinetic parameters obtained for this substrate.

3.3.2 Design of probes RBM7–077 and RBM7–148

With the aim of improving the kinetics of the fluorogenic substrate **RBM13**, we designed compounds **RBM7–077** and **RBM7–148** as two new putative S1PL fluorogenic substrates (Figure 3.3.1). We reasoned that placing the bulky coumarin group two carbons away from the C2–C3 cleavable bond could provide better S1PL substrates. Structurally, probes **RBM7–077** and **RBM7–148** are formally derived from **RBM13** by intercalation of a vinyl group between the naturally *anti*–configured amino alcohol phosphate framework and the ω–coumarin group. In the case of **RBM7–077**, the vinyl unit was placed at the C4–C5 position, which retained the allylic alcohol motif

of the natural substrate. In contrast, in order to increase the reactivity of the S1PL–generated aldehyde (see below), the vinyl moiety in **RBM7–148** was located at C5–C6. The *E* configuration of the natural substrate S1P was also conserved in compounds **RBM7–077** and **RBM7–148**. However, both the chemical synthesis and the biological activity of the corresponding *Z*–isomers could be interesting subjects for further studies.

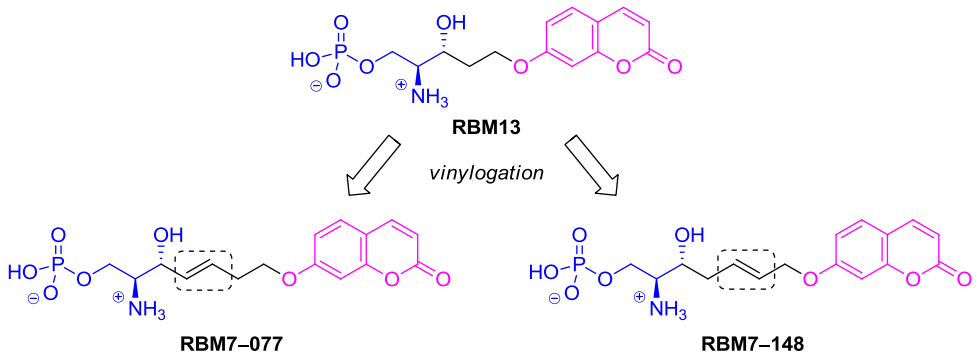

Figure 3.3.1. Design of coumarin–based probes **RBM7–077** and **RBM7–148**.

Upon incubation in the presence of S1PL, **RBM7–077** and **RBM7–148** are expected to be metabolized to the corresponding unsaturated aldehydes **RBM7–083** and **RBM7–136**, which should undergo subsequent elimination at alkaline pH to finally release the fluorescent umbelliferone **7** and the diene **17** (Figure 3.3.2).

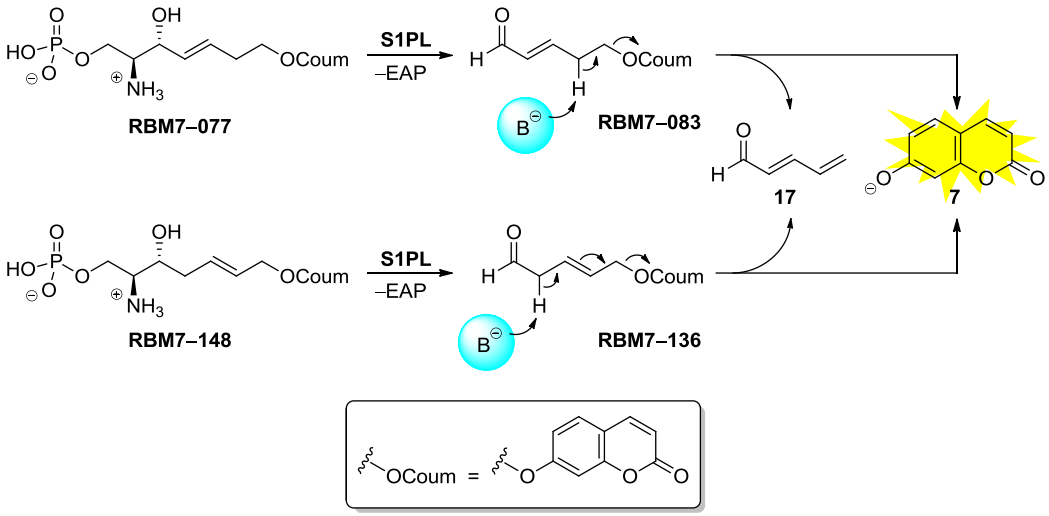

Figure 3.3.2. Proposed mechanism for the S1PL–catalyzed release of **7**.

Based on the principle of vinilogy,[8] we reasoned that the proton at the allylic position in **RBM7–083** would be acidic enough to be abstracted by a base, allowing the concerted release of **7** *via* an E2–type mechanism, as postulated for **RBM13**.[6] On the other hand, different putative mechanisms can be envisioned for the release of **7** from aldehyde **RBM7–136** (Figure 3.3.3). Firstly, since the leaving group is at the allylic position, it is reasonable to think that the elimination reaction could proceed following an E1–mechanism (Figure 3.3.3A) in which **7** could be initially released, yielding a terminal allylic carbocation, which is stabilized by resonance. Subsequent proton abstraction should generate diene **17**. In a second scenario (Figure 3.3.3B), the elimination reaction could take place in a concerted manner following an E2'–type mechanism. In this case, the abstraction of the proton at the α–position with respect to the carbonyl and the release of **7** should occur simultaneously with transposition of the double bond at the C4–C5 position. Finally, due to the expected acidity of the α–proton of **RBM7–136**, the base–mediated formation of the corresponding enolate could also take place (Figure 3.3.3C). Then, the resulting enolate could either evolve to give **7** and **17** in a E1cB'–type mechanism or isomerize to yield the α,β–unsaturated aldehyde **RBM7–083**.

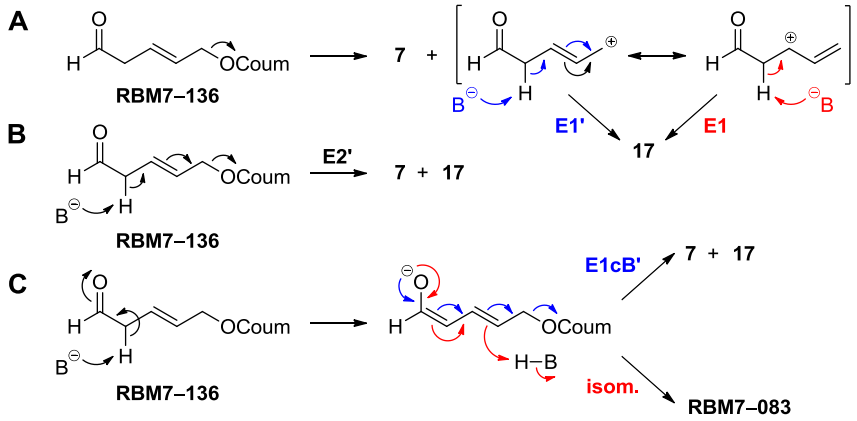

Figure 3.3.3. Proposed mechanisms for the base–mediated release of **7** using aldehyde **RBM7–136**.

3.3.3 Synthetic approach to probes RBM7–077 and RBM7–148

Access to probes **RBM7–077** and **RBM7–148** was planned by a two–step site–selective phosphorylation and deprotection sequence of *N*–Boc aminodiols **RBM7–079** and **RBM7–143** (Scheme 3.3.1).

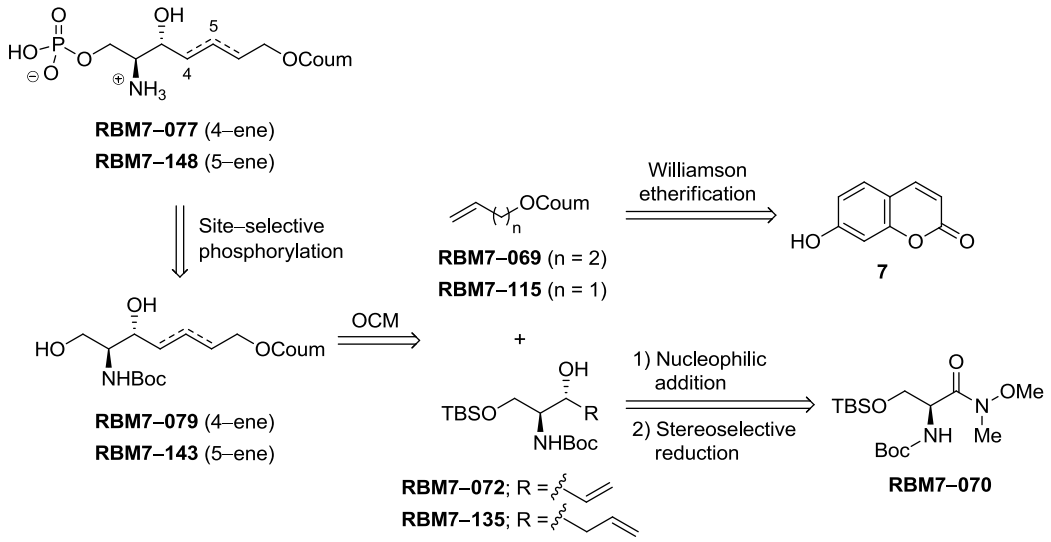

Scheme 3.3.1. Synthetic approach to coumarin–based probes **RBM7–077** and **RBM7–148**.

According to the synthetic strategy reported by Yamamoto *et al*.,[9] olefin cross–metathesis (OCM) reaction between building blocks **RBM7–069** and **RBM7–072** or **RBM7–115** and **RBM7–135**, followed by silyl removal, was envisaged as a suitable route to obtain alkenes **RBM7–079** and **RBM7–143** as major *E*–stereoisomers.

Coumarin derivatives **RBM7–069** and **RBM7–115** would be obtained by direct alkylation of **7**, whereas *anti*–configured aminodiols **RBM7–072** and **RBM7–135** would arise from Weinreb's amide **RBM7–070**, which is readily accessible from *L*-serine.[9] In this context, we expected that the nucleophilic addition of a suitable Grignard reagent to **RBM7–070**, followed by a diastereoselective reduction of the resulting ketones would provide allylic alcohol **RBM7–072** and its homoallylic analog **RBM7–135**.

3.3.4 Synthesis of coumarinic precursors RBM7–069 and RBM7–115

Alkenes **RBM7–069** and **RBM7–115** were obtained by nucleophilic substitution of the *in situ* generated umbelliferone anion and the appropriate electrophile (Scheme 3.3.2). Following the methodology described by Magolan *et al*.,[10] Williamson reaction using allyl bromide gave the desired allyl ether **RBM7–115** in good yield. Contrarily, initial attempts to prepare **RBM7–069** using 4–bromo–1–butene as electrophile proved unsatisfactory, since the desired product was obtained in low yields (30–40 %), regardless of the reaction conditions (base, solvent or temperature). We hypothesized

that elimination of 4–bromo–1–butene to 1,4–butadiene can compete with the expected nucleophilic displacement of the bromine atom. Gratifyingly, when the leaving group was replaced by a tosylate,[11] the reaction with **7** proceeded smoothly, yielding the homoallylic derivative **RBM7–069** in 85 % yield. In this case, tosylate **RBM7–084** was obtained from the commercially available 3–buten–1–ol (**18**), following a reported method.[12]

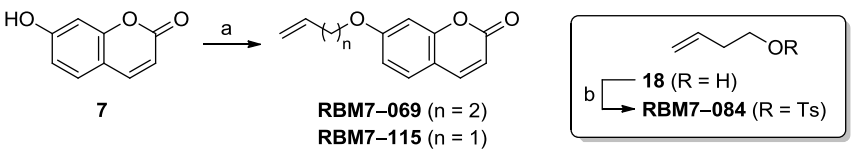

Scheme 3.3.2. Synthesis of coumarinic precursors **RBM7–069** and **RBM7–115**. Reagents and conditions: (a) for **RBM7–115**: allyl bromide, K_2CO_3, acetone, reflux, 88 %; for **RBM7–069**: NaH, **RBM7–084**, DMF, 80 ºC, 85 %; (b) TsCl, py, CH_2Cl_2, rt, 72 %.

3.3.5 Synthesis of the sphingoid precursors RBM7–072 and RBM7–135

As depicted in Scheme 3.3.3, the synthesis of the desired sphingoid precursors **RBM7–072** and **RBM7–135** started with the transformation of *L*–serine to the protected Weinreb's amide **RBM7–070**, which was obtained over three steps, in excellent yield and without any purification stage, according to a reported methodology.[9] We next explored the introduction of the required vinyl or allyl moiety by means of a nucleophilic addition of the corresponding Grignard reagent to **RBM7–070** and subsequent hydrolysis of the resulting intermediate.[9,13] Deceivingly, initial attempts at the synthesis of vinyl ketone **RBM7–071** using vinylmagnesium bromide in THF were unsuccessful. In this case, although the presence of the desired ketone was observed by TLC along the reaction progress, usual acidic workup of the reaction mixture led to the formation of a major product, which was further identified as the β–aminoketone **19** resulting from the 1,4–addition of the liberated *N*,*O*–dimethylhydroxylamine to **RBM7–071** (see Scheme 3.3.3). Examination of the literature revealed that the observed reactivity had been widely studied by other authors, giving rise to new methodologies to synthesize a variety of β–aminoketones.[14,15] In our case, the problem was circumvented by performing an inverse acidic workup at 0 ºC (see section 5.1.5.2), which provided vinyl ketone **RBM7–071** in good yield and with negligible formation of the Michael adduct.

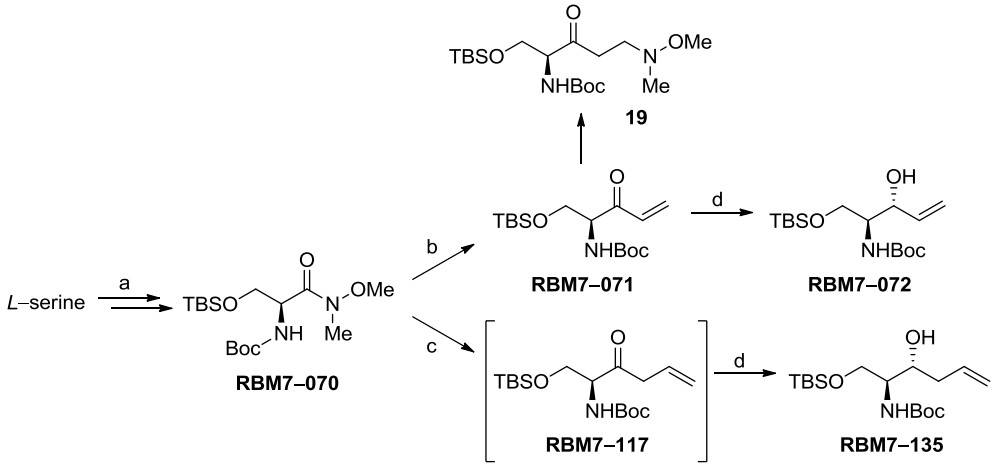

Scheme 3.3.3. Synthesis of sphingoid precursors **RBM7–072** and **RBM7–135**. Reagents and conditions: (a) Ref. 9; (b) vinylmagnesium bromide, THF, 0 ºC to rt, 71 %; (c) allylmagnesium chloride, THF, –20 ºC to rt, (d) $LiAlH(O^tBu)_3$, EtOH, –78 ºC, 90 % for **RBM7–072** (dr = 98:2) and 78 % (2 steps) for **RBM7–135** (dr = 99:1).

On the other hand, treatment of **RBM7–070** with allylmagnesium chloride provided ketone **RBM7–117**, as observed by TLC. However, purification attempts by direct phase chromatography resulted on an inseparable mixture of **RBM7–117** and the isomeric α,β–unsaturated ketone, which was presumably formed during the chromatographic process. Thus, due to its instability, crude **RBM7–117** was immediately used in the next synthetic step without further purification. Final diastereoselective reduction of ketones **RBM7–071** and **RBM7–117** using $LiAlH(O^tBu)_3$ in EtOH at –78 ºC,[9,13,16] provided the protected aminoalcohols **RBM7–072** and **RBM7–135** in good yields and excellent diastereoselectivities. In both cases, *anti*–configured aminoalcohols were separated from the small amount of the corresponding *syn* diastereomers by flash chromatography.

The high *anti*–selectivity of the last reduction step can be rationalized by the Cram's chelation control model, in which the aluminum atom coordinates to the carbonyl oxygen and the nitrogen of the protected amine, enforcing a *syn*–periplanar relationship between both groups, and leading to the *anti* diastereomer, since the hydride anion is forced to attack from the *si*–side (Figure 3.3.4).[16] Hoffman *et al*. postulated that the EtOH may play an important role since it may be converted to ethoxide by reaction with the metallic hydride. The resulting ethoxide would then deprotonate the carbamate of the protected amino ketone initiating the chelate formation.

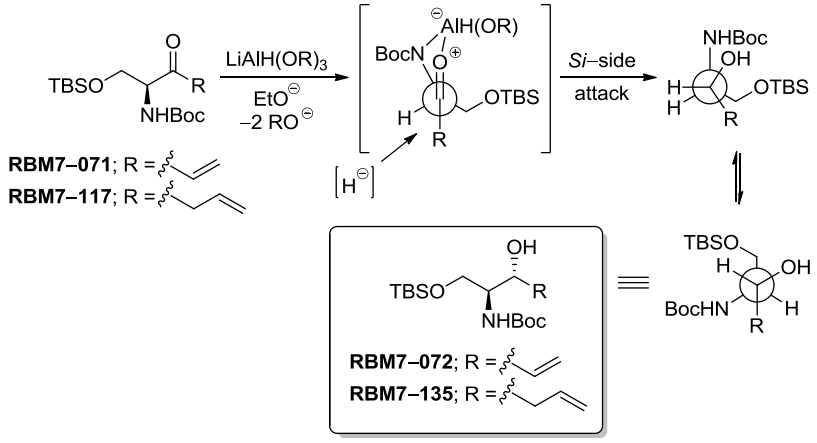

Figure 3.3.4. Proposed mechanism for the diastereoselective reduction of *N*–carbamate protected amino ketones **RBM7–071** and **RBM7–117** using $LiAlH(O^tBu)_3$ in EtOH. Adapted from Ref. 16.

Both the spectroscopic data and the optical rotation obtained for **RBM7–072** were in agreement with those previously reported.[9] However, in the case of **RBM7–135**, although the spectroscopic data matched those described, some discrepancies were observed regarding the sign of the optical rotation. In this case, our experimental value ($[\alpha]^{20}_D$ = +32.6 (*c* 1.0, $CHCl_3$)) was in agreement with that reported by Francson *et al*. ($[\alpha]_D$ = +32.2 (*c* 1.32, $CHCl_3$)),[17] but was opposite in sign to that reported by Huang *et al*. ($[\alpha]^{25}_D$ = –28.1 (*c* 1.0, $CHCl_3$)).[13]

Therefore, in order to unambiguously confirm the configuration of **RBM7–135**, the absolute configuration of the stereocenter at C3 was determined. This was also applied to **RBM7–072** to double check the assigned configuration based on the optical rotation data. In both cases, the 3*R* configuration was corroborated after derivatization of the free hydroxyl groups to the corresponding (*R*)– and (*S*)–α–methoxy–α–phenylacetic (MPA) esters[18] and ^{1}H NMR analysis of selected chemical shifts increments ($\Delta\delta^{RS}$), according to the model proposed by Seco *et al*.[19,20] (see Scheme 3.3.4 and Tables 5.1 and 5.2).

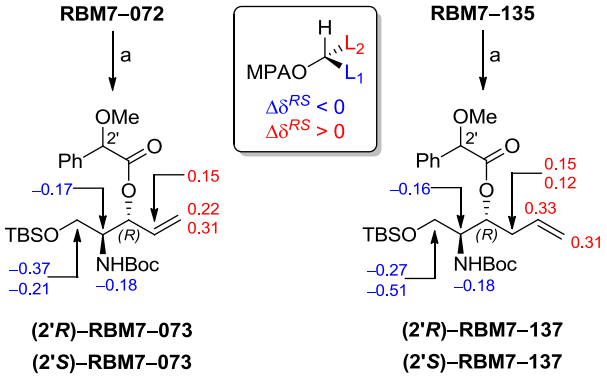

Scheme 3.3.4. Configurational assignment of C3 in **RBM7–072** and **RBM7–135**. Reagents and conditions: (a) (R)–(–)– or (S)–(+)–MPA, EDC, DMAP, CH_2Cl_2, 0 ºC to rt, 64 % for **(2'R)–RBM7–073**, 82 % for **(2'S)–RBM7–073**, 36 % for **(2'R)–RBM7–137** and 68 % for **(2'S)–RBM7–137**.

3.3.6 Synthesis of probes RBM7-077 and RBM7-148

With both sphingoid and coumarinic precursors in hand, the synthesis of probes **RBM7–077** and **RBM7–148** continued as shown in Scheme 3.3.5. Namely, Ru–catalyzed olefin cross–metathesis reaction between alkenes **RBM7–072** and **RBM7–069** provided allylic alcohol **RBM7–078** whereas coupling between **RBM7–135** and **RBM7–115**, under the same conditions, afforded the homoallylic derivative **RBM7–141**. Both reactions proceeded smoothly yielding the desired coupling products, as highly enriched *E*:*Z* mixtures (*E*/*Z* = 94:6 for **RBM7–078** and 93:7 for **RBM7–141**), in moderate yields. In the case of **RBM7–141**, both isomers were cleanly separated by direct phase chromatography. In contrast, separation of *E*– and *Z*–**RBM7–078** resulted in a tedious process, since they co–eluted in different solvent systems. Hence, although fractions containing pure, major *E* isomer could be obtained, most of the material was obtained as *E*/*Z* mixtures. These mixtures were used as such in the subsequent synthetic stages, which allowed the removal of the minor *Z* isomer along the required purification steps.

Fluoride–mediated deprotection of **RBM7–078** and **RBM7–141** gave diols **RBM7–079** and **RBM7–143**, which were site–selectively phosphorylated at the primary hydroxyl group yielding dimethyl phosphates **RBM7–076** and **RBM7–144** in good yields. Phosphorylation of **RBM7–079** proceeded with moderate selectivity, since small amounts of other phosphorous–containing byproducts were detected by ^{31}P NMR.

Nevertheless, pure phosphate triester was obtained after careful purification of the crude reaction mixture by flash chromatography. Contrarily, phosphorylation of **RBM7–143** yielded phosphate **RBM7–144** as a single compound in 78 % yield. Final treatment of **RBM7–076** and **RBM7–144** with Me_3SiBr, followed by methanolysis, gave the zwitterionic amino phosphates **RBM7–077** and **RBM7–148** in good yields.

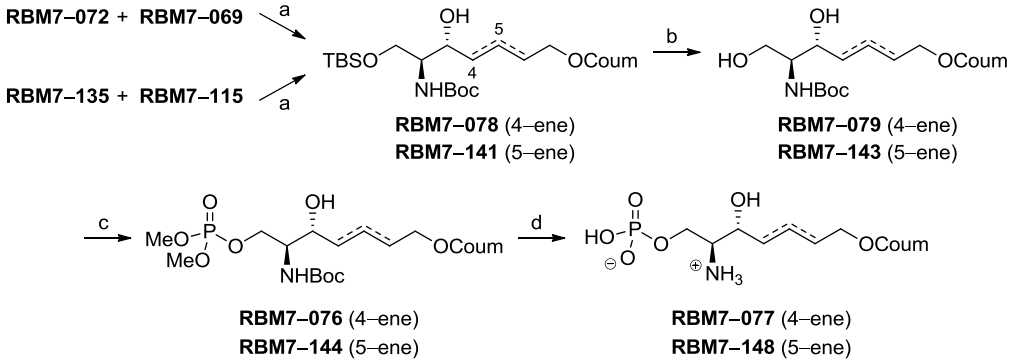

Scheme 3.3.5. Synthesis of probes **RBM7–077** and **RBM7–148**. Reagents and conditions: (a) Grubbs catalyst 2nd gen., CH_2Cl_2, reflux, 63 % for **RBM7–078** (*E*/*Z* = 94:6) and 66 % for **RBM7–141** (*E*/*Z* = 93:7); (b) TBAF, THF, 0 ºC, 95 % for **RBM7–079**, 88 % for **RBM7–143**; (c) Dimethyl chlorophosphate, *N*–methylimidazole, CH_2Cl_2, 0 ºC to rt, 69 % for **RBM7–076**, 78 % for **RBM7–144**; (d) (i) Me_3SiBr, MeCN, 0 ºC to rt (ii) MeOH/H_2O (95:5), rt, 85 % for **RBM7–077**, 82 % for **RBM7–148**.

3.3.7 Synthesis of unsaturated aldehydes RBM7–083 and RBM7–136

Once we had obtained probes **RBM7–077** and **RBM7–148**, we next focused on the preparation of unsaturated aldehydes **RBM7–083** and **RBM7–136** in order to study and optimize the reaction conditions of its base–mediated elimination. In our retrosynthetic analysis (Scheme 3.3.6), we envisioned that the oxidation of primary alcohols **RBM7–081** and **RBM7–134** would provide the desired aldehydes.

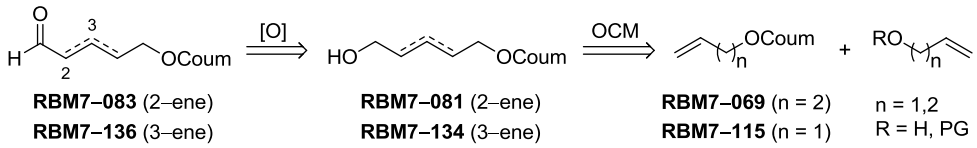

Scheme 3.3.6. Synthetic approach to aldehydes **RBM7–083** and **RBM7–136**.

Olefin cross–metathesis reaction between the above mentioned coumarinic precursors **RBM7–069** or **RBM7–115** and the appropriate terminal alkene hydroxylated at the ω–position would afford the *E*–configured alkenes **RBM7–081** and **RBM7–134**.

3.3.8 Synthesis of aldehyde RBM7–083

According to our proposed approach to aldehyde **RBM7–083** (Scheme 3.3.6), we initially attempted the synthesis of **RBM7–081** by means of an olefin cross–metathesis between **RBM7–069** and allyl alcohol (Scheme 3.3.7). Under the same conditions described in section 3.3.6, compound **RBM7–081** was obtained as an 85:15 inseparable *E*,*Z*–mixture of alkenes, in low yield (33 %). The use of longer reaction times (up to 16 h), lower temperatures,[21] higher amounts of catalyst (up to 20 mol %),[22] a different solvent (Et_2O)[21] or even the repeated addition of up to 10 eq. of allyl alcohol[21] did not improve the outcome of the reaction. We hypothesized that the high reactivity of the starting material was probably responsible for the moderate yields of the hetero–coupling adduct, since a significant formation of the allyl alcohol homo–coupling product was evidenced by TLC in all cases.

Oxidation of the inseparable mixture of *E*/*Z*–**RBM7–081** using IBX in refluxing EtOAc[23,24] led to total degradation. However, when the same mixture was oxidized under milder conditions, using Dess–Martin periodinane in CH_2Cl_2 at low temperature,[25] aldehyde **RBM7–083** was satisfactorily obtained in 64 % yield. Careful purification of the crude reaction mixture by flash chromatography allowed the isolation of a 95:5 enriched mixture of *E*/*Z*–**RBM7–083**, which was considered suitable for further studies.

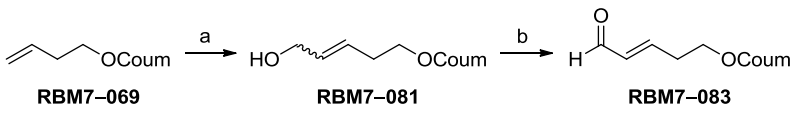

Scheme 3.3.7. Synthesis of aldehyde **RBM7–083**. Reagents and conditions: (a) allyl alcohol, Grubbs cat. 2nd gen., CH_2Cl_2, reflux, 33 %, *E*/*Z* = 85:15; (b) DMP, CH_2Cl_2, 0 ºC to rt, 64 %.

3.3.9 Attempts to synthesize aldehyde RBM7–136

In view of the moderate results obtained using simple unsaturated alcohols such as allyl alcohol in the cross–metathesis reaction, we explored the use of a protected alcohol as

an alternative to access compound **RBM7–134**. We envisaged that the protection of the corresponding unsaturated alcohol with a bulky group such as TBDPS, would lower its reactivity in terms of auto–metathesis and, therefore, would increase the yield of the hetero–coupling adduct. In this regard, homoallyl alcohol **18** was quantitatively protected as the TBDPS derivative **RBM7–116**, which was next subjected to olefin cross–metathesis using **RBM7–115** as olefinic partner. To our delight, the reaction proceeded satisfactorily giving protected homoallylic alcohol **RBM7–118** in acceptable yield (58 %) and with an improved *E*:*Z* ratio (91:9), as compared with that obtained using allyl alcohol (see Scheme 3.3.7). Since both isomers could not be cleanly separated at this stage, the above *E*:*Z* mixture was used in the next steps. Fortunately, this mixture was gradually enriched in the desired *E*–alkene throughout the subsequent purification steps of the route (up to *E*/*Z* = 98:2, see Section 5.1.5.4).

Further deprotection of the silyl ether group using TBAF furnished alcohol **RBM7–134** in near–quantitative yield. However, attempts to oxidize **RBM7–134** under the conditions described above for the preparation of **RBM7–083** proved unsuccessful. Although the consumption of the starting alcohol and the formation of a more polar fluorescent product were evidenced by TLC, purification of the crude mixture by flash chromatography led to the isolation of a major product which was further identified as umbelliferone (**7**). The same result was obtained when the crude mixture was purified on silica gel previously neutralized with a 1 % (v/v) TEA solution in hexane. These results corroborated the instability of the β,γ–unsaturated aldehyde **RBM7–136**, which was prone to spontaneously eliminate **7** on exposure to slightly acidic or alkaline conditions, instead of undergoing isomerization to the α,β–unsaturated isomer. In light of these results, the synthesis of aldehyde **RBM7–136** was disregarded.

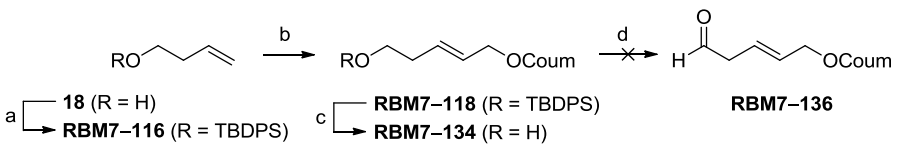

Scheme 3.3.8. Attempted synthesis of aldehyde **RBM7–136**. Reagents and conditions: (a) TBDPSCl, imidazole, DMF, rt, quant. yield; (b) **RBM7–115**, Grubbs cat. 2nd gen., CH_2Cl_2, reflux, 58 %, *E*/*Z* = 91:9; (c) TBAF, THF, 0 ºC to rt, 96 %; (d) DMP, CH_2Cl_2, 0 ºC to rt.

3.3.10 Optimization of the reaction conditions for the base–mediated release of umbelliferone using aldehyde RBM7–083

Initially, the release of umbelliferone using aldehyde **RBM7–083** was evaluated (Figure 3.3.5). Similarly to the experiments with **RBM13**, studies were performed using a 5 μM solution of **RBM7–083**, which corresponds to the equivalent amount of aldehyde that would be released if a ~5 % of the substrate **RBM7–077** (tested at 125 μM) was metabolized after S1PL incubation. Firstly, the release of **7** was examined after incubation of **RBM7–083** with a 200 mM glycine/NaOH buffer solution (pH 10.6), as previously described for **RBM13**.[6,26] Results showed that the release of **7** took place at lower rates than those described for aldehyde **5**, arising from the decomposition of **RBM13** by S1PL. In this case, the maximum release of umbelliferone was observed after 20 min of incubation, whereas aldehyde **RBM7–083** required up to 6 h of incubation to achieve the maximum release of umbelliferone (Figure 3.3.5A).

In view of these results, we disregarded the use of a glycine/NaOH buffer for the generation of umbelliferone from **RBM7–083**. Hence, we explored the use of alternative bases to increase the reaction rate. In this regard, aqueous NaOH and ethanolic KOH solutions were first considered as suitable candidates, mainly for their miscibility with the enzymatic reaction buffers required for the S1PL activity assays. However, incubation of **7** with these basic solutions at concentrations ranging from 200 to 1000 mM, resulted in a decrease of the fluorescence signal over time (Figure 3.3.5B). At concentrations ≥ 500 mM, almost a total loss of the fluorescence signal was observed after 3 h of incubation. In this case, we hypothesized that the opening of the lactone ring of **7** under alkaline conditions may account for the observed phenomenon. Thus, aqueous NaOH was disregarded at this stage, since it induced a more pronounced degradation of **7**. Subsequent experiments, however, showed that treatment of **7** with lower concentrations of ethanolic KOH at shorter incubation times gave a constant fluorescence signal after up to 60 min (Figure 3.3.5C). Surprisingly, despite the amount of **7** was constant in all experiments (5 μM), different fluorescence intensities were detected depending on the concentration of the basic solution. We speculated that low base concentrations can be inefficient to completely shift the ionization of umbelliferone towards the highly fluorescent anionic form. Thus, the use of two different base systems was considered (Figure 3.3.5C (+B)). In this regard, the successive treatment of **7** with KOH in EtOH followed by 200 mM glycine/NaOH

buffer (pH = 10.6) provided the highest fluorescence signals with an intensity maximum at KOH concentrations ≥ 50 mM. The use of 10 mM KOH was disregarded for further studies due to lower fluorescence intensity.

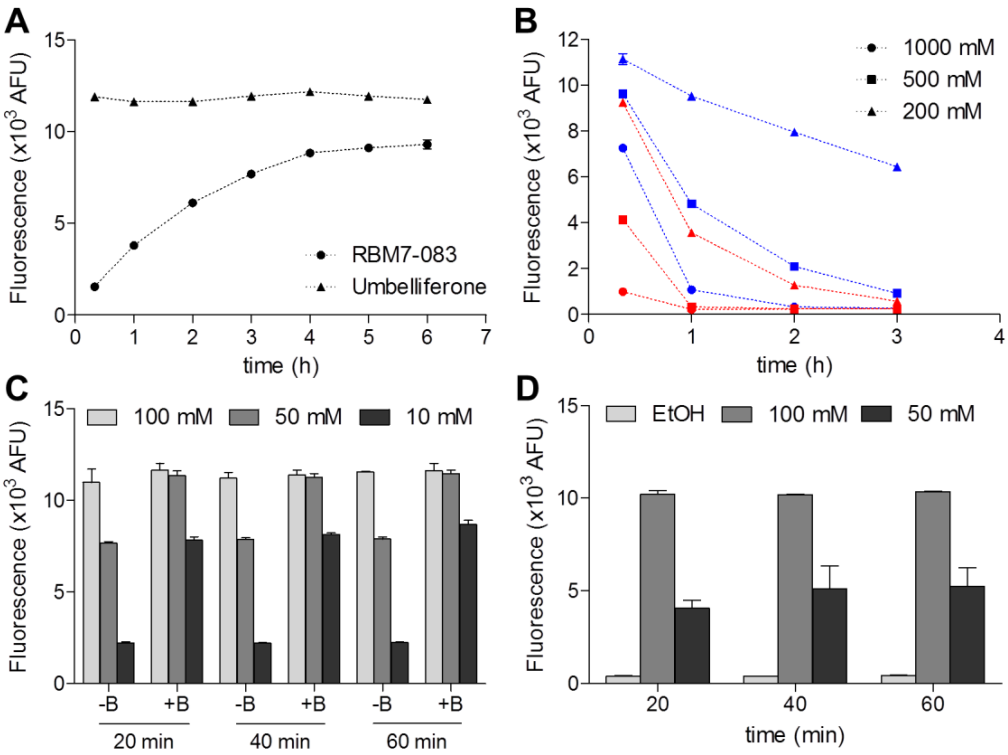

Figure 3.3.5. Optimization of the conditions for the base–mediated release of **7**. A 5 µM solution of either **RBM7-083** or **7** in a 100 mM HEPES buffer, pH 7.4, containing 0.1 mM EDTA, 0.05 % Triton X–100, 0.01 % Pluronic F127 (Biotium), and 100 µM pyridoxal 5′–phosphate (final volume: 100 µL) were successively treated with the corresponding basic solution (at the indicated concentrations) and/or solvent and incubated at 37 ºC for the indicated times before fluorescence reading ($\lambda_{ex/em}$ = 355/460 nm). In all cases, **7** and **RBM7-083** were added from 100 µM stock solutions in DMSO (5 µL). (A) **7** and **RBM7–083** were treated with 50 µL of MeOH and 100 µL of a 200 mM glycine/NaOH buffer solution (pH 10.6). (B) **7** was treated with 50 µL of MeOH and 100 µL of KOH in EtOH (blue) or aq. NaOH (red). (C) **7** was treated with 50 µL of MeOH and 100 µL of KOH in EtOH, incubated at 37 ºC and read (–B) or treated with 100 µL of KOH in EtOH, incubated at 37 ºC and further treated with 50 µL of a 200 mM glycine/NaOH buffer solution immediately before reading (+B). (D) **RBM7–083** was treated with 100 µL of KOH in EtOH, incubated at 37 ºC and further treated with 50 µL of a 200 mM glycine/NaOH buffer solution immediately before reading. Data are means ± SD of one representative experiment with triplicates.

Finally, **RBM7–083** was subjected to the above optimized conditions and the release of **7** was evaluated (Figure 3.3.5D). Results showed that treatment of **RBM7–083** with 100 mM KOH in EtOH provided a fluorescence intensity comparable to that obtained from **7** under the same conditions (Figure 3.3.5C), regardless of the incubation time employed. These results suggested that the elimination reaction with **RBM7–083** occurred in less than 20 min and confirmed that the released umbelliferone was stable under the assayed conditions, since no loss of fluorescence was observed up to 60 min of incubation time. The use of 50 mM KOH was disregarded since lower fluorescence values were achieved even at higher incubation times. From these overall results, incubation of **RBM7–083** with 100 mM ethanolic KOH for 20 min and further adjustment of the pH with 200 mM glycine/NaOH (pH = 10.6) was established as optimal. Under these conditions, the production of fluorescence increased linearly with the concentration of **RBM–083** up to 25 μM (results not shown).

3.3.11 Validation of RBM7–077 and RBM7–148 as hS1PL substrates

Once the conditions for the elimination of **7** from aldehyde **RBM7–083** were optimized, we next tested **RBM7–077** as S1PL substrate. For these experiments, recombinant hS1PL was used as enzyme source. Incubation of **RBM7–077** (125 μM) with hS1PL at graded enzyme concentrations showed a linear increase in product formation for up to 3 μg/mL of enzyme (Figure 3.3.6A). Product formation also increased in a linear manner up to 3 h of incubation time (Figure 3.3.6C). Taking into account these results we considered as optimal conditions an enzyme concentration of 0.8 μg/mL and 60 min of incubation time. Under these conditions, only around 5 % of the substrate was metabolized giving rise to a 30–fold increase of the fluorescence intensity with respect to the blank. Interestingly, although harsh basic conditions were employed, **7** was not formed from **RBM7–077** upon incubation with ethanolic KOH, since no significant production of fluorescence was observed in blank experiments without the enzyme.

Probe **RBM7–148** was also tested as hS1PL substrate. In this case, we were not able to optimize the conditions for the monitorization of the released umbelliferone, since the synthesis of the required model aldehyde **RBM7–136** was not possible (see Section 3.3.9). Therefore, **RBM7–148** was incubated with different amounts of hS1PL and the resulting enzymatic reaction mixture was independently treated with two different alkaline solutions in order to promote the formation of **7** (Figure 3.3.6B).

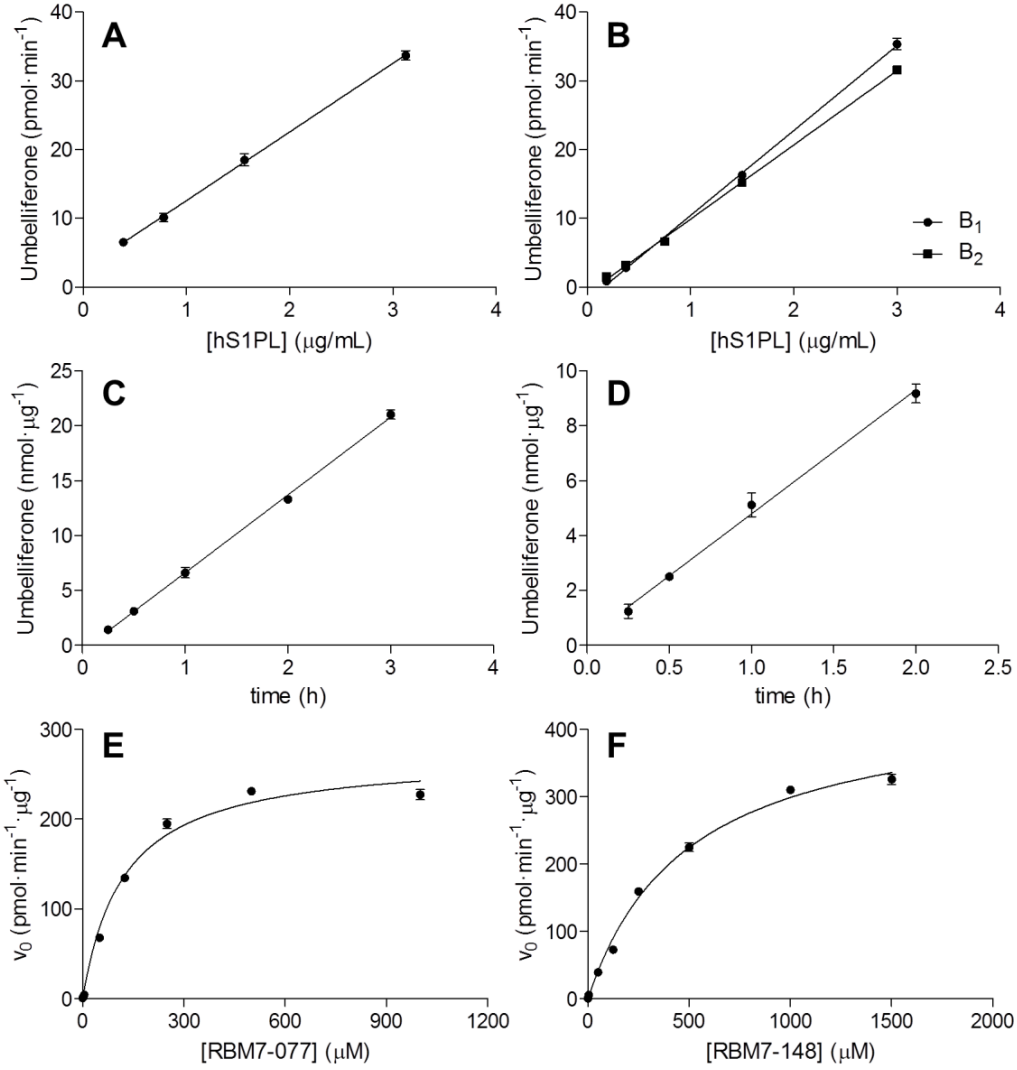

Figure 3.3.6. Enzyme concentration (A,B) and time (C,D) dependence of the hS1PL catalyzed reaction using **RBM7–077** (A,C) and **RBM7–148** (B,D) as substrates at a final concentration of 125 µM. A and B: Incubation time was 60 min. C and D: hS1PL concentration was 0.8 µg/mL. In B, the resulting enzymatic mixture was either diluted with MeOH (50 µL) and treated with 100 µL of 200 mM glycine/NaOH buffer (pH 10.6) (B_1) or alternatively, treated with 100 mM KOH/EtOH (100 µL), incubated for 20 min and the pH was further adjusted with the addition of 50 µL of a 200 mM glycine/NaOH buffer solution (pH 10.6) immediately before reading (B_2). Data are means ± SD of one representative experiment with triplicates. In E and F, the substrate concentration dependence of the initial velocity (V_O, expressed as pmol of **7** formed per minute and per µg of enzyme) of the hS1PL catalyzed reaction is represented. In both cases, hS1PL (0.8 µg/mL) was incubated for 60 min with **RBM7–077** (E) or **RBM7–148** (F) at graded concentrations. Data correspond to the mean ± SD of one representative experiment out of three performed with triplicates.

Results showed that similar fluorescence intensity was obtained regardless of the conditions employed. In both cases, the resulting fluorescence signal was constant up to 60 min of incubation time under basic conditions, indicating that the full release of **7** was accomplished in less than 20 min (results not shown). From these results we concluded that **RBM7–148** was indeed acting as substrate of S1PL, since product formation increased linearly with the amount of hS1PL up to 3 μg/mL. As stated above for **RBM7–077**, an enzyme concentration of 0.8 μg/mL, in which around 3 % of the substrate was metabolized, was established as optimal. Under these conditions and using a glycine/NaOH buffer solution as the base source (B_1), an 8–fold increase of the fluorescence signal was observed with respect to the blank. In contrast, the signal–to–noise ratio increased up to 25 times when ethanolic KOH was used instead (B_2). In this case, the observed differences were due to the lower fluorescence values obtained in blank experiments using the latter conditions. According to the observed ability of aldehyde **RBM7–136** in releasing **7** under milder basic conditions, we decided to perform the elimination reaction using a 200 mM glycine/NaOH buffer solution (pH 10.6). Under the optimized assay conditions, the product formation also increased linearly up to 2 h of incubation (Figure 3.3.6D). Thus, the optimal incubation time was established at 1h.

Kinetic parameters for **RBM7–077** and **RBM7–148** against hS1PL were next determined (Figures 3.3.6E and 3.3.6F, respectively). The results showed that the position of the double bond on these novel vinylogated probes had a significant effect on their enzymatic kinetic constants (Table 3.3.1). In terms of affinity, both compounds were much better substrates in comparison with **RBM13**, as deduced from their lower K_M values. Pleasingly, the determined K_M value for compound **RBM7–077** was more than one order of magnitude lower (15–fold decrease) compared to that obtained for **RBM13**. In the case of **RBM7–148**, however, a less pronounced decrease was observed since the determined K_M value was around 4–times lower. We speculated that the presence of the natural–like allyl alcohol moiety on **RBM7–077** would account for its lower K_M value. Furthermore, in comparison with **RBM13**, higher V_{max} values were determined for **RBM7–077** and **RBM7–148**, being the latter the best substrate with a 4–fold observed increase on its V_{max} value.

Table 3.3.1. Kinetic parameters for the hS1PL–catalyzed cleavage of **RBM7–077** and **RBM7–148**.[a]

Substrate	K_M (μM)	V_{max} (pmol·min^{-1}·μg^{-1})	V_{max}/K_M	IC_{50} 3c (nM)
RBM13[b]	1994 ± 121	107 ± 11	0.05	93.5 ± 6.0
RBM7–077	132 ± 14	263 ± 13	1.99	91.2 ± 7.1
RBM7–148	530 ± 52	452 ± 8	0.85	98.3 ± 6.2

[a]Data correspond to the mean ± SD of three independent experiments with triplicates. [b]See Section 3.1.4.1.

Overall, the calculated V_{max}/K_M ratios indicate that amino phosphates **RBM7–077** and **RBM7–148** are better substrates than **RBM13**, being compound **RBM7–077** the best substrate with a V_{max}/K_M =1.99. These results clearly validated our initial hypothesis, since the introduction of two carbon atoms between the polar head and the coumarin moiety in **RBM13** gives rise to better S1PL substrates with up to 40–times higher V_{max}/K_M ratios.

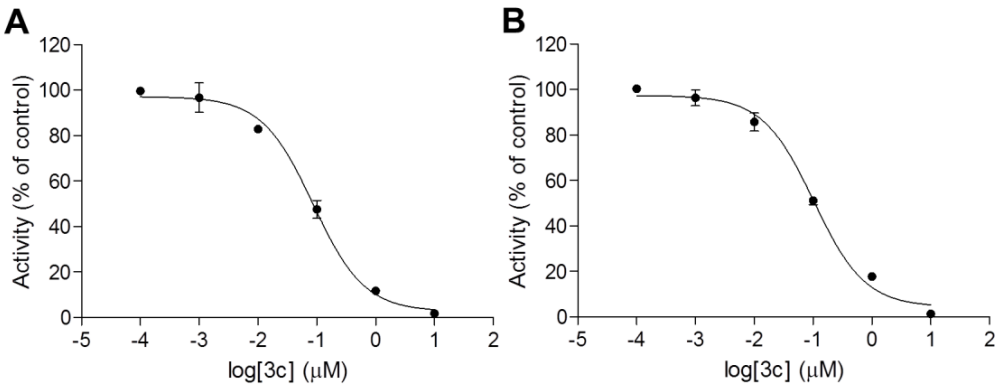

Figure 3.3.7. Activity (% of control) of hS1PL (final concentration: 0.8 μg/mL) at graded concentrations of **3c** using **RBM7–077** (A) or **RBM7–148** (B) as substrate (final concentration: 125 μM). Data correspond to the mean ± SD of one representative experiment out of three performed with triplicates

Finally, an IC_{50} value for the reference hS1PL inhibitor **3c** was determined in order to validate substrates **RBM7–077** and **RBM7–148** in our previously developed activity

assays. Results are summarized in Table 3.3.1. In both cases, an IC_{50} in the 90–100 nM range was determined (see Figure 3.3.7), which were almost identical to that determined for inhibitor **3c** using **RBM13** as substrate (see Section 3.1.4.2). All IC_{50} values were in the same order of magnitude than that originally reported for **3c** (IC_{50} = 24.0 ± 5.0 nM),[27] thus confirming the reliability of our novel series of fluorogenic S1PL substrates reported herein.

3.3.12 Computational studies

To this point, it was shown that the position of the coumarin unit with respect to the polar head of the fluorogenic probes studied in this section had a significant effect on their kinetic parameters as hS1PL substrates. In addition, the position of the double bound in **RBM7–077** and **RBM7–148** was also found to have an influence, as evidenced by the different kinetics determined for these two new vinylogated probes against the human enzyme. Thus, in an attempt to rationalize the obtained results, substrates **RBM13**, **RBM7–077** and **RBM7–148** were modeled covalently bound to PLP, as external aldimines **20a–c** (Figure 3.3.8A), in the hS1PL (PDB 4Q6R) active site.

For this purpose, after removing the bound ligands from the 4Q6R structure of hS1PL, the imine bond between the essential Lys353 and the PLP cofactor was cleaved and structures **20a–c** were manually build on the resulting PLP moiety. Figures 3.3.8B–D show the minimized structures of the three hS1PL–aldimine complexes. In all cases, the reactive C3–OH group establishes hydrogen bond interactions with the phosphate group of the PLP cofactor and with the side chain of His242. In the case of **RBM13**, the modeled structure shows that the coumarin unit is placed in the above mentioned hydrophobic patch formed by residues L173, H174, F290, W382 and Y387 (see Figure 3.3.8B). This disposition is in disagreement with our initial hypothesis, which proposed that the coumarin group could hinder the substrate–enzyme interaction because of its proximity to the C2–C3 cleavable bond. Similarly, the structures for the enzyme–bound aldimines **20b** and **20c** show the ω–coumarin group placed even further away from the reactive site, interacting not only with some of the residues of the above mentioned hydrophobic patch, but also with some residues which are closer to the entrance to the active site, such as I386, Y526 and F545 (see Figures 3.3.8C and 3.3.8D). Comparison of the spatial arrangement of aldimines **20b** and **20c** revealed that the position of the

double bond does not have significant influence in the disposition of both the linker and the coumarin group. However, the possibility that the different position of the double bond in **RBM7–077** and **RBM7–148**, or its absence in **RBM13**, could affect some steps of the enzymatic cycle, for example by modifying the acidity of the reactive C3−OH group, could not be discarded. Such effects could possibly explain the significant variation of the kinetic parameters of the three substrates.

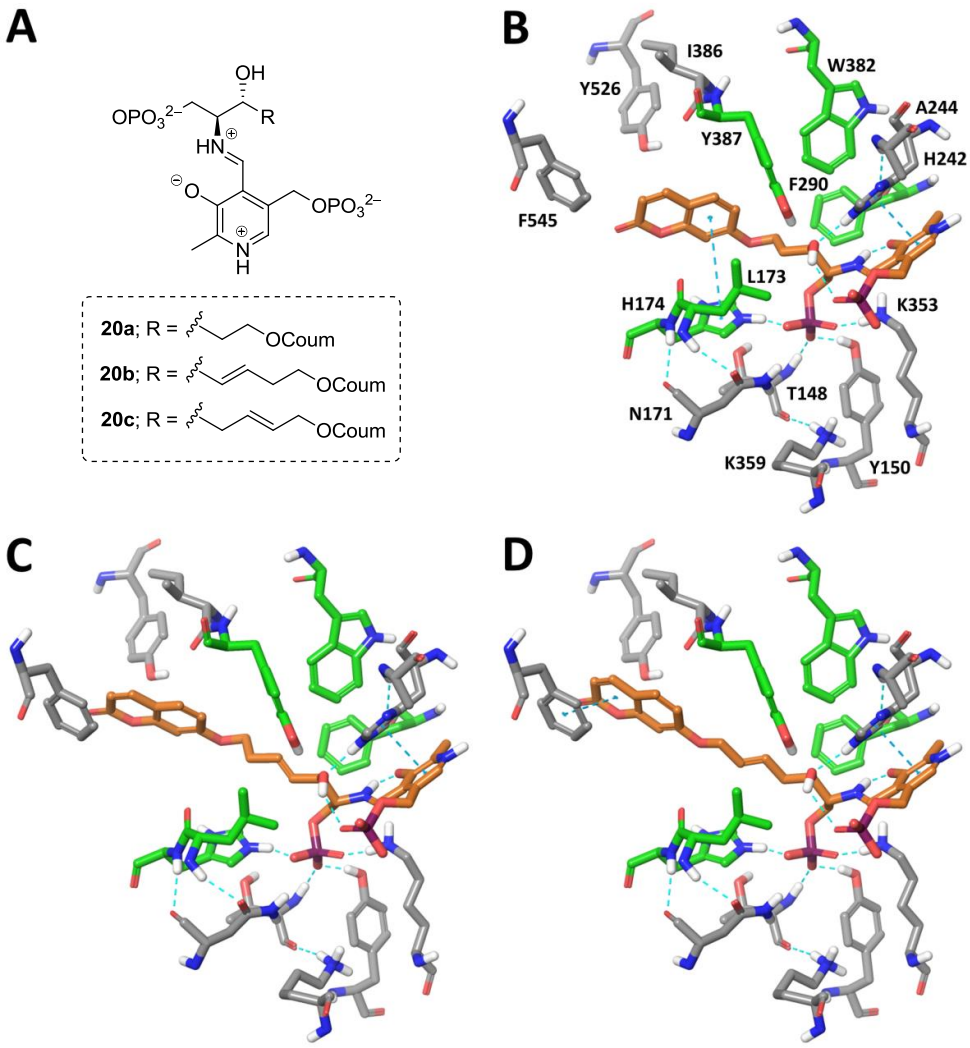

Figure 3.3.8. (A) Structures of modelled aldimines **20a–c**. (B–D) Complexes of aldimines **20a–c** (orange) bound into the active site of hS1PL. Residues forming a hydrophobic patch close to the PLP-binding site are highlighted in green.

To further asses the plausibility of such structures, the modelled aldimine **20a** complex was used as starting point to run a 50 ns molecular dynamics simulation (300 K, periodic boundary conditions, NPT ensemble) in explicit water, which better reflects the biological conditions. The simulation showed that the structure was mostly stable after an initial slight and normal rearrangement of the whole protein, with an RMSD of around 1.4 Å relative to the starting structure (see Figure 3.3.9A). Analysis of the hydrogen–bond interactions established by aldimine **20a** showed that the hydrogen bond between the C3–OH and the PLP–phosphate was kept for about 95 % of the simulation time whilst that between the C3–OH and His242 is being established only intermittently during the simulation, as it is also observed with Tyr387 (see Figure 3.3.9B). Analogous simulations with the complexes from aldimines **20b** and **20c** are currently underway in our group, however, given the similarity between the arrangements of the three aldimines in the context of the active site of hS1PL, similar results could be expected, and these could probably be extended also to the natural substrate S1P.

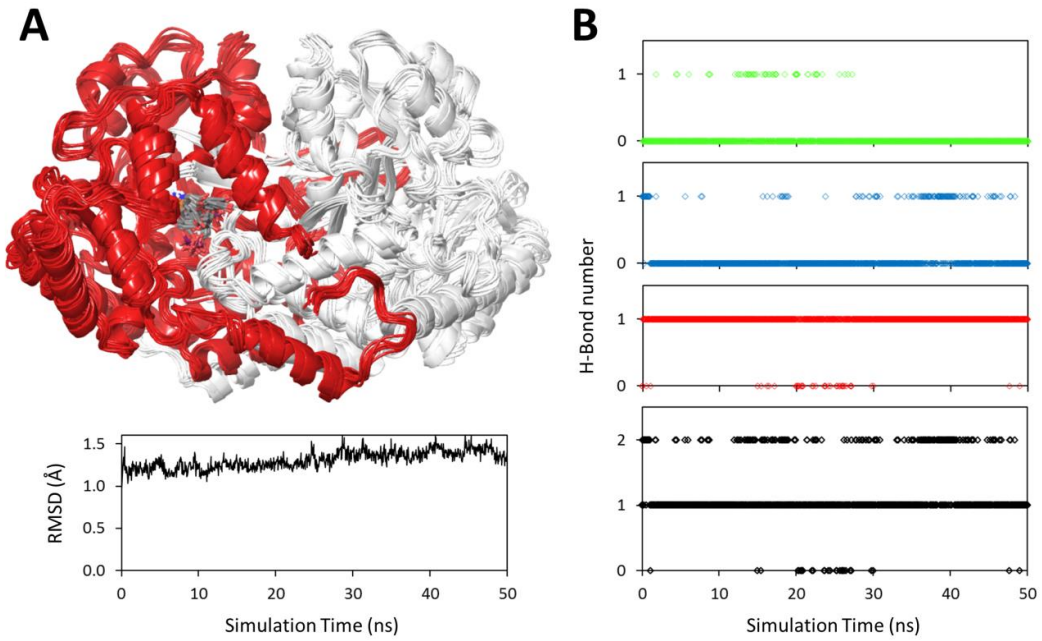

Figure 3.3.9. (A) Snapshots from the 50 ns MD simulation of the complex between aldimine **20a** and hS1PL, and RMSD plot. (B) Dependence of the number of hydrogen bond interactions established between the C3–OH of aldimine **20a** and the rest of the protein (black), the PLP phosphate group (red), His242 (blue) or Tyr387 (green) with simulation time.

Therefore, if confirmed, these simulations would suggest that the PLP-phosphate group could be the base responsible of the C3–OH deprotonation that is previous to the C–C bond cleavage in the enzymatic cycle. Similarly, the phosphate group of dihydroxyacetone phosphate (DHAP) has also been proposed as catalytic acid–base group in fructose–1,6–bisphosphate aldolase.[28]

The only other candidate base that apparently is close enough to the reactive C3–OH would be His242. However, that His242 could act as such a base seems less likely since the crystal structure of hS1PL shows that the δ–N of its imidazole ring accepts a hydrogen bond from the backbone amide of Ala244, thus forcing the ε–N to be protonated and becoming unable to act as acceptor of another proton. Instead, as observed in our simulation, the ε–NH of the imidazole is suitable to act as a hydrogen–bond donor if an acceptor group is placed appropriately, as the C3–OH of **RBM13** or the corresponding hydroxyl group on the other substrates considered. Therefore, it seems reasonable to propose that such hydrogen–bond interaction between His242 and the C3–OH of the substrate, as well as that formed with Tyr387 which is also observed although less frequently during the simulation, could serve to increase the acidity of this reactive OH, thus promoting the cleavage of the C–C bond and the concerted release of the corresponding aldehyde, both essential steps of the catalytic cycle of S1PL. If this hypothesis could be confirmed, it would add to clarify the identity of the catalytic base, which for now is unknown,[26] and the function of some of the essential residues of the S1PL active site.

3.3.13 References

(1) Van Veldhoven, P. P.; Mannaerts, G. P. Subcellular Localization and Membrane Topology of Sphingosine-1-Phosphate Lyase in Rat Liver. *J. Biol. Chem.* **1991**, *266* (19), 12502–12507.

(2) Van Veldhoven, P. P. [28] Sphingosine-1-Phosphate Lyase. In *Sphingolipid Metabolism and Cell Signaling Part A*; Enzymology, B. T.-M. in, Ed.; Academic Press, 2000; Vol. Volume 311, pp 244–254.

(3) Kashem, M. A.; Wa, C.; Wolak, J. P.; Grafos, N. S.; Ryan, K. R.; Sanville-Ross, M. L.; Fogarty, K. E.; Rybina, I. V; Shoultz, A.; Molinaro, T.; et al. A High-Throughput Scintillation Proximity Assay for Sphingosine-1-Phosphate Lyase. *Assay Drug Dev. Technol.* **2014**, *12* (5), 293–302.

(4) Bandhuvula, P.; Fyrst, H.; Saba, J. D. A Rapid Fluorescence Assay for Sphingosine-1-Phosphate Lyase Enzyme Activity. *J. Lipid Res.* **2007**, *48* (12), 2769–2778.

(5) Bandhuvula, P.; Li, Z.; Bittman, R.; Saba, J. D. Sphingosine 1-Phosphate Lyase Enzyme Assay Using a BODIPY-Labeled Substrate. *Biochem. Biophys. Res. Commun.* **2009**, *380* (2), 366–370.

(6) Bedia, C.; Camacho, L.; Casas, J.; Abad, J. L.; Antonio, D.; Van Veldhoven, P. P.; Fabriàs, G. Synthesis of a Fluorogenic Analogue of Sphingosine-1-Phosphate and Its Use to Determine Sphingosine-1-Phosphate Lyase Activity. *ChemBioChem* **2009**, *10* (5), 820–822.

(7) Berdyshev, E. V.; Goya, J.; Gorshkova, I.; Prestwich, G. D.; Byun, H. S.; Bittman, R.; Natarajan, V. Characterization of Sphingosine-1-Phosphate Lyase Activity by Electrospray Ionization-Liquid Chromatography/tandem Mass Spectrometry Quantitation of (2E)-Hexadecenal. *Anal. Biochem.* **2011**, *408* (1), 12–18.

(8) Krishnamurthy, S. The Principle of Vinylogy. *J. Chem. Educ.* **1982**, *59* (7), 543.

(9) Yamamoto, T.; Hasegawa, H.; Hakogi, T.; Katsumura, S. Versatile Synthetic Method for Sphingolipids and Functionalized Sphingosine Derivatives via Olefin Cross Metathesis. *Org. Lett.* **2006**, *8* (24), 5569–5572.

(10) Magolan, J.; Coster, M. J. Total Synthesis of (+)-Angelmarin. *J. Org. Chem.* **2009**, *74* (14), 5083–5086.

(11) Wahler, D.; Badalassi, F.; Crotti, P.; Reymond, J.-L. Enzyme Fingerprints of Activity, and Stereo- and Enantioselectivity from Fluorogenic and Chromogenic Substrate Arrays. *Chem. – A Eur. J.* **2002**, *8* (14), 3211–3228.

(12) Ren, X.-F.; Turos, E.; Lake, C. H.; Churchill, M. R. Regiochemical and Stereochemical Studies on Halocyclization Reactions of Unsaturated Sulfides. *J. Org. Chem.* **1995**, *60* (20), 6468–6483.

(13) Huang, W.; Ma, J.-Y.; Yuan, M.; Xu, L.-F.; Wei, B.-G. A Facile Approach to Trans-4,5-Pyrrolidine Lactam and Application in the Synthesis of Nemonapride and Streptopyrrolidine. *Tetrahedron* **2011**, *67* (40), 7829–7837.

(14) Gomtsyan, A. Direct Synthesis of β-Aminoketones from Amides via Novel Sequential Nucleophilic Substitution/Michael Reaction. *Org. Lett.* **2000**, *2* (1), 11–13.

(15) Gomtsyan, A.; Koenig, R. J.; Lee, C.-H. Novel Sequential Process from N-

Methoxyamides and Vinyl Grignard Reagents: New Synthesis of β-Aminoketones. *J. Org. Chem.* **2001**, *66* (10), 3613–3616.

(16) Hoffman, R. V; Maslouh, N.; Cervantes-Lee, F. Highly Stereoselective Syntheses of Syn- and Anti-1,2-Amino Alcohols. *J. Org. Chem.* **2002**, *67* (4), 1045–1056.

(17) Fransson, R.; McCracken, A. N.; Chen, B.; McMonigle, R. J.; Edinger, A. L.; Hanessian, S. Design, Synthesis, and Antileukemic Activity of Stereochemically Defined Constrained Analogues of FTY720 (Gilenya). *ACS Med. Chem. Lett.* **2013**, *4* (10), 969–973.

(18) Abad, J.-L.; Camps, F. Arylacetic Acid Derivatization of 2,3- and Internal Erythro-Squalene Diols. Separation and Absolute Configuration Determination. *Tetrahedron* **2004**, *60* (50), 11519–11525.

(19) Seco, J. M.; Quiñoá, E.; Riguera, R. The Assignment of Absolute Configuration by NMR. *Chem. Rev.* **2004**, *104* (1), 17–118.

(20) Seco, J. M.; Quiñoá, E.; Riguera, R. A Practical Guide for the Assignment of the Absolute Configuration of Alcohols, Amines and Carboxylic Acids by NMR. *Tetrahedron: Asymmetry* **2001**, *12* (21), 2915–2925.

(21) Wang, X.-L.; Yang, Y.-Y.; Chen, H.-J.; Wu, Y.; Ma, D.-S. Synthesis of a Vinylchlorine-Containing 1,3-Diol from a Marine Cyanophyte. *Tetrahedron* **2014**, *70* (30), 4571–4579.

(22) Postema, M. H. D.; Piper, J. L. Cross-Metathesis and Ring-Closing Metathesis of Olefinic Monosaccharides. *Tetrahedron Lett.* **2002**, *43* (39), 7095–7099.

(23) Bartlett, N.; Gross, L.; Péron, F.; Asby, D. J.; Selby, M. D.; Tavassoli, A.; Linclau, B. Stereocontrol by Quaternary Centres: A Stereoselective Synthesis of (−)-Luminacin D. *Chem. – A Eur. J.* **2014**, *20* (12), 3306–3310.

(24) Bartlett, S. L.; Beaudry, C. M. High-Yielding Oxidation of β-Hydroxyketones to β-Diketones Using O-Iodoxybenzoic Acid. *J. Org. Chem.* **2011**, *76* (23), 9852–9855.

(25) Caron, P.-Y.; Deslongchamps, P. Versatile Strategy to Access Tricycles Related to Quassinoids and Triterpenes. *Org. Lett.* **2010**, *12* (3), 508–511.

(26) Bourquin, F.; Riezman, H.; Capitani, G.; Grütter, M. G. Structure and Function of Sphingosine-1-Phosphate Lyase, a Key Enzyme of Sphingolipid Metabolism. *Structure* **2010**, *18*, 1054–1065.

(27) Weiler, S.; Braendlin, N.; Beerli, C.; Bergsdorf, C.; Schubart, A.; Srinivas, H.; Oberhauser, B.; Billich, A. Orally Active 7-Substituted (4-Benzylphthalazin-1-Yl)-2-Methylpiperazin-1-Yl]nicotinonitriles as Active-Site Inhibitors of Sphingosine 1-Phosphate Lyase for the Treatment of Multiple Sclerosis. *J. Med. Chem.* **2014**, *57*, 5074–5084.

(28) St-Jean, M.; Sygusch, J. Stereospecific Proton Transfer by a Mobile Catalyst in Mammalian Fructose-1,6-Bisphosphate Aldolase. *J. Biol. Chem.* **2007**, *282* (42), 31028–31037.

4. Summary and conclusions

The most remarkable conclusions derived from each of the topics presented in the present doctoral thesis are highlighted in this section.

1) A structure–based drug design (SBDD) of S1PL inhibitors was performed using the crystal structures of the bacterial (StS1PL) and human (hS1PL) enzymes. From this analysis, a pharmacophoric model was derived consisting on: a carboxylate group linked to an aromatic moiety by means of a short spacer of variable nature. Taking into account the above features, the general structure **9** was proposed as a suitable scaffold for the development of a small library of potential S1PL binders. Consequently, a series of *N*–acylanilino carboxylates was designed, synthesized and tested against both enzyme sources.

2) Our previously reported fluorogenic probe **RBM13** was found to be a suitable substrate for bacterial and human S1PL, thus allowing the development of a HTS amenable on–plate S1PL activity assay using purified enzymes. In addition, both enzymes showed comparable experimental kinetic parameters using substrate **RBM13**.

3) Unfortunately, attempts to rationally design a set of active–site directed S1PL inhibitors have met with limited success, as evidenced by the modest activity found for the designed *N*–acylanilino carboxylates. Either overestimation of the ionic interactions in the active site or the inability of our compounds to reach it, may explain the observed results. Surprisingly, the known hS1PL inhibitor **3c** did not show any activity on StS1PL. Comparison of the structures of both enzymes suggested that this lack of activity could be due to the structural differences between both enzymes found at the access channel to the enzyme active site.

4) Based on S1PL mechanistic considerations, two kinds of S1PL inhibitors were designed and tested using bacterial (StS1PL) and human (hS1PL) enzyme sources. Compounds **RBM7–001**, **RBM7–012** and **RBM7–032**, were designed as non–reactive analogs of the corresponding internal aldimines **13** and **15**. These compounds were obtained by reductive amination of PLP with either *O*–phosphorylethanolamine, dhS1P or S1P, respectively, and they were weak inhibitors on both enzyme sources, probably due to the steric constraints imposed by the PLP moiety.

5) On the other hand, a series of stereodefined azido phosphates were conceived as non–reactive, potential S1PL competitive inhibitors, since the amino group of both enzyme substrates (dhS1P and S1P) was replaced by an azido group.

6) The synthesis of the differently configured azidophosphates was carried out from the corresponding stereodefined sphingosines, whose synthesis was successfully accomplished after a key diastereocontrolled addition to L– or D–Garner's aldehyde. Diazo transfer reaction followed by a site–selective phosphorylation at the C1–OH gave the required azido phosphates in 15–25 % overall yields from the starting Garner's aldehydes.

7) All the azido phosphates behaved as competitive inhibitors in the low μM range on the two S1PL isozymes tested, being the *anti*–isomers with the non–natural enantiomeric configuration slightly more potent inhibitors on hS1PL. For this series of compounds, the presence of a phosphate group at C1 was found to be crucial to ensure a strong enzyme binding.

8) Taken together, these results provide support to the hypothesis that the more easily available StS1PL can be a useful model for the design of hS1PL inhibitors that bind into the active site. However, considering the results obtained for the described inhibitor **3c**, the usefulness of this model protein is more limited if one wants to design compounds that target the active site access channel.

9) Two new vinyl derivatives of the previously reported compound **RBM13** were designed, synthesized and evaluated as hS1PL substrates. In both cases, a vinyl group was intercalated between the amino alcohol phosphate moiety and the ω–coumarin group of the parent compound. While the vinyl unit in **RBM7–077** was placed at the C4–C5 position, which retained the allylic alcohol motif of the natural substrate, the double bond in **RBM7–148** was located at C5–C6.

10) Nucleophilic addition of the appropriate alkenyl Grignard reagent to Weinreb's amide **RBM7–070**, followed by a diasteroselective reduction yielded alkenes **RBM7–072** and **RBM–135** with the required (2*S*,3*R*) configuration.

11) The olefin cross–metathesis reaction of alkenes **RBM7–071** and **RBM7–135** with their corresponding olefin partners **RBM7–069** and **RBM7–115** was found to be a suitable way to access the required coupling products **RBM7–078** and

RBM7–141 with excellent *E*:*Z* ratios. Subsequent site–selective phosphorylation at the C1–OH group afforded zwitterionic probes **RBM7–077** and **RBM7–148** in good yields.

12) Oxidation of allylic alcohol **RBM7–081** yielded aldehyde **RBM7–083**, whereas attempts to oxidize the corresponding homoallylic derivative **RBM7–134** were unsuccessful likely due to the instability of the resulting aldehyde **RBM7–136**. Studies on the base–mediated elimination of umbelliferone from aldehyde **RBM7–083** revealed that incubation with KOH in ethanol and further adjustment of the pH with 200 mM Gly/NaOH (pH = 10.6) were the optimal conditions for the complete and efficient release of umbelliferone from the model aldehyde.

13) Probes **RBM7–077** and **RBM7–148** were validated as hS1PL substrates. In terms of V_{max}/K_M, both compounds were much better than **RBM13**, being the naturally configured compound **RBM7–077** the best substrate with a 40–fold improvement in the V_{max}/K_M ratio. Both probes were revealed as suitable non–natural hS1PL substrates for the identification of putative S1PL inhibitors, as illustrated by the determination of IC_{50} values for the reference hS1PL inhibitor **3c**, which were consistent with that originally reported using S1P as substrate.

5. Experimental section

5.1 Chemistry

5.1.1 General remarks

Unless otherwise stated, reactions were carried out under argon atmosphere. Dry solvents were obtained by passing through an activated alumina column on a Solvent Purification System (SPS). Methanol and ethanol were dried over CaH_2 and distilled prior to use. Commercially available reagents and solvents were used with no further purification. All reactions were monitored by TLC analysis using ALUGRAM® SIL G/UV_{254} precoated aluminum sheets (Machery–Nagel). UV light was used as the visualizing agent and a 5% (w/v) ethanolic solution of phosphomolybdic acid as the developing agent. Flash column chromatography was carried out with the indicated solvents using flash–grade silica gel (37–70 μm). Preparative reversed–phase purifications were performed on a Biotage® Isolera™ One equipment with the indicated solvents using a Biotage® SNAP cartridge (KP–C18–HS, 12 g) at a flow rate of 12 mL/min. Yields refer to chromatographically and spectroscopically pure compounds, unless otherwise stated.

NMR spectra were recorded at room temperature on a Varian Mercury 400 instrument. The chemical shifts (δ) are reported in ppm relative to the solvent signal, and coupling constants (*J*) are reported in Hertz (Hz). ^{31}P chemical shifts are relative to a 85 % H_3PO_4 external reference (0 ppm). For ^{13}C NMR spectra recorded in D_2O, a 0.5 % (w/v) solution of DSS (4,4–dimethyl–4–silapentane–1–sulfonic acid) in D_2O was used as external reference (0 ppm). In the case of NMR spectra recorded in $CDCl_3/CD_3OD$ mixtures, chemical shifts are expressed relative to the residual peak of CD_3OD. The following abbreviations are used to define the multiplicities in ^1H NMR spectra: s = singlet, d = doublet, t = triplet, q = quartet, dd = doublet of doublets, ddd = doublet of doublet of doublets, m = multiplet, br = broad signal and app = apparent. High Resolution Mass Spectrometry analyses were carried out on an Acquity UPLC system coupled to a LCT Premier orthogonal accelerated time–of–flight mass spectrometer (Waters) using electrospray ionization (ESI) technique. Optical rotations were measured at room temperature on a Perkin Elmer 341 polarimeter.

HPLC analyses were carried out on an Alliance HPLC system consisting of a 2695 Separation Module (Waters) coupled to a 2996 PDA detector (Waters) and a light scattering ELS–1000 detector (Polymer Laboratories). Column A corresponds to a

Phenomenex® Lux Amylose–2 (250 x 4.60 mm) and column B corresponds to a Chiralpak® IA (250 x 4.60 mm). Hexane/isopropanol mixtures at a flow rate of 1 mL/min were used as mobile phase and the monitoring wavelength was set at 220 nm. Injection volume was 5 μL. Retention times (R_T) correspond to peaks observed using the PDA detector.

Garner's aldehyde,[1] amide **RBM7–070**[2] and ISA·HCl[3] were synthesized following previously described methods.

5.1.2 General synthetic methods

General procedure 1: CuAAC between 3–ethynylaniline and selected azides

To a solution of 3–ethynylaniline (13 mmol) and the selected azide (1.2 equiv./mol) in a mixture H_2O/THF (1:1) (75 mL), $CuSO_4 \cdot 5H_2O$ (0.1 equiv./mol) and sodium ascorbate (0.1 equiv./mol) were added. After stirring under argon at rt for 1 h, the reaction mixture was extracted with EtOAc (3 x 50 mL). The combined organic layers were dried over anhydrous $MgSO_4$ and concentrated to give a residue which was purified by flash chromatography on elution with DCM/MeOH (98.5:1.5) to afford the corresponding cycloaddition adducts.

General procedure 2: HATU–mediated coupling for amide–bond formation

A 15 mL screw cap tube was charged with the selected carboxylic acid (1.1 equiv./mol), HATU (2 equiv./mol), DMF (1 mL) and DIPEA (2 equiv./mol). A solution of the selected aniline (0.4 mmol) in DMF (1 ml) was then added dropwise. The tube was flushed with argon, sealed and the mixture was stirred overnight at 40 ºC. After cooling down to rt, the crude reaction mixture was diluted with water (10 mL) and extracted with EtOAc (3 x 15 mL). The combined organic layers were washed with brine (3 x 15 mL), dried over anhydrous $MgSO_4$, filtered and concentrated under reduced pressure to give a residue, which was purified as indicated for each compound.

General procedure 3: EDC/HOBt–mediated coupling for amide–bond formation

To a stirred solution of the selected carboxylic acid (0.5 mmol) and HOBt (1.2 equiv./mol) in DMF (2 mL), was added dropwise a solution of the selected aniline (1 equiv./mol) in DMF (2 mL). EDC (1.2 equiv./mol) was then added portionwise and the mixture was stirred overnight at rt. The crude reaction mixture was diluted with water (10 mL) and extracted with EtOAc (3 x 15 mL). The combined organic layers were washed with brine (3 x 15 mL), dried over anhydrous $MgSO_4$, filtered and concentrated under reduced pressure to give a crude mixture, which was purified as indicated for each compound.

General procedure 4: Base–mediated hydrolysis of methyl esters

To a stirred solution of the selected methyl ester (0.1 mmol) in THF/H_2O (3:1) (20 mL), LiOH (3 equiv./mol) was added at 0 ºC. After stirring at the same temperature for 1.5 h,

the reaction mixture was acidified with 1*N* HCl and extracted with EtOAc (3 x 15 mL). The combined organic layers were dried over anhydrous $MgSO_4$, filtered and concentrated under reduced pressure to give a residue, which, unless otherwise noted, was purified by preparative RP chromatography (Solvent A: 0.2 % (v/v) formic acid in CH_3CN; Solvent B: 0.2 % (v/v) aq. formic acid; from 5 to 100 % A in B), to give pure carboxylic acids.

General procedure 5: Reductive amination between PLP and selected amines

To an ice cooled solution of the selected amine (0.1 mmol) in dry CH_3OH (3 mL) was added KO*t*–Bu (2 equiv./mol) and the mixture was stirred at rt for 30 min (Solution A). Simultaneously, KO*t*–Bu (2 equiv./mol of PLP) was added to a solution of PLP (1.3 equiv./mol) in CH_3OH (3 mL) at 0 ºC and the mixture was stirred at rt for 30 min (Solution B). Solution A was then added dropwise to solution B at 0 ºC and the mixture was refluxed in the dark for 3 h, cooled to 0 ºC and treated with $NaBH_4$ (1.3 equiv./mol). After stirring at rt for 1h, the reaction mixture was acidified by the dropwise addition of 6 M aq. HCl and the solvent was evaporated to dryness to give a residue, which was purified as indicated for each compound.

General procedure 6: Ru–catalyzed olefin cross metathesis reactions

To a stirred solution of the starting olefins (1.5 and 6 mmol, respectively) in degassed CH_2Cl_2 (20 mL), Grubbs catalyst 2nd generation (0.03 equiv./mol) was added portionwise at rt. The resulting mixture was refluxed in the dark for 2 h, cooled down to rt and concentrated *in vacuo* to afford a crude, which was purified as indicated for each compound.

General procedure 7: Acid–mediated removal of isopropylidene groups

To a solution of the protected amino diol (1.0 mmol) in MeOH (35 mL) was added *p*–TsOH (0.1 equiv./mol) and the mixture was stirred overnight at room temperature. Et_3N (0.1 equiv./mol) was then added and the solvent was removed under reduced pressure to give a residue, which was purified by flash chromatography on silica gel (from 0 to 40 % EtOAc in hexane) to afford the required products.

General procedure 8: Catalytic hydrogenation of double bonds

To a solution of the corresponding allylic alcohol (1.3 mmol) in degassed MeOH (50 mL) was added Rh/Al_2O_3 (10 % w/w) and the mixture was stirred for 2.5 h at rt under hydrogen atmosphere (balloon). The reaction mixture was then filtered through Celite and the particles were rinsed with MeOH (3 x 5 mL). The combined filtrates were concentrated *in vacuo* to give a residue, which was purified by flash chromatography on silica gel (from 0 to 45 % EtOAc in hexane), yielding the required compounds.

General procedure 9: Acid–mediated removal of *N*–Boc protecting groups

To an ice cooled solution of the corresponding *N*–Boc protected aminodiol (0.8 mmol) in MeOH (12 mL) was added dropwise neat acetyl chloride (5 equiv./mol). After stirring at rt overnight, the reaction mixture was concentrated *in vacuo* to give a crude mixture, which was purified by flash chromatography on silica gel (from 0 to 20 % MeOH in CH_2Cl_2), to afford the required amine hydrochlorides.

General procedure 10: Cu–catalyzed diazotransfer reaction

To a stirred mixture of the corresponding amine hydrochloride (0.7 mmol), K_2CO_3 (2.7 equiv./mol) and $CuSO_4 \cdot 5H_2O$ (0.01 equiv./mol) in MeOH (7 mL) was added ISA·HCl (1.2 equiv./mol) in one portion. After stirring at rt overnight, the mixture was concentrated, diluted with H_2O (5 mL), acidified with 1 M aqueous HCl and extracted with EtOAc (3 x 10 mL). The combined organic layers were washed with brine (2 x 10 mL), dried over anhydrous $MgSO_4$, filtered and evaporated *in vacuo*. Purification of the residue by flash chromatography (from 0 to 25 % EtOAc in hexane) gave the required azido derivatives.

General procedure 11: Site–selective phosphorylation of 1,3–diols

A solution of the starting diol (0.5 mmol) in CH_2Cl_2 (15 mL) at 0 ºC was treated successively with *N*–methylimidazole (1.5 equiv./mol) and dimethyl chlorophosphate (1.2 equiv./mol). The reaction mixture was stirred at rt for 1 h, cooled down to 0 ºC and quenched by the dropwise addition of saturated aqueous NH_4Cl (10 mL). The resulting mixture was extracted with CH_2Cl_2 (3 x 15 mL) and the combined organic layers were washed with brine (2 x 20 mL), dried over anhydrous $MgSO_4$ and filtered. Evaporation

of the solvent afforded a crude mixture, which was purified as indicated for each compound.

General procedure 12: TMSBr–mediated deprotection of dimethyl phosphates and *N*–Boc amino groups.

To an ice cooled solution of the starting dimethyl phosphate (0.2 mmol) in dry CH_3CN (8 mL), was added dropwise TMSBr (4–5 equiv./mol). After stirring for 3 h at rt, the reaction mixture was concentrated under reduced pressure. The residue was then redissolved in MeOH/H_2O (95:5, same reaction volume) and stirred for an additional hour at rt. Evaporation of the solvent afforded a crude mixture, which was purified as indicated for each compound.

General procedure 13: Synthesis of (R)– and (S)–MPA esters

DMAP (1.1 equiv./mol) was added portionwise at 0 ºC to a solution of the starting alcohol (0.2 mmol) in CH_2Cl_2 (2 mL) containing (*R*)–(–)– or (*S*)–(+)–MPA (1.6 equiv./mol) and EDC (1.5 equiv./mol). After stirring for 6 h at rt, the reaction mixture was washed with saturated aq. $NaHCO_3$ (2 x 2 mL) and the organic phase was separated, dried over anhydrous $MgSO_4$, filtered and evaporated to dryness. The resulting residue was flash chromatographed on silica gel (from 0 to 8 % EtOAc in hexane) to give the corresponding MPA esters.

General procedure 14: fluoride–mediated deprotection of TBS groups

To a solution of the corresponding TBS–protected alcohol (1 mmol) in THF (10 mL) was added dropwise TBAF (1 M in THF, 2 equiv./mol) at 0 ºC. After stirring at the same temperature for 30 min, the reaction was quenched with saturated aqueous NH_4Cl (10 mL) and the resulting mixture was extracted with Et_2O (3 x 15 mL). The combined organic layers were washed with brine (2 x 20 mL), dried over anhydrous $MgSO_4$, filtered, and evaporated to give the crude products. Purification by flash chromatography on silica gel (from 0 to 3 % MeOH in CH_2Cl_2) afforded the required alcohols.

5.1.3 Synthesis and characterization of compounds from Section 3.1

5.1.3.1 Synthesis of scaffolds **RBM7–021** and **RBM7–022**

Methyl 2–azidoacetate (RBM7–019)

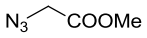

Sodium azide (829 mg, 12.8 mmol) was added to a solution of methyl 2–bromoacetate (1.3 g, 8.5 mmol) in DMSO (35 mL). The mixture was stirred at rt for 20 h and then poured into cold water (80 mL). The resulting solution was extracted with Et_2O (3 x 50 mL) and the combined organic fractions were washed with brine (3 x 50 mL), dried over anhydrous $MgSO_4$ and carefully concentrated to afford the methyl ester **RBM7–019** (902 mg, 92%) as a colourless oil that was suitable for use without further purification.

^{1}H NMR (400 MHz, $CDCl_3$) δ 3.89 (s, 2H), 3.80 (s, 3H). ^{13}C NMR (101 MHz, $CDCl_3$) δ 168.9, 52.8, 50.4. HRMS calcd. for $C_3H_6N_3O_2$ ($[M + H]^+$): 116.0460, found: 116.0462.

Methyl 3–azidopropionate (RBM7–020)

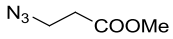

Sodium azide (655 mg, 10.1 mmol) was dissolved in water (10 mL) and DMF (10 mL) was added. To this solution, methyl 3–bromopropionate (1 mL, 9.16 mmol) was added dropwise and the biphasic mixture was stirred at 55 ºC for 18 h. After cooling to rt, the crude reaction mixture was extracted with Et_2O (3 x 50 mL). The combined organic layers were washed with brine (3 x 50 mL), dried over anhydrous $MgSO_4$ and carefully concentrated to afford the methyl ester **RBM7–020** (1.05 g, 89%) as a yellow oil that was suitable for use without further purification.

^{1}H NMR (400 MHz, $CDCl_3$) δ 3.73 (s, 3H), 3.58 (t, J = 6.5 Hz, 2H), 2.59 (t, J = 6.5 Hz, 2H). ^{13}C NMR (101 MHz, $CDCl_3$) δ 171.4, 52.2, 46.9, 33.9. HRMS calcd. for $C_4H_8N_3O_2$ ($[M + H]^+$): 130.0616, found: 130.0619.

Methyl 2–(4–(3–aminophenyl)–1*H*–1,2,3–triazol–1–yl)acetate (RBM7–021)

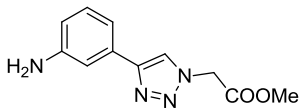

Compound **RBM7–021** (pale yellow solid, 3.72 g, quantitative yield) was obtained from 3–ethynylaniline (1.8 mL, 15.98 mmol), azide **RBM7–019** (2.21 g, 19.18 mmol), $CuSO_4 \cdot 5H_2O$ (399 mg, 1.6 mmol) and sodium ascorbate (317 mg, 1.6 mmol), according to general procedure 1.

^{1}H NMR (400 MHz, $CDCl_3$) δ 7.86 (s, 1H), 7.29 – 7.27 (m, 1H), 7.23 – 7.14 (m, 2H), 6.68 (ddd, *J* = 7.7, 2.4, 1.2 Hz, 1H), 5.21 (s, 2H), 3.83 (s, 3H). ^{13}C NMR (101 MHz, $CDCl_3$) δ 166.9, 148.4, 146.8, 131.3, 129.9, 121.2, 116.3, 115.3, 112.5, 53.2, 50.9. HRMS calcd. for $C_{11}H_{13}N_4O_2$ ($[M + H]^+$): 233.1039, found: 233.1037.

Methyl 3–(4–(3–aminophenyl)–1*H*–1,2,3–triazol–1–yl)propionate (RBM7–022)

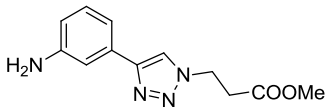

Compound **RBM7–022** (pale yellow solid, 2.54 g, 97 %) was obtained from 3–ethynylaniline (1.2 mL, 10.65 mmol), azide **RBM7–020** (1.65 g, 12.78 mmol), $CuSO_4 \cdot 5H_2O$ (266 mg, 1.07 mmol) and sodium ascorbate (211 mg, 1.07 mmol), according to general procedure 1.

^{1}H NMR (400 MHz, $CDCl_3$) δ 7.82 (s, 1H), 7.26 – 7.25 (m, 1H), 7.22 – 7.12 (m, 2H), 6.66 (ddd, *J* = 7.8, 2.4, 1.2 Hz, 1H), 4.69 (t, *J* = 6.4 Hz, 2H), 3.71 (s, 3H), 3.01 (t, *J* = 6.4 Hz, 2H). ^{13}C NMR (101 MHz, $CDCl_3$) δ 171.2, 147.9, 146.9, 131.5, 129.8, 120.7, 116.1, 115.1, 112.4, 52.3, 45.6, 34.6. HRMS calcd. for $C_{12}H_{15}N_4O_2$ ($[M + H]^+$): 247.1195, found: 247.1188.

5.1.3.2 Synthesis of *N*–acylanilino carboxylates

(*S*)–methyl 2–(4–(3–(1–(2–(((benzyloxy)carbonyl)amino)acetyl)pyrrolidine–2–carboxamido)phenyl)–1*H*–1,2,3–triazol–1–yl)acetate (RBM7–027)

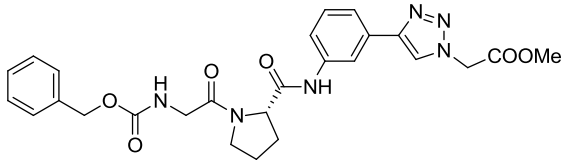

Compound **RBM7–027** (white solid, 42 mg, 54 %) was obtained from aniline **RBM7–021** (35 mg, 0.151 mmol), Z–Gly–Pro–OH (51 mg, 0.166 mmol), HATU (115 mg, 0.301 mmol) and DIPEA (53 µL, 0.301 mmol), according to general procedure 2. The title compound was purified by preparative RP chromatography (from 5 to 100 % CH_3CN in H_2O).

^{1}H NMR (400 MHz, $CDCl_3$) δ 9.36 (s, 1H), 7.89 (s, 1H), 7.87 (s, 1H), 7.56 (d, *J* = 7.7 Hz, 1H), 7.51 (ddd, *J* = 8.1, 2.0, 0.9 Hz, 1H), 7.37 – 7.27 (m, 6H), 5.79 (t, *J* = 4.3 Hz, 1H), 5.19 (s, 2H), 5.11 (s, 2H), 4.75 (dd, *J* = 8.1, 1.6 Hz, 1H), 4.05 (dd, *J* = 12.0, 4.7 Hz, 2H, major rotamer), 3.81 (s, 3H), 3.63 – 3.55 (m, 1H), 3.48 – 3.38 (m, 1H), 2.53 – 2.44 (m, 1H), 2.25 – 2.12 (m, 1H), 2.11 – 2.00 (m, 1H), 1.98 – 1.85 (m, 1H). ^{13}C NMR (101 MHz, $CDCl_3$) δ 169.2, 169.0, 166.9, 156.5, 148.0, 138.7, 136.4, 130.9, 129.5, 128.6, 128.3, 128.2, 121.6, 121.5, 119.7, 117.1, 67.1, 61.3, 53.2, 50.9, 46.7, 43.6, 27.7, 25.0. HRMS calcd. for $C_{26}H_{29}N_6O_6$ ($[M + H]^+$): 521.2149, found: 521.2181.

(*S*)–methyl 3–(4–(3–(1–(2–(((benzyloxy)carbonyl)amino)acetyl)pyrrolidine–2–carboxamido) phenyl)–1*H*–1,2,3–triazol–1–yl)propanoate (RBM7–028)

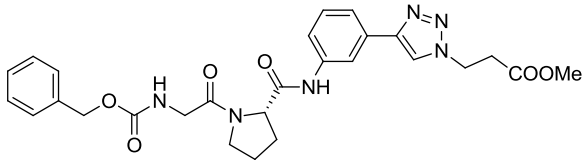

Compound **RBM7–028** (white solid, 40 mg, 61%) was obtained from aniline **RBM7–022** (30 mg, 0.122 mmol), Z–Gly–Pro–OH (41 mg, 0.134 mmol), HATU (93 mg, 0.244 mmol) and DIPEA (42 µL, 0.244 mmol), according to general procedure 2. The title compound was purified by preparative RP chromatography (from 5 to 100 % CH_3CN in H_2O).

^{1}H NMR (400 MHz, $CDCl_3$) δ 9.39 (s, 1H), 7.87 – 7.84 (m, 1H), 7.82 (s, 1H), 7.54 – 7.49 (m, 2H), 7.34 – 7.25 (m, 6H), 5.86 (t, *J* = 4.4 Hz, 1H), 5.10 (s, 2H), 4.75 (dd, *J* = 8.1, 1.9 Hz, 1H), 4.65 (t, *J* = 6.5 Hz, 2H), 4.04 (dd, *J* = 8.9, 4.8 Hz, 2H), 3.69 (s, 3H), 3.63 – 3.55 (m, 1H), 3.46 – 3.36 (m, 1H), 2.99 (t, *J* = 6.5 Hz, 2H), 2.48 – 2.40 (m, 1H), 2.24 – 2.12 (m, 1H), 2.08 – 1.98 (m, 1H), 1.98 – 1.88 (m, 1H). ^{13}C NMR (101 MHz, $CDCl_3$) δ 171.1, 169.1, 169.1, 156.5, 147.4, 138.7, 136.4, 131.2, 129.5, 128.6, 128.3, 128,2, 121.5, 121.0, 119.6, 117.1, 67.2, 61.2, 52.3, 46.7, 45.7, 43.6, 34.5, 27.5, 25.0. HRMS calcd. for $C_{27}H_{31}N_6O_6$ ($[M + H]^+$): 535.2305, found: 535.2318.

(*S*)–methyl 2–(4–(3–(2–((((9*H*–fluoren–9–yl)methoxy)carbonyl)amino)–3–cyclohexyl propanamido)phenyl)–1*H*–1,2,3–triazol–1–yl)acetate (RBM7–033)

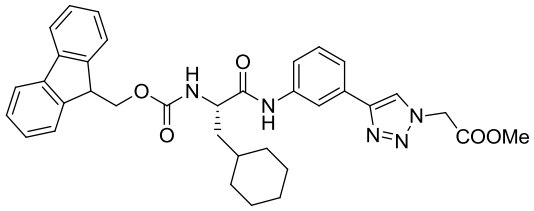

Compound **RBM7–033** (white solid, 161 mg, 62 %) was obtained from aniline **RBM7–021** (100 mg, 0.43 mmol), Fmoc–Cha–OH (186 mg, 0.47 mmol), HATU (328 mg, 0.86 mmol) and DIPEA (150 µL, 0.86 mmol), according to general procedure 2. The title compound was purified by flash chromatography on silica gel (CH_2Cl_2/MeOH = 98.5:1.5).

^{1}H NMR (400 MHz, $CD_3OD/CDCl_3$ (1:1)) δ 8.14 (s, 1H), 7.95 (t, *J* = 1.7 Hz, 1H), 7.73 (app d, *J* = 7.5 Hz, 2H), 7.64 – 7.51 (m, 4H), 7.40 – 7.31 (m, 3H), 7.26 (app t, *J* = 7.4 Hz, 2H), 5.28 (s, 2H), 4.44 – 4.32 (m, 3H), 4.20 (app t, *J* = 6.8 Hz, 1H), 3.80 (s, 3H), 1.87 – 1.53 (m, 7H), 1.48 – 1.34 (m, 1H), 1.33 – 1.07 (m, 4H), 1.05 – 0.86 (m, 2H). ^{13}C NMR (101 MHz, $CD_3OD/CDCl_3$ (1:1)) δ 173.1, 167.9, 157.6, 148.3, 144.5, 144.4 141.9, 139.3, 131.3, 130.1, 128.3, 127.6, 127.6, 125.6, 123.0, 122.2, 120.9, 120.4, 118.0, 67.5, 54.3, 53.3, 51.3, 47.8, 40.5, 34.8, 34.3, 32.9, 27.0, 26.8, 26.6. HRMS calcd. for $C_{35}H_{38}N_5O_5$ ($[M + H]^+$): 608.2873, found: 608.2866.

Methyl 2–(4–(3–(2–(2–fluoro–[1,1'–biphenyl]–4–yl)propanamido)phenyl)–1*H*–1,2,3–triazol–1–yl)acetate (RBM7–034)

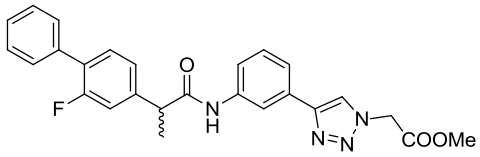

Compound **RBM7–034** (white solid, 166 mg, 84 %) was obtained from aniline **RBM7–021** (100 mg, 0.43 mmol), 2–fluoro–α–methyl–4–biphenylacetic acid (116 mg, 0.47 mmol), HATU (328 mg, 0.86 mmol) and DIPEA (150 µL, 0.86 mmol), according to general procedure 2. The title compound was purified by flash chromatography on silica gel (CH_2Cl_2/MeOH = 98.5:1.5).

^{1}H NMR (400 MHz, $CD_3OD/CDCl_3$ (1:1)) δ 8.17 (s, 1H), 7.96 (t, *J* = 1.8 Hz, 1H), 7.60 (ddd, *J* = 8.1, 2.1, 1.0 Hz, 1H), 7.54 – 7.51 (m, 1H), 7.51 – 7.47 (m, 2H), 7.42 – 7.22 (m, 7H), 5.29 (s, 2H), 3.84 (q, *J* = 7.0 Hz, 1H), 3.80 (s, 3H), 1.57 (d, *J* = 7.0 Hz, 3H). ^{13}C NMR (101 MHz, $CD_3OD/CDCl_3$ (1:1)) δ 174.0, 167.8, 160.3 (d, $J_{C–F}$ = 248.5 Hz), 148.3, 143.5 (d, $J_{C–F}$ = 8.1 Hz), 139.7, 136.2 (d, $J_{C–F}$ = 2.0 Hz), 131.3 (d, $J_{C–F}$ = 4.0 Hz), 131.2, 130.0, 129.4 (d, $J_{C–F}$ = 3.0 Hz), 128.9, 128.3 (d, $J_{C–F}$ = 14.1 Hz), 128.1, 124.0 (d, $J_{C–F}$ = 4.0 Hz), 123.0, 122.0, 120.7, 117.8, 115.6 (d, $J_{C–F}$ = 23.2 Hz), 53.3, 51.3, 47.2, 18.9. HRMS calcd. for $C_{26}H_{24}FN_4O_3$ ($[M + H]^+$): 459.1832, found: 459.1848.

(*S*)–methyl 2–(4–(3–(2,6–bis(((benzyloxy)carbonyl)amino)hexanamido)phenyl)–1*H*–1,2,3–triazol–1–yl)acetate (RBM7–035)

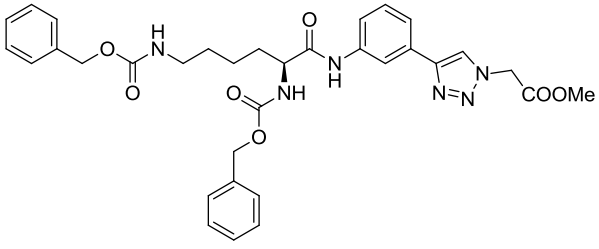

Compound **RBM7–035** (pale yellow solid, 243 mg, 90 %) was obtained from aniline **RBM7–021** (100 mg, 0.43 mmol), Z–Lys(Z)–OH (196 mg, 0.47 mmol), HATU (328 mg, 0.86 mmol) and DIPEA (150 µL, 0.86 mmol), according to general procedure 2. The title compound was purified by flash chromatography on silica gel (CH_2Cl_2/MeOH = 98:2).

^{1}H NMR (400 MHz, $CD_3OD/CDCl_3$ (1:1)) δ 8.15 (s, 1H), 7.96 (br s, 10H), 7.55 (dd, *J* = 7.2, 1.9 Hz, 2H), 7.38 – 7.21 (m, 10H), 5.29 (s, 2H), 5.07 (s, 2H), 5.01 (s, 2H), 4.25 (dd, *J* = 8.0, 5.5 Hz, 1H), 3.80 (s, 3H), 3.11 (t, *J* = 6.5 Hz, 2H), 1.90 – 1.78 (m, 1H), 1.78 – 1.64 (m, 1H), 1.59 – 1.35 (m, 4H). ^{13}C NMR (101 MHz, $CD_3OD/CDCl_3$ (1:1)) δ 172.3, 167.8, 158.1, 157.6, 148.3, 139.2, 137.3, 136.9, 131.3, 130.0, 129.0, 128.9, 128.6, 128.5, 128.4, 128.2, 123.0, 122.2, 120.8, 118.0, 67.5, 67.0, 56.2, 53.3, 51.3, 40.8, 32.7, 29.8, 23.2. HRMS calcd. for $C_{33}H_{37}N_6O_7$ ($[M + H]^+$): 629.2724, found: 629.2758.

(*R*)–methyl 3–(4–(3–(2–(((benzyloxy)carbonyl)amino)–2–henylacetamido)phenyl)–1*H*–1,2,3–triazol–1–yl)propanoate (RBM7–038)

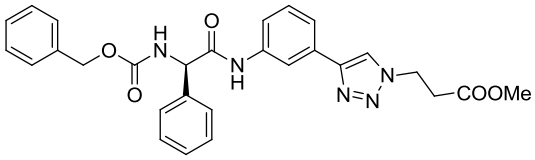

Compound **RBM7–038** (white solid, 178 mg, 85 %) was obtained from aniline **RBM7–022** (100 mg, 0.40 mmol), *N*–Carbobenzoxy–D–2–phenylglycine (127 mg, 0.45 mmol), HATU (309 mg, 0.81 mmol) and DIPEA (142 µL, 0.81 mmol), according to general procedure 2. The title compound was purified by flash chromatography on silica gel (CH_2Cl_2/MeOH = 98.5:1.5).

^{1}H NMR (400 MHz, $CDCl_3$) δ 8.37 (br s, 1H), 7.80 (s, 2H), 7.56 – 7.42 (m, 4H), 7.36 – 7.24 (m, 9H), 6.28 (br d, *J* = 5.4 Hz, 1H), 5.54 (br d, *J* = 4.7 Hz, 1H), 5.11 (d, *J* = 4.4 Hz, 2H, major rotamer), 4.64 (t, *J* = 6.4 Hz, 2H), 3.69 (s, 3H), 2.97 (t, *J* = 6.4 Hz, 2H). ^{13}C NMR (101 MHz, $CDCl_3$) δ 171.2, 168.5, 156.1, 147.1, 138.1, 137.5, 136.1, 131.1, 129.6, 129.3, 128.8, 128.6, 128.3, 128.2, 127.4, 122.0, 121.1, 119.9, 117.2, 67.4, 59.6, 52.3, 45.8, 34.5. HRMS calcd. for $C_{28}H_{28}N_5O_5$ ($[M + H]^+$): 514.2090, found: 514.2097.

(*R*)–methyl 3–(4–(3–(2–(((benzyloxy)carbonyl)amino)–2–cyclohexylacetamido) phenyl)–1*H*–1,2,3–triazol–1–yl)propanoate (RBM7–039)

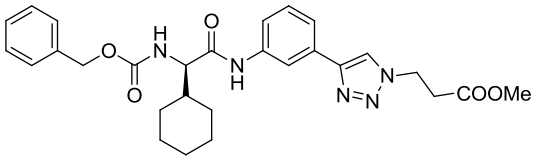

Compound **RBM7–039** (white solid, 124 mg, 59 %) was obtained from aniline **RBM7–022** (100 mg, 0.41 mmol), Z–D–Chg–OH (130 mg, 0.45 mmol), HATU (309 mg, 0.81 mmol) and DIPEA (142 µL, 0.81 mmol), according to general procedure 2. The title compound was purified by flash chromatography on silica gel (CH_2Cl_2/MeOH = 98.5:1.5).

^{1}H NMR (400 MHz, $CD_3OD/CDCl_3$ (1:1)) δ 8.02 (s, 1H), 7.87 (s, 1H), 7.60 (d, *J* = 8.0 Hz, 1H), 7.49 (d, *J* = 7.7 Hz, 1H), 7.37 – 7.17 (m, 6H), 5.07 (s, 2H, major rotamer), 4.67 (t, *J* = 6.5 Hz, 2H), 4.09 (d, *J* = 6.9 Hz, 1H), 3.68 (s, 3H), 3.01 (t, *J* = 6.5 Hz, 2H), 1.83 – 1.58 (m, 6H), 1.30 – 0.95 (m, 5H). ^{13}C NMR (101 MHz, $CD_3OD/CDCl_3$ (1:1)) δ 171.5, 171.3, 157.2, 147.6, 138.8, 136.6, 130.9, 129.8, 128.8, 128.4, 128.2, 121.9, 121.8, 120.4, 117.5, 67.3, 60.9, 52.4, 46.1, 41.3, 34.5, 29.9, 28.8, 26.3, 26.2, 26.2. HRMS calcd. for $C_{28}H_{34}N_5O_5$ ($[M + H]^+$): 520.2560, found: 520.2549.

Benzyl 3–((3–(1–(2–methoxy–2–oxoethyl)–1*H*–1,2,3–triazol–4–yl)phenyl) carbamoyl)piperidine–1–carboxylate (RBM7–041)

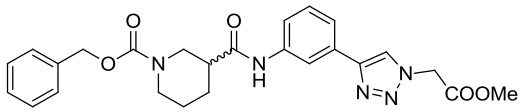

Compound **RBM7–041** (white solid, 189 mg, 92 %) was obtained from aniline **RBM7–021** (100 mg, 0.43 mmol), 1–[(benzyloxy)carbonyl]–3–piperidinecarboxylic acid (125 mg, 0.47 mmol), HATU (328 mg, 0.86 mmol) and DIPEA (150 µL, 0.86 mmol), according to general procedure 2. The title compound was purified by flash chromatography on silica gel (CH_2Cl_2/MeOH = 98.5:1.5).

^{1}H NMR (400 MHz, $CDCl_3$) δ 7.97 (br s, 1H), 7.89 (s, 1H), 7.61 – 7.50 (m, 2H), 7.36 – 7.25 (m, 6H), 5.20 (s, 2H), 5.15 (br s, 2H, major rotamer), 4.12 (br s, 1H), 3.90 – 3.74 (br s, 1H) 3.80 (s, 3H), 3.36 (br s, 1H), 3.16 (br s, 1H), 2.51 (br s, 1H), 2.22 (br s, 1H),

1.97 (br s, 2H), 1.70 (br s, 1H), 1.56 – 1.45 (m, 1H). ^{13}C NMR (101 MHz, $CDCl_3$) δ 171.6, 166.8, 155.7, 148.0, 138.7, 136.7, 131.0, 129.7, 128.7, 128.2, 128.0, 121.7, 121.5, 119.9, 117.2, 67.5, 53.2, 51.0, 46.4, 44.6, 44.1, 27.8, 24.3. HRMS calcd. for $C_{25}H_{27}N_5NaO_5$ ($[M + Na]^+$): 500.1910, found: 500.1912.

Methyl 3–(4–(3–(2–phenylacetamido)phenyl)–1*H*–1,2,3–triazol–1–yl)propanoate (RBM7–054)

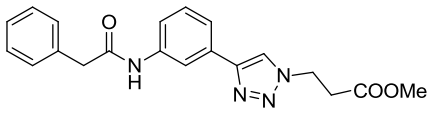

Compound **RBM7–054** (white solid, 330 mg, 74 %) was obtained from aniline **RBM7–022** (300 mg, 1.22 mmol), phenylacetic acid (182 mg, 1.34 mmol), HATU (926 mg, 2.44 mmol) and DIPEA (424 µL, 2.44 mmol), according to general procedure 2. The title compound was purified by flash chromatography on silica gel (from 0 to 2 % MeOH in CH_2Cl_2).

^{1}H NMR (400 MHz, $CDCl_3$) δ 7.83 (s, 1H), 7.77 (t, *J* = 1.6 Hz, 1H), 7.57 (dd, *J* = 8.2, 1.1 Hz, 1H), 7.52 (app d, *J* = 7.8 Hz, 1H), 7.42 – 7.30 (m, 7H), 4.66 (t, *J* = 6.4 Hz, 2H), 3.75 (s, 2H), 3.69 (s, 3H), 2.99 (t, *J* = 6.4 Hz, 2H). ^{13}C NMR (101 MHz, $CDCl_3$) δ 171.1, 169.4, 147.3, 138.4, 134.4, 131.3, 129.7, 129.4, 127.9, 121.8, 121.0, 119.7, 116.9, 52.3, 45.7, 45.0, 34.6. HRMS calcd. for $C_{20}H_{21}N_4O_3$ ($[M + H]^+$): 365.1614, found: 351.1618.

Methyl 3–(4–(3–benzamidophenyl)–1*H*–1,2,3–triazol–1–yl)propanoate (RBM7–065)

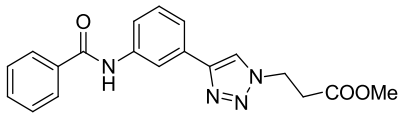

Compound **RBM7–065** (pale yellow solid, 272 mg, 64 %) was obtained from aniline **RBM7–022** (300 mg, 1.22 mmol), benzoic acid (164 mg, 1.34 mmol), HATU (926 mg, 2.44 mmol) and DIPEA (424 µL, 2.44 mmol), according to general procedure 2. The title compound was purified by flash chromatography on silica gel (from 0 to 2 % MeOH in CH_2Cl_2).

^{1}H NMR (400 MHz, $CDCl_3$) δ 8.06 (t, *J* = 1.8 Hz, 1H), 7.96 (br s, 1H), 7.91 (s, 1H), 7.91 – 7.87 (m, 2H), 7.77 (dd, *J* = 8.1, 1.3 Hz, 1H), 7.63 – 7.60 (m, 1H), 7.59 – 7.54 (m, 1H), 7.53 – 7.48 (m, 2H), 7.43 (t, *J* = 7.9 Hz, 1H), 4.70 (t, *J* = 6.4 Hz, 2H), 3.72 (s, 3H), 3.02 (t, *J* = 6.4 Hz, 2H). ^{13}C NMR (101 MHz, $CDCl_3$) δ 171.1, 166.1, 147.3, 138.7, 134.9, 132.0, 131.4, 129.7, 128.9, 127.2, 121.8, 121.0, 120.1, 117.4, 52.3, 45.7, 34.5. HRMS calcd. for $C_{19}H_{19}N_4O_3$ ($[M + H]^+$): 351.1457, found: 351.1462.

Methyl 3–(4–(3–(2–hydroxy–2–(4–hydroxy–3–methoxyphenyl)acetamido)phenyl)–1*H*–1,2,3–triazol–1–yl)propanoate (RBM7–037)

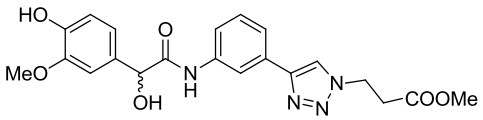

Compound **RBM7–037** (white solid, 178 mg, 83 %) was obtained from aniline **RBM7–022** (124 mg, 0.51 mmol), 4–hydroxy–3–methoxy–DL–mandelic acid (100 mg, 0.51 mmol), EDC (116 mg, 0.61 mmol) and HOBt (82 mg, 0.61 mmol), according to general procedure 3. The title compound was purified by flash chromatography on silica gel (CH_2Cl_2/MeOH = 96.5:3.5).

^{1}H NMR (400 MHz, $CD_3OD/CDCl_3$ (1:1)) δ 9.49 (br s, 1H), 8.12 (s, 1H), 7.99 – 7.94 (m, 1H), 7.63 – 7.52 (m, 2H), 7.37 (t, *J* = 7.9 Hz, 1H), 7.04 (d, *J* = 1.7 Hz, 1H), 6.95 (dd, *J* = 8.2, 1.8 Hz, 1H), 6.80 (d, *J* = 8.1 Hz, 1H), 5.08 (s, 1H), 4.69 (t, *J* = 6.5 Hz, 2H), 3.86 (s, 3H), 3.68 (s, 3H), 3.02 (t, *J* = 6.5 Hz, 2H). ^{13}C NMR (101 MHz, $CD_3OD/CDCl_3$ (1:1)) δ 172.6, 171.6, 147.9, 147.7, 146.6, 138.5, 131.7, 131.2, 130.0, 122.1, 121.9, 120.4, 120.1, 117.6, 115.3, 110.4, 74.7, 56.1, 52.4, 46.2, 34.6. HRMS calcd. for $C_{21}H_{23}N_4O_6$ ($[M + H]^+$): 427.1618, found: 427.1607.

(*R*)–methyl 3–(4–(3–(2–(((benzyloxy)carbonyl)amino)–3–(4–hydroxyphenyl) propanamido)phenyl)–1*H*–1,2,3–triazol–1–yl)propanoate (RBM7–040)

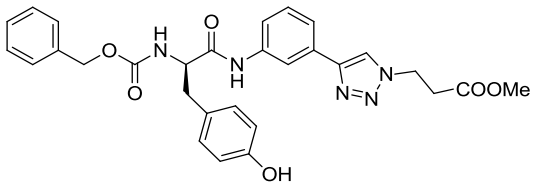

Compound **RBM7–040** (colorless oil, 75 mg, 87 %) was obtained from aniline **RBM7–022** (39 mg, 0.16 mmol), Z–D–Tyr–OH (50 mg, 0.16 mmol), EDC (37 mg, 0.19 mmol)

and HOBt (26 mg, 0.19 mmol), according to general procedure 3. The title compound was purified by flash chromatography on silica gel (CH_2Cl_2/MeOH = 97.5:2.5).

^{1}H NMR (400 MHz, $CD_3OD/CDCl_3$ (1:1)) δ 8.11 (s, 1H), 7.81 (br s, 1H), 7.55 – 7.51 (m, 1H), 7.47 (ddd, *J* = 8.1, 2.1, 1.0 Hz, 1H), 7.34 (t, *J* = 7.9 Hz, 1H), 7.31 – 7.23 (m, 4H), 7.18 (br s, 1H), 7.04 (app d, *J* = 8.5 Hz, 2H), 6.73 – 6.67 (m, 2H), 5.10 – 4.98 (m, 2H), 4.70 (t, *J* = 6.5 Hz, 2H), 4.46 (t, *J* = 7.0 Hz, 1H), 3.69 (s, 3H), 3.10 – 3.00 (m, 1H), 3.03 (t, *J* = 6.5 Hz, 2H), 2.91 (dd, *J* = 13.8, 7.6 Hz, 1H). ^{13}C NMR (101 MHz, $CD_3OD/CDCl_3$ (1:1)) δ 171.9, 171.8, 157.4, 156.5, 147.9, 139.0, 137.1, 131.4, 131.0, 130.0, 129.0, 128.6, 128.3, 128.0, 122.2, 120.9, 118.2, 115.9, 67.4, 57.9, 52.5, 46.4, 38.5, 34.7. HRMS calcd. for $C_{29}H_{30}N_5O_6$ ($[M + H]^+$): 544.2196, found: 544.2208.

(*S*)–3–(4–(3–(1–(2–(((benzyloxy)carbonyl)amino)acetyl)pyrrolidine–2–carboxamido) phenyl)–1*H*–1,2,3–triazol–1–yl)propanoic acid (RBM7–030)

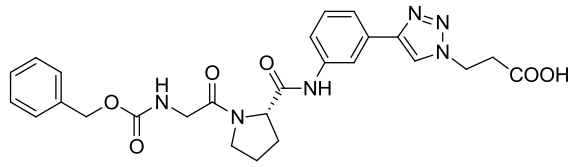

Compound **RBM7–030** (white solid, 31 mg, 91 %) was obtained from methyl ester **RBM7–028** (35 mg, 0.07 mmol) and LiOH (5 mg, 0.20 mmol), according to general procedure 4.

^{1}H NMR (400 MHz, CD_3OD, major rotamer) δ 8.26 (s, 1H), 7.98 (t, *J* = 1.8 Hz, 1H), 7.60 – 7.51 (m, 1H), 7.42 – 7.22 (m, 6H), 5.09 (s, 2H), 4.69 (t, *J* = 6.6 Hz, 2H), 4.58 (dd, *J* = 8.3, 3.7 Hz, 2H), 4.02 (app q, *J* = 17.1 Hz, 2H), 3.74 – 3.66 (m, 1H), 3.65 – 3.58 (m, 1H), 3.00 (t, *J* = 6.6 Hz, 2H), 2.32 – 2.21 (m, 1H), 2.19 – 1.92 (m, 3H). ^{13}C NMR (101 MHz, CD_3OD, major rotamer) δ 173.9, 172.9, 170.4, 159.1, 148.4, 140.2, 138.2, 132.3, 130.4, 129.4, 129.0, 128.8, 122.9, 122.5, 121.3, 118.6, 67.8, 62.5, 47.8, 47.2, 44.2, 35.2, 30.7, 25.9. HRMS calcd. for $C_{26}H_{29}N_6O_6$ ($[M + H]^+$): 521.2149, found: 521.2178.

(*S*)–2–(4–(3–(1–(2–(((benzyloxy)carbonyl)amino)acetyl)pyrrolidine–2–carboxamido) phenyl)–1*H*–1,2,3–triazol–1–yl)acetic acid (RBM7–031)

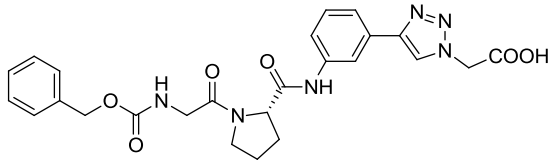

Compound **RBM7–031** (white solid, 32 mg, 82 %) was obtained from methyl ester **RBM7–027** (40 mg, 0.08 mmol) and LiOH (6 mg, 0.23 mmol), according to general procedure 4.

^{1}H NMR (400 MHz, CD_3OD, major rotamer) δ 8.28 (s, 1H), 8.00 (t, *J* = 1.8 Hz, 1H), 7.60 – 7.52 (m, 2H), 7.41 – 7.22 (m, 5H), 5.30 (s, 2H), 5.08 (s, 2H), 4.57 (dd, *J* = 8.3, 3.7 Hz, 1H), 4.01 (app q, *J* = 17.1 Hz, 2H), 3.73 – 3.64 (m, 1H), 3.64 – 3.56 (m, 1H), 2.32 – 2.19 (m, 1H), 2.17 – 1.95 (m, 3H). ^{13}C NMR (101 MHz, CD_3OD, major rotamer) δ 172.9, 170.4, 169.9, 159.1, 148.6, 140.2, 138.2, 132.3, 130.4, 129.4, 129.0, 128.8, 123.9, 122.5, 121.3, 118.6, 67.8, 62.5, 51.8, 47.8, 44.2, 30.7, 25.9. HRMS calcd. for $C_{25}H_{27}N_6O_6$ ($[M + H]^+$): 507.1992, found: 507.1996.

2–(4–(3–(2–(2–fluoro–[1,1'–biphenyl]–4–yl)propanamido)phenyl)–1*H*–1,2,3–triazol–1–yl)acetic acid (RBM7–042)

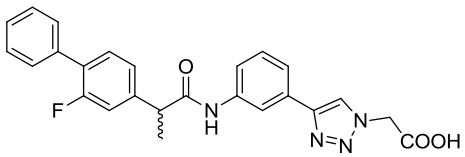

Compound **RBM7–042** (white solid, 27 mg, 56 %) was obtained from methyl ester **RBM7–034** (50 mg, 0.11 mmol) and LiOH (8 mg, 0.33 mmol), according to general procedure 4.

^{1}H NMR (400 MHz, $CD_3OD/CDCl_3$ (1:1)) δ 8.15 (s, 1H), 7.93 (t, *J* = 1.8 Hz, 1H), 7.62 (ddd, *J* = 8.1, 2.1, 0.9 Hz, 1H), 7.54 – 7.46 (m, 3H), 7.42 – 7.21 (m, 7H), 5.22 (s, 2H), 3.84 (q, *J* = 7.0 Hz, 1H), 1.57 (d, *J* = 7.0 Hz, 3H). ^{13}C NMR (101 MHz, $CD_3OD/CDCl_3$ (1:1)) δ 174.0, 168.9, 160.3 (d, $J_{C–F}$ = 248.5 Hz), 148.2, 143.6 (d, $J_{C–F}$ = 7.1 Hz), 139.7, 136.2 (d, $J_{C–F}$ = 1.0 Hz), 131.3 (d, $J_{C–F}$ = 8.1 Hz), 131.3, 130.0, 129.4 (d, $J_{C–F}$ = 3.0 Hz), 128.9, 128.3 (d, $J_{C–F}$ = 14.1 Hz), 128.1, 124.0 (d, $J_{C–F}$ = 3.0 Hz), 123.0, 122.0, 120.7,

117.8, 115.6 (d, $J_{C–F}$ = 24.2 Hz), 51.4, 47.2, 18.9. HRMS calcd. for $C_{25}H_{22}FN_4O_3$ ([M + H]$^+$): 445.1676, found: 445.1664.

(*S*)–2–(4–(3–(2,6–bis(((benzyloxy)carbonyl)amino)hexanamido)phenyl)–1*H*–1,2,3–triazol–1–yl)acetic acid (RBM7–043)

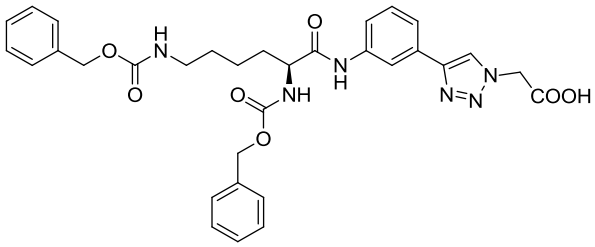

Compound **RBM7–043** (white solid, 31 mg, 63 %) was obtained from methyl ester **RBM7–035** (50 mg, 0.08 mmol) and LiOH (6 mg, 0.24 mmol), according to general procedure 4.

^{1}H NMR (400 MHz, $CD_3OD/CDCl_3$ (1:1)) δ 8.16 (s, 1H), 7.94 (br s, 1H), 7.59 – 7.54 (m, 3H), 7.39 – 7.14 (m, 10H), 5.23 (s, 2H), 5.08 (s, 2H), 5.01 (s, 2H), 4.25 (dd, *J* = 8.1, 5.5 Hz, 1H), 3.12 (t, *J* = 6.5 Hz, 2H), 1.91 – 1.78 (m, 1H), 1.77 – 1.64 (m, 1H), 1.58 – 1.36 (m, 4H). ^{13}C NMR (101 MHz, $CD_3OD/CDCl_3$ (1:1)) δ 172.4, 168.9, 158.1, 157.6, 148.2, 139.2, 137.3, 137.0, 131.4, 130.0, 129.0, 128.9, 128.6, 128.5, 128.4, 128.3, 123.0, 122.2, 120.8, 118.0, 67.5, 67.0, 56.2, 51.4, 40.8, 32.7, 29.8, 23.3. HRMS calcd. for $C_{32}H_{35}N_6O_7$ ([M + H]$^+$): 615.2567, found: 615.2552.

(*S*)–2–(4–(3–(2–((((9*H*–fluoren–9–yl)methoxy)carbonyl)amino)–3–cyclohexylpropana–mido)phenyl)–1*H*–1,2,3–triazol–1–yl)acetic acid (RBM7–044)

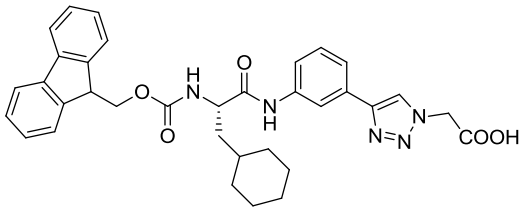

Compound **RBM7–044** (white solid, 20 mg, 41 %) was obtained from methyl ester **RBM7–033** (50 mg, 0.08 mmol) and LiOH (6 mg, 0.25 mmol), according to general procedure 4.

^{1}H NMR (400 MHz, $CD_3OD/CDCl_3$ (1:1)) δ 8.15 (s, 1H), 7.93 (t, *J* = 1.8 Hz, 1H), 7.74 (d, *J* = 7.5 Hz, 2H), 7.65 – 7.53 (m, 4H), 7.40 – 7.32 (m, 3H), 7.27 (app t, *J* = 7.4 Hz, 2H), 5.24 (s, 2H), 4.46 – 4.31 (m, 3H), 4.22 (t, *J* = 6.8 Hz, 1H), 1.82 (br d, *J* = 11.8 Hz, 1H), 1.77 – 1.56 (m, 6H), 1.40 (br s, 1H), 1.32 – 1.09 (m, 3H), 1.04 – 0.88 (m, 2H). ^{13}C NMR (101 MHz, $CD_3OD/CDCl_3$ (1:1)) δ 173.2, 168.9, 157.7, 148.2, 144.5, 144.4, 142.0, 139.3, 131.4, 130.1, 128.3, 127.7, 125.6, 123.1, 122.3, 120.9, 120.5, 118.1, 67.5, 54.3, 51.5, 47.8, 40.5, 34.8, 34.3, 33.0, 27.0, 26.9, 26.7. HRMS calcd. for $C_{34}H_{36}N_5O_5$ ($[M + H]^+$): 594.2716, found: 594.2716.

(*R*)–3–(4–(3–(2–(((benzyloxy)carbonyl)amino)–2–phenylacetamido)phenyl)–1*H*–1,2,3–triazol–1–yl)propanoic acid (RBM7–045)

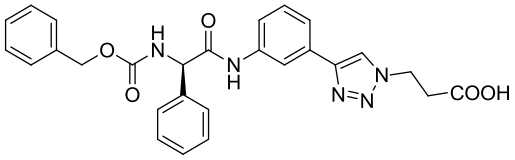

Compound **RBM7–045** (white solid, 36 mg, 74 %) was obtained from methyl ester **RBM7–038** (50 mg, 0.10 mmol) and LiOH (7 mg, 0.29 mmol), according to general procedure 4.

^{1}H NMR (400 MHz, $CD_3OD/CDCl_3$ (1:1)) δ 8.10 (s, 1H), 7.89 (br s, 1H), 7.59 – 7.53 (m, 2H), 7.52 – 7.44 (m, 3H), 7.37 – 7.22 (m, 8H), 5.40 (br s, 1H), 5.09 (d, *J* = 2.6 Hz, 2H), 4.67 (t, *J* = 6.5 Hz, 2H), 2.98 (t, *J* = 6.5 Hz, 2H). ^{13}C NMR (101 MHz, $CD_3OD/CDCl_3$ (1:1)) δ 173.1, 170.1, 157.1, 147.8, 139.2, 138.0, 136.9, 131.4, 130.0, 129.4, 129.0, 128.6, 128.4, 127.8, 122.2, 120.7, 117.8, 67.6, 59.9, 46.6, 34.8. HRMS calcd. for $C_{27}H_{26}N_5O_5$ ($[M + H]^+$): 500.1934, found: 500.1917.

(*R*)–3–(4–(3–(2–(((benzyloxy)carbonyl)amino)–2–cyclohexylacetamido)phenyl)–1*H*–1,2,3–triazol–1–yl)propanoic acid (RBM7–046)

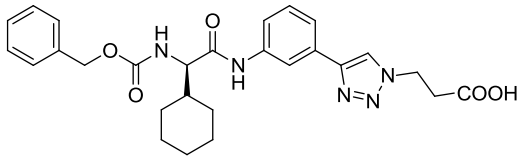

Compound **RBM7–046** (white solid, 21 mg, 43 %) was obtained from methyl ester **RBM7–039** (50 mg, 0.10 mmol) and LiOH (7 mg, 0.29 mmol), according to general procedure 4.

^{1}H NMR (400 MHz, $CD_3OD/CDCl_3$ (1:1)) δ 8.15 (s, 1H), 7.92 (br s, 1H), 7.61 – 7.56 (m, 1H), 7.54 – 7.50 (m, 1H), 7.39 – 7.16 (m, 6H), 5.08 (s, 2H), 4.69 (t, *J* = 6.5 Hz, 2H), 4.10 (d, *J* = 7.1 Hz, 1H), 2.99 (t, *J* = 6.5 Hz, 2H), 1.83 – 1.61 (m, 6H), 1.28 – 1.03 (m, 5H). ^{13}C NMR (101 MHz, $CD_3OD/CDCl_3$ (1:1)) δ 173.1, 171.9, 157.7, 147.9, 139.1, 137.1, 131.4, 130.1, 129.0, 128.6, 128.4, 122.2, 120.8, 117.9, 67.5, 61.3, 46.6, 41.5, 34.8, 30.3, 29.2, 26.6, 26,5, 26.5. HRMS calcd. for $C_{27}H_{32}N_5O_5$ ($[M + H]^+$): 506.2403, found: 506.2391.

2–(4–(3–(1–((benzyloxy)carbonyl)piperidine–3–carboxamido)phenyl)–1*H*–1,2,3–triazol–1–yl)acetic acid (RBM7–047)

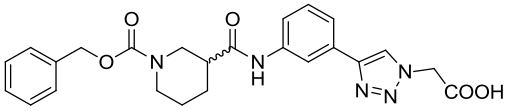

Compound **RBM7–047** (white solid, 20 mg, 41 %) was obtained from methyl ester **RBM7–041** (50 mg, 0.11 mmol) and LiOH (8 mg, 0.31 mmol), according to general procedure 4.

^{1}H NMR (400 MHz, $CD_3OD/CDCl_3$ (1:1)) δ 8.15 (s, 1H), 7.90 (br s, 1H), 7.59 (br d, J = 7.6 Hz, 1H), 7.52 (br d, *J* = 7.6 Hz, 1H), 7.39 – 7.22 (m, 6H), 5.23 (s, 2H), 5.15 – 5.06 (m, 2H), 4.28 – 4.21 (m, 1H), 4.10 (app d, *J* = 13.0 Hz, 1H), 3.06 (br s, 1H), 2.88 (br s, 1H), 2.50 (tt, *J* = 11.0, 3.7 Hz, 1H), 2.05 (br d, *J* = 10.8 Hz, 1H), 1.86 – 1.70 (m, 2H), 1.59 – 1.43 (m, 1H). ^{13}C NMR (101 MHz, $CD_3OD/CDCl_3$ (1:1)) δ 174.0, 169.4, 156.7, 148.5, 140.0, 137.6, 131.9, 130.3, 129.3, 128.9, 128.6, 123.5, 122.3, 120.9, 118.1, 68.2,

51.6, 47.3, 45.1 (br), 44.7, 28.8 (br), 25.4 (br). HRMS calcd. for $C_{24}H_{26}N_5O_5$ ([M + H]$^+$): 464.1934, found: 464.1924.

(*R*)–3–(4–(3–(2–(((benzyloxy)carbonyl)amino)–3–(4–hydroxyphenyl)propanamido) phenyl)–1*H*–1,2,3–triazol–1–yl)propanoic acid (RBM7–048)

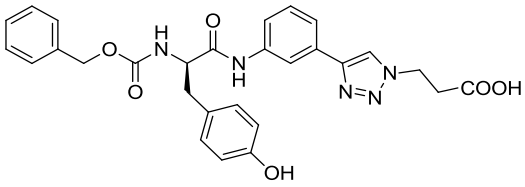

Compound **RBM7–048** (white solid, 19 mg, 39 %) was obtained from methyl ester **RBM7–040** (50 mg, 0.09 mmol) and LiOH (7 mg, 0.28 mmol), according to general procedure 4.

^{1}H NMR (400 MHz, $CD_3OD/CDCl_3$ (1:1)) δ 8.11 (s, 1H), 7.78 (br s, 1H), 7.54 – 7.51 (m, 1H), 7.49 (ddd, *J* = 8.1, 2.1, 1.1 Hz, 1H), 7.37 – 7.16 (m, 6H), 7.04 (d, *J* = 8.5 Hz, 2H), 6.73 – 6.68 (m, 2H), 5.05 (d, *J* = 11.4 Hz, 2H, major rotamer), 4.68 (t, *J* = 6.5 Hz, 2H), 4.46 (t, *J* = 7.0 Hz, 1H), 3.05 (dd, *J* = 13.7, 6.7 Hz, 1H), 2.99 (t, *J* = 6.5 Hz, 2H), 2.91 (dd, *J* = 13.6, 7.6 Hz, 1H). ^{13}C NMR (101 MHz, $CD_3OD/CDCl_3$ (1:1)) δ 173.1, 171.7, 157.3, 156.4, 147.8, 139.0, 137.0, 131.4, 130.9, 130.0, 129.0, 128.6, 128.3, 127.9, 122.3, 122.2, 120.9, 118.1, 115.9, 67.4, 57.8, 46.6, 38.5, 34.8. HRMS calcd. for $C_{28}H_{28}N_5O_6$ ([M + H]$^+$): 530.2040, found: 530.2048.

3–(4–(3–(2–hydroxy–2–(4–hydroxy–3–methoxyphenyl)acetamido)phenyl)–1*H*–1,2,3–triazol–1–yl)propanoic acid (RBM7–049)

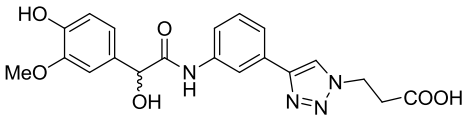

Compound **RBM7–049** (white solid, 59 mg, 91 %) was obtained from methyl ester **RBM7–037** (67 mg, 0.16 mmol) and LiOH (11 mg, 0.47 mmol), according to general procedure 4. Once evaporated, the crude reaction mixture was dissolved in DMSO/H_2O (1:1) and loaded on an Amberlite® XAD4 column (5 g), which had been washed thoroughly with acetone and then equilibrated with water. Elution with a linear gradient from 0 to 40 % CH_3CN in H_2O provided pure **RBM7–049**.

^{1}H NMR (400 MHz, $CD_3OD/CDCl_3$ (1:1)) δ 8.13 (s, 1H), 7.95 (t, *J* = 1.8 Hz, 1H), 7.61 (ddd, *J* = 8.1, 2.1, 1.0 Hz, 1H), 7.56 – 7.52 (m, 1H), 7.37 (t, *J* = 7.9 Hz, 1H), 7.04 (d, *J* = 2.0 Hz, 1H), 6.95 (dd, *J* = 8.2, 2.0 Hz, 1H), 6.80 (d, *J* = 8.1 Hz, 1H), 5.08 (s, 1H), 4.68 (t, *J* = 6.5 Hz, 2H), 3.86 (s, 3H), 2.98 (t, *J* = 6.5 Hz, 2H). ^{13}C NMR (101 MHz, $CD_3OD/CDCl_3$ (1:1)) δ 173.2 (br), 173.0, 148.2, 147.8, 146.8, 138.7, 131.9, 131.5, 130.1, 122.3, 122.2, 120.6, 120.2, 117.9, 115.5, 110.6, 74.9, 56.1, 46.6, 34.9. HRMS calcd. for $C_{20}H_{21}N_4O_6$ ($[M + H]^+$): 413.1461, found: 413.1473.

3–(4–(3–benzamidophenyl)–1*H*–1,2,3–triazol–1–yl)propanoic acid (RBM7–066)

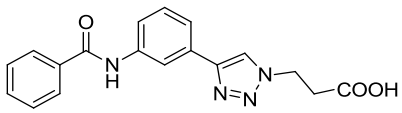

Compound **RBM7–066** (white solid, 111 mg, 93 %) was obtained from methyl ester **RBM7–065** (125 mg, 0.36 mmol) and LiOH (26 mg, 1.07 mmol), according to general procedure 4.

^{1}H NMR (400 MHz, CD_3OD) δ 8.33 (s, 1H), 8.12 (t, *J* = 1.8 Hz, 1H), 7.98 – 7.94 (m, 2H), 7.73 (ddd, *J* = 8.1, 2.1, 1.0 Hz, 1H), 7.63 – 7.56 (m, 2H), 7.56 – 7.50 (m, 2H), 7.44 (t, *J* = 7.9 Hz, 1H), 4.72 (t, *J* = 6.6 Hz, 2H), 3.02 (t, *J* = 6.6 Hz, 2H). ^{13}C NMR (101 MHz, $CD_3OD/CDCl_3$ (1:1)) δ 173.6, 168.6, 148.1, 140.0, 135.7, 132.6, 131.7, 130.2, 129.2, 128.3, 122.5, 122.5, 121.8, 118.9, 46.9, 35.1. HRMS calcd. for $C_{18}H_{17}N_4O_3$ ($[M + H]^+$): 337.1301, found: 337.1299.

3–(4–(3–(2–phenylacetamido)phenyl)–1*H*–1,2,3–triazol–1–yl)propanoic acid (RBM7–067)

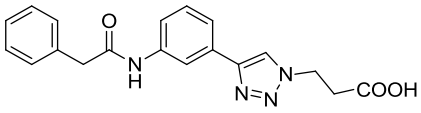

Compound **RBM7–067** (white solid, 114 mg, 79 %) was obtained from methyl ester **RBM7–54** (150 mg, 0.41 mmol) and LiOH (30 mg, 1.23 mmol), according to general procedure 4.

^{1}H NMR (400 MHz, $CD_3OD/CDCl_3$ (1:1)) δ 8.12 (s, 1H), 7.88 (t, *J* = 1.8 Hz, 1H), 7.60 (ddd, *J* = 8.1, 2.1, 1.0 Hz, 1H), 7.52 – 7.48 (m, 1H), 7.37 – 7.28 (m, 5H), 7.26 – 7.20 (m, 1H), 4.67 (t, *J* = 6.5 Hz, 2H), 3.68 (s, 2H), 2.98 (t, *J* = 6.5 Hz, 2H). ^{13}C NMR (101

MHz, $CD_3OD/CDCl_3$ (1:1)) δ 173.2, 171.6, 147.9, 139.6, 135.7, 131.3, 130.0, 129.6, 129.1, 127.5, 122.1, 122.0, 120.6, 117.7, 46.6, 44.4, 34.9. HRMS calcd. for $C_{19}H_{19}N_4O_3$ ($[M + H]^+$): 351.1457, found: 351.1454.

5.1.4 Synthesis and characterization of compounds from Section 3.2

5.1.4.1 Synthesis of PLP–derivatives

Phosphopyridoxyl ethanolamine phosphate (RBM7–001) and Pyridoxine–5'–phosphate (RBM7–002)

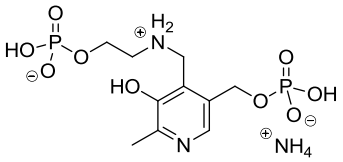

RBM7-001

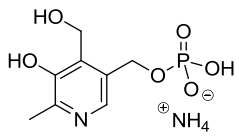

RBM7-002

Compound **RBM7–001** (pale yellow solid, 110 mg, 79 %) was obtained from solution A (*O*–phosphorylethanolamine (50 mg, 0.36 mmol), KO^{t}Bu (80 mg, 0.71 mmol)), solution B (PLP monohydrate (122 mg, 0.46 mmol), KO^{t}Bu (103 mg, 0.92 mmol) and $NaBH_4$ (17 mg, 0.46 mmol), according to general procedure 5. The crude material was dissolved in 10 mM aq. NH_4HCO_3 and applied to a DEAE–Sephadex A–25–120 ion exchange column (10 g) previously equilibrated with the same buffer. Elution with a linear gradient from 10 to 300 mM aq. NH_4HCO_3 yielded the title compound. Monophosphate **RBM7–002** (22 mg, white solid) was also isolated.

For **RBM7–001**:

^{1}H NMR (400 MHz, D_2O) δ 7.68 (s, 1H), 4.86 (d, J = 6.3 Hz, 2H), 4.45 (s, 2H), 4.10 – 4.01 (m, 2H), 3.38 – 3.30 (m, 2H), 2.48 (s, 3H). ^{13}C NMR (101 MHz, D_2O) δ 165.7, 147.4, 137.6 (d, $J_{C–P}$ = 7.9 Hz), 134.12, 126.1, 64.2 (d, $J_{C–P}$ = 4.3 Hz), 62.3 (d, $J_{C–P}$ = 4.4 Hz), 50.7 (d, $J_{C–P}$ = 6.9 Hz), 47.0, 17.6. ^{31}P NMR (162 MHz, D_2O) δ 2.93, 2.76. HRMS calcd. for $C_{10}H_{19}N_2O_9P_2$ ($[M + H]^+$): 373.0566, found: 373.0565.

For **RBM7–002**:

^{1}H NMR (400 MHz, D_2O) δ 7.78 (s, 1H), 4.96 (d, J = 6.4 Hz, 2H), 4.85 (s, 2H), 2.49 (s, 3H). ^{13}C NMR (101 MHz, D_2O) δ 172.7, 146.8, 141.9, 136.7 (d, $J_{C–P}$ = 8.2 Hz), 128.1,

64.3 (d, J_{C-P} = 4.3 Hz), 58.8, 18.1. ^{31}P NMR (162 MHz, D_2O) δ 2.01. HRMS calcd. for $C_8H_{13}NO_6P$ ([M + H]$^+$): 250.0481, found: 250.0486.

Phosphopyridoxyl sphingosine–1–phosphate (RBM7–032)

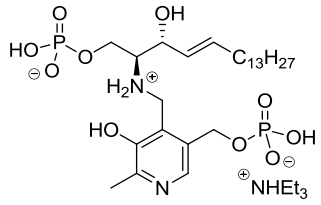

Compound **RBM7–032** (pale yellow solid, 47 mg, 74%) was obtained from solution A (S1P (34 mg, 0.09 mmol), KO^{t}Bu (20 mg, 0.18 mmol)), solution B (PLP monohydrate (31 mg, 0.12 mmol), KO^{t}Bu (26 mg, 0.23 mmol)) and $NaBH_4$ (4 mg, 0.12 mmol), according to general procedure 5. The title compound was purified by preparative RP chromatography (from 5 to 100 % CH_3CN in 100 mM TEAA buffer (pH 7.0)).

$[\alpha]^{20}_D$ = –14.1 (*c* 1.0, CH_3OH). ^{1}H NMR (400 MHz, CD_3OD) δ 7.82 (s, 1H), 5.93 – 5.82 (m, 1H), 5.54 (dd, *J* = 15.4, 6.6 Hz, 1H), 4.99 – 4.92 (m, 2H), 4.58 (d, *J* = 13.9 Hz, 1H), 4.46 (app t, J = 5.8 Hz, 1H), 4.41 (d, *J* = 13.9 Hz, 1H), 4.23 (ddd, *J* = 11.7, 6.6, 3.4 Hz, 1H), 4.16 – 4.07 (m, 1H), 3.26 (ddd, *J* = 8.2, 5.1, 3.5 Hz, 1H), 3.19 (q, *J* = 7.3 Hz, 6H), 2.46 (s, 3H), 2.11 (dd, *J* = 14.1, 7.1 Hz, 2H), 1.56 – 1.17 (m, 31H), 0.90 (t, *J* = 6.9 Hz, 3H). ^{13}C NMR (101 MHz, CD_3OD) δ 157.2, 147.6, 135.9, 135.7, 133.2 (d, J_{C-P} = 8.7 Hz), 131.4, 129.7, 71.2, 63.8 (d, J_{C-P} = 6.9 Hz), 63.7 (d, J_{C-P} = 4.8 Hz), 62.5 (d, J_{C-P} = 4.8 Hz), 47.5, 45.5, 33.5, 33.1, 30.8, 30.8, 30.8, 30.8, 30.7, 30.5, 30.2, 23.7, 17.7, 14.5, 9.2. ^{31}P NMR (162 MHz, CD_3OD) δ 2.64, 1.76. HRMS calcd. for $C_{26}H_{49}N_2O_{10}P_2$ ([M + H]$^+$): 611.2862, found: 611.2859.

Phosphopyridoxyl sphinganine–1–phosphate (RBM7–012)

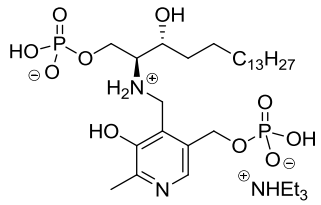

Compound **RBM7–012** (pale yellow solid, 40 mg, 71%) was obtained from solution A (dhS1P (30 mg, 0.08 mmol), KO^{t}Bu (18 mg, 0.16 mmol)), solution B (PLP monohydrate (27 mg, 0.10 mmol), KO^{t}Bu (23 mg, 0.21 mmol) and $NaBH_4$ (4 mg, 0.10

mmol), according to general procedure 1. The title compound was purified by preparative RP chromatography (from 5 to 100 % CH_3CN in 100 mM TEAA buffer (pH 7.0)).

$[\alpha]^{20}_D$ = –4.5 (*c* 1.0, CH_3OH). ^{1}H NMR (400 MHz, CD_3OD) δ 7.83 (s, 1H), 5.01 – 4.92 (m, 2H), 4.54 (d, *J* = 13.8 Hz, 1H), 4.43 (d, *J* = 13.8 Hz, 1H), 4.29 – 4.21 (m, 1H), 4.18 – 4.09 (m, 1H), 4.02 – 3.95 (m, 1H), 3.26 (dt, *J* = 7.6, 3.7 Hz, 1H), 3.19 (q, *J* = 7.3 Hz, 6H), 2.47 (s, 3H), 1.72 – 1.17 (m, 37H), 0.90 (t, *J* = 6.9 Hz, 3H). ^{13}C NMR (101 MHz, CD_3OD) δ 157.9, 147.5, 134.5, 134.0 (d, J_{C-P} = 8.1 Hz), 130.9, 69.5, 64.0 (d, J_{C-P} = 6.5 Hz), 63.7 (d, J_{C-P} = 4.6 Hz), 62.0 (d, J_{C-P} = 4.9 Hz), 47.6, 44.6, 34.4, 33.1, 30.8, 30.8, 30.8, 30.7, 30.5, 27.1, 23.7, 17.7, 14.5, 9.2. ^{31}P NMR (162 MHz, CD_3OD) δ 2.78, 1.92. HRMS calcd. for $C_{26}H_{51}N_2O_{10}P_2$ ($[M + H]^+$): 613.3019, found: 613.3024.

5.1.4.2 Synthesis of azido–S1P/dhS1P stereosiomers

(*S*)–*tert*–butyl 4–((*R*)–1–hydroxyallyl)–2,2–dimethyloxazolidine–3–carboxylate (RBM7–023)

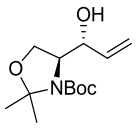

Vinylmagnesium bromide (24.9 mL, 17.45 mmol, 0.7 M in THF) was added dropwise to a solution of (*S*)–(–)–Garner's aldehyde (2.0 g, 8.72 mmol) in THF (35 mL) at –78 ºC. After stirring at this temperature for 3 h, the reaction mixture was allowed to warm to 0 ºC and then quenched by the dropwise addition of saturated aqueous NH_4Cl (20 mL). The mixture was extracted with Et_2O (3 x 25 mL) and the combined organic layers were washed with brine (2 x 20 mL), dried over anhydrous $MgSO_4$, filtered and evaporated *in vacuo*. Flash chromatography of the residue (from 0 to 15 % EtOAc in hexane) gave **RBM7–023** (*anti*/*syn* = 86:14) as a colourless oil (1.43 g, 64 %). Subsequent purification of the diastereomeric mixture by flash chromatography afforded pure *anti*–**RBM7–023**.

$[\alpha]^{20}_D$ = –26.2 (*c* 1.0, CH_3OH) [lit.[4] $[\alpha]^{20}_D$ = –32.0 (*c* 1.0, CH_3OH)]. ^{1}H NMR (400 MHz, CD_3OD) δ 5.89 (ddd, *J* = 17.0, 10.4, 6.3 Hz, 1H), 5.26 (d, *J* = 17.2 Hz, 1H), 5.18 – 5.08 (m, 1H), 4.29 – 4.14 (m, 1H), 4.07 – 3.77 (m, 3H), 1.65 – 1.42 (m, 15H). ^{13}C

NMR (101 MHz, CD_3OD) (mixture of rotamers) δ 154.6, 153.7, 140.1, 139.6, 116.3, 116.1, 95.4, 95.3, 81.8, 81.3, 74.2, 74.0, 65.5, 65.1, 62.7, 62.5, 28.7, 28.6, 27.3, 27.0, 24.9, 23.4. HRMS calcd. for $C_{13}H_{23}NO_4Na$ ($[M + Na]^+$): 280.1525, found: 280.1519.

(*R*)–*tert*–butyl 4–((*S*)–1–hydroxyallyl)–2,2–dimethyloxazolidine–3–carboxylate (*ent*–RBM7–023)

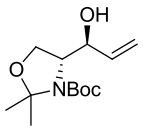

Compound ***ent*–RBM7–023** was obtained from (*R*)–(+)–Garner's aldehyde following the procedure described for the preparation of **RBM7–023**. Spectroscopic data were identical to those reported for **RBM7–023**.

$[\alpha]^{20}_D$ = +31.3 (*c* 1.0, CH_3OH) [lit.[5] $[\alpha]^{25}_D$ = +54.6 (*c* 1.47, $CHCl_3$)]

(*S*)–*tert*–butyl 4–((*R*,*E*)–1–hydroxyhexadec–2–en–1–yl)–2,2–dimethyloxazolidine–3–carboxylate (RBM7–024)

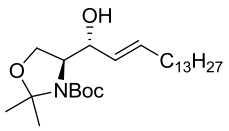

Compound **RBM7–024** (inseparable 94:6 *E*/*Z* mixture, colourless oil, 501 mg, 78 %) was obtained from **RBM7–023** (374 mg, 1.45 mmol), 1–pentadecene (1.58 mL, 5.81 mmol) and Grubbs catalyst 2nd generation (37 mg, 0.04 mmol), according to general procedure 6. The title compound was purified by flash chromatography on silica gel (from 0 to 10 % EtOAc in hexane). Pure *E* alkene was obtained in further purification steps along the synthetic route.

$[\alpha]^{20}_D$ = –26.1 (*c* 0.25, $CHCl_3$) [lit.[6] $[\alpha]^{22}_D$ = –26.0 (*c* 0.25, $CHCl_3$)]. ^{1}H NMR (400 MHz, CD_3OD) δ 5.65 (dt, *J* = 13.4, 6.4 Hz, 1H), 5.55 – 5.44 (m, 1H), 4.11 (t, *J* = 6.7 Hz, 1H), 4.07 – 3.84 (m, 3H), 3.83 – 3.74 (m, 1H), 2.04 (td, *J* = 14.4, 7.8 Hz, 2H), 1.54 (s, 3H), 1.48 (s, 12H), 1.44 – 1.23 (m, 22H), 0.90 (t, *J* = 6.9 Hz, 3H). ^{13}C NMR (101 MHz, CD_3OD) (mixture of rotamers) δ 154.6, 153.6, 134.0, 133.9, 131.5, 131.0, 95.3, 95.1, 81.7, 81.0, 74.3, 74.2, 65.8, 65.6, 62.9, 62.8, 33.7, 33.4, 33.1, 30.8, 30.8, 30.8,

30.7, 30.7, 30.5, 30.4, 28.9, 28.8, 27.5, 27.0, 25.0, 23.8, 23.5, 14.5. HRMS calcd. for $C_{26}H_{50}NO_4$ ($[M + H]^+$): 440.3740, found: 440.3741.

(*R*)–*tert*–butyl 4–((*S*,*E*)–1–hydroxyhexadec–2–en–1–yl)–2,2–dimethyloxazolidine–3–carboxylate (*ent*–RBM7–024)

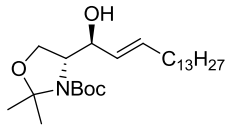

Compound ***ent*–RBM7–024** was obtained from ***ent*–RBM7–023** following the procedure described for the preparation of **RBM7–024**. Spectroscopic data were identical to those reported for **RBM7–024**.

$[\alpha]^{20}_D$ = +26.9 (*c* 0.25, $CHCl_3$)

(*S*)–*tert*–butyl 4–((*S*,*E*)–1–hydroxyhexadec–2–en–1–yl)–2,2–dimethyloxazolidine–3–carboxylate (RBM7–093)

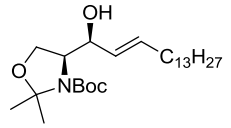

To an ice–cooled stirred suspension of $Cp_2Zr(H)Cl$ (773 mg, 3.00 mmol) in CH_2Cl_2 (5 mL) at 0 ºC was added neat 1–pentadecyne (787 µL, 3.00 mmol), and the mixture was stirred at rt for 40 min and then cooled to –40 ºC. To the resulting solution was added Et_2Zn (3.36 mL, 3.36 mmol, 1.0 M in hexanes) followed by (*S*)–(–)–Garner's aldehyde (550 mg, 2.40 mmol) in CH_2Cl_2 (4 mL). The reaction mixture was allowed to warm to 0 ºC and then quenched by the dropwise addition of saturated aqueous sodium potassium tartrate (10 mL) at the same temperature. The mixture was extracted with CH_2Cl_2 (3 x 25 mL) and the combined organic layers were washed with brine (2 x 20 mL), dried over anhydrous $MgSO_4$, filtered and evaporated *in vacuo*. Flash chromatography of the residue (from 0 to 12 % EtOAc in hexane) gave an inseparable 93:7 mixture of *syn*/*anti*–**RBM7–093** as a colourless oil (789 mg, 75 %). Pure *syn* diastereomer was obtained in further purification steps along the synthetic route.

$[\alpha]^{20}_D$ = –40.2 (*c* 1.0, $CHCl_3$). [lit.[7] $[\alpha]^{24}_D$ = –37.8 (*c* 0.84, $CHCl_3$)]. ^{1}H NMR (400 MHz, CD_3OD) δ 5.71 – 5.60 (m, 1H), 5.56 – 5.44 (m, 1H), 4.46 – 4.36 (m, 1H), 4.15 – 3.86

(m, 4H), 2.11 – 2.01 (m, 2H), 1.56 – 1.24 (m, 37H), 0.90 (t, *J* = 6.7 Hz, 3H). ^{13}C NMR (101 MHz, CD_3OD) (mixture of rotamers) δ 154.6, 153.6, 135.6, 135.5, 129.8, 129.6, 95.6, 95.3, 81.9, 81.2, 72.9, 64.3, 62.6, 62.1, 33.4, 33.1, 30.8, 30.8, 30.7, 30.7, 30.5, 30.3, 30.2, 28.8, 28.7, 27.3, 26.3, 24.6, 23.7, 23.2, 14.5. HRMS calcd. for $C_{26}H_{49}NO_4Na$ ($[M + Na]^+$): 462.3559, found: 462.3547.

(*R*)–*tert*–butyl 4–((*R*,*E*)–1–hydroxyhexadec–2–en–1–yl)–2,2–dimethyloxazolidine–3–carboxylate (*ent*–RBM7–093)

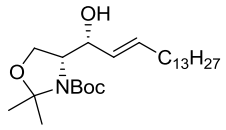

Compound ***ent*–RBM7–093** was obtained from (*R*)–(+)–Garner's aldehyde following the procedure described for the preparation of **RBM7–093**. Spectroscopic data were identical to those reported for **RBM7–093**.

$[\alpha]^{20}_D$ = +39.7 (*c* 1.0, $CHCl_3$)

***tert*–butyl ((2*S*,3*R*,*E*)–1,3–dihydroxyoctadec–4–en–2–yl)carbamate (RBM7–025)**

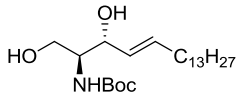

Compound **RBM7–025** (white solid, 402 mg, 94 %) was obtained from **RBM7–024** (470 mg, 1.07 mmol) and *p*–TsOH (20 mg, 0.11 mmol), according to general procedure 7.

$[\alpha]^{20}_D$ = –1.9 (*c* 1.0, $CHCl_3$). [lit.[7] $[\alpha]^{24}_D$ = –1.4 (*c* 1.25, $CHCl_3$)]. ^{1}H NMR (400 MHz, $CDCl_3$) δ 5.83 – 5.73 (m, 1H), 5.53 (dd, *J* = 15.4, 6.4 Hz, 1H), 5.28 (br s, 1H), 4.37 – 4.28 (m, 1H), 3.94 (dd, *J* = 11.3, 3.7 Hz, 1H), 3.71 (dd, *J* = 11.4, 3.7 Hz, 1H), 3.60 (br s, 1H), 2.05 (dd, *J* = 14.3, 7.0 Hz, 2H), 1.45 (s, 9H), 1.42 – 1.19 (m, 22H), 0.88 (t, *J* = 6.8 Hz, 3H). ^{13}C NMR (101 MHz, $CDCl_3$) δ 156.4, 134.3, 129.1, 80.0, 74.9, 62.8, 55.6, 32.4, 32.1, 29.8, 29.8, 29.8, 29.8, 29.6, 29.5, 29.4, 29.3, 28.5, 22.8, 14.3. HRMS calcd. for $C_{23}H_{45}NO_4Na$ ($[M + Na]^+$): 422.3246, found: 422.3268.

***tert*–butyl ((2*R*,3*S*,*E*)–1,3–dihydroxyoctadec–4–en–2–yl)carbamate (*ent*–RBM7–025)**

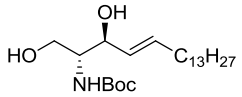

Compound ***ent*–RBM7–025** was obtained from ***ent*–RBM7–024** following the procedure described for the preparation of **RBM7–025**. Spectroscopic data were identical to those reported for **RBM7–025**.

$[\alpha]^{20}_{D}$ = +1.4 (*c* 1.0, $CHCl_3$) [lit.[8] $[\alpha]^{25}_{D}$ = +1.4 (*c* 1.0, $CHCl_3$)].

***tert*–butyl ((2*S*,3*S*,*E*)–1,3–dihydroxyoctadec–4–en–2–yl)carbamate (RBM7–094)**

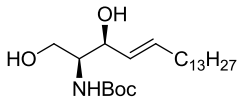

Compound **RBM7–094** (colorless oil, 566 mg, 92 %) was obtained from **RBM7–093** (675 mg, 1.54 mmol) and *p*–TsOH (29 mg, 0.15 mmol), according to general procedure 7.

$[\alpha]^{20}_{D}$ = –0.6 (*c* 1.0, $CHCl_3$). [lit.[9] $[\alpha]^{25}_{D}$ = –0.4 (*c* 1.0, $CHCl_3$)]. ^{1}H NMR (400 MHz, $CDCl_3$) δ 5.81 – 5.70 (m, 1H), 5.52 (dd, *J* = 15.4, 6.6 Hz, 1H), 5.14 (br s, 1H), 4.34 (dd, *J* = 6.3, 3.6 Hz, 1H), 3.80 (app d, *J* = 3.8 Hz, 2H), 3.63 (td, *J* = 8.3, 4.4 Hz, 1H), 2.39 (br s, 2H), 2.09 – 1.98 (m, 2H), 1.65 – 1.17 (m, 37H), 0.88 (t, *J* = 6.8 Hz, 3H). ^{13}C NMR (101 MHz, $CDCl_3$) δ 156.8, 133.9, 129.1, 79.8, 73.1, 64.1, 55.7, 32.4, 32.0, 29.8, 29.8, 29.8, 29.7, 29.6, 29.5, 29.4, 29.2, 28.5, 22.8, 14.2. HRMS calcd. for $C_{23}H_{45}NO_4Na$ ([M + Na]$^+$): 422.3246, found: 422.3247.

***tert*–butyl ((2*R*,3*R*,*E*)–1,3–dihydroxyoctadec–4–en–2–yl)carbamate (*ent*–RBM7–094)**

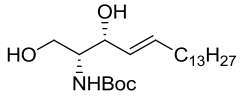

Compound ***ent*–RBM7–094** was obtained from ***ent*–RBM7–093** following the procedure described for the preparation of **RBM7–094**. Spectroscopic data were identical to those reported for **RBM7–094**.

$[\alpha]^{20}_D$ = +0.9 (*c* 1.0, $CHCl_3$) [lit.[10] $[\alpha]^{25}_D$ = +0.4 (*c* 0.9, $CHCl_3$)].

***tert*–butyl ((2*S*,3*R*)–1,3–dihydroxyoctadecan–2–yl)carbamate (RBM7–009)**

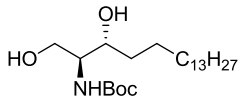

Compound **RBM7–009** (white solid, 485 mg, 97 %) was obtained from alkene **RBM7–025** (500 mg, 1.25 mmol) and Rh/Al_2O_3 (50 mg), according to general procedure 8.

$[\alpha]^{20}_D$ = +8.3 (*c* 1.0, $CHCl_3$). [lit.[11] $[\alpha]^{24}_D$ = +8.2 (*c* 1.0, $CHCl_3$)]. ^{1}H NMR (400 MHz, $CDCl_3$) δ 5.38 (br s, 1H), 3.99 (dd, *J* = 11.4, 3.4 Hz, 1H), 3.84 – 3.71 (m, 2H), 3.52 (br s, 1H), 1.63 – 1.15 (m, 37H), 0.88 (t, *J* = 6.8 Hz, 3H). ^{13}C NMR (101 MHz, $CDCl_3$) δ 156.2, 79.9, 74.5, 62.8, 55.0, 34.6, 32.1, 29.8, 29.8, 29.8, 29.7, 29.7, 29.5, 28.5, 26.1, 22.8, 14.3. HRMS calcd. for $C_{23}H_{47}NO_4Na$ ($[M + Na]^+$): 424.3403, found: 424.3401.

tert–butyl ((2*R*,3*S*)–1,3–dihydroxyoctadecan–2–yl)carbamate (*ent*–RBM7–009)

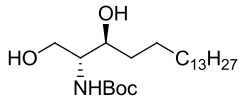

Compound ***ent*–RBM7–009** was obtained from alkene ***ent*–RBM7–025** following the procedure described for the preparation of **RBM7–009**. Spectroscopic data were identical to those reported for **RBM7–009**.

$[\alpha]^{20}_D$ = –9.3 (*c* 1.0, $CHCl_3$).

***tert*–butyl ((2*S*,3*S*)–1,3–dihydroxyoctadecan–2–yl)carbamate (RBM7–099)**

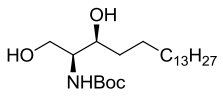

Compound **RBM7–099** (colourless oil, 474 mg, 91 %) was obtained from alkene **RBM7–094** (520 mg, 1.30 mmol) and Rh/Al_2O_3 (52 mg), according to general procedure 8.

$[\alpha]^{20}_D$ = +7.5 (*c* 1.0, $CHCl_3$) [lit.[11] $[\alpha]^{21}_D$ = +19.8 (*c* 1.0, $CHCl_3$)]. ^{1}H NMR (400 MHz, $CDCl_3$) δ 5.20 (br d, J = 7.7 Hz, 1H), 3.91 (app t, *J* = 5.9 Hz, 1H), 3.82 (app d, *J* = 3.8 Hz, 2H), 3.59 (br s, 1H), 2.44 (br s, 2H), 1.60 – 1.16 (m, 37H), 0.88 (t, *J* = 6.8 Hz, 3H).

^{13}C NMR (101 MHz, $CDCl_3$) δ 156.7, 79.8, 73.2, 65.6, 54.4, 34.4, 32.1, 29.9, 29.8, 29.8, 29.8, 29.7, 29.5, 28.5, 25.7, 22.8, 14.3. HRMS calcd. for $C_{23}H_{47}NO_4Na$ ([M + Na]$^+$): 424.3403, found: 424.3374.

***tert*–butyl ((2*R*,3*R*)–1,3–dihydroxyoctadecan–2–yl)carbamate (*ent*–RBM7–099)**

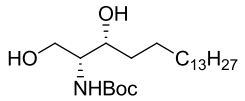

Compound ***ent*–RBM7–099** was obtained from ***ent*–RBM7–094** following the procedure described for the preparation of **RBM7–099**. Spectroscopic data were identical to those reported for **RBM7–099**.

$[\alpha]^{20}_D$ = –8.6 (*c* 1.0, $CHCl_3$) [lit.[12] $[\alpha]^{20}_D$ = –20.6 (*c* 1.0, $CHCl_3$)].

(2S,3R,E)–2–aminooctadec–4–ene–1,3–diol hydrochloride (RBM7–086)

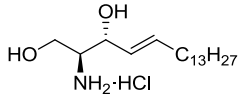

Compound **RBM7–086** (white solid, 243 mg, 84 %) was obtained from **RBM7–025** (345 mg, 0.86 mmol) and AcCl (308 µL, 4.32 mmol), according to general procedure 9.

^{1}H NMR (400 MHz, CD_3OD) δ 5.90 – 5.77 (m, 1H), 5.48 (dd, *J* = 15.4, 6.9 Hz, 1H), 4.30 – 4.20 (m, 1H), 3.78 (dd, *J* = 11.5, 4.1 Hz, 1H), 3.64 (dd, *J* = 11.5, 8.1 Hz, 1H), 3.14 (dt, *J* = 8.7, 4.4 Hz, 1H), 2.10 (dd, *J* = 14.1, 7.1 Hz, 2H), 1.48 – 1.21 (m, 22H), 0.90 (t, *J* = 6.8 Hz, 3H). ^{13}C NMR (101 MHz, CD_3OD) δ 136.3, 128.7, 71.3, 59.8, 58.5, 33.4, 33.1, 30.8, 30.8, 30.7, 30.6, 30.5, 30.4, 30.2, 23.7, 14.5. HRMS calcd. for $C_{18}H_{38}NO_2$ ([M + H]$^+$): 300.2903, found: 300.2884.

(2*R*,3*S*,*E*)–2–aminooctadec–4–ene–1,3–diol hydrochloride (*ent*–RBM7–086)

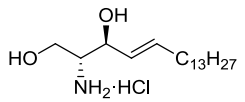

Compound ***ent*–RBM7–086** was obtained from ***ent*–RBM7–025** following the procedure described for the preparation of **RBM7–086**. Spectroscopic data were identical to those reported for **RBM7–086**.

(2*S*,3*S*,*E*)–2–aminooctadec–4–ene–1,3–diol hydrochloride (RBM7–095)

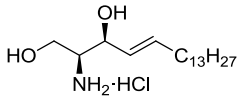

Compound **RBM7–095** (white solid, 222 mg, 90 %) was obtained from **RBM7–094** (295 mg, 0.74 mmol) and AcCl (263 µL, 3.69 mmol), according to general procedure 9.

^{1}H NMR (400 MHz, CD_3OD) δ 5.91 – 5.78 (m, 1H), 5.45 (dd, *J* = 15.4, 7.5 Hz, 1H), 4.11 (app t, *J* = 7.8 Hz, 1H), 3.74 (dd, *J* = 11.7, 3.6 Hz, 1H), 3.59 (dd, *J* = 11.7, 6.5 Hz, 1H), 3.08 – 3.00 (m, 1H), 2.15 – 2.04 (m, 2H), 1.52 – 1.16 (m, 28H), 0.90 (t, *J* = 6.6 Hz, 3H). ^{13}C NMR (101 MHz, CD_3OD) δ 136.8, 129.7, 71.0, 60.1, 58.9, 33.3, 33.0, 30.8, 30.7, 30.7, 30.6, 30.4, 30.3, 30.1, 23.7, 14.5. HRMS calcd. for $C_{18}H_{38}NO_2$ ($[M + H]^+$): 300.2903, found: 300.2878.

(2*R*,3*R*,*E*)–2–aminooctadec–4–ene–1,3–diol hydrochloride (*ent*–RBM7–095)

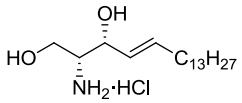

Compound ***ent*–RBM7–095** was obtained from ***ent*–RBM7–094** following the procedure described for the preparation of **RBM7–095**. Spectroscopic data were identical to those reported for **RBM7–095**.

(2*S*,3*R*)–2–aminooctadecane–1,3–diol hydrochloride (RBM7–062)

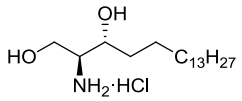

Compound **RBM7–062** (white solid, 336 mg, quant. yield) was obtained from **RBM7–009** (400 mg, 0.996 mmol) and AcCl (355 µL, 4.98 mmol), according to general procedure 9.

^{1}H NMR (400 MHz, CD_3OD) δ 3.83 (dd, *J* = 11.5, 4.0 Hz, 1H), 3.80 – 3.74 (m, 1H), 3.70 (dd, *J* = 11.5, 8.7 Hz, 1H), 3.23 – 3.16 (m, 1H), 1.60 – 1.21 (m, 28H), 0.90 (t, *J* = 6.8 Hz, 3H). ^{13}C NMR (101 MHz, CD_3OD) δ 70.3, 58.9, 58.4, 34.2, 33.0, 30.8, 30.7, 30.7, 30.7, 30.6, 30.4, 27.0, 23.7, 14.4. HRMS calcd. for $C_{18}H_{40}NO_2$ ($[M + H]^+$): 302.3059, found: 302.3047.

(2*R*,3*S*)–2–aminooctadecane–1,3–diol hydrochloride (*ent*–RBM7–062)

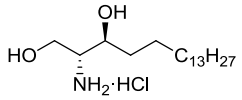

Compound ***ent*–RBM7–062** was obtained from ***ent*–RBM7–009** following the procedure described for the preparation of **RBM7–062**. Spectroscopic data were identical to those reported for **RBM7–062**.

(2*S*,3*S*)–2–aminooctadecane–1,3–diol hydrochloride (RBM7–100)

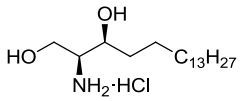

Compound **RBM7–100** (white solid, 258 mg, 85 %) was obtained from **RBM7–099** (363 mg, 0.90 mmol) and AcCl (323 µL, 4.52 mmol), according to general procedure 9.

^{1}H NMR (400 MHz, CD_3OD) δ 4.58 (s, 2H), 3.76 (dd, *J* = 11.6, 4.1 Hz, 1H), 3.70 – 3.61 (m, 2H), 3.03 (td, *J* = 6.8, 4.2 Hz, 1H), 1.64 – 1.16 (m, 28H), 0.90 (t, *J* = 6.9 Hz, 3H). ^{13}C NMR (101 MHz, CD_3OD) δ 69.2, 60.6, 59.1, 34.9, 33.1, 30.8, 30.8, 30.7, 30.7, 30.6, 30.5, 26.3, 23.7, 14.4. HRMS calcd. for $C_{18}H_{40}NO_2$ ($[M + H]^+$): 302.3059, found: 302.3047.

(2*R*,3*R*)–2–aminooctadecane–1,3–diol hydrochloride (*ent*–RBM7–100)

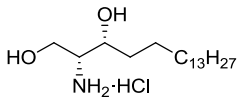

Compound ***ent*–RBM7–100** was obtained from ***ent*–RBM7–099** following the procedure described for the preparation of **RBM7–100**. Spectroscopic data were identical to those reported for **RBM7–100**.

(2*S*,3*R*,*E*)–2–azidooctadec–4–ene–1,3–diol (RBM7–087)

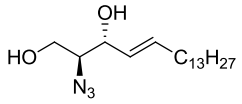

Compound **RBM7–087** (white solid, 152 mg, 91%) was obtained from **RBM7–086** (173 mg, 0.52 mmol), K_2CO_3 (192 mg, 1.39 mmol), $CuSO_4 \cdot 5H_2O$ (0.8 mg, 5 μmol) and ISA·HCl (130 mg, 0.62 mmol), according to general procedure 10.

$[\alpha]^{20}_D$ = –34.6 (*c* 1.0, $CHCl_3$) [lit.[13] $[\alpha]^{25}_D$ = –33.2 (*c* 2.0, $CHCl_3$)]. ^{1}H NMR (400 MHz, $CDCl_3$) δ 5.89 – 5.75 (m, 1H), 5.59 – 5.48 (m, 1H), 4.28 – 4.21 (m, 1H), 3.84 – 3.73 (m, 2H), 3.51 (dd, *J* = 10.4, 5.5 Hz, 1H), 2.12 – 1.99 (m, 4H), 1.46 – 1.18 (m, 22H), 0.88 (t, *J* = 6.8 Hz, 3H). ^{13}C NMR (101 MHz, $CDCl_3$) δ 136.1, 128.1, 73.9, 66.9, 62.7, 32.5, 32.1, 29.8, 29.8, 29.8, 29.8, 29.7, 29.6, 29.5, 29.3, 29.1, 22.8, 14.2. HRMS calcd. for $C_{18}H_{35}N_3O_2Na$ ($[M + Na]^+$): 348.2627, found: 348.2637. R_T (Column B, hexane/isopropanol (96.5:3.5)): 16.5 min. *ca*. 99 % *ee*.

(2*R*,3*S*,*E*)–2–azidooctadec–4–ene–1,3–diol (*ent*–RBM7–087)

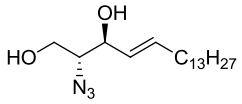

Compound ***ent*–RBM7–087** was obtained from ***ent*–RBM7–086** following the procedure described for the preparation of **RBM7–087**. Spectroscopic data were identical to those reported for **RBM7–087**.

$[\alpha]^{20}_D$ = +32.4 (*c* 1.0, $CHCl_3$) [lit.[14] $[\alpha]^{24}_D$ = +39.3 (*c* 1.0, $CHCl_3$)]. R_T (Column B, hexane/isopropanol (96.5:3.5)): 15.4 min. *ca*. 99 % *ee*.

(2*S*,3*S*,*E*)–2–azidooctadec–4–ene–1,3–diol (RBM7–096)

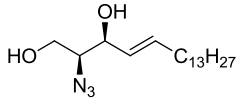

Compound **RBM7–096** (white solid, 217 mg, 82 %) was obtained from **RBM7–095** (272 mg, 0.81 mmol), K_2CO_3 (302 mg, 2.19 mmol), $CuSO_4 \cdot 5H_2O$ (1.3 mg, 8 μmol) and ISA·HCl (204 mg, 0.97 mmol), according to general procedure 10.

$[\alpha]^{20}_D$ = +1.0 (*c* 1.0, $CHCl_3$) [lit.[15] $[\alpha]^{26}_D$ = +0.9 (*c* 1.0, $CHCl_3$)]. ^{1}H NMR (400 MHz, $CDCl_3$) δ 5.86 – 5.74 (m, 1H), 5.52 (dd, *J* = 15.4, 7.1 Hz, 1H), 4.21 (app t, *J* = 6.2 Hz, 1H), 3.82 (dd, *J* = 11.4, 3.8 Hz, 1H), 3.70 (dd, *J* = 11.4, 6.4 Hz, 1H), 3.52 – 3.42 (m, 1H), 2.12 – 1.95 (m, 4H), 1.48 – 1.10 (m, 22H), 0.88 (t, *J* = 6.7 Hz, 3H). ^{13}C NMR (101 MHz, $CDCl_3$) δ 135.8, 128.4, 73.7, 67.7, 63.1, 32.4, 32.1, 29.8, 29.8, 29.7, 29.6, 29.5, 29.3, 29.1, 22.8, 14.3. HRMS calcd. for $C_{18}H_{35}N_3O_2Na$ ($[M + Na]^+$): 348.2627, found: 348.2595. R_T (Column A, hexane/isopropanol (95:5)): 15.3 min. *ca*. 97 % *ee*.

(2*R*,3*R*,*E*)–2–azidooctadec–4–ene–1,3–diol (ent–RBM7–096)

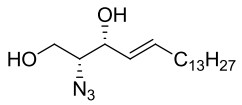

Compound **ent–RBM7–096** was obtained from ***ent*–RBM7–095** following the procedure described for the preparation of **RBM7–096**. Spectroscopic data were identical to those reported for **RBM7–096**.

$[\alpha]^{20}_D$ = –1.5 (*c* 1.0, $CHCl_3$) [lit.[16] $[\alpha]^{24}_D$ = –2.4 (*c* 0.3, $CHCl_3$)]. R_T (Column A, hexane/isopropanol (95:5)): 13.1 min. *ca*. >99 % *ee*.

(2*S*,3*R*)–2–azidooctadecane–1,3–diol (RBM7–112)

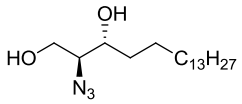

Compound **RBM7–112** (white solid, 201 mg, 86 %) was obtained from **RBM7–062** (240 mg, 0.71 mmol), K_2CO_3 (265 mg, 1.92 mmol), $CuSO_4 \cdot 5H_2O$ (1.1 mg, 7 μmol) and ISA·HCl (179 mg, 0.85 mmol), according to general procedure 10.

$[\alpha]^{20}_D$ = +7.9 (*c* 1.0, $CHCl_3$) [lit.[17] $[\alpha]^{24}_D$ = +4.1 (*c* 0.5, $CHCl_3$)]. ^{1}H NMR (400 MHz, $CDCl_3$) δ 3.94 – 3.85 (m, 2H), 3.81 – 3.74 (m, 1H), 3.43 (dd, *J* = 10.1, 5.1 Hz, 1H), 2.03 (br s, 2H), 1.66 – 1.17 (m, 28H), 0.88 (t, *J* = 6.8 Hz, 3H). ^{13}C NMR (101 MHz, $CDCl_3$) δ 72.8, 67.0, 62.7, 33.9, 32.1, 29.8, 29.8, 29.8, 29.7, 29.7, 29.6, 29.5, 25.7, 22.8, 14.3. HRMS calcd. for $C_{18}H_{37}N_3O_2Na$ ($[M + Na]^+$): 350.2783, found: 350.2780. R_T (Column A, hexane/isopropanol (95:5)): 9.7 min. *ca*. 98 % *ee*.

(2*R*,3*S*)–2–azidooctadecane–1,3–diol (*ent*–RBM7–112)

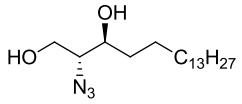

Compound ***ent*–RBM7–112** was obtained from ***ent*–RBM7–062** following the procedure described for the preparation of **RBM7–112**. Spectroscopic data were identical to those reported for **RBM7–112**.

$[\alpha]^{20}_D$ = –10.6 (*c* 1.0, $CHCl_3$). R_T (Column A, hexane/isopropanol (95:5)): 7.8 min. *ca*. 98 % *ee*.

(2*S*,3*S*)–2–azidooctadecane–1,3–diol (RBM7–101)

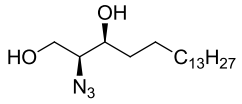

Compound **RBM7–101** (white solid, 225 mg, 80 %) was obtained from **RBM7–100** (289 mg, 0.86 mmol), K_2CO_3 (319 mg, 2.31 mmol), $CuSO_4 \cdot 5H_2O$ (1.4 mg, 9 µmol) and ISA·HCl (215 mg, 1.03 mmol), according to general procedure 10.

$[\alpha]^{20}_D$ = +7.3 (*c* 1.0, $CHCl_3$). ^{1}H NMR (400 MHz, $CDCl_3$) δ 3.97 – 3.82 (m, 2H), 3.79 – 3.70 (m, 1H), 3.44 (dt, *J* = 6.1, 4.2 Hz, 1H), 2.07 – 2.00 (m, 1H), 1.91 – 1.86 (m, 1H), 1.62 – 1.20 (m, 28H), 0.88 (t, *J* = 6.8 Hz, 3H). ^{13}C NMR (101 MHz, $CDCl_3$) δ 72.5, 67.0, 63.8, 34.6, 32.1, 29.8, 29.8, 29.8, 29.8, 29.8, 29.7, 29.7, 29.6, 29.5, 25.7, 22.8, 14.3. HRMS calcd. for $C_{18}H_{37}N_3O_2Na$ ($[M + Na]^+$): 350.2783, found: 350.2755. R_T (Column A, hexane/isopropanol (96.5:3.5)): 19.3 min. *ca*. 95 % *ee*.

(2*R*,3*R*)–2–azidooctadecane–1,3–diol (*ent*–RBM7–101)

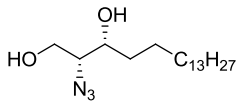

Compound ***ent*–RBM7–101** was obtained from ***ent*–RBM7–100** following the procedure described for the preparation of **RBM7–101**. Spectroscopic data were identical to those reported for **RBM7–101**.

$[\alpha]^{20}_D$ = –8.3 (*c* 1.0, $CHCl_3$). R_T (Column A, hexane/isopropanol (96.5:3.5)): 15.2 min. *ca*. 99 % *ee*.

(2*S*,3*R*,*E*)–2–azido–3–hydroxyoctadec–4–en–1–yl dimethyl phosphate (RBM7–088)

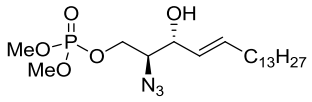

Compound **RBM7–088** (colorless oil, 171 mg, 85%) was obtained from alcohol **RBM7–087** (152 mg, 0.47 mmol), *N*–methylimidazole (56 μL, 0.70 mmol) and dimethyl chlorophosphate (60 μL, 0.56 mmol), according to general procedure 11. The title compound was purified by flash chromatography on silica gel (from 0 to100 % Et_2O in hexane).

$[\alpha]^{20}_D$ = –7.4 (*c* 1.0, $CHCl_3$). ^{1}H NMR (400 MHz, $CDCl_3$) δ 5.88 – 5.77 (m, 1H), 5.57 – 5.46 (m, 1H), 4.28 – 4.15 (m, 3H), 3.82 (d, *J* = 3.7 Hz, 3H), 3.80 (d, *J* = 3.7 Hz, 3H), 3.57 (dd, *J* = 10.3, 5.8 Hz, 1H), 2.11 – 2.02 (m, 2H), 1.45 – 1.19 (m, 22H), 0.88 (t, *J* = 6.8 Hz, 3H). ^{13}C NMR (101 MHz, $CDCl_3$) δ 136.2, 127.7, 71.8, 67.2 (d, $J_{C–P}$ = 5.4 Hz), 65.6 (d, $J_{C–P}$ = 6.6 Hz), 54.7 (d, $J_{C–P}$ = 6.1 Hz), 54.7 (d, $J_{C–P}$ = 6.1 Hz), 32.4, 32.0, 29.8, 29.8, 29.8, 29.7, 29.6, 29.5, 29.3, 29.0, 22.8, 14.2. ^{31}P NMR (162 MHz, $CDCl_3$) δ 2.07. HRMS calcd. for $C_{20}H_{40}N_3O_5PNa$ ($[M + Na]^+$): 456.2603, found: 456.2603.

(2*R*,3*S*,*E*)–2–azido–3–hydroxyoctadec–4–en–1–yl dimethyl phosphate (*ent*–RBM7–088)

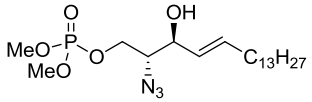

Compound ***ent*–RBM7–088** was obtained from ***ent*–RBM7–087** following the procedure described for the preparation of **RBM7–088**. Spectroscopic data were identical to those reported for **RBM7–088**.

$[\alpha]^{20}_D$ = +6.8 (*c* 1.0, $CHCl_3$).

(2*S*,3*S*,*E*)–2–azido–3–hydroxyoctadec–4–en–1–yl dimethyl phosphate (RBM7–097)

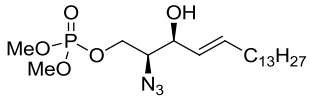

Compound **RBM7–097** (colorless oil, 99 mg, 68 %) was obtained from alcohol **RBM7–096** (110 mg, 0.34 mmol), *N*–methylimidazole (40 µL, 0.51 mmol) and dimethyl chlorophosphate (44 µL, 0.41 mmol), according to general procedure 11. The title compound was purified by flash chromatography on silica gel (from 0 to100 % Et_2O in hexane).

$[\alpha]^{20}_D$ = –1.6 (*c* 1.0, $CHCl_3$). ^{1}H NMR (400 MHz, $CDCl_3$) δ 5.86 – 5.72 (m, 1H), 5.49 (dd, *J* = 15.4, 6.9 Hz, 1H), 4.29 – 4.20 (m, 1H), 4.18 – 4.12 (m, 1H), 4.12 – 4.02 (m, 1H), 3.80 (s, 3H), 3.77 (s, 3H), 3.63 – 3.55 (m, 1H), 2.10 – 1.99 (m, 2H), 1.47 – 1.12 (m, 22H), 0.86 (t, *J* = 6.6 Hz, 3H). ^{13}C NMR (101 MHz, $CDCl_3$) δ 135.8, 127.8, 72.1, 67.2 (d, $J_{C–P}$ = 5.4 Hz), 66.0 (d, $J_{C–P}$ = 7.0 Hz), 54.7 (d, $J_{C–P}$ = 5.9 Hz), 32.4, 32.0, 29.8, 29.8, 29.7, 29.6, 29.5, 29.3, 29.0, 22.8, 14.2. ^{31}P NMR (162 MHz, $CDCl_3$) δ 1.38. HRMS calcd. for $C_{20}H_{40}N_3O_5PNa$ ($[M + Na]^+$): 456.2603, found: 456.2591.

(2*R*,3*R*,*E*)–2–azido–3–hydroxyoctadec–4–en–1–yl dimethyl phosphate (*ent*–RBM7–097)

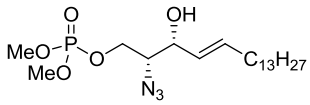

Compound ***ent*–RBM7–097** was obtained from ***ent*–RBM7–096** following the procedure described for the preparation of **RBM7–097**. Spectroscopic data were identical to those reported for **RBM7–097**.

$[\alpha]^{20}_D$ = +2.3 (*c* 1.0, $CHCl_3$).

(2*S*,3*R*)–2–azido–3–hydroxyoctadecyl dimethyl phosphate (RBM7–113)

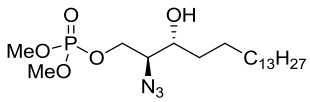

Compound **RBM7–113** (colorless oil, 66 mg, 76 %) was obtained from alcohol **RBM7–112** (65 mg, 0.20 mmol), *N*–methylimidazole (24 µL, 0.30 mmol) and dimethyl

chlorophosphate (26 µL, 0.24 mmol), according to general procedure 11. The title compound was purified by flash chromatography on silica gel (from 0 to100 % Et_2O in hexane).

$[\alpha]^{20}_D$ = +22.0 (*c* 1.0, $CHCl_3$). ^{1}H NMR (400 MHz, $CDCl_3$) δ 4.43 – 4.26 (m, 2H), 3.83 (d, *J* = 4.7 Hz, 3H), 3.80 (d, *J* = 4.7 Hz, 3H), 3.74 – 3.67 (m, 1H), 3.43 – 3.36 (m, 1H), 1.67 – 1.20 (m, 28H), 0.88 (t, *J* = 6.8 Hz, 3H). ^{13}C NMR (101 MHz, $CDCl_3$) δ 70.0, 67.3 (d, J_{C-P} = 5.4 Hz), 65.8 (d, J_{C-P} = 5.9 Hz), 54.9 (d, J_{C-P} = 6.1 Hz), 54.8 (d, J_{C-P} = 6.1 Hz), 33.6, 32.1, 29.8, 29.8, 29.8, 29.7, 29.7, 29.7, 29.5, 25.6, 22.8, 14.3. ^{31}P NMR (162 MHz, $CDCl_3$) δ 2.44. HRMS calcd. for $C_{20}H_{42}N_3O_5PNa$ ($[M + Na]^+$): 458.2760, found: 458.2765.

(2*R*,3*S*)–2–azido–3–hydroxyoctadecyl dimethyl phosphate (*ent*–RBM7–113)

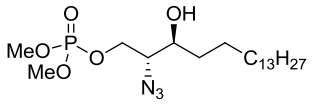

Compound ***ent*–RBM7–113** was obtained from ***ent*–RBM7–112** following the procedure described for the preparation of **RBM7–113**. Spectroscopic data were identical to those reported for **RBM7–113**.

$[\alpha]^{20}_D$ = –22.6 (*c* 1.0, $CHCl_3$).

(2*S*,3*S*)–2–azido–3–hydroxyoctadecyl dimethyl phosphate (RBM7–102)

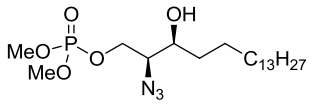

Compound **RBM7–102** (colorless oil, 66 mg, 64 %) was obtained from alcohol **RBM7–101** (78 mg, 0.24 mmol), *N*–methylimidazole (29 µL, 0.36 mmol) and dimethyl chlorophosphate (31 µL, 0.29 mmol), according to general procedure 11. The title compound was purified by flash chromatography on silica gel (from 0 to1 % CH_3OH in CH_2Cl_2).

$[\alpha]^{20}_D$ = +4.3 (*c* 1.0, $CHCl_3$). ^{1}H NMR (400 MHz, $CDCl_3$) δ 4.35 – 4.27 (m, 1H), 4.25 – 4.16 (m, 1H), 3.82 (s, 3H), 3.80 (s, 3H), 3.71 – 3.64 (m, 1H), 3.57 (ddd, *J* = 8.0, 5.1, 3.3 Hz, 1H), 1.68 – 1.17 (m, 28H), 0.88 (t, *J* = 6.8 Hz, 3H). ^{13}C NMR (101 MHz, $CDCl_3$) δ 70.7, 67.6 (d, J_{C-P} = 5.5 Hz), 65.4 (d, J_{C-P} = 6.8 Hz), 54.8 (d, J_{C-P} = 6.1 Hz), 54.7 (d, J_{C-}

$_P$ = 6.1 Hz), 34.3, 32.1, 29.8, 29.8, 29.8, 29.8, 29.7, 29.7, 29.6, 29.5, 25.8, 22.8, 14.2. ^{31}P NMR (162 MHz, $CDCl_3$) δ 1.96. HRMS calcd. for $C_{20}H_{42}N_3O_5PNa$ ($[M + Na]^+$): 458.2760, found: 458.2764.

(2*R*,3*R*)–2–azido–3–hydroxyoctadecyl dimethyl phosphate (*ent*–RBM7–102)

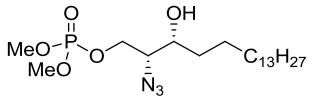

Compound ***ent*–RBM7–102** was obtained from ***ent*–RBM7–101** following the procedure described for the preparation of **RBM7–102**. Spectroscopic data were identical to those reported for **RBM7–102**.

$[\alpha]^{20}_D$ = –3.4 (*c* 1.0, $CHCl_3$).

(2*S*,3*R*,*E*)–2–azido–3–hydroxyoctadec–4–en–1–yl dihydrogen phosphate (RBM7–089)

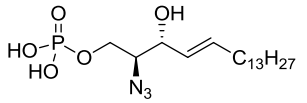

Compound **RBM7–089** (pale yellow solid, 52 mg, 71%) was obtained from dimethyl phosphate **RBM7–088** (78 mg, 0.18 mmol) and TMSBr (95 µL, 0.72 mmol), according to general procedure 12. The crude reaction mixture was dissolved in methanol and loaded on an Amberlite® XAD4 column (10 g), which had been washed thoroughly with acetone and then equilibrated with water. Elution with a linear gradient from 0 to 70 % CH_3CN in H_2O provided the title compound.

$[\alpha]^{20}_D$ = –18.5 (*c* 1.0, CH_3OH). ^{1}H NMR (400 MHz, CD_3OD) δ 5.83 – 5.72 (m, 1H), 5.51 (dd, *J* = 15.3, 7.4 Hz, 1H), 4.16 – 4.08 (m, 2H), 3.98 – 3.89 (m, 1H), 3.64 – 3.56 (m, 1H), 2.13 – 2.02 (m, 2H), 1.48 – 1.21 (m, 22H), 0.90 (t, *J* = 6.7 Hz, 3H). ^{13}C NMR (101 MHz, CD_3OD) δ 136.0, 129.6, 73.1, 67.5 (d, $J_{C–P}$ = 7.8 Hz), 67.1 (d, $J_{C–P}$ = 5.1 Hz), 33.4, 33.1, 30.8, 30.8, 30.8, 30.8, 30.7, 30.6, 30.5, 30.2, 30.2, 23.7, 14.4. ^{31}P NMR (162 MHz, CD_3OD) δ 1.22. HRMS calcd. for $C_{18}H_{36}N_3O_5PNa$ ($[M + Na]^+$): 428.2290, found: 428.2287.

(2*R*,3*S*,*E*)–2–azido–3–hydroxyoctadec–4–en–1–yl dihydrogen phosphate (*ent*–RBM7–089)

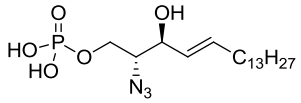

Compound ***ent*–RBM7–089** was obtained from ***ent*–RBM7–088** following the procedure described for the preparation of **RBM7–089**. Spectroscopic data were identical to those reported for **RBM7–089**.

$[\alpha]^{20}_{D}$ = +16.8 (*c* 1.0, CH_3OH).

(2*S*,3*S*,*E*)–2–azido–3–hydroxyoctadec–4–en–1–yl dihydrogen phosphate (RBM7–098)

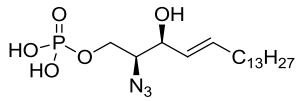

Compound **RBM7–098** (pale yellow solid, 57 mg, 68 %) was obtained from dimethyl phosphate **RBM7–097** (90 mg, 0.21 mmol) and TMSBr (110 µL, 0.83 mmol), according to general procedure 12. The crude material was purified as described above for **RBM7–089**.

$[\alpha]^{20}_{D}$ = –5.1 (*c* 0.7, $CHCl_3$). ^{1}H NMR (400 MHz, CD_3OD) 5.85 – 5.72 (m, 1H), 5.53 (dd, *J* = 15.4, 6.9 Hz, 1H), 4.20 – 4.04 (m, 2H), 3.96 (br s, 1H), 3.53 (br s, 1H), 2.14 – 2.01 (m, 2H), 1.62 – 1.19 (m, 22H), 0.90 (t, *J* = 6.8 Hz, 3H). ^{13}C NMR (101 MHz, CD_3OD) δ 135.3, 130.1, 73.1, 67.7 (d, $J_{C–P}$ = 4.1 Hz), 66.9 (d, $J_{C–P}$ = 4.2 Hz), 33.4, 33.1, 30.8, 30.8, 30.7, 30.6, 30.5, 30.3, 30.2, 23.7, 14.4. ^{31}P NMR (162 MHz, CD_3OD) δ 3.05. HRMS calcd. for $C_{18}H_{36}N_3O_5PNa$ ($[M + Na]^+$): 428.2290, found: 428.2287.

(2*R*,3*R*,*E*)–2–azido–3–hydroxyoctadec–4–en–1–yl dihydrogen phosphate (*ent*–RBM7–098)

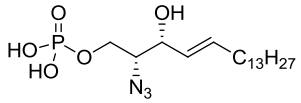

Compound ***ent*–RBM7–098** was obtained from ***ent*–RBM7–097** following the procedure described for the preparation of **RBM7–098**. Spectroscopic data were identical to those reported for **RBM7–098**.

$[\alpha]^{20}_{D}$ = +4.2 (*c* 0.7, $CHCl_3$).

(2*S*,3*R*)–2–azido–3–hydroxyoctadecyl dihydrogen phosphate (RBM7–114)

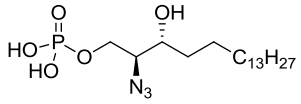

Compound **RBM7–114** (pale yellow solid, 39 mg, 56 %) was obtained from dimethyl phosphate **RBM7–113** (75 mg, 0.17 mmol) and TMSBr (91 µL, 0.69 mmol), according to general procedure 12. The crude material was purified as described above for **RBM7–089**.

$[\alpha]^{20}_{D}$ = +21.3 (*c* 0.7, $CHCl_3$). ^{1}H NMR (400 MHz, CD_3OD) δ 4.31 – 4.21 (m, 1H), 4.09 – 3.98 (m, 1H), 3.61 – 3.49 (m, 2H), 1.64 – 1.21 (m, 28H), 0.90 (t, *J* = 6.7 Hz, 3H). ^{13}C NMR (101 MHz, CD_3OD) δ 71.6, 67.7 (d, $J_{C–P}$ = 6.6 Hz), 67.4 (d, $J_{C–P}$ = 3.1 Hz), 34.4, 33.1, 30.8, 30.8, 30.8, 30.7, 30.7, 30.7, 30.5, 26.6, 23.7, 14.5. ^{31}P NMR (162 MHz, CD_3OD) δ 1.58. HRMS calcd. for $C_{18}H_{38}N_3O_5PNa$ ($[M + Na]^+$): 430.2447, found: 430.2441.

(2*R*,3*S*)–2–azido–3–hydroxyoctadecyl dihydrogen phosphate (ent–RBM7–114)

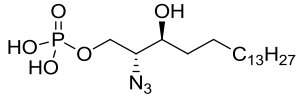

Compound **ent–RBM7–114** was obtained from **ent–RBM7–113** following the procedure described for the preparation of **RBM7–114**. Spectroscopic data were identical to those reported for **RBM7–114**.

$[\alpha]^{20}_D$ = –23.7 (*c* 0.7, $CHCl_3$).

(2*S*,3*S*)–2–azido–3–hydroxyoctadecyl dihydrogen phosphate (RBM7–103)

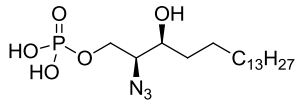

Compound **RBM7–103** (pale yellow solid, 50 mg, 69 %) was obtained from dimethyl phosphate **RBM7–102** (78 mg, 0.18 mmol) and TMSBr (95 µL, 0.72 mmol), according to general procedure 12. The crude material was purified as described above for **RBM7–089**.

$[\alpha]^{20}_D$ = +8.4 (*c* 0.5, $CHCl_3$). ^{1}H NMR (400 MHz, CD_3OD) δ 4.19 – 4.05 (m, 2H), 3.73 – 3.65 (m, 1H), 3.57 – 3.50 (m, 1H), 1.63 – 1.18 (m, 28H), 0.90 (t, *J* = 6.8 Hz, 3H). ^{13}C NMR (101 MHz, CD_3OD) δ 71.7, 67.4 (d, $J_{C–P}$ = 5.1 Hz), 67.1 (d, $J_{C–P}$ = 7.6 Hz), 34.9, 33.1, 30.8, 30.8, 30.7, 30.7, 30.7, 30.5, 26.8, 23.7, 14.5. ^{31}P NMR (162 MHz, CD_3OD) δ 1.29. HRMS calcd. for $C_{18}H_{38}N_3O_5PNa$ ($[M + Na]^+$): 430.2447, found: 430.2445.

(2*R*,3*R*)–2–azido–3–hydroxyoctadecyl dihydrogen phosphate (*ent*–RBM7–103)

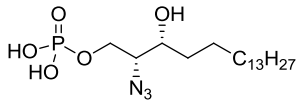

Compound ***ent*–RBM7–103** was obtained from ***ent*–RBM7–102** following the procedure described for the preparation of **RBM7–103**. Spectroscopic data were identical to those reported for **RBM7–103**.

$[\alpha]^{20}_D$ = –8.1 (*c* 0.5, $CHCl_3$).

5.1.4.3 Synthesis of S1P and dhS1P

***tert*–butyl ((2*S*,3*R*,*E*)–1–((dimethoxyphosphoryl)oxy)–3–hydroxyoctadec–4–en–2–yl) carbamate (RBM7–026)**

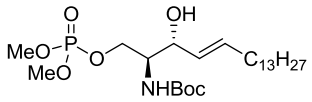

Compound **RBM7–026** (white solid, 192 mg, 76 %) was obtained from alcohol **RBM7–025** (200 mg, 0.50 mmol), *N*–methylimidazole (60 µL, 0.75 mmol) and dimethyl chlorophosphate (65 µL, 0.60 mmol), according to general procedure 11. The title compound was purified by flash chromatography on silica gel (from 0 to 60 % EtOAc in hexane).

$[\alpha]^{20}_D$ = +3.9 (*c* 1.0, $CHCl_3$) [lit.[18] $[\alpha]^{20}_D$ = +4.7 (*c* 1.1, $CHCl_3$)]. ^{1}H NMR (400 MHz, $CDCl_3$) δ 5.81 – 5.70 (m, 1H), 5.50 (dd, *J* = 15.4, 7.0 Hz, 1H), 5.00 (br d, *J* = 7.9 Hz, 1H), 4.33 (ddd, *J* = 10.9, 7.9, 4.7 Hz, 1H), 4.19 – 4.08 (m, 2H), 3.90 – 3.65 (m, 7H), 2.78 (br d, *J* = 3.9 Hz, 1H), 2.03 (dd, *J* = 14.1, 7.0 Hz, 2H), 1.52 – 1.14 (m, 31H), 0.87 (t, *J* = 6.8 Hz, 3H). ^{13}C NMR (101 MHz, $CDCl_3$) δ 155.8, 134.9, 128.7, 79.8, 72.6, 66.8 (d, $J_{C–P}$ = 5.8 Hz), 55.0 (d, $J_{C–P}$ = 5.1 Hz), 54.7 (d, $J_{C–P}$ = 6.0 Hz), 32.5, 32.1, 29.8, 29.8, 29.7, 29.6, 29.5, 29.4, 29.2, 28.5, 22.8, 14.2. ^{31}P NMR (162 MHz, $CDCl_3$) δ 2.31. HRMS calcd. for $C_{25}H_{51}NO_7P$ ($[M + H]^+$): 508.3403, found: 508.3408.

***tert*–butyl ((2*S*,3*R*)–1–((dimethoxyphosphoryl)oxy)–3–hydroxyoctadecan–2–yl) carbamate (RBM7–010)**

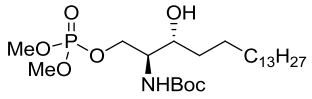

Compound **RBM7–010** (white solid, 465 mg, 75 %) was obtained from alcohol **RBM7–009** (486 mg, 1.21 mmol), *N*–methylimidazole (145 µL, 1.82 mmol) and dimethyl chlorophosphate (157 µL, 1.45 mmol), according to general procedure 11. The title compound was purified by flash chromatography on silica gel (from 0 to 60 % EtOAc in hexane).

$[\alpha]^{20}_D$ = +20.5 (*c* 1.0, $CHCl_3$). ^{1}H NMR (400 MHz, $CDCl_3$) δ 5.07 (br d, *J* = 8.4 Hz, 1H), 4.44 – 4.34 (m, 1H), 4.16 – 4.05 (m, 1H), 3.80 (d, *J* = 2.9 Hz, 3H), 3.77 (d, *J* = 2.9

Hz, 3H), 3.68 (br s, 1H), 3.60 (br s, 1H), 3.08 (br s, 1H), 1.62 – 1.17 (m, 37H), 0.87 (t, *J* = 6.8 Hz, 3H). ^{13}C NMR (101 MHz, $CDCl_3$) δ 155.8, 79.9, 71.5, 67.1 (d, J_{C-P} = 5.8 Hz), 55.0 (d, J_{C-P} = 5.6 Hz), 54.7 (d, J_{C-P} = 6.0 Hz) 33.9, 32.0, 29.8, 29.8, 29.8, 29.8, 29.7, 29.5, 28.5, 26.0, 22.8, 14.2. ^{31}P NMR (162 MHz, $CDCl_3$) δ 2.53. HRMS calcd. for $C_{25}H_{53}NO_7P$ ($[M + H]^+$): 510.3560, found: 510.3577.

(2*S*,3*R*,*E*)–2–ammonio–3–hydroxyoctadec–4–en–1–yl hydrogen phosphate: Sphingosine–1–phosphate (S1P)

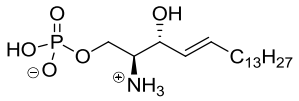

Compound **RBM7–029** (white solid, 81 mg, 54 %) was obtained from dimethyl phosphate **RBM7–026** (200 mg, 0.39 mmol) and TMSBr (234 µL, 1.77 mmol), according to general procedure 12. The crude material was recrystallized from THF/H_2O (2:1, v/v) and the precipitate was collected by centrifugation of the mixture and removal of the supernatant. Following the same procedure (vortexing / centrifuging at 4 ºC for 3 min (2000 rpm)), the white pellet was washed with H_2O (2 x 2 mL), $(CH_3)_2CO$ (2 x 2 mL) and Et_2O (2 x 2 mL) and dried under vacuum to give the title compound.

HRMS calcd. for $C_{18}H_{39}NO_5P$ ($[M + H]^+$): 380.2566, found: 380.2583.

(2*S*,3*R*)–2–ammonio–3–hydroxyoctadecyl hydrogen phosphate: Sphinganine–1–phosphate (dhS1P)

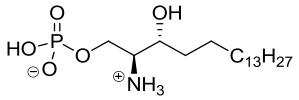

Compound **RBM7–011** (white solid, 177 mg, 79 %) was obtained from dimethyl phosphate **RBM7–010** (300 mg, 0.59 mmol) and TMSBr (350 µL, 2.65 mmol), according to general procedure 12. The crude material was worked–up as described for **S1P**.

HRMS calcd. for $C_{18}H_{41}NO_5P$ ($[M + H]^+$): 382.2722, found: 382.2707.

5.1.5 Synthesis and characterization of compounds from Section 3.3

5.1.5.1 Synthesis of coumarinic precursors **RBM7–069** and **RBM7–115**

But–3–en–1–yl 4–methylbenzenesulfonate (RBM7–084)

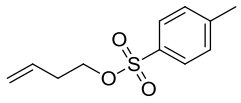

To a solution of 3–buten–1–ol (1.5 g, 20.8 mmol) in CH_2Cl_2 (50 mL) at 0 ºC were added pyridine (1.85 mL, 22.9 mmol) and *p*–TsCl (4.36 g, 22.9 mmol). After stirring at rt for 12 h, the reaction mixture was poured into 1 M aq. HCl (30 mL) and extracted with CH_2Cl_2 (3 x 50 mL). The combined organic layers were washed with brine (2 x 50 mL), dried over anhydrous $MgSO_4$, filtered and evaporated to dryness. Flash chromatography of the residue (from 0 to 5 % EtOAc in hexane) afforded tosylate **RBM7–084** (3.40 g, 72 %) as a colourless oil.

^{1}H NMR (400 MHz, $CDCl_3$) δ 7.79 (d, *J* = 8.3 Hz, 2H), 7.34 (d, *J* = 8.0 Hz, 2H), 5.67 (ddt, *J* = 17.1, 10.4, 6.7 Hz, 1H), 5.11 – 5.04 (m, 2H), 4.06 (t, *J* = 6.7 Hz, 2H), 2.45 (s, 3H), 2.44 – 2.36 (m, 2H). ^{13}C NMR (101 MHz, $CDCl_3$) δ 144.9, 133.3, 132.5, 129.9, 128.0, 118.3, 69.5, 33.3, 21.8. HRMS calcd. for $C_{11}H_{15}O_3S$ ($[M + H]^+$): 227.0742, found: 227.0743.

7–(but–3–en–1–yloxy)–2*H*–chromen–2–one (RBM7–069)

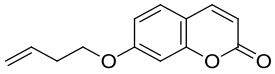

To a suspension of NaH (60 % in mineral oil, 581 mg, 14.5 mmol) in DMF (10 mL) at 0 ºC was added dropwise a solution of umbelliferone (2.29 g, 14.1 mmol) in DMF (10 mL). The resulting mixture was stirred at the same temperature for 10 min and then treated with a solution of **RBM7–084** (3.19 g, 14.1 mmol) in DMF (10 mL). After stirring for 16 h at 80 ºC, the reaction mixture was carefully diluted with water (20 mL) and extracted with diethyl ether (3 x 20 mL). The combined organic layers were washed with brine (2 x 25 mL), dried over anhydrous $MgSO_4$, filtered and evaporated *in vacuo*. Flash chromatography of the residue (from 0 to 21 % EtOAc in hexane) gave **RBM7–069** (2.58 g, 85 %) as a white solid.

^{1}H NMR (400 MHz, $CDCl_3$) δ 7.63 (d, *J* = 9.5 Hz, 1H), 7.36 (d, *J* = 8.5 Hz, 1H), 6.87 – 6.79 (m, 2H), 6.25 (d, *J* = 9.5 Hz, 1H), 5.90 (ddt, *J* = 17.0, 10.2, 6.7 Hz, 1H), 5.19 (dq, *J* = 17.2, 1.6 Hz, 1H), 5.14 (ddd, *J* = 10.2, 2.8, 1.2 Hz, 1H), 4.07 (t, *J* = 6.7 Hz, 2H), 2.58 (qt, *J* = 6.7, 1.3 Hz, 2H). ^{13}C NMR (101 MHz, $CDCl_3$) δ 162.3, 161.3, 156.0, 143.5, 133.9, 128.9, 117.7, 113.2, 113.1, 112.6, 101.5, 67.9, 33.4. HRMS calcd. for $C_{13}H_{13}O_3$ ($[M + H]^+$): 217.0865, found: 217.0869.

7–(allyloxy)–2*H*–chromen–2–one (RBM7–115)

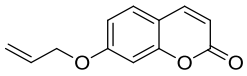

Allyl bromide (3.36 mL, 38.9 mmol) was added dropwise to a stirred mixture of umbelliferone (3.0 g, 18.5 mmol) and K_2CO_3 (3.58 g, 25.9 mmol) in acetone (75 mL). The reaction mixture was refluxed for 4 h, then cooled to rt, diluted with water (50 mL) and extracted with EtOAc (3 x 40 mL). The combined organic layers were washed with brine (2 x 30 mL), dried over anhydrous $MgSO_4$, filtered and concentrated under reduced pressure. Recrystallization of the residue from methanol in two consecutive crops yielded allyl ether **RBM7–115** (3.29 g, 88 %) as creamy–yellow crystals.

^{1}H NMR (400 MHz, $CDCl_3$) δ 7.63 (d, *J* = 9.5 Hz, 1H), 7.37 (d, *J* = 8.6 Hz, 1H), 6.89 – 6.81 (m, 2H), 6.25 (d, *J* = 9.5 Hz, 1H), 6.05 (ddt, *J* = 17.2, 10.6, 5.3 Hz, 1H), 5.44 (ddd, *J* = 17.3, 3.0, 1.5 Hz, 1H), 5.34 (dq, *J* = 10.5, 1.3 Hz, 1H), 4.60 (dt, *J* = 5.3, 1.5 Hz, 2H). ^{13}C NMR (101 MHz, CDCl3) δ 161.9, 161.3, 155.9, 143.5, 132.3, 128.9, 118.7, 113.3, 113.2, 112.8, 101.9, 69.4. HRMS calcd. for $C_{12}H_{11}O_3$ ($[M + H]^+$): 203.0708, found: 203.0701.

5.1.5.2 Synthesis of sphingoid precursors **RBM7–072** and **RBM7–135**

(*S*)–*tert*–butyl (1–((*tert*–butyldimethylsilyl)oxy)–3–oxopent–4–en–2–yl)carbamate (RBM7–071)

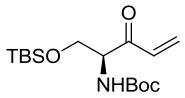

Vinylmagnesium bromide (82.8 mL, 57.9 mmol, 0.7 M in THF) was added dropwise to a solution of **RBM7–070** (6.0 g, 16.60 mmol) in THF (50 mL) at 0 ºC. After stirring at rt for 1 h, the reaction mixture was added dropwise *via* canula to a 1 M aq. solution of

HCl (50 mL) at 0 ºC and the resulting mixture was extracted with EtOAc (3 x 50 mL) The organic layers were combined, washed with brine (2 x 50 mL), dried over anhydrous $MgSO_4$, filtered and concentrated *in vacuo* to give the crude product. Flash chromatography (from 0 to 5 % EtOAc in hexane) gave **RBM7–071** (3.85 g, 71 %) as a colourless oil.

$[\alpha]^{20}_D$ = +62.2 (*c* 1.0, $CHCl_3$) [lit.[2] $[\alpha]^{24}_D$ = +63.3 (*c* 0.62, $CHCl_3$)]. ^{1}H NMR (400 MHz, $CDCl_3$) δ 6.56 (dd, *J* = 17.5, 10.6 Hz, 1H), 6.35 (dd, *J* = 17.4, 1.3 Hz, 1H), 5.83 (d, *J* = 10.6 Hz, 1H), 5.52 (br d, *J* = 7.0 Hz, 1H), 4.60 (dt, *J* = 7.6, 3.9 Hz, 1H), 4.01 (dd, *J* = 10.3, 3.3 Hz, 1H), 3.85 (dd, *J* = 10.3, 4.4 Hz, 1H), 1.45 (s, 9H), 0.84 (s, 9H), 0.01 (s, 3H), 0.00 (s, 3H). ^{13}C NMR (101 MHz, $CDCl_3$) δ 197.0, 155.4, 133.3, 129.5, 79.9, 63.6, 59.7, 28.5, 25.9, 18.3, –5.5, –5.5. HRMS calcd. for $C_{16}H_{31}NO_4SiNa$ ($[M + Na]^+$): 352.1920, found: 352.1937.

***tert*–butyl ((2*S*,3*R*)–1–((*tert*–butyldimethylsilyl)oxy)–3–hydroxypent–4–en–2–yl) carbamate (RBM7–072)**

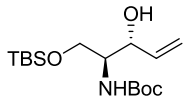

A solution of **RBM7–071** (1.01 g, 3.08 mmol) in ethanol (12 mL) was added dropwise to a suspension of lithium tri–*tert*–butoxyaluminum hydride (1.72 g, 6.78 mmol) in ethanol (30 mL) at –78 ºC. After stirring at the same temperature for 30 min, the reaction mixture was allowed to warm to 0 ºC and was quenched with 10 % (w/v) aqueous citric acid (20 mL). The resulting mixture was extracted with EtOAc (3 x 50 mL) and the combined organic layers were washed with brine (2 x 50 mL), dried over anhydrous $MgSO_4$, filtered, and concentrated *in vacuo* to give a 98:2 *anti*/*syn* crude mixture of diastereomers. Flash chromatography of the residue (from 0 to 11 % EtOAc in hexane) gave pure *anti*–**RBM7–072** (922 mg, 90 %) as a colourless oil.

$[\alpha]^{20}_D$ = +28.1 (*c* 1.0, $CHCl_3$) [lit.[2] $[\alpha]^{23}_D$ = +24.8 (*c* 1.45, $CHCl_3$)]. ^{1}H NMR (400 MHz, $CDCl_3$) δ 5.93 (ddd, *J* = 17.2, 10.6, 4.9 Hz, 1H), 5.39 (dt, *J* = 17.2, 1.7 Hz, 1H), 5.32 – 5.19 (m, 2H), 4.27 (s, 1H), 3.93 (dd, *J* = 10.4, 2.9 Hz, 1H), 3.76 (dd, *J* = 10.3, 2.6 Hz, 1H), 3.63 (dd, *J* = 7.3, 3.5 Hz, 2H), 3.44 (br s, 1H), 1.45 (s, 9H), 0.90 (s, 9H), 0.07 (s, 3H), 0.07 (s, 3H). ^{13}C NMR (101 MHz, $CDCl_3$) δ 156.0, 138.0, 116.0, 79.7, 75.0, 63.6,

54.2, 28.5, 25.9, 18.3, –5.5, –5.5. HRMS calcd. for $C_{16}H_{34}NO_4Si$ ($[M + H]^+$): 332.2257, found: 332.2267.

***tert*–butyl ((2*S*,3*R*)–1–((*tert*–butyldimethylsilyl)oxy)–3–hydroxyhex–5–en–2–yl) carbamate (RBM7–135)**

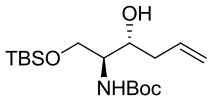

Allylmagnesium chloride (6.9 mL, 13.79 mmol, 2.0 M in THF) was added dropwise to a solution of **RBM7–070** (2.50 g, 6.90 mmol) in THF (30 mL) at –20 ºC. The reaction mixture was allowed to warm to 0 ºC over 5 h with stirring and was then quenched with saturated aqueous NH_4Cl (25 mL). The resulting mixture was extracted with EtOAc (3 x 50 mL) and the combined organic layers were washed with brine (2 x 50 mL), dried over anhydrous $MgSO_4$, filtered, and concentrated under reduced pressure. The resulting residue was dissolved in ethanol (15 mL) and was added dropwise to a suspension of lithium tri–*tert*–butoxyaluminum hydride (3.86 g, 15.18 mmol) in ethanol (60 mL) at –78 ºC. After stirring at the same temperature for 30 min, the reaction mixture was allowed to warm to 0 ºC and was quenched with 10 % (w/v) aqueous citric acid (40 mL). The resulting mixture was carefully concentrated under reduced pressure and then extracted with EtOAc (3 x 50 mL). The organic layers were combined and were washed with brine (2 x 50 mL), dried over anhydrous $MgSO_4$, filtered, and concentrated *in vacuo* to give a 99:1 *anti*/*syn* crude mixture of diastereomers. Flash chromatography of the residue (from 0 to 9 % EtOAc in hexane) gave pure *anti*–**RBM7–135** (1.85 g, 78 %) as a colourless oil.

$[\alpha]^{20}_D$ = +32.6 (*c* 1.0, $CHCl_3$) [lit.[19] $[\alpha]_D$ = +32.2 (*c* 1.32, $CHCl_3$)]. ^{1}H NMR (400 MHz, $CDCl_3$) δ 5.85 (ddt, *J* = 17.2, 10.2, 7.0 Hz, 1H), 5.23 (br d, *J* = 7.9 Hz, 1H), 5.19 – 5.06 (m, 2H), 3.98 (dd, *J* = 10.6, 2.9 Hz, 1H), 3.84 – 3.76 (m, 1H), 3.76 – 3.67 (m, 1H), 3.60 – 3.48 (m, 1H), 3.02 (br s, 1H), 2.42 – 2.27 (m, 2H), 1.45 (s, 9H), 0.90 (s, 9H), 0.08 (s, 6H). ^{13}C NMR (101 MHz, $CDCl_3$) δ 155.8, 134.7, 117.9, 79.6, 73.0, 63.4, 53.8, 39.5, 28.5, 26.0, 18.3, –5.5, –5.5. HRMS calcd. for $C_{17}H_{35}NO_4NaSi$ ($[M + Na]^+$): 368.2233, found: 368.2235.

(*R*)–(–)–MPA ester of alcohol RBM7–072 ((2'*R*)–RBM7–073)

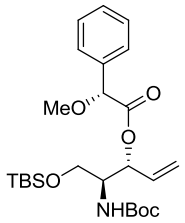

Compound **(2'*R*)–RBM7–073** (colorless oil, 52 mg, 64 %) was obtained from **RBM7–072** (56 mg, 0.17 mmol), (*R*)–(–)–MPA (45 mg, 0.27 mmol), EDC (49 mg, 0.25 mmol) and DMAP (23 mg, 0.19 mmol), according to general procedure 13.

^{1}H NMR (400 MHz, $CDCl_3$) δ 7.46 – 7.40 (m, 2H), 7.40 – 7.29 (m, 3H), 5.82 (ddd, *J* = 17.3, 10.5, 6.8 Hz, 1H), 5.37 – 5.21 (m, 3H), 4.75 (s, 1H), 4.49 (br d, *J* = 9.4 Hz, 1H), 3.78 – 3.69 (m, 1H), 3.43 – 3.36 (m, 4H), 3.19 (dd, *J* = 10.3, 3.5 Hz, 1H), 1.40 (s, 9H), 0.81 (s, 9H), –0.10 (s, 3H), –0.13 (s, 3H). ^{13}C NMR (101 MHz, $CDCl_3$) δ 169.4, 155.4, 136.4, 133.3, 128.9, 128.8, 127.3, 119.3, 82.6, 79.6, 74.2, 61.2, 57.5, 53.9, 28.5, 25.9, 18.3, –5.5, –5.6. HRMS calcd. for $C_{25}H_{42}NO_6Si$ ($[M + H]^+$): 480.2781, found: 480.2782.

(*S*)–(+)–MPA ester of alcohol RBM7–072 ((2'*S*)–RBM7–073)

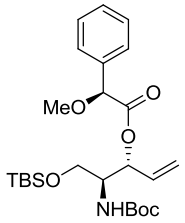

Compound **(2'*S*)–RBM7–073** (colorless oil, 72 mg, 82 %) was obtained from **RBM7–072** (61 mg, 0.184 mmol), (*S*)–(+)–MPA (49 mg, 0.29 mmol), EDC (53 mg, 0.28 mmol) and DMAP (25 mg, 0.20 mmol), according to general procedure 13.

^{1}H NMR (400 MHz, $CDCl_3$) δ 7.45 – 7.39 (m, 2H), 7.38 – 7.29 (m, 3H), 5.68 (ddd, *J* = 17.1, 10.7, 6.3 Hz, 1H), 5.39 (t, *J* = 6.5 Hz, 1H), 5.07 (d, *J* = 10.7 Hz, 1H), 4.95 (d, *J* = 17.2 Hz, 1H), 4.77 (s, 1H), 4.67 (br d, *J* = 9.4 Hz, 1H), 3.95 – 3.84 (m, 1H), 3.62 (dd, *J* = 10.3, 3.5 Hz, 1H), 3.55 (dd, *J* = 10.3, 4.6 Hz, 1H), 3.43 (s, 3H), 1.43 (s, 9H), 0.87 (s, 9H), 0.00 (s, 3H), –0.01 (s, 3H). ^{13}C NMR (101 MHz, $CDCl_3$) δ 169.4, 155.5, 136.3,

132.5, 128.8, 128.7, 127.3, 118.9, 82.7, 79.6, 74.1, 61.8, 57.6, 53.7, 28.5, 25.9, 18.3, –5.4, –5.5. HRMS calcd. for $C_{25}H_{42}NO_6Si$ ($[M + H]^+$): 480.2781, found: 480.2762.

Table 5.1. Absolute configuration determination of alcohol **RBM7–072**.[a]

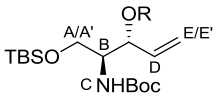

	δ H_A	δ $H_{A'}$	δ H_B	δ H_C	δ H_D	δ H_E	δ $H_{E'}$
R = (*R*)–MPA	3.18	3.40	3.73	4.49	5.82	5.29	5.25
R = (*S*)–MPA	3.55	3.61	3.90	4.67	5.67	5.07	4.94
$\Delta\delta^{RS}$	**–0.37**	**–0.21**	**–0.17**	**–0.18**	**0.15**	**0.22**	**0.31**

[a]Chemical shifts (δ) are reported in ppm relative to the solvent signal

(*R*)–(–)–MPA ester of alcohol RBM7–135 ((2'*R*)–RBM7–137)

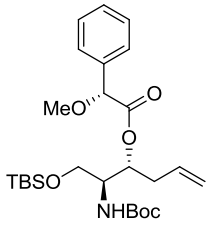

Compound **(2'*R*)–RBM7–137** (yellow oil, 38 mg, 36 %) was obtained from **RBM7–135** (75 mg, 0.22 mmol), (*R*)–(–)–MPA (58 mg, 0.35 mmol), EDC (62 mg, 0.33 mmol) and DMAP (29 mg, 0.24 mmol), according to general procedure 13.

^{1}H NMR (400 MHz, $CDCl_3$) δ 7.45 – 7.38 (m, 2H), 7.38 – 7.28 (m, 3H), 5.83 – 5.69 (m, 1H), 5.09 – 4.98 (m, 3H), 4.70 (s, 1H), 4.53 (br d, *J* = 9.5 Hz, 1H), 3.73 – 3.63 (m, 1H), 3.40 (s, 3H), 3.31 (dd, *J* = 10.3, 3.7 Hz, 1H), 3.06 (dd, *J* = 10.4, 3.5 Hz, 1H), 2.55 – 2.45 (m, 1H), 2.38 – 2.28 (m, 1H), 1.41 (s, 9H), 0.81 (s, 9H), –0.12 (s, 3H), –0.15 (s, 3H). ^{13}C NMR (101 MHz, $CDCl_3$) δ 169.7, 155.5, 136.5, 133.6, 128.9, 128.8, 127.3, 118.1, 82.6, 79.6, 72.5, 61.3, 57.5, 53.5, 36.0, 28.5, 25.9, 18.3, –5.5, –5.6. HRMS calcd. for $C_{26}H_{44}NO_6Si$ ($[M + H]^+$): 494.2938, found: 494.2926.

(*S*)–(+)–MPA ester of alcohol RBM7–135 ((2'*S*)–RBM7–137)

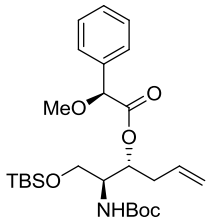

Compound **(2'*S*)–RBM7–137** (yellow oil, 73 mg, 68 %) was obtained from **RBM7–135** (75 mg, 0.22 mmol), (*S*)–(+)–MPA (58 mg, 0.35 mmol), EDC (62 mg, 0.33 mmol) and DMAP (29 mg, 0.24 mmol), according to general procedure 13.

^{1}H NMR (400 MHz, $CDCl_3$) δ 7.45 – 7.37 (m, 2H), 7.37 – 7.28 (m, 3H), 5.43 (ddt, *J* = 17.0, 10.2, 7.2 Hz, 1H), 5.01 (td, *J* = 7.5, 4.0 Hz, 1H), 4.81 – 4.65 (m, 4H), 3.89 – 3.79 (m, 1H), 3.57 (d, *J* = 3.6 Hz, 2H), 3.42 (s, 3H), 2.40 – 2.31 (m, 1H), 2.26 – 2.16 (m, 1H), 1.44 (s, 9H), 0.87 (s, 9H), 0.01 (s, 3H), –0.01 (s, 3H). ^{13}C NMR (101 MHz, $CDCl_3$) δ 170.0, 155.5, 136.4, 132.9, 128.8, 128.6, 127.4, 118.0, 82.8, 79.7, 73.1, 61.8, 57.6, 53.2, 35.4, 28.5, 26.0, 18.3, –5.4, –5.5. HRMS calcd. for $C_{26}H_{44}NO_6Si$ ($[M + H]^+$): 494.2938, found: 494.2933.

Table 5.2. Absolute configuration determination of alcohol **RBM7–135**.[a]

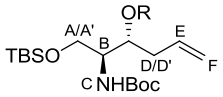

	δ H_A	**δ $H_{A'}$**	**δ H_B**	**δ H_C**	**δ H_D**	**δ $H_{D'}$**	**δ H_E**	**δ H_F**
R = (*R*)–MPA	3.31	3.07	3.68	4.54	2.51	2.33	5.76	5.03
R = (*S*)–MPA	3.58	3.58	3.84	4.72	2.36	2.21	5.43	4.72
$\Delta\delta^{RS}$	**–0.27**	**–0.51**	**–0.16**	**–0.18**	**0.15**	**0.12**	**0.33**	**0.31**

[a]Chemical shifts (δ) are reported in ppm relative to the solvent signal

5.1.5.3 Synthesis of probes **RBM7–077** and **RBM7–148**

***Tert*–butyl ((2*S*,3*R*,*E*)–1–((*tert*–butyldimethylsilyl)oxy)–3–hydroxy–7–((2–oxo–2*H*–chromen–7–yl)oxy)hept–4–en–2–yl)carbamate (RBM7–078)**

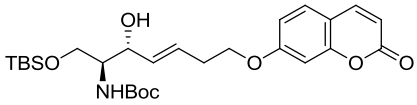

Compound **RBM7–078** (inseparable 94:6 *E*/*Z* mixture, colourless oil, 860 mg, 63 %) was obtained from **RBM7–072** (875 mg, 2.64 mmol), **RBM7–069** (2.28 g, 10.56 mmol) and Grubbs catalyst 2nd generation (67 mg, 0.08 mmol), according to general procedure 6. The title compound was purified by flash chromatography on silica gel (from 0 to 1 % CH_3OH in CH_2Cl_2). Early–eluting fractions were independently collected to give a sample of pure *E*–alkene, from which the following data were acquired.

$[\alpha]^{20}_D$ = +11.1 (*c* 1.0, $CHCl_3$) ^{1}H NMR (400 MHz, $CDCl_3$) δ 7.63 (d, *J* = 9.5 Hz, 1H), 7.36 (d, *J* = 8.6 Hz, 1H), 6.85 – 6.76 (m, 2H), 6.25 (d, *J* = 9.5 Hz, 1H), 5.92 – 5.81 (m, 1H), 5.71 (dd, *J* = 15.4, 5.4 Hz, 1H), 5.24 (br d, *J* = 8.2 Hz, 1H), 4.29 – 4.22 (m, 1H), 4.06 (t, *J* = 6.5 Hz, 2H), 3.94 (dd, *J* = 10.4, 2.9 Hz, 1H), 3.80 – 3.70 (m, 1H), 3.65 – 3.55 (m, 1H), 2.60 (app q, *J* = 6.6 Hz, 2H), 1.45 (s, 9H), 0.88 (s, 9H), 0.06 (s, 3H), 0.05 (s, 3H). ^{13}C NMR (101 MHz, $CDCl_3$) δ 162.2, 161.3, 156.0, 155.9, 143.5, 132.9, 128.9, 127.5, 113.2, 113.0, 112.7, 101.5, 79.7, 74.5, 67.8, 63.5, 54.5, 32.1, 28.5, 25.9, 18.2, –5.5, –5.5. HRMS calcd. for $C_{27}H_{41}NO_7NaSi$ ($[M + Na]^+$): 542.2550, found: 542.2557.

***tert*–butyl ((2*S*,3*R*,*E*)–1–((*tert*–butyldimethylsilyl)oxy)–3–hydroxy–7–((2–oxo–2*H*–chromen–7–yl)oxy)hept–5–en–2–yl)carbamate (RBM7–141)**

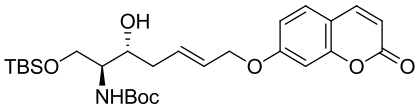

Compound **RBM7–141** (93:7 *E*/*Z* mixture, colourless oil, 865 mg, 66 %) was obtained from **RBM7–135** (868 mg, 2.51 mmol), **RBM7–115** (2.03 g, 10.05 mmol) and Grubbs catalyst 2nd generation (64 mg, 0.08 mmol), according to general procedure 6. The title compound was purified by flash chromatography on silica gel (from 0 to 27 % EtOAc in hexane). Pure *E*–alkene was obtained after purification of the diastereomeric mixture by flash chromatography using the same gradient.

$[\alpha]^{20}_D$ = +16.5 (*c* 1.0, $CHCl_3$). ^{1}H NMR (400 MHz, $CDCl_3$) δ 7.62 (d, *J* = 9.5 Hz, 1H), 7.36 (d, *J* = 8.5 Hz, 1H), 6.87 – 6.78 (m, 2H), 6.24 (d, *J* = 9.5 Hz, 1H), 6.00 – 5.90 (m, 1H), 5.80 (dt, *J* = 15.5, 5.8 Hz, 1H), 5.22 (br d, *J* = 8.3 Hz, 1H), 4.55 (d, *J* = 5.8 Hz, 2H), 3.97 (dd, *J* = 10.6, 2.9 Hz, 1H), 3.85 – 3.69 (m, 2H), 3.60 – 3.49 (m, 2H), 3.14 (br s, 1H), 2.46 – 2.32 (m, 2H), 1.45 (s, 9H), 0.90 (s, 9H), 0.08 (s, 6H). ^{13}C NMR (101 MHz, $CDCl_3$) δ 161.9, 161.3, 155.9, 155.8, 143.5, 132.1, 128.9, 126.9, 113.2, 113.1, 112.7, 101.8, 79.7, 73.1, 69.1, 63.4, 53.9, 37.9, 28.5, 25.9, 18.3, –5.5, –5.5. HRMS calcd. for $C_{27}H_{41}NO_7NaSi$ ($[M + Na]^+$): 542.2550, found: 542.2556.

***tert*–butyl ((2*S*,3*R*,*E*)–1,3–dihydroxy–7–((2–oxo–2*H*–chromen–7–yl)oxy)hept–4–en–2–yl) carbamate (RBM7–079)**

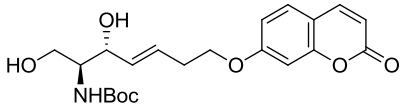

Diol **RBM7–079** (colorless oil, 345 mg, 95 %) was obtained from **RBM7–078** (465 mg, 0.90 mmol) and TBAF (1.79 mL, 1.79 mmol), according to general procedure 14.

$[\alpha]^{20}_D$ = –3.6 (*c* 1.0, $CHCl_3$). ^{1}H NMR (400 MHz, $CDCl_3$) δ 7.63 (d, *J* = 9.5 Hz, 1H), 7.36 (d, *J* = 8.5 Hz, 1H), 6.86 – 6.76 (m, 2H), 6.25 (d, *J* = 9.5 Hz, 1H), 5.94 – 5.83 (m, 1H), 5.74 (dd, *J* = 15.5, 6.0 Hz, 1H), 5.33 (br d, *J* = 7.2 Hz, 1H), 4.40 – 4.35 (m, 1H), 4.07 (t, *J* = 6.4 Hz, 2H), 3.94 (dd, *J* = 11.4, 3.5 Hz, 1H), 3.73 (dd, *J* = 11.4, 3.7 Hz, 1H), 3.65 (br s, 1H), 2.65 – 2.55 (m, 1H), 1.45 (s, 9H). ^{13}C NMR (101 MHz, $CDCl_3$) δ 162.1, 161.5, 156.4, 155.9, 143.6, 132.6, 128.9, 128.3, 113.1, 113.1, 112.7, 101.5, 80.0, 74.4, 67.8, 62.5, 55.4, 32.1, 28.5. HRMS calcd. for $C_{21}H_{27}NO_7Na$ ($[M + Na]^+$): 428.1685, found: 428.1691.

***tert*–butyl ((2*S*,3*R*,*E*)–1,3–dihydroxy–7–((2–oxo–2*H*–chromen–7–yl)oxy)hept–5–en–2–yl) carbamate (RBM7–143)**

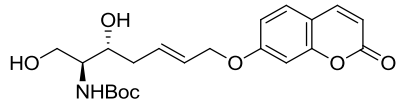

Diol **RBM7–143** (colorless oil, 427 mg, 88 %) was obtained from **RBM7–141** (620 mg, 1.19 mmol) and TBAF (2.39 mL, 2.39 mmol), according to general procedure 14.

$[\alpha]^{20}_D$ = +4.5 (*c* 1.0, $CHCl_3$). ^{1}H NMR (400 MHz, $CDCl_3$) δ 7.63 (d, *J* = 9.5 Hz, 1H), 7.37 (d, *J* = 8.5 Hz, 1H), 6.87 – 6.78 (m, 2H), 6.25 (d, *J* = 9.5 Hz, 1H), 5.99 – 5.88 (m, 1H), 5.83 (dt, *J* = 15.5, 5.5 Hz, 1H), 5.31 (br d, J = 10.4 Hz, 1H), 4.56 (d, *J* = 5.6 Hz, 2H), 4.01 (dd, *J* = 11.4, 3.4 Hz, 1H), 3.92 – 3.83 (m, 1H), 3.77 (dd, *J* = 11.4, 3.4 Hz, 1H), 3.61 – 3.50 (m, 1H), 2.46 – 2.33 (m, 3H), 1.45 (s, 9H). ^{13}C NMR (101 MHz, $CDCl_3$) δ 161.9, 161.5, 156.2, 155.8, 143.7, 131.7, 128.9, 127.4, 113.3, 113.1, 112.7, 101.8, 80.0, 72.9, 69.0, 62.5, 54.8, 37.5, 28.5. HRMS calcd. for $C_{21}H_{27}NO_7Na$ ([M + Na]$^+$): 428.1685, found: 428.1682.

***tert*–butyl ((2*S*,3*R*,*E*)–1–((dimethoxyphosphoryl)oxy)–3–hydroxy–7–((2–oxo–2*H*–chromen–7–yl)oxy)hept–4–en–2–yl)carbamate (RBM7–076)**

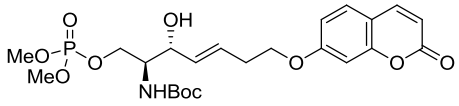

Compound **RBM7–076** (colorless oil, 105 mg, 69 %) was obtained from alcohol **RBM7–079** (120 mg, 0.30 mmol), *N*–methylimidazole (35 μL, 0.44 mmol) and dimethyl chlorophosphate (38 μL, 0.36 mmol), according to general procedure 11. The title compound was purified by flash chromatography on silica gel (from 0 to100 % EtOAc in hexane).

$[\alpha]^{20}_D$ = +6.4 (*c* 0.9, $CHCl_3$). ^{1}H NMR (400 MHz, $CDCl_3$) δ 7.63 (d, *J* = 9.5 Hz, 1H), 7.36 (d, *J* = 8.6 Hz, 1H), 6.87 – 6.77 (m, 2H), 6.24 (d, *J* = 9.5 Hz, 1H), 5.91 – 5.81 (m, 1H), 5.70 (dd, *J* = 15.5, 6.4 Hz, 1H), 5.09 (br d, *J* = 7.8 Hz, 1H), 4.35 (ddd, *J* = 10.8, 8.2, 4.7 Hz, 1H), 4.20 (t, *J* = 6.3 Hz, 1H), 4.16 – 4.08 (m, 1H), 4.05 (t, *J* = 6.5 Hz, 2H), 3.88 – 3.73 (m, 7H), 2.62 – 2.53 (m, 2H), 1.42 (s, 9H). ^{13}C NMR (101 MHz, $CDCl_3$) δ 162.2, 161.33, 156.0, 155.8, 143.5, 132.0, 128.9, 113.2, 113.0, 112.7, 101.5, 80.0, 72.2, 67.8, 66.7 (d, $J_{C–P}$ = 5.7 Hz), 55.0 (br d, $J_{C–P}$ = 4.4 Hz), 54.7 (d, $J_{C–P}$ = 5.9 Hz), 32.1, 28.5. ^{31}P NMR (162 MHz, $CDCl_3$) δ 2.65. HRMS calcd. for $C_{23}H_{32}NO_{10}NaP$ ([M + Na]$^+$): 536.1662, found: 536.1670.

***tert*–butyl ((2*S*,3*R*,*E*)–1–((dimethoxyphosphoryl)oxy)–3–hydroxy–7–((2–oxo–2*H*–chromen–7–yl)oxy)hept–5–en–2–yl)carbamate (RBM7–144)**

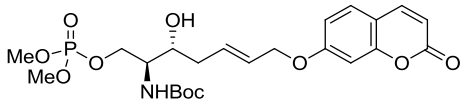

Compound **RBM7–144** (colorless oil, 232 mg, 78 %) was obtained from alcohol **RBM7–143** (236 mg, 0.58 mmol), *N*–methylimidazole (70 µL, 0.87 mmol) and dimethyl chlorophosphate (75 µL, 0.70 mmol), according to general procedure 11. The title compound was purified by flash chromatography on silica gel (from 0 to100 % EtOAc in hexane).

$[\alpha]^{20}_{D}$ = +14.1 (*c* 1.0, $CHCl_3$). ^{1}H NMR (400 MHz, $CDCl_3$) δ 7.63 (d, *J* = 9.5 Hz, 1H), 7.36 (d, *J* = 8.5 Hz, 1H), 6.87 – 6.78 (m, 2H), 6.24 (d, *J* = 9.5 Hz, 1H), 6.02 – 5.91 (m, 1H), 5.82 (dt, *J* = 15.5, 5.8 Hz, 1H), 5.05 (br d, *J* = 8.1 Hz, 1H), 4.56 (d, *J* = 5.7 Hz, 2H), 4.50 – 4.41 (m, 1H), 4.15 – 4.05 (m, 1H), 3.81 (d, *J* = 3.4 Hz, 3H), 3.78 (d, *J* = 3.4 Hz, 3H), 3.71 (br s, 2H), 3.34 (br s, 1H), 2.53 – 2.40 (m, 1H), 2.31 (dt, *J* = 14.1, 6.9 Hz, 1H), 1.44 (s, 9H). ^{13}C NMR (101 MHz, $CDCl_3$) δ 161.9, 161.3, 155.9, 155.6, 143.6, 131.9, 128.9, 127.3, 113.2, 113.2, 112.7, 101.8, 80.1, 70.1, 69.1, 67.0 (d, $J_{C–P}$ = 5.7 Hz), 54.8 (d, $J_{C–P}$ = 6.0 Hz), 54.8 (d, $J_{C–P}$ = 6.0 Hz), 54.7 (br d, $J_{C–P}$ = 5.4 Hz), 36.8, 28.5. ^{31}P NMR (162 MHz, $CDCl_3$) δ 2.96. HRMS calcd. for $C_{23}H_{32}NO_{10}NaP$ ($[M + Na]^+$): 536.1662, found: 536.1660.

(2*S*,3*R*,*E*)–2–ammonio–3–hydroxy–7–((2–oxo–2*H*–chromen–7–yl)oxy)hept–4–en–1–yl hydrogen phosphate (RBM7–077)

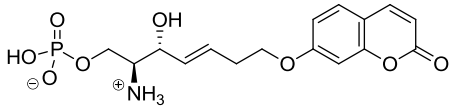

Compound **RBM7–077** (white solid, 49 mg, 85 %) was obtained from dimethyl phosphate **RBM7–076** (77 mg, 0.15 mmol) and TMSBr (99 µL, 0.75 mmol), according to general procedure 12. The crude reaction mixture was dissolved in methanol and loaded on an Amberlite ® XAD4 column (10 g), which had been washed thoroughly with acetone and then equilibrated with water. Elution with a linear gradient from 0 to 50 % CH_3CN in H_2O provided pure **RBM7–077**.

$[\alpha]^{20}_D$ = +14.7 (*c* 0.7, DMSO). ^{1}H NMR (400 MHz, CD_3OD) δ 7.88 (d, *J* = 9.5 Hz, 1H), 7.54 (d, *J* = 8.6 Hz, 1H), 6.99 – 6.89 (m, 2H), 6.25 (d, *J* = 9.5 Hz, 1H), 6.06 – 5.93 (m, 1H), 5.68 (dd, *J* = 15.4, 6.6 Hz, 1H), 4.34 (t, *J* = 5.6 Hz, 1H), 4.20 – 4.07 (m, 3H), 4.00 (dt, *J* = 11.8, 7.9 Hz, 1H), 3.43 – 3.36 (m, 1H), 2.67 – 2.58 (m, 2H). ^{13}C NMR (101 MHz, DMSO–d_6) δ 161.6, 160.3, 155.4, 144.3, 131.0, 129.5, 128.4, 112.7, 112.4, 112.3, 101.1, 69.0, 67.5, 61.5 (br d, $J_{C–P}$ = 2.7 Hz), 56.2 (br d, $J_{C–P}$ = 2.7 Hz), 31.3. ^{31}P NMR (162 MHz, DMSO–d_6) δ 1.84. HRMS calcd. for $C_{16}H_{21}NO_8P$ ($[M + H]^+$): 386.1005, found: 386.0997.

(2*S*,3*R*,*E*)–2–ammonio–3–hydroxy–7–((2–oxo–2*H*–chromen–7–yl)oxy)hept–5–en–1–yl hydrogen phosphate (RBM7–148)

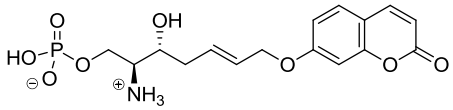

Compound **RBM7–148** (white solid, 45 mg, 82 %) was obtained from dimethyl phosphate **RBM7–144** (73 mg, 0.14 mmol) and TMSBr (94 μL, 0.71 mmol), according to general procedure 12. The title compound was purified as described above for **RBM7–077**.

$[\alpha]^{20}_D$ = +4.2 (*c* 1.0, DMSO). ^{1}H NMR (400 MHz, CD_3OD) δ 7.89 (d, *J* = 9.5 Hz, 1H), 7.54 (d, *J* = 8.5 Hz, 1H), 6.98 – 6.90 (m, 2H), 6.25 (d, *J* = 9.5 Hz, 1H), 6.01 – 5.84 (m, 2H), 4.65 (d, *J* = 4.9 Hz, 2H), 4.18 (ddd, *J* = 10.8, 6.9, 3.7 Hz, 1H), 4.08 (dt, *J* = 11.5, 7.9 Hz, 1H), 3.88 (dt, *J* = 9.4, 4.8 Hz, 1H), 3.39 (dt, *J* = 8.2, 3.9 Hz, 1H), 2.45 – 2.29 (m, 2H). ^{13}C NMR (101 MHz, DMSO–d_6) δ 161.4, 160.3, 155.3, 144.3, 131.7, 129.5, 126.6, 112.8, 112.4, 112.3, 101.4, 68.8, 68.1, 61.4 (d, $J_{C–P}$ = 5.7 Hz), 55.8 (d, $J_{C–P}$ = 3.4 Hz), 35.6. ^{31}P NMR (162 MHz, DMSO–d_6) δ 2.08. HRMS calcd. for $C_{16}H_{21}NO_8P$ ($[M + H]^+$): 386.1005, found: 386.0994.

5.1.5.4 Synthesis of aldehydes **RBM7–083** and **RBM7–136**

(*E*)–7–((5–hydroxypent–3–en–1–yl)oxy)–2*H*–chromen–2–one (RBM7–081)

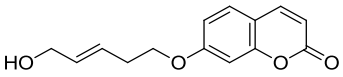

Compound **RBM7–081** (inseparable 85:15 *E*/*Z* mixture, brownish oil, 114 mg, 33 %) was obtained from **RBM7–069** (300 mg, 1.39 mmol), allyl alcohol (377 µL, 5.55 mmol) and Grubbs catalyst 2nd generation (35 mg, 0.04 mmol), according to general procedure 6. The title compound was purified by flash chromatography on silica gel (from 0 to 1.5 % MeOH in CH_2Cl_2).

^{1}H NMR (400 MHz, $CDCl_3$, major isomer) δ 7.63 (d, *J* = 9.5 Hz, 1H), 7.36 (d, *J* = 8.6 Hz, 1H), 6.86 – 6.76 (m, 2H), 6.24 (d, *J* = 9.5 Hz, 1H), 5.87 – 5.74 (m, 2H), 4.15 (br s, 2H), 4.06 (t, *J* = 6.6 Hz, 2H), 2.66 – 2.52 (m, 2H). ^{13}C NMR (101 MHz, $CDCl_3$, major isomer) δ 162.2, 161.4, 156.0, 143.6, 132.2, 128.9, 127.6, 113.2, 113.1, 112.7, 101.5, 68.0, 63.5, 32.0. HRMS calcd. for $C_{14}H_{15}O_4$ ($[M + H]^+$): 247.0970, found: 247.0961.

(*E*)–5–((2–oxo–2*H*–chromen–7–yl)oxy)pent–2–enal (RBM7–083)

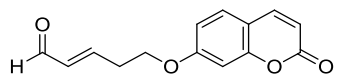

Dess–Martin periodinane (530 mg, 1.25 mmol) was added to a solution of allylic alcohol **RBM7–081** (205 mg, 0.83 mmol) in CH_2Cl_2 (4 mL) at 0°C. After stirring for 2 h at rt, the reaction mixture was filtered through a plug of Celite and the filtrate was evaporated to dryness. The residue was purified by flash chromatography (from 0 to 50 % EtOAc in hexane) to afford aldehyde **RBM7–083** (130 mg, 64 %) as a white solid. Late–eluting fractions were independently collected to give a 95:5 *E*:*Z* mixture of **RBM7–083**, from which the following data were acquired.

^{1}H NMR (400 MHz, $CDCl_3$, major isomer) δ 9.57 (d, *J* = 7.8 Hz, 1H), 7.64 (d, *J* = 9.5 Hz, 1H), 7.39 (d, *J* = 8.5 Hz, 1H), 6.93 (dt, *J* = 15.7, 6.7 Hz, 1H), 6.88 – 6.78 (m, 2H), 6.31 – 6.21 (m, 2H), 4.20 (t, *J* = 6.1 Hz, 2H), 2.91 – 2.83 (m, 2H). ^{13}C NMR (101 MHz, $CDCl_3$, major isomer) δ 193.7, 161.7, 161.2, 156.0, 153.0, 143.4, 134.9, 129.0, 113.6, 113.0, 101.5, 66.2, 32.3. HRMS calcd. for $C_{14}H_{13}O_4$ ($[M + H]^+$): 245.0814, found: 245.0810.

(But–3–en–1–yloxy)(*tert*–butyl)diphenylsilane (RBM7–116)

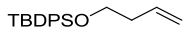

A solution of 3–buten–1–ol (500 mg, 6.93 mmol) in DMF (10 mL) was treated successively with imidazole (1.04 g, 15.26 mmol) and TBDPSCl (1.98 mL, 7.63 mmol). The resulting mixture was stirred overnight at rt, diluted with Et_2O (10 mL) and poured into 1 M aqueous HCl (10 mL). The mixture was extracted with Et_2O (3 x 10 mL) and the combined organic layers were washed with brine (2 x 15 mL), dried over anhydrous $MgSO_4$, filtered and evaporated *in vacuo*. Flash chromatography of the residue (from 0 to 1 % EtOAc in hexane) gave **RBM7–116** (2.17 g, quant. yield) as a colorless oil.

^{1}H NMR (400 MHz, $CDCl_3$) δ 7.72 – 7.64 (m, 4H), 7.46 – 7.33 (m, 6H), 5.83 (ddt, *J* = 17.1, 10.2, 6.9 Hz, 1H), 5.09 – 4.99 (m, 2H), 3.71 (t, *J* = 6.7 Hz, 2H), 2.32 (qt, *J* = 6.8, 1.3 Hz, 2H), 1.05 (s, 9H). ^{13}C NMR (101 MHz, $CDCl_3$) δ 135.7, 135.6, 134.1, 129.7, 127.7, 116.5, 63.7, 37.4, 27.0, 19.4. HRMS calcd. for $C_{20}H_{27}OSi$ ($[M + H]^+$): 311.1831, found: 311.1834.

(*E*)–7–((5–((*tert*–butyldiphenylsilyl)oxy)pent–2–en–1–yl)oxy)–2*H*–chromen–2–one (RBM7–118)

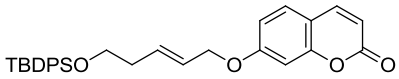

Compound **RBM7–118** (inseparable 91:9 *E*/*Z* mixture, colourless oil, 347 mg, 58 %) was obtained from **RBM7–115** (250 mg, 1.24 mmol), **RBM7–116** (1.54 g, 4.95 mmol and Grubbs catalyst 2nd generation (32 mg, 0.04 mmol), according to general procedure 6. The title compound was purified by flash chromatography on silica gel (from 0 to 16 % EtOAc in hexane). Late–eluting fractions were independently collected to give a 94:6 *E*:*Z* mixture of **RBM7–118**, from which the following data were acquired.

^{1}H NMR (400 MHz, $CDCl_3$, major isomer) δ 7.69 – 7.60 (m, 4H), 7.46 – 7.32 (m, 6H), 6.86 – 6.76 (m, 2H), 6.25 (d, *J* = 9.5 Hz, 1H), 5.93 – 5.82 (m, 1H), 5.73 (dt, *J* = 15.5, 5.9 Hz, 1H), 4.51 (d, *J* = 5.8 Hz, 2H), 3.74 (t, *J* = 6.5 Hz, 2H), 2.42 – 2.31 (m, 2H), 1.04 (s, 9H). ^{13}C NMR (101 MHz, $CDCl_3$, major isomer) δ 162.0, 161.4, 156.0, 143.5, 135.7, 134.0, 133.1, 129.8, 128.9, 127.8, 125.8, 113.2, 112.7, 101.8, 69.3, 63.3, 35.8, 27.0, 19.4. HRMS calcd. for $C_{30}H_{32}O_4NaSi$ ($[M + Na]^+$): 507.1968, found: 507.1972.

(*E*)–7–((5–hydroxypent–2–en–1–yl)oxy)–2*H*–chromen–2–one (RBM7–134)

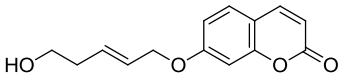

To an ice cooled solution of **RBM7–118** (175 mg, 0.36 mmol) in THF (3.5 mL) was added dropwise TBAF (1 M in THF, 722 μL, 0.72 mmol). After completion of addition the ice bath was removed and the mixture was stirred for 2 h at rt. The reaction was then quenched with saturated aqueous NH_4Cl (5 mL) and the resulting mixture was extracted with Et_2O (3 x 10 mL). The combined organic layers were washed with brine (2 x 15 mL), dried over anhydrous $MgSO_4$, filtered, and evaporated to give the crude product. Purification by flash chromatography on silica gel (from 0 to 70 % AcOEt in hexane) afforded homoallylic alcohol **RBM7–134** (85 mg, 96 %) as a colourless oil. Late–eluting fractions were independently collected to give a 98:2 *E*:*Z* mixture of **RBM7–134**, from which the following data were acquired.

^{1}H NMR (400 MHz, $CDCl_3$, major isomer) δ 7.63 (d, *J* = 9.5 Hz, 1H), 7.36 (d, *J* = 8.5 Hz, 1H), 6.88 – 6.78 (m, 2H), 6.24 (d, *J* = 9.5 Hz, 1H), 5.95 – 5.86 (m, 1H), 5.81 (dt, *J* = 15.5, 5.6 Hz, 1H), 4.55 (dd, *J* = 5.5, 0.7 Hz, 2H), 3.72 (t, *J* = 6.3 Hz, 2H), 2.46 – 2.35 (m, 2H), 1.61 (s, 1H). ^{13}C NMR (101 MHz, $CDCl_3$, major isomer) δ 161.9, 161.4, 155.8, 143.6, 132.4, 128.9, 126.5, 113.2, 113.0, 112.6, 101.7, 69.1, 61.7, 35.7. HRMS calcd. for $C_{14}H_{14}O_4Na$ ($[M + Na]^+$): 269.0790, found: 269.0785.

5.2 Biological studies

5.2.1 General remarks

All biochemical reagents were commercially available and were used without further purification. **RBM13**,[20] pentadecanal,[21] and S1P[18,22,23] (see Section 5.1.4.3) were synthesized in our laboratories following previously described methods. Inhibitor **3c** and recombinant hS1PL were from Novartis.

Fluorogenic assays were performed on flat–bottom 96–well plates. Substrates and inhibitors were added from stock solutions in H_2O (**RBM7–001**, **RBM7–002**, **RBM7–012** and **RBM7–032**), DMSO (**umbelliferone (7)**, **3c**, **RBM7–077**, **RBM7–148**, *N*–acylanilino carboxylates and **VS01–28**), 0.5 M potassium phosphate buffer pH 7.2 (**RBM13**) or 1 % (v/v) aq. Triton X–100 (S1P and azido–S1P/dhS1P stereoisomers). Buffer solution A corresponds to a 1 mM potassium phosphate buffer pH 7.2, containing 100 mM NaCl, 1 mM EDTA, 1 mM DTT and 10 µM pyridoxal 5'–phosphate. Buffer solution B corresponds to a 100 mM HEPES buffer pH 7.4, containing 0.1 mM EDTA, 0.05 % Triton X–100, 0.01 % Pluronic F127 (Biotium), and 100 µM pyridoxal 5′–phosphate.

V_{max} and K_M values were determined by measuring initial velocities at different substrate concentrations and fitting the data to the Michaelis–Menten equation in Prism 5 (GraphPad Software, La Jolla). IC_{50} values were determined by plotting percent activity versus log [I] and fitting the data to the log(inhibitor) vs. response equation in Prism 5 (GraphPad Software, La Jolla). In both cases, settings for curve adjustments were kept with their default values. Type of inhibition and K_I values for more active compounds were determined by Lineweaver–Burk plots of assays performed with different concentrations of inhibitor and substrate.

5.2.2 Expression and purification of StS1PL

Plasmid (pQE70–StSPL)[24] was transformed into *E. coli* strain M–15 [pREP–4] from QIAGEN and grown in 100 mL of LB medium containing ampicillin (100 µg/mL) and kanamycin (50 µg/mL) for 14 h at 30 °C on a rotary shaker at 160 rpm. A final optical density at 600 nm (OD_{600}) of 2 was usually achieved. An aliquot of the pre–culture (5 mL) was transferred into a shake–flask (2 L) containing LB medium (final volume: 500 mL) with ampicillin (100 µg/mL), kanamycin (50 µg/mL) and pyridoxine (0.1 g/L) and

incubated for 2.5 h at 37 ºC with shaking at 100 rpm. The culture was then cooled down to 30 °C while maintaining the shaking at 100 rpm for 30 min. Protein expression was finally induced at an OD_{600} of 0.8 by adding cold ethanol, pyridoxine and IPTG at final concentrations of 2 % (v/v), 0.1 g/L and 0.1 mM, respectively.

After incubation for 14 h at 30 ºC with shaking (100 rpm), cells were harvested by centrifuging at 8000 g for 30 min at 4 ºC. The obtained pellet (from 2 L induced–culture broths) was frozen overnight at –20 ºC, thawed on ice and resuspended with 100 ml of sodium phosphate buffer (50 mM, pH 7.2), containing NaCl (300 mM), imidazole (10 mM), PLP (200 µM), DTT (1 mM) and cOmplete^{TM} ULTRA tablets (Mini, EDTA–free) Protease Inhibitor Cocktail (4 tablets). Cells were lysed using a Cell Disrupter (Constant Systems). Cellular debris was removed by centrifugation at 30000 g for 30 min at 4 ºC and the supernatant was incubated at 60 ºC for 1 h. After centrifugation to pellet the precipitated thermolabile proteins, the clear supernatant was collected and purified by affinity chromatography (IMAC) in a FPLC system (Amersham Biosciences). The crude supernatant was applied to a cooled HisTrapTM HP 5 mL column (GE Healthcare) previously equilibrated with a sodium phosphate buffer (50 mM, pH 7.2), containing NaCl (300 mM) and imidazole (10 mM), and washed with the same buffer containing 20 mM imidazole. Finally, the protein was eluted at a flow rate of 3 mL/min by increasing the imidazole concentration up to 250 mM. Fractions containing the recombinant protein were pooled and dialyzed against buffer solution A. The dialyzed solution (12 mL) was separated into 20 µL aliquots and stored at –80 ºC. A protein concentration of 600 µg/mL was determined following the Bradford assay and using BSA as standard for quantification.[25] Purity and identity of purified StS1PL was confirmed by SDS–PAGE (Figure 3.1.9) and LC/MS analysis (See Section 5.2.3 and Figure 3.1.10). In both cases, results are in full agreement with those reported by Bourquin and coworkers.[24]

5.2.3 LC/MS analysis of StS1PL

To 100 µL of a 60 µg/mL solution of purified StS1PL in buffer solution A were added 50 µL of 0.5 % (v/v) aq. TFA and 50 µL of 0.5 % (v/v) TFA in CH_3CN. A 10 µL aliquot of the resulting solution was subjected to HPLC chromatography (C4 reverse phase column, 300 Å) coupled to an ESI spectrometer, under the following chromatographic conditions: mobile phase A, 0.5 % (v/v) aq. TFA; mobile phase B, 0.5

% (v/v) TFA in CH_3CN; gradient elution, from 10 to 100 % B in A over 20 min at a flow rate of 1 mL/min. Multiple–charged protein ion signals were deconvoluted to produce zero–charge spectra using ProMass Xcali software.

5.2.4 Assays of S1PL enzyme activity

5.2.4.1 Fluorogenic assay using **RBM13** as substrate

Recombinant bacterial or human S1PL (50 µL from stock solutions in buffer A (StS1PL) or B (hS1PL), final concentration: 25 µg/mL for StS1PL and 3 µg/mL for hS1PL) was added to a mixture of **RBM13** (final concentration: 125 µM) and putative inhibitors (at the indicated concentrations) in either buffer solution A (StS1PL) or B (hS1PL) (final volume: 100 µL). The mixture was incubated at 37 ºC for 1 h and the enzymatic reaction was stopped by the addition of 50 µL of MeOH. Finally, 100 µL of a 200 mM glycine–NaOH buffer, pH 10.6, were added to the resulting solution and the mixture was incubated for 20 additional min at 37 ºC in order to complete the β–elimination reaction. The amount of umbelliferone formed was determined on either a SpectraMax M5 (Molecular Devices) or Synergy 2 (BioTek) microplate readers ($\lambda_{ex/em}$ = 355/460 nm), using a calibration curve.

5.2.4.2 Fluorogenic assay using **RBM7–077** as substrate

hS1PL (50 µL from stock solutions in buffer B, final concentration: 0.8 µg/mL) was added to a mixture of **RBM7–077** (final concentration: 125 µM) and putative inhibitors (at the indicated concentrations) in buffer solution B (final volume: 100 µL). The mixture was incubated at 37 ºC for 1 h and the enzymatic reaction was stopped by the addition of 100 µL of KOH/EtOH (100 mM). After incubation at 37 ºC for 20 min, the resulting mixture was treated with 50 µL of a 200 mM glycine–NaOH buffer, pH 10.6, and the amount of umbelliferone formed was determined as described for **RBM13** (See Section 5.2.4.1).

5.2.4.3 Fluorogenic assay using **RBM7–148** as substrate

The assay was performed as described above for **RBM13** (See Section 5.2.4.1) using hS1PL at a final concentration of 0.8 µg/mL.

5.2.4.4 LC/MS assay

Recombinant bacterial or human S1PL (50 µL from stock solutions in buffer B; final concentration: 0.8 µg/mL) was added to a mixture of S1P (final concentration: 10 µM) and compound **3c** (final concentration: 50 µM) in buffer solution B (final volume: 100 µL). The reaction mixture was incubated at 37 ºC for 1 h and stopped by the successive addition of pentadecanal (5 µL of a stock solution in ACN; final concentration: 3.7 µM) and isoniazid (95 µL of a stock solution in ACN/300 mM aq. H_2SO_4 (1:1); final concentration: 3.1 mM). A 10 µL aliquot of the resulting solution was analyzed using a Waters Aquity UPLC system connected to a Waters LCT Premier Orthogonal Accelerated Time of Flight Mass Spectrometer (Waters, Millford, MA), operated in positive ESI mode. Full scan spectra from 50 to 1500 Da were obtained. Mass accuracy and reproducibility were maintained by using an independent reference spray via LockSpray. A C18 Acquity UPLC BEH analytical column (Waters, 100 mm x 2.1 mm, 1.7 µm) was used. The two mobile phases were CH_3CN (phase A) and water (phase B), both phases with 0.2 % (v/v) of formic acid. The linear gradient was: 0 min, 90% B; 5 min, 100% A; 6.5 min, 100% A; 7.2 min, 90% B and 8 min, 90% B at 0.3 mL/min. The column was held at 30 ºC. Positive identification of compounds was based on the accurate mass measurement with an error < 5 ppm and its LC retention time calculated with authentic 2EC16–ISO and C15–ISO standards. Exact masses ($[M + H]^+$) of both (*E*)–*N*'–((*E*)–hexadec–2–en–1–ylidene)isonicotinohydrazide (2EC16–ISO) and (*E*)–*N*'–pentadecylideneisonicotinohydrazide (C15–ISO) (m/z: 358.2858 and 346.2858, respectively) were extracted from TIC chromatograms and the area of the resulting peaks was calculated using MassLynx. The area ratio between 2EC16–ISO and C15–ISO was used as a measure of S1PL activity.

5.3 Computational virtual screening and docking methods

All the computational work was carried out with the Schrödinger Suite 2015,[26] through its graphical interface Maestro.[27] Coordinates of StS1PL and hS1PL (PDB codes 3MAD and 4Q6R)[24,28] were obtained from the Protein Data Bank[29] at Brookhaven National Laboratory. The protein X–ray structures were prepared using the Protein Preparation Wizard[30–34] included in Maestro to remove solvent molecules and ions, adding hydrogens, setting protonation states[35] and minimizing the energies.

Ligands were set up with the LigPrep module[36] included in Maestro to generate ionization states, tautomers, ring conformers and stereoisomers, as well as for geometry optimization previous to docking.

A virtual database of over 650000 commercial lead–like compounds[37] was screened against both S1PL proteins using the virtual screening workflow implemented in the Schrödinger Suite.[38] This workflow uses the docking program Glide[39–42] at different levels of accuracy to successively filter the compounds according to their predicted binding potency. Thus, initially all the compounds in the database were docked at the HTVS level, then the best 10 % was subjected to a second round of docking at the SP level, and finally the best 10 % was submitted to a third round of docking at the XP level, from which the best 10 % hits were reported. Among the final hits from screening against both protein targets in the two ionization states considered (see Section 3.1.2), compounds that bound to the anion binding site and that exhibited scores better than 9 kcal/mol were considered as positive hits.

A second virtual database of compounds based on scaffold **9** was generated. For that purpose, a diverse collection of commercial carboxylic acids was extracted from the clean lead–like subset from the ZINC database.[43,44] Compounds were selected according to different criteria: molecular weight <500; a single carboxylic group present; no undesirable chemical functions present. Additional compounds available in house were also considered resulting in a collection of 6048 carboxylic acids. These were combined with scaffold **10a** and **10b** (setting n = 1 or 2), using the CombiGlide[45] application of the Schrodinger Suite to enumerate a virtual library of 12096 compounds. This library was virtually screened as described above, but this time performing only the SP and XP docking steps and considering only the neutral state for the phenol–imine pair of the lysine–bound PLP complex, to yield 120 hits for each protein target. The hits from both

proteins were then submitted to the Induced Fit Docking Protocol[46] of the Schrödinger Suite, which takes in consideration the flexibility of the protein residues within a given distance (5 Å) from the bound ligands, in order to refine the geometries and scores of the docked poses.

In the case of the azido–S1P/dhS1P series, docking studies were conducted considering the 3–hydroxypyridine and imino groups of the Lys–bound PLP prosthetic group in their neutral state. The azido phosphate structures were built within Maestro and set up with the LigPrep module (see above) to generate ionization states, as well as for geometry optimization previous to docking. Ligands were docked into the active site of S1PL using the Induced Fit Docking Protocol (see above).

5.4 References

(1) Campbell, A. D.; Raynham, T. M.; Taylor, R. J. K. A Simplified Route to the (R)-Garner Aldehyde and (S)-Vinyl Glycinol. *Synthesis (Stuttg)*. **1998**, *1998* (12), 1707–1709.

(2) Yamamoto, T.; Hasegawa, H.; Hakogi, T.; Katsumura, S. Versatile Synthetic Method for Sphingolipids and Functionalized Sphingosine Derivatives via Olefin Cross Metathesis. *Org*. *Lett*. **2006**, *8* (24), 5569–5572.

(3) Goddard-Borger, E. D.; Stick, R. V. An Efficient, Inexpensive, and Shelf-Stable Diazotransfer Reagent: Imidazole-1-Sulfonyl Azide Hydrochloride. *Org*. *Lett*. **2007**, *9* (19), 3797–3800.

(4) Bhabak, K. P.; Proksch, D.; Redmer, S.; Arenz, C. Novel Fluorescent Ceramide Derivatives for Probing Ceramidase Substrate Specificity. *Bioorg*. *Med*. *Chem*. **2012**, *20* (20), 6154–6161.

(5) Srivastava, A. K.; Panda, G. Total Synthesis of (−)-Balanol, All Stereoisomers, Their N-Tosyl Analogues, and Fully Protected Ophiocordin: An Easy Route to Hexahydroazepine Cores from Garner Aldehydes. *Chem*. *– A Eur*. *J*. **2008**, *14* (15), 4675–4688.

(6) Wisse, P.; Gold, H.; Mirzaian, M.; Ferraz, M. J.; Lutteke, G.; van den Berg, R. J. B. H. N.; van den Elst, H.; Lugtenburg, J.; van der Marel, G. A.; Aerts, J. M. F. G.; et al. Synthesis of a Panel of Carbon-13-Labelled (Glyco)Sphingolipids. *Eur*. *J*. *Org*. *Chem*. **2015**, *2015* (12), 2661–2677.

(7) Murakami, T.; Furusawa, K. Efficient Stereodivergent Synthesis of Erythro- and Threo-Sphingosines: Unprecedented Reversal of the Stereochemistry in the Addition. *Tetrahedron* **2002**, *58* (45), 9257–9263.

(8) Raghavan, S.; Rajender, A. Novel, Short, Stereospecific Synthesis of Lyxo-(2R,3R,4R)-Phytosphingosine and Erythro-(2R,3S)-Sphingosine. *J*. *Org*. *Chem*. **2003**, *68* (18), 7094–7097.

(9) Herold, P. Synthesis of D-Erythro- and D-Threo-Sphingosine Derivatives From L-Serine. *Helv*. *Chim*. *Acta* **1988**, *71* (2), 354–362.

(10) Raghavan, S.; Rajender, A.; Yadav, J. S. Novel, Efficient and Stereospecific Synthesis of Xylo-(2R,3S,4S)-Phytosphingosine and Threo-(2R,3R)-Sphingosine. *Tetrahedron: Asymmetry* **2003**, *14* (14), 2093–2099.

(11) Yun, J. M.; Sim, T. B.; Hahm, H. S.; Lee, W. K.; Ha, H.-J. Efficient Synthesis of Enantiomerically Pure 2-Acylaziridines: Facile Syntheses of N-Boc-Safingol, N-Boc-D-Erythro-Sphinganine, and N-Boc-Spisulosine from a Common Intermediate. *J*. *Org*. *Chem*. **2003**, *68* (20), 7675–7680.

(12) Mukherjee, M.; Zhou, Y.; Gupta, A. K.; Guan, Y.; Wulff, W. D. A General Synthesis of Sphinganines through Multicomponent Catalytic Asymmetric Aziridination. *Eur*. *J*. *Org*. *Chem*. **2014**, *2014* (7), 1386–1390.

(13) Sandbhor, M. S.; Key, J. A.; Strelkov, I. S.; Cairo, C. W. A Modular Synthesis of Alkynyl-Phosphocholine Headgroups for Labeling Sphingomyelin and Phosphatidylcholine. *J*. *Org*. *Chem*. **2009**, *74* (22), 8669–8674.

(14) Parameswar, A. R.; Hawkins, J. A.; Mydock, L. K.; Sands, M. S.; Demchenko, A. V. Concise Synthesis of the Unnatural Sphingosine and Psychosine Enantiomer. *Eur*. *J*.

Org. *Chem*. **2010**, *2010* (17), 3269–3274.

(15) Enders, D.; Whitehouse, D. L.; Runsink, J. Diastereo- and Enantioselective Synthesis of L-Threo- and D-Erythro-Sphingosine. *Chem*. *– A Eur*. *J*. **1995**, *1* (6), 382–388.

(16) Nugent, T. C.; Hudlicky, T. Chemoenzymatic Synthesis of All Four Stereoisomers of Sphingosine from Chlorobenzene: Glycosphingolipid Precursors1a. *J*. *Org*. *Chem*. **1998**, *63* (3), 510–520.

(17) Fernandes, R. A.; Kumar, P. A Stereoselective Synthesis of Dihydrosphingosine. *Eur*. *J*. *Org*. *Chem*. **2000**, *2000* (20), 3447–3449.

(18) Yang, H.; Liebeskind, L. S. A Concise and Scalable Synthesis of High Enantiopurity (−)-D-Erythro-Sphingosine Using Peptidyl Thiol Ester−Boronic Acid Cross-Coupling. *Org*. *Lett*. **2007**, *9* (16), 2993–2995.

(19) Fransson, R.; McCracken, A. N.; Chen, B.; McMonigle, R. J.; Edinger, A. L.; Hanessian, S. Design, Synthesis, and Antileukemic Activity of Stereochemically Defined Constrained Analogues of FTY720 (Gilenya). *ACS Med*. *Chem*. *Lett*. **2013**, *4* (10), 969–973.

(20) Bedia, C.; Camacho, L.; Casas, J.; Abad, J. L.; Antonio, D.; Van Veldhoven, P. P.; Fabriàs, G. Synthesis of a Fluorogenic Analogue of Sphingosine-1-Phosphate and Its Use to Determine Sphingosine-1-Phosphate Lyase Activity. *ChemBioChem* **2009**, *10* (5), 820–822.

(21) Sbardella, G.; Castellano, S.; Vicidomini, C.; Rotili, D.; Nebbioso, A.; Miceli, M.; Altucci, L.; Mai, A. Identification of Long Chain Alkylidenemalonates as Novel Small Molecule Modulators of Histone Acetyltransferases. *Bioorg*. *Med*. *Chem*. *Lett*. **2008**, *18* (9), 2788–2792.

(22) Szulc, Z. M.; Hannun, Y. A.; Bielawska, A. A Facile Regioselective Synthesis of Sphingosine 1-Phosphate and Ceramide 1-Phosphate. *Tetrahedron Lett*. **2000**, *41* (41), 7821–7824.

(23) Boumendjel, A.; Miller, S. P. Synthesis of Sphingosine-1-Phosphate and Dihydrosphingosine-1-Phosphate. *J*. *Lipid Res*. **1994**, *35* (12), 2305–2311.

(24) Bourquin, F.; Riezman, H.; Capitani, G.; Grütter, M. G. Structure and Function of Sphingosine-1-Phosphate Lyase, a Key Enzyme of Sphingolipid Metabolism. *Structure* **2010**, *18*, 1054–1065.

(25) Bradford, M. M. A Rapid and Sensitive Method for the Quantitation of Microgram Quantities of Protein Utilizing the Principle of Protein-Dye Binding. *Anal*. *Biochem*. **1976**, *72* (1), 248–254.

(26) Schrödinger Suite 2015 Update 2, Schrödinger, LLC: New York, NY, 2015.

(27) Schrödinger Maestro, Version 10.2, Schrödinger, LLC: New York, NY, 2015.

(28) Weiler, S.; Braendlin, N.; Beerli, C.; Bergsdorf, C.; Schubart, A.; Srinivas, H.; Oberhauser, B.; Billich, A. Orally Active 7-Substituted (4-Benzylphthalazin-1-Yl)-2-Methylpiperazin-1-Yl]nicotinonitriles as Active-Site Inhibitors of Sphingosine 1-Phosphate Lyase for the Treatment of Multiple Sclerosis. *J*. *Med*. *Chem*. **2014**, *57*, 5074–5084.

(29) Berman, H. M.; Westbrook, J.; Feng, Z.; Gilliland, G.; Bhat, T. N.; Weissig, H.; Shindyalov, I. N.; Bourne, P. E. The Protein Data Bank. *Nucleic Acids Res* **2000**, *28* (1),

235–242.

(30) Schrödinger Protein Preparation Wizard 2015-2, Schrödinger, LLC: New York, NY, 2015.

(31) Schrödinger Epik, Version 2.4, Schrödinger, LLC: New York, NY, 2015.

(32) Schrödinger Impact, Version 5.9, Schrödinger, LLC: New York, NY, 2015.

(33) Schrödinger Prime, Version 3.2, Schrödinger, LLC: New York, NY, 2015.

(34) Madhavi Sastry, G.; Adzhigirey, M.; Day, T.; Annabhimoju, R.; Sherman, W. Protein and Ligand Preparation: Parameters, Protocols, and Influence on Virtual Screening Enrichments. *J. Comput. Aided. Mol. Des.* **2013**, *27* (3), 221–234.

(35) Olsson, M. H. M.; Søndergaard, C. R.; Rostkowski, M.; Jensen, J. H. PROPKA3: Consistent Treatment of Internal and Surface Residues in Empirical pKa Predictions. *J. Chem. Theory Comput.* **2011**, *7* (2), 525–537.

(36) Schrödinger LigPrep, Version 3.4, Schrödinger, LLC: New York, NY, 2015.

(37) MOE Leadlike Database, v. 2011.10, Chemical Comuting Group Inc.: Montreal, QC, Canada, 2011.

(38) Schrödinger Virtual Screening Workflow 2015-2, Schrödinger, LLC: New York, NY, 2015.

(39) Schrödinger Glide, Version 6.7, Schrödinger, LLC: New York, NY, 2015.

(40) Friesner, R. A.; Banks, J. L.; Murphy, R. B.; Halgren, T. A.; Klicic, J. J.; Mainz, D. T.; Repasky, M. P.; Knoll, E. H.; Shelley, M.; Perry, J. K.; et al. Glide: A New Approach for Rapid, Accurate Docking and Scoring. 1. Method and Assessment of Docking Accuracy. *J Med Chem* **2004**, *47* (7), 1739–1749.

(41) Halgren, T. A.; Murphy, R. B.; Friesner, R. A.; Beard, H. S.; Frye, L. L.; Pollard, W. T.; Banks, J. L. Glide: A New Approach for Rapid, Accurate Docking and Scoring. 2. Enrichment Factors in Database Screening. *J Med Chem* **2004**, *47* (7), 1750–1759.

(42) Friesner, R. A.; Murphy, R. B.; Repasky, M. P.; Frye, L. L.; Greenwood, J. R.; Halgren, T. A.; Sanschagrin, P. C.; Mainz, D. T. Extra Precision Glide: Docking and Scoring Incorporating a Model of Hydrophobic Enclosure for Protein-Ligand Complexes. *J Med Chem* **2006**, *49* (21), 6177–6196.

(43) Irwin, J. J.; Shoichet, B. K. ZINC--a Free Database of Commercially Available Compounds for Virtual Screening. *J. Chem. Inf. Model.* **2005**, *45* (1), 177–182.

(44) Irwin, J. J.; Sterling, T.; Mysinger, M. M.; Bolstad, E. S.; Coleman, R. G. ZINC: A Free Tool to Discover Chemistry for Biology. *J. Chem. Inf. Model.* **2012**, *52* (7), 1757–1768.

(45) Schrödinger CombiGlide, Version 3.7, Schrödinger, LLC: New York, NY, 2015.

(46) Schrödinger Induced Fit Docking Protocol 2015-2, Scrödinger, LCC: New York, NY, 2015.

6. Summary in catalan

Els esfingolípids (SLs) són components estructurals essencials de les membranes cel·lulars. A més, una bona part dels seus metabòlits actuen com a molècules de senyalització en cèl·lules eucariotes. Els SLs fosforilats, els quals presenten un grup fosfat en l'hidroxil terminal, formen un grup rellevant de metabòlits d'aquesta gran família de lípids d'origen natural. Entre ells, l'esfigosina–1–fosfat (S1P) és una reconeguda molècula de senyalització, la qual pot actuar com a missatger secundari intracel·lular o com lligand d'una sèrie de receptors acoblats a proteïnes G ($S1P_{1–5}$), activant diverses vies de senyalització, les quals estan involucrades en el desenvolupament vascular, la integritat endotelial, el control del ritme cardíac o la resposta immunitària, entre d'altres.

L'esfingosina–1–fosfat liasa (S1PL), és un enzim depenent de piridoxal 5'–fosfat (PLP) situat al reticle endoplasmàtic, el qual catalitza la degradació irreversible de la S1P, per donar fosfat d'etanolamina (EAP) i *trans*–2–hexacedenal (Figura 6.1). Juntament amb la S1P fosfatasa i la esfingosina cinasa, la S1PL regula els nivells intracel·lulars de la S1P i contribueix a l'anomenat "reòstat esfingolipídic", un sistema que controla el destí cel·lular, basant-se en la relació de concentracions entre la S1P, que actua com a agent proliferatiu, i l'esfingosina i/o la ceramida, les quals són molècules apoptogèniques. Addicionalment, s'ha demostrat que la S1PL té un paper important en la regulació del sistema immunitari, ja que la seva inhibició altera el gradient de concentració de S1P que promou la sortida de cèl·lules T dels teixits limfoides. En aquest context, la S1PL ha estat recentment validada com a diana terapèutica per al tractament d'algunes malalties autoimmunes, tals com l'esclerosi múltiple o l'artritis reumatoide.

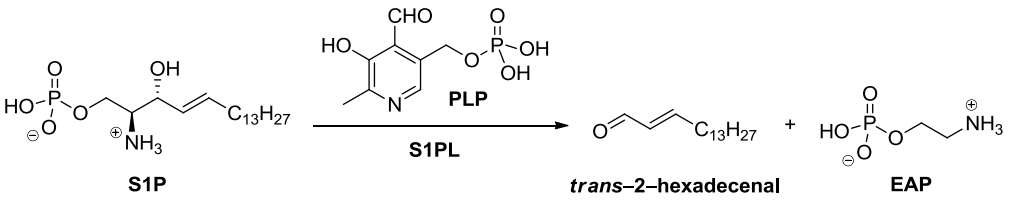

Figura 6.1. Reacció retroaldòlica de degradació de la S1P catalitzada per la S1PL.

Degut al potencial terapèutic associat a la modulació de l'activitat S1PL, en la present tesi doctoral s'ha abordat el disseny de nous inhibidors de la S1PL des de dues aproximacions diferents. Primerament, es va duu a terme un disseny basat en la estructura (SBDD) de nous inhibidors de la S1PL emprant les estructures cristal·lines de

la S1PL humana (hS1PL) i la de *Symbiobacterium thermophilum* (StS1PL), les quals varen presentar un elevat grau de similitud estructural i de seqüència. Atenent als trets estructurals comuns presents en una sèrie de compostos identificats com a *hits* en un cribratge preliminar d'inhibidors de la S1PL, i basant-se en els resultats de *docking* duts a terme amb les estructures de raig X de la hS1PL i la StS1PL, una col·lecció de potencials inhibidors de la S1PL derivats de l'estructura general **9**, va ser dissenyada i sintetitzada (Figura 6.2)

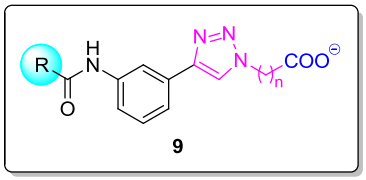

Figura 6.2. Estructura general dels potencials inhibidors de la S1PL sintetitzats.

Per tal d'avaluar l'activitat biològica de possibles inhibidors de la S1PL, es va desenvolupar un assaig basat en l'ús d'enzims recombinants purificats, tals com la StS1PL o la hS1PL. En aquest cas, el compost **RBM13**, un substrat fluorogènic de la S1PL prèviament reportat en el nostre grup de recerca, va ser emprat com a substrat del nou assaig (Figura 6.3). Malauradament, però, les modestes activitats presentades per els inhibidors dissenyats en el nou assaig desenvolupat, va permetre concloure que la primera aproximació en el disseny racional d'inhibidors de la S1PL no va ser exitosa.

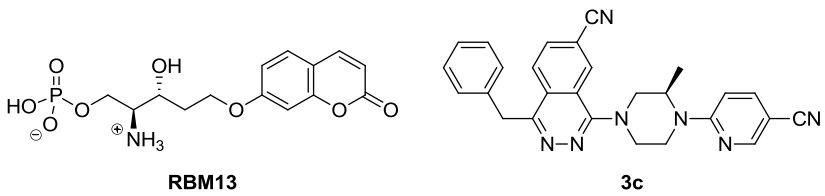

Figura 6.3. Estructures del substrat fluorogènic **RBM13** i de l'inhibidor de la hS1PL **3c**.

Sorprenentment, tot i que el compost **RBM13** va presentar uns paràmetres cinètics molt semblants vers els dos enzims, quan el compost **3c** (Figura 6.3), un inhibidor de referència de la hS1PL, va ser testat contra l'enzim bacterià, aquest no va resultar ser actiu. No obstant, la comparació de les estructures d'ambdós enzims va permetre

identificar algunes diferències estructurals en el canal d'entrada al centre actiu d'aquests, les quals podrien explicar la manca d'activitat observada per al compost **3c**.

En una segona aproximació, basant-se en consideracions mecanístiques del cicle catalític de l'enzim, es van dissenyar i sintetitzar dues famílies d'inhibidors de la S1PL. D'aquesta manera, una família d'anàlegs no reactius d'alguns intermedis clau del cicle catalític (compostos **RBM7–001**, **RBM7–012** i **RBM7–032**) així com una sèrie d'azido-derivats del substrat natural S1P (compostos d'estructural general **A**) varen ser dissenyats, sintetitzats i testats vers la hS1PL i la StS1PL (Figura 6.4). Tot i que alguns dels mimètics dels intermedis del procés catalític van ser inhibidors de potència moderada, tots els azido fosfats sintetitzats van resultar ser inhibidors competitius en el rang μM baix en els dos isoenzims.

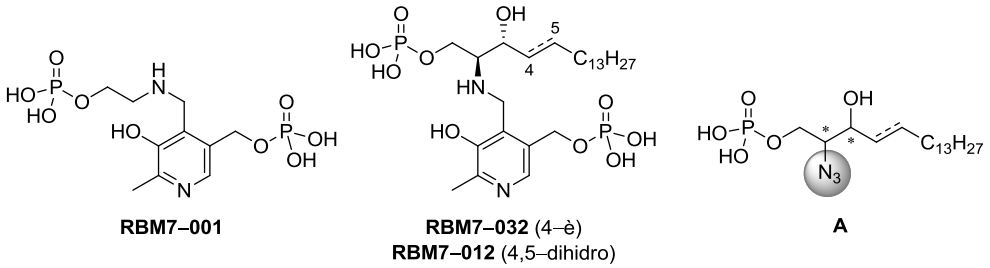

Figura 6.4. Estructura dels inhibidors de la S1PL basats en el mecanisme de reacció.

Amb tot, els resultats obtinguts suggereixen que la StS1PL és un bon model per al disseny i identificació de nous inhibidors de la hS1PL, sempre que aquests siguin concebuts per unir-se al centre actiu de l'enzim. No obstant, atenent als resultats obtinguts per a l'inhibidor de referència de la hS1PL (**3c**), la utilitat de la StS1PL com a model de l'enzim humà esdevé limitada, especialment quan hom vol dissenyar inhibidors que interaccionin amb el canal d'entrada al centre actiu de l'enzim.

Finalment, dues noves sondes fluorogèniques amb potencial aplicabilitat en assaigs HTS van ser dissenyades i sintetitzades (compostos **RBM7–077** i **RBM7–148**, Figura 6.5). Estructuralment, ambdues sondes deriven formalment del compost **RBM13**, en els quals un grup vinil va ser intercalat entre la fracció d'amino alcohol fosfat i la unitat de cumarina situada en la posició ω. En aquest cas, els dos compostos varen ser validats com a substrats de la hS1PL, els quals van presentar millors paràmetres cinètics que els determinats per al substrat **RBM13**. Ambdues sondes van resultar ser substrats no–

naturals adequats per al cribratge d'inhibidors de la S1PL, ja que van permetre la determinació de diferents valors d'IC_{50} de l'inhibidor de referència **3c**, els quals van resultar ser del mateix ordre de magnitud que els determinats pel mateix inhibidor emprant la S1P natural com a substrat.

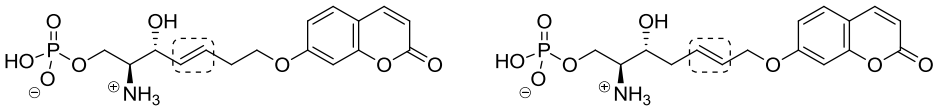

Figura 6.5. Estructura de les sondes fluorogèniques **RBM7–077** i **RBM7–148**.

7. Supporting information

Supplementary data related to the present doctoral thesis can be found in the attached CD. The following material is included:

- PDF file of the Doctoral Thesis.
- Dose–response curves of compounds from Section 3.2.
- Lineweaver–Burk plots of compounds from Section 3.2.
- HPLC chromatograms of compounds **RBM7–087**, ***ent*–RBM7–087**, **RBM7–096**, ***ent*–RBM7–096**, **RBM7–112**, ***ent*–RBM7–112**, **RBM7–101** and ***ent*–RBM7–101**.
- NMR spectra of compounds from Sections 3.1, 3.2 and 3.3.